Radioactive Waste Management
2022

Clay Club Catalogue of Characteristics of Argillaceous Rocks

2022 Update

OECD
BETTER POLICIES FOR BETTER LIVES

NEA
NUCLEAR ENERGY AGENCY

Radioactive Waste Management and Decommissioning

Clay Club Catalogue of Characteristics of Argillaceous Rocks:

2022 Update

NEA No. 7249

NUCLEAR ENERGY AGENCY
ORGANISATION FOR ECONOMIC CO-OPERATION AND DEVELOPMENT

ORGANISATION FOR ECONOMIC CO-OPERATION AND DEVELOPMENT

The OECD is a unique forum where the governments of 38 democracies work together to address the economic, social and environmental challenges of globalisation. The OECD is also at the forefront of efforts to understand and to help governments respond to new developments and concerns, such as corporate governance, the information economy and the challenges of an ageing population. The Organisation provides a setting where governments can compare policy experiences, seek answers to common problems, identify good practice and work to co-ordinate domestic and international policies.

The OECD member countries are: Australia, Austria, Belgium, Canada, Chile, Colombia, Costa Rica, the Czech Republic, Denmark, Estonia, Finland, France, Germany, Greece, Hungary, Iceland, Ireland, Israel, Italy, Japan, Korea, Latvia, Lithuania, Luxembourg, Mexico, the Netherlands, New Zealand, Norway, Poland, Portugal, the Slovak Republic, Slovenia, Spain, Sweden, Switzerland, Turkey, the United Kingdom and the United States. The European Commission takes part in the work of the OECD.

OECD Publishing disseminates widely the results of the Organisation's statistics gathering and research on economic, social and environmental issues, as well as the conventions, guidelines and standards agreed by its members.

NUCLEAR ENERGY AGENCY

The OECD Nuclear Energy Agency (NEA) was established on 1 February 1958. Current NEA membership consists of 34 countries: Argentina, Australia, Austria, Belgium, Bulgaria, Canada, the Czech Republic, Denmark, Finland, France, Germany, Greece, Hungary, Iceland, Ireland, Italy, Japan, Korea, Luxembourg, Mexico, the Netherlands, Norway, Poland, Portugal, Romania, Russia, the Slovak Republic, Slovenia, Spain, Sweden, Switzerland, Turkey, the United Kingdom and the United States. The European Commission and the International Atomic Energy Agency also take part in the work of the Agency.

The mission of the NEA is:

- to assist its member countries in maintaining and further developing, through international co-operation, the scientific, technological and legal bases required for the safe, environmentally sound and economical use of nuclear energy for peaceful purposes.
- to provide authoritative assessments and to forge common understandings on key issues as input to government decisions on nuclear energy policy and to broader OECD analyses in areas such as energy and the sustainable development of low-carbon economies.

Specific areas of NEA competence include the safety and regulation of nuclear activities, radioactive waste management, radiological protection, nuclear science, economic and technical analyses of the nuclear fuel cycle, nuclear law and liability, and public information. The NEA Data Bank provides nuclear data and computer program services for participating countries.

Cover photos: A gallery in the Meuse/Haute Marne Underground Research Laboratory (A. Daste, Andra); Ammonite found at a depth of 652 metres in the Opalinus Clay of the Benken borehole (Comet, provided courtesy of Nagra).

Foreword

Countries around the world are considering a wide variety of argillaceous media – from soft, plastic and poorly indurated clays, to brittle, hard mudstones or shales – as potential host rocks for the deep geological disposal of radioactive waste. Such argillaceous media are typically characterised as being favourable or unfavourable for the long-term passive isolation of safety-relevant radionuclides, based on a number of parameters. Characteristics that are typically evaluated for argillaceous media being considered as a potential host for a deep geological repository (DGR) include:

- thickness and continuity;
- low permeability;
- chemical buffering capacity;
- potential for plastic deformation and self-sealing of fractures;
- geochemical characteristics that favour low solubility of radionuclides; and
- high capacity to delay the migration of radionuclides to the accessible environment (e.g. through sorption and/or diffusion-dominated transport).

Information required to evaluate the performance of deep geological formations is drawn from detailed site characterisation programmes and regional observations/understanding (e.g. hydromechanical characteristics are gathered during borehole drilling, underground excavation and underground rock laboratory [URL] activities; and geochemical characteristics are used to indicate the ability of the formation to limit radionuclide migration obtained from groundwater/porewater analyses).

The Nuclear Energy Agency Working Group on the Characterisation, the Understanding and the Performance of Argillaceous Rocks as Repository Host Formations (hereinafter the "Clay Club") began, in 1990, examining the various argillaceous rocks that are being considered for the deep geological disposal of radioactive waste. The Clay Club promotes: 1) continuing inter-comparison of the properties of different argillaceous media; 2) exchange of technical and scientific information on clay properties and behaviour, and on testing that is being carried out in underground research facilities; and 3) detailed review of the available and most promising investigation techniques for site characterisation.

With these overall objectives, one of the first initiatives of the Clay Club was to gather the key geoscientific characteristics of the various argillaceous formations that were – or had been – studied in NEA member countries in the context of radioactive waste disposal. This work resulted in the publication of the *Clay Club Catalogue of Characteristics of Argillaceous Rocks* (NEA, 2005). The present publication builds upon this earlier report by providing updated datasets for a select number of argillaceous formations that were presented in the 2005 catalogue, and by providing an expanded discussion of: 1) the formations and their properties; 2) the radioactive waste management organisations responsible for implementation of the DGR concept; 3) the design concept proposed for a DGR in the respective countries, specific to the rock formations; and 4) some of the favourable properties of argillaceous formations. A key goal of this 2022 updated catalogue is to present the data in a manner that allows reasonable comparability (in both scale and methods) of the included parameters in order to support formal assessment and demonstration of the capacity of clay-rich formations to securely contain and isolate radioactive waste from the natural environment.

Argillaceous formations included in this updated catalogue are listed under their respective countries below:

Belgium

- Boom Clay at Mol
- Ypresian clays at Kallo/Doel (Beveren)

Canada

- Queenston Formation Shale at Tiverton (Bruce nuclear site)
- Georgian Bay Formation at Tiverton (Bruce nuclear site)

France

- Callovo-Oxfordian at Bure
- Toarcian-Domerian at Tournemire

Hungary

- Boda Claystone at Boda
- Boda Claystone at Gorica

Japan

- Wakkanai at Horonobe
- Koetoi at Horonobe

Switzerland

- Opalinus Clay at Mont Terri
- Opalinus Clay in north-east Switzerland.

Acknowledgements

This updated 2022 Clay Club Catalogue has been compiled by the Nuclear Waste Management Organization (NWMO) of Canada with the help of the Clay Club members (see the list of contributors below) and officials from the Nuclear Energy Agency (NEA). The NEA appreciates in particular the work of L. Kennell-Morrison (NWMO), T. Yang (NWMO) and M. Jensen (NWMO) in compiling the updated 2022 Clay Club Catalogue.

Contributors:

Belgium	L. Wouters (ONDRAF/NIRAS)
Canada	L. Kennell-Morrison (NWMO), M. Jensen (NWMO), T. Lam (NWMO), R. Crowe (NWMO), M. Hobbs (NWMO), T. Yang (NWMO), E. Sykes (NWMO)
France	J.Y. Boisson (IRSN), C. Wittebroodt (IRSN), A. Chabiron (Andra), F. Plas (Andra)
Hungary	G. Tungli (PURAM), Z. Nagy (Consultant – Geology and Geophysics), J. Csicsák (MECSEKERC Environmental Co.), F. Fedor (GEOCHEM Ltd.), G. Földing (MECSEKERC Environmental Co.), G. Hámos (MECSEKERC Environmental Co.), G. Konrád (University of Pecs), L. Kovács (KOMERO Ltd.), Z Máthé (MECSEKERC Environmental Co.), J. Osan (Centre for Energy Research, Hungarian Academy of Sciences)
Japan	H. Sasamoto (JAEA), K. Tsusaka (INPEX), E. Ishii (JAEA), T. Mizuno (JAEA), K. Aoyagi (JAEA)
Switzerland	A. Gautschi (Nagra), M. Mazurek (University of Bern), D. Traber (Nagra), S. Giger (Nagra)

Dedicated to the memory of Mark Jensen, whose leadership and dedication to advancing geoscientific understanding inspired this updated compilation of the Clay Club Catalogue of Characteristics of Argillaceous Media. Mark's contributions to his peers, both in Canada and internationally, are beyond measure.

Table of contents

List of figures

List of tables

List of abbreviations and acronyms

BCF	Boda Claystone Formation
CT	Computed tomography
D_e	Effective diffusion coefficient
DGR	Deep geologic(al) repository
EBS	Engineered barrier system
HLW	High-level waste
HTO	Tritiated water
ILLW	Intermediate- and low-level waste
ILW	Intermediate-level waste
IRSN	French Institute for Radiological Protection and Nuclear Safety
JAEA	Japan Atomic Energy Agency
L&ILW	Low- and intermediate-level waste
LLW	Low-level waste
NUMO	Nuclear Waste Management Organization (Japan)
NWMO	Nuclear Waste Management Organization (Canada)
NEA	Nuclear Energy Agency
PURAM	Public Limited Company for Radioactive Waste Management (Hungary)
R&D	Research and development
RD&D	Research, Design and Development
SFC	Safety and Feasibility Case
TDS	Total dissolved solids
URF	Underground research facility
URL	Underground rock (or research) laboratory

List of units

cm	centimetre
°C	degrees Celsius
kg/m^3	kilogram per cubic metre
km	kilometre
km^2	square kilometres
Ma	million years
MPa	megapascal
m	metre(s)
m/s	metres per second
mg/L	milligrams per litre
mm	millimetre
mV	millivolt
m^2/g	square metres per gram
m^2/s	square metres per second
vol.%	percent by volume
wt.%	percent by weight
‰ V-SMOW	per mille Vienna Standard Mean Ocean Water

Chapter 1. **Objectives of the report**

The primary aims of the 2005 Clay Club Catalogue (NEA, 2005) were to:

- provide an overview of key geoscientific data that are necessary inputs in clay characterisation and performance assessments (e.g. geology, mineralogy, geochemistry, petrophysics, hydrogeology, solute transport, rock mechanics) for each argillaceous formation included in the catalogue;
- assist in understanding both the similarities and differences between formations;
- assess the possibilities of transferring knowledge and/or characterisation methodologies from one formation to another (or from one site to another);
- illustrate the wide spectrum of characteristics corresponding to "clays as host formations".

The present report builds upon the knowledge and experience gained during the compilation of the catalogue in 2005 and brings together a small collection of datasets compiled over the last decade, which document the key geoscientific characteristics of argillaceous formations that are most relevant in the context of demonstrating passive safety and confirming deep system longevity and stability. The updated 2022 report 1) highlights key attributes and characteristics of argillaceous sediments, some of which are being considered as host media for the long-term containment of radioactive waste; and 2) provides a vetted database documenting representative formation properties. Emphasis is placed on the understanding of geosphere properties, coupled with understanding of behaviour in the geological past, and how such information underpins and establishes confidence in the context of long-term deep geological repository (DGR) safety considerations for the future.

The parameters selected to structure the datasets were included on the basis of their relevance, according to the performance assessment ranking system presented in the Nuclear Energy Agency publication *Features, Events and Processes Evaluation Catalogue for Argillaceous Media* (FEPCAT) (NEA, 2003). An evaluation of the performance assessment Level 1-ranked features, events and processes yields the following three hypotheses suggested to be highly relevant in establishing confidence in formation suitability to host a DGR.

1. The areal extent and thickness of the lithological units at the sites allow for predictability at scales relevant to establishing safety.
2. The presence of natural barriers (host and enclosing formations) acts to isolate the host rock and to contain solutes for time frames necessary to establish safety:
   - shallow groundwater resources are isolated;
   - the nature of the argillaceous rock allows for sorption of solutes and retardation of radionuclide transport.
3. Stability of the geosphere on timescales relevant to establishing safety is supported by multiple lines of geoscientific reasoning:
   - Transport processes are anticipated to remain diffusion-dominated over geological time frames (hundreds of thousands to millions of years).
   - The groundwater-porewater system is anticipated to remain geochemically stable over geological time frames.
   - The formations are characterised by geomechanical stability.

Each formation description (see Annex III: Document 1) included in this report contains a summary section, "Favourable Formation Attributes", detailing site- or formation-specific information that has been collected during characterisation activities. This information has been organised into groupings based on their relevance to the three hypotheses presented above.

Key goals of the 2022 Clay Club Catalogue include:

1. providing a reasonably comparable database of select physical and chemical properties (e.g. geochemical, hydrogeological and geomechanical) representative of clay-rich sedimentary formations, from the last decade of international research on long-term radioactive waste management;
2. emphasising the breadth and scope of international knowledge and experience associated with the characterisation of argillaceous rocks for long-term radioactive waste management purposes;
3. highlighting features and attributes, as well as the versatility, of argillaceous formations, with emphasis on those characteristics that would be most relevant for consideration in the context of DGR safety (note that ranking of the sedimentary formations is not a component of this report).

The catalogue includes data that have been acquired from both surface-based investigations (borehole logging and core analysis, seismic surveys, etc.) and underground rock laboratories (URLs). The measured data are presented as a range in the data tables, using minimum and maximum values, as well as by a quantitative best-estimate value for most parameters. The report should not be used for the following purposes:

- as a detailed description of a particular geological formation;
- as an assessment of the abilities of a particular geological formation to host a radioactive waste disposal facility;
- as an evaluation/comparison of the respective performance of the various formations;
- as direct quantitative input for assessments without any consideration of the origin of the data and the related terms of their measurements;
- as a provision of a guarantee of the applicability of a given value to a specific location, depth, lithostratigraphic interval within the formation, etc., without further checking with pertinent specialists.

Each contributing organisation is responsible for the content of its formation-specific text and data. Neither the NEA nor the participating national organisations can be held responsible for any use that might be made of the information considered in this catalogue.

This catalogue is open and freely available. In addition to Clay Club members, the catalogue targets radioactive waste disposal experts and external geoscientific experts as its main audience. A comprehensive database is included as an Annex of this report. Annex III of this catalogue is a comprehensive compilation that has been updated from the 2005 version of the Clay Club Catalogue to include information on: i) the current waste disposal concept (where applicable) of the respective organisations; and ii) the key characteristics of the various formations that are/can be used to provide confidence in the ability of argillaceous formations to safely isolate radioactive waste over long time frames.

Chapter 2. Description of the catalogue and guidelines for its use

2.1. Context for the presented formations

This updated 2022 catalogue documents key properties and attributes of clay formations, based on geoscience research in radioactive waste management programmes around the world. Unlike the previous (2005) version of the catalogue, key formation properties are selected and presented here according to the three key geoscientific hypotheses (see Chapter 1) that are considered highly relevant to demonstrating long-term passive performance in the context of deep geological repository (DGR) safety.

In this report, the formations presented include those studied in national repository (siting or licensing) site characterisation programmes and/or those in which an underground rock laboratory (URL) has been established for the purpose of assessing formation properties (i.e. gaining process understanding) relevant to predicting long-term evolution. Included in the catalogue is a comprehensive compilation of high-quality datasets (Master Database; see Annex III: Table 1) that highlight the natural properties of argillaceous rock most influencing the understanding of geosphere stability, as well as detailed formation descriptions (Annex III: Document 1). Section 4.1 contains brief geological summaries for each argillaceous formation included in the Master Database. The detailed descriptions of the various argillaceous formations found in Annex III: Document 1 include information on the national context in which all the data were gathered, the disposal concept being considered (where applicable), the key formation properties (i.e. geology and geomechanics, hydrogeology, geochemistry and solute transport) and, wherever possible and relevant, data applicability in the context of suitability of argillaceous formations to host a DGR and contain/isolate waste over safety-relevant time frames. Other relevant information presented includes:

- geological environment;
- illustrated map(s) and cross-sections;
- data acquisition techniques (i.e. geophysical survey, outcrops, boreholes/drillings, existence of a URL).

It should be noted that the intention of this data compilation is not to promote inter-site comparison or ranking of sites relative to one another based solely on the presented data. Instead, this report aims to document characteristics of a variety of argillaceous formations that span a broad range of clay contents, mineralogies, ages and degrees of induration, as well as to depict the range in key parameters that are encountered in a variety of argillaceous media considered potentially suitable for the long-term management and isolation of radioactive waste.

2.2. Selection of clay properties in the catalogue

The parameters included in this update are selected and presented based on three key geoscientific hypotheses that are of relevance to demonstrating system longevity and stability, as stated in Chapter 1. These parameters are selected, in part, based on their role and importance to understanding long-term geosphere behaviour, as well as on data availability from the participating national organisations. The data are prioritised in terms of relevance to the assessment of long-term safety in line with the properties and parameters identified in Mazurek et al. (2011) and assigned a Level 1 ranking in NEA FEPCAT (NEA, 2003).

For each argillaceous formation, the presented parameters are grouped into the following main categories:

- geological parameters;
- mineralogical parameters;
- porewater chemistry parameters;
- petrophysical parameters;
- flow and solute transport parameters;
- geomechanical parameters.

For each category, a list of the included parameters is presented in Table 1.

2.3. Confidence in clay characteristics and properties

A number of steps have been taken to validate the datasets included in the Master Database. Such steps have included review of the datasets for charge balance and for major mineral composition balance, and review of the methods used to measure the respective parameters to ensure reasonable comparability of the data. Where it has been noted that the methods used would preclude or limit comparability, a note to that effect has been included in Chapter 3, "Limitations of the Catalogue". Chapter 4 highlights some of the key features of argillaceous media that render them feasible for the purpose of long-term radioactive waste storage and isolation, with emphasis in Section 4.2 on the figures and correlation plots in Annex I and II. It is noted in Section 4.2 that, for the formations included in this report, the various methods used to measure individual parameters generally produce similar/consistent results for the individual formations. In addition, for clarity, the measurement methods employed are indicated in a number of the data figures included in Annex I and are tabulated in Annex III (Annex III: Table 2) along with the scales of measurement for each parameter.

The datasets included are of high quality and have undergone extensive review at NWMO, Nagra, Andra, ONDRAF/NIRAS, JAEA and IRSN.

2.4. General guidelines

- An assessment of the quality of, and confidence in, the data is provided (low, medium and high) in Annex III: Table 1, and is indicated in various figures in Annex I.
- The conditions of measurement (i.e. in situ versus laboratory, sample orientation) of a given parameter, where appropriate, are noted in the Master Database (see Annex III: Table 1) and in the summary table of method(s) and scale(s) of measurement (see Annex III: Table 2).
- Scale(s) of measurement and/or method(s) of measurement for each parameter are tabulated, in as much detail as possible, in Annex III: Table 2.
- Parameters are expressed as "minimum", "best estimate" (most representative or best estimate from experts) and "maximum" values.
  - The meaning of min/max/best estimate for each parameter may reflect different measures. In some circumstances, the min/max values reflect the range of values measured for the formation (lowest/highest, with best estimate as the mean), while in others the min/max may represent the analytical precision of the methods and encompass the 1σ or 2σ range of the mean or central tendency (or "best estimate"). The meaning of these values is defined wherever possible in Annex III: Table 2.
  - The meaning of "best estimate" may differ between the respective formations and is intended as a reference value (selected or calculated based on expertise from the available data). In some circumstances, the "best estimate" represents mean values measured for the formation (possibly at multiple locations) near repository depth, as part of site selection or multiple site investigation activities. In other circumstances, it represents values for the formation from an underground rock laboratory (URL)

location, which likely will not be used as a future site for a DGR. And finally, in a few circumstances the data represent the best estimates from repository depth at a site that has undergone extensive characterisation activities and has been proposed as a potential repository location. The number of measurements performed, and the location(s) from which the samples were taken, are provided wherever possible in Annex III: Table 2 to clarify the meaning of "best estimate" for the various parameters.

- Wherever possible, anisotropy of any parameter measured in both horizontal and vertical orientations is noted in Annex III: Table 1.
- Parameters are not anticipated to be affected by surface effects such as weathering or decompression.

To the greatest extent possible, bibliographic references refer to open, published literature.

Table 1: **Master Database compilation – listing of included parameters**

Geological parameters	Mineralogical parameters	Porewater chemistry parameters	Petrophysical parameters	Flow and solute transport parameters	Geomechanical parameters
Depositional environment	Clay minerals – sum of all (% total dry weight)	Porewater type	Cation-exchange capacity [meq/100 g of rock]	Hydraulic conductivity (⊥) lab tests [m/s]	Uniaxial compressive strength (⊥) lab tests [MPa]
Age (Ma)	Clay minerals-Illite [% total dry weight]	TDS – salinity [mg/L]	Specific surface external [m^2/g]	Hydraulic conductivity (//) lab tests [m/s]	Uniaxial compressive strength (//) lab tests [MPa]
Burial depth present-day (top formation)	Clay minerals-smectite [% total dry weight]	Eh [mV]	Specific surface total [m^2/g]	Hydraulic conductivity in situ tests [m/s]	Young's modulus static (⊥) lab tests [MPa]
Burial depth present-day (bottom formation)	Clay minerals-chlorite [% total dry weight]	pH	Density bulk saturated [kg/m^3]	Diffusion effective coefficient De (^3H) (⊥) lab tests [m^2/s]	Young's modulus static (//) lab tests [MPa]
Thickness (m)	Clay minerals-kaolinite [% total dry weight]	$\delta^{18}O$ [‰ V-SMOW]	Density bulk dry [kg/m^3]	Diffusion effective coefficient De (^3H) (//) lab tests [m^2/s]	Young's modulus dynamic (⊥) lab tests [MPa]
Burial depth maximum (m)	Clay minerals-illite/smectite [% total dry weight]	δ^2H [‰ V-SMOW]	Density grain average [kg/m^3]	Diffusion effective coefficient De (I^-) (⊥) lab tests [m^2/s]	Young's modulus dynamic (//) lab tests [MPa]
Over-consolidation ratio	Quartz [% total dry weight]	Cations: Ca, Mg, K, Na (mg/L)	Water content (water weight/dry weight) [%]	Diffusion effective coefficient De (I^-) (//) lab tests [m^2/s]	Young's modulus static (⊥) in situ tests [MPa]
Maximum temperature reached during diagenesis (oC)	Feldspars [% total dry weight]	Anions: Cl, SO4, HCO3, Br (mg/L)	Porosity calculated from water content at 105-110 °C [% by volume]	Diffusion effective coefficient De (Cl^-) (⊥) lab tests [m^2/s]	Young's modulus static (//) in situ tests [MPa]
	Carbonates [% total dry weight]		Physical porosity	Diffusion effective coefficient De (Cl^-) (//) lab tests [m^2/s]	Poisson's ratio static lab tests (⊥) [-]
	Calcite [% total dry weight]		Porosity other methods [% by volume]		Poisson's ratio static lab tests (//)
	Dolomite/ankerite [% total dry weight]		Anion-accessible porosity		Poisson's ratio dynamic (⊥) lab tests [-]
	Pyrite [% total dry weight]		Seismic velocity Vp (⊥) lab tests [m/s]		Poisson's ratio dynamic (//) lab tests [-]

Table 1: **Master Database compilation – listing of included parameters** *(cont'd)*

Geological parameters	Mineralogical parameters	Porewater chemistry parameters	Petrophysical parameters	Flow and solute transport parameters	Geomechanical parameters
	Carbon organic [%]		Seismic velocity Vp (∥) lab tests [m/s]		Cohesion (⊥) lab tests [MPa]
			Seismic velocity Vs (⊥) lab tests [m/s]		Cohesion (∥) lab tests [MPa]
			Seismic velocity Vs (∥) lab tests [m/s]		Internal friction angle (⊥) lab tests [°]
			Seismic velocity Vp in situ tests [m/s]		Internal friction angle (∥) lab tests [°]
			Seismic velocity Vs in situ tests [m/s]		Swelling pressure (⊥) lab tests [MPa]
					Swelling pressure (∥) lab tests [MPa]

Chapter 3. **Limitations of the catalogue**

The following sub-sections focus on specific challenges with respect to data comparison and transferability, as determined subsequent to detailed review of the datasets. Observations with respect to potential heterogeneity of methods and the comparability of laboratory versus in situ data are documented here, as well as brief discussions of data reliability, potential issues associated with upscaling and anisotropy, and any key property uncertainties.

Data transferability

As noted in Chapter 2, comparison of the data between formations must be performed with caution. Methods used to determine several of the included parameters are not the same between organisations/sites, with different approaches employed based on the nature of the rock (e.g. depth of the formation – application of pressure in laboratory to imitate in situ pressure conditions, typical/known salinity of the porewater/groundwater, porosity and water content).

As observed in Annex I, II and III, differences can often be observed in measured values for the same parameter when the measurement is performed in laboratory versus in situ. Consideration must be given to these differences in both scale and methodology (see Annex III: Table 2) when comparing such results. These differences may be real, potentially representing the differences between the in situ pressure conditions at depth and those measured in the laboratory (i.e. following core relaxation – use of ambient pressure/temperature or applied pressure), or may be a reflection of the various methods applied and the potential for those to measure parameters to a different degree of accuracy/confidence/certainty.

The data for site-specific and/or URL locations can be used to make some conclusive statements regarding the nature of the argillaceous rock mass at that location, and potentially the surrounding area (km to tens of km scale); however, the potential for heterogeneity within and across argillaceous rock formations must be considered in any overall generalisation about the nature of these formations in a broader scale or context.

Effort has been made to ensure the data presented are reasonably comparable, based on assessments of methodology, sample orientation and scales of measurement; however, it must be understood that differences do exist and must be considered in any evaluation or comparison of parameters between the formations (or between sites), which is not the intended purpose of this compilation.

Data reliability

The parameters included in the Master Database have been ranked in terms of level of confidence in the values (high, medium, low). The confidence levels reflect a number of factors, including the uncertainties associated with the methods employed.

In a general sense, parameters can be compared between locations despite differences in the analytical methods; however, direct comparison is not appropriate, as conditions of measurement (i.e. pressure, temperature, displacing medium, sample size, number of samples analysed, etc.) cannot be assumed to be the same between laboratories. To the extent that it is available such information is presented in Annex III: Table 2, where the methods employed, scales of measurement and any relevant notes are included for the parameters measured.

Annex III: Table 2 indicates, wherever possible, the number of samples analysed to determine the minimum, best estimate and maximum values presented in the Master Database (Annex III: Table 1) and in the figures (Annex I and II).

Upscaling and anisotropy

A number of parameters in the Master Database have been measured at varying scales and varying degrees of confidence/certainty with respect to the measured values. As a result, it is difficult to make general assessments about the potential representativeness of the parameter in the context of the formation as a whole. Wherever possible, anisotropy values (i.e. where values have been measured both parallel and perpendicular to bedding, or at different orientations) for a parameter have been provided (i.e. calculated) in the Master Database (Annex III: Table 1).

Key property uncertainties

The limitations of the catalogue are outlined below, in order to avoid mis- or over-interpretation of the data:

- The Master Database contains results and data that are more than 10 years old for some formations, and also contains relatively new data (<10 years old) from recent and/or ongoing investigation programmes for radioactive waste management.
- Differences exist with respect to the scale of measurement of a given parameter or the number of samples analysed to achieve the minimum, maximum and best-estimate values. As a result, scale of measurement, sample numbers and methodology must all be considered when making any type of assessment of the respective datasets. In the context of direct comparison, parameters should be compared with caution, after making reference to the method(s)/scale(s) of measurement information tabulated in Annex III: Table 2.
- Because each parameter is presented in the context of minimum, maximum and best-estimate values, an assessment of spatial heterogeneity is not considered appropriate. Heterogeneity has been observed in some of the included formations, as indicated in the text (see Section 4.1 and formation summaries in Annex III: Document 1), but such information cannot be used to define parameters or generalise heterogeneity for the whole formation beyond the borehole- or site-scales.
- A variety of consistency cross-checks have been applied, in an attempt to minimise internal inconsistencies in the Master Database. Such cross-checks include:
  - thickness of formation vs bottom minus top of formation;
  - sum of clay minerals vs calculated sum of individual clay species (best-estimate values for total clay minerals are equivalent to the sum of the individual clay species for all included formations);
  - sum of all minerals vs sum of best estimates of individual species (best-estimate values for total mineralogy sum to 100 ± 1% for all included formations);
  - total dissolved solids (TDS) vs sum of all best-estimate chemical species;
  - charge balance with respect to porewater chemical composition (charge balance error for best-estimate porewater chemistries are all < 5%);
  - water content porosity and gravimetric water content;
  - anisotropies of various parameters, when values have been given for both parallel and perpendicular orientations with respect to bedding of the samples.
- In some circumstances, no “best-estimate value” is provided, only the data range, i.e. minimum or maximum values. Reporting in this manner may be justified by the current level of knowledge of a parameter, but may also largely limit certain dataset comparisons (i.e. parameter[s] defined only by minimum/maximum values in one dataset must not be compared to another dataset that may contain only best-estimate values for the same parameter[s]). In that respect, this catalogue must not be used as a tool for making a performance assessment of any included formation without the requisite data checks, consultation with the contributing organisation(s) and/or any additional quality checks/procedures.

Chapter 4. List of clay formations considered

The formations included in the Master Database (and the organisation providing the data) are listed below under the respective countries:

- Belgium (ONDRAF/NIRAS)
  - Boom Clay at Mol
  - Ypresian clays at Kallo/Doel (Beveren)
- Canada (NWMO)
  - Georgian Bay at Tiverton Ontario (Bruce nuclear site)
  - Queenston Shale at Tiverton Ontario (Bruce nuclear site)
- France (Andra, IRSN)
  - Callovo-Oxfordian at Meuse/Haute-Marne (Andra)
  - Toarcian-Domerian at Tournemire (IRSN)
- Hungary (PURAM)
  - Boda Claystone at Boda
  - Boda Claystone at Gorica)
- Japan (JAEA)
  - Wakkanai at Horonobe
  - Koetoi at Horonobe
- Switzerland (Nagra)
  - Opalinus Clay in north-east Switzerland
  - Opalinus Clay at Mont Terri

The country locations of the various argillaceous formations that are characterised within the catalogue are depicted in Figure 1.

Figure 1: **Country locations of the argillaceous rock formations included in the catalogue**

Table 2 presents a list of the argillaceous rock formations included in the catalogue, as well as their estimated age, present-day depth (top of formation), typical clay contents and dominant rock types. A brief description of each formation included in the database is presented below and detailed formation descriptions can be found in Annex III: Document 1.

Table 2: **Formations included in the Master Database**

Formation (Fm)	Country	Rock type	Clay content	Age	Burial depth (present day)
			(total clay, wt.%)	*(Ma)*	*(m)*
Ypresian clays (Kortrijk and Tielt Fms)	Belgium	Clay	25-65	55-51	289-329
Boom Clay (Boom Fm)	Belgium	Clay	25-71	32-28	190
Georgian Bay Fm	Canada	Shale	10-65	450	520
Queenston Fm	Canada	Shale	25-55	445	450
Callovo-Oxfordian	France	Argillite	29-49	163-158	490
Toarcian-Domerian	France	Marl and clay	25-50	180	250
Boda Claystone Fm (Gorica Block)	Hungary	Albitic argillite	15-45	265-260	350-600
Boda Claystone Fm (Boda Block)	Hungary	Albitic argillite	11-56	265-260	0-600
Wakkanai Fm	Japan	Siliceous mudstone	19-33	7-3	230-350
Koetoi Fm	Japan	Diatomaceous mudstone	17-25	4-2	0-20
Opalinus Clay (NE)	Switzerland	Clay	43-63	172	539-831
Opalinus Clay (Mont Terri)	Switzerland	Clay	45-72	172	200

4.1. Formation summaries

Boom Clay – Belgium

The Boom Clay, a non-indurated clay unit, has been studied for almost 40 years in Belgium in the context of the long-term management of radioactive waste. The Boom Clay is present in the north-eastern part of Belgium and it outcrops along the Rupel River (refer to Vandenberghe et al., 2014). The Boom Clay Formation is, from base to top, subdivided into four members: Belsele-Waas Member, Terhagen Member, Putte Member and Boeretang Member, and is covered by glauconitic and clayey sands of the Eigenbilzen Formation (Figure 2). At Mol, the Boom Clay is present at depths between 185 and 285 m below ground surface.

The basal member of the Boom Clay (Belsele-Waas) is comprised of two thick silt layers. It is overlain by the Terhagen Member, a grey clay with a small number of distinct black stained layers. This unit contains dispersed carbonate in its lower part, and three septaria horizons. It also contains the “pink” layer, a reddish- to brown-coloured band, depending on humidity conditions of the clay surface, which corresponds to a maximum flooding surface. The top of the member is defined by the sudden and systematic occurrence of black bands in the overlying clay. This clay, the Putte Member, is rich in organic matter. A large amount of pyrite is associated with this organic matter. The top unit or Boeretang Member is defined on the basis of geophysical logs. This member gradually becomes coarser, with silty clay layers and clayey silt to fine sand. The most distinguishing characteristic of the Boom Clay, directly visible where the formation outcrops, is the presence of horizontal layering, which is the result of variations in grain size, organic matter content and carbonate content. Within this layering, several “marker” horizons (i.e. layers with distinct characteristics) are recognised and these horizons can be seen in outcrops and in boreholes, which has enabled study of the continuity of the Boom Clay over long lateral distances.

The formation has been subjected consistently to subsidence, with the exception of a short period of uplift during the Chattian (27-24 million years [Ma] before present). Research indicates that large-scale erosion and denudation over the last 1 Ma has occurred. The Boom Clay at Mol may have been buried as much as 20 to 30 metres deeper than its present depth.

Figure 2: **Geological column of the Boom Clay showing the distribution of the formation members**

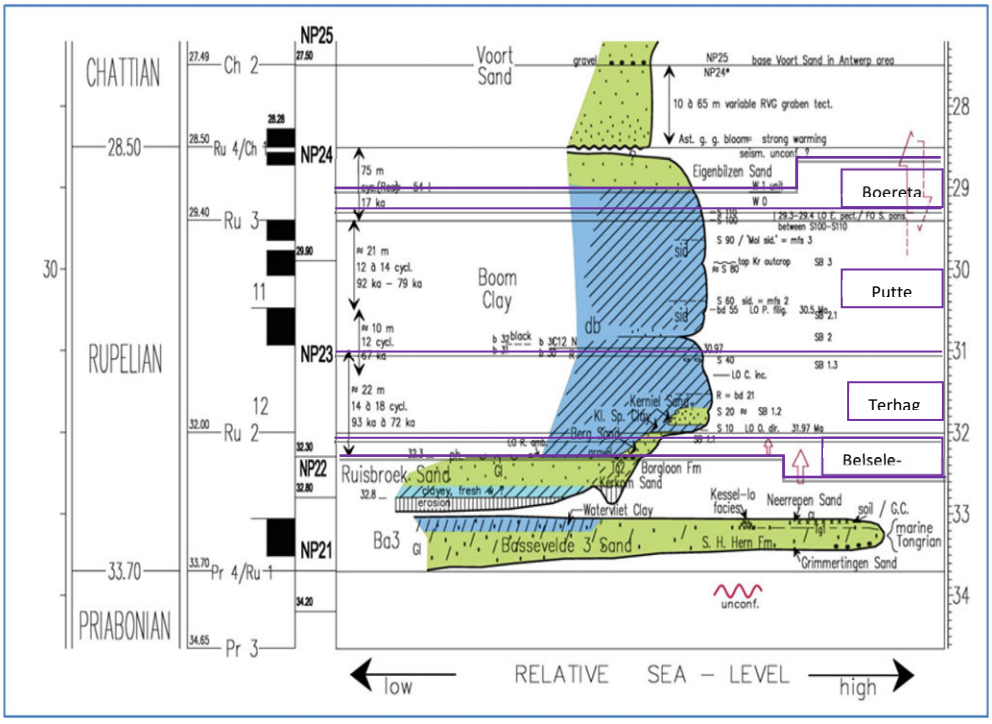

Source: modified after Vandenberghe et al. (2004).

Ypresian clays (Kortrijk and Tielt Formations) – Belgium

The Ypresian clays are a relatively thick sequence of predominantly fine-grained sediments deposited early in the Eocene (~54-51 Ma before present). These clay-rich units are part of the larger Kortrijk and Tielt formations. The area of occurrence of the Kortrijk Formation in Belgium is bordered in the south-east by a practically straight line, roughly tracing the original paleo-coastline (see Figure 3). The Ypresian clays dip towards the north and, in northern Belgium, they are unaffected by erosion and are covered by sediments of younger age. The northerly dip angle increases slightly from west to east, and towards the north, with a true dip of about 0.5°–0.6° in a north-northeast direction.

There is little evidence of major tectonic faults cross-cutting the Ypresian clays in the study area (Kallo and Doel near Antwerp). In outcrop, where the Ypresian clays are exposed, an orthogonal system of two sets of vertical joints has been observed. These joints are in the same orientation as a sub-vertical joint system observed in outcrop areas of the Boom Clay (Dehandschutter, 2004). Fracture patterns similar to this also are recognised in northern France in the London Clay, the lateral equivalent of the Ypresian clays. No observations or estimations are yet available for the Ypresian clays that would 1) provide insight into the penetration depth of these joints and/or 2) indicate if they are present at proposed repository depths.

The Ypresian clays consist of several members characterised by different clayey lithologies. Their identification on the basis of geophysical borehole measurements was subject to a revision by the Belgian National Commission for Stratigraphy in order to harmonise the different

interpretations. From bottom to top, the Ypresian clays consist of the Orchies Member (with significant kaolinite content), the more silty and heterogeneous Roubaix Member, the clay-rich Aalbeke Member, the silty Kortemark Member, and the thin Egemkapel clay. As the Roubaix Member tends to evolve to a sand in the eastern part of the depositional area, and due to the absence of useful reconnaissance boreholes, the eastern boundary of the area of interest is not yet clearly defined.

Figure 3: **Map of northern Belgium, showing the depth below sea level for the top of the Kortrijk Formation and the thickness of the formation**

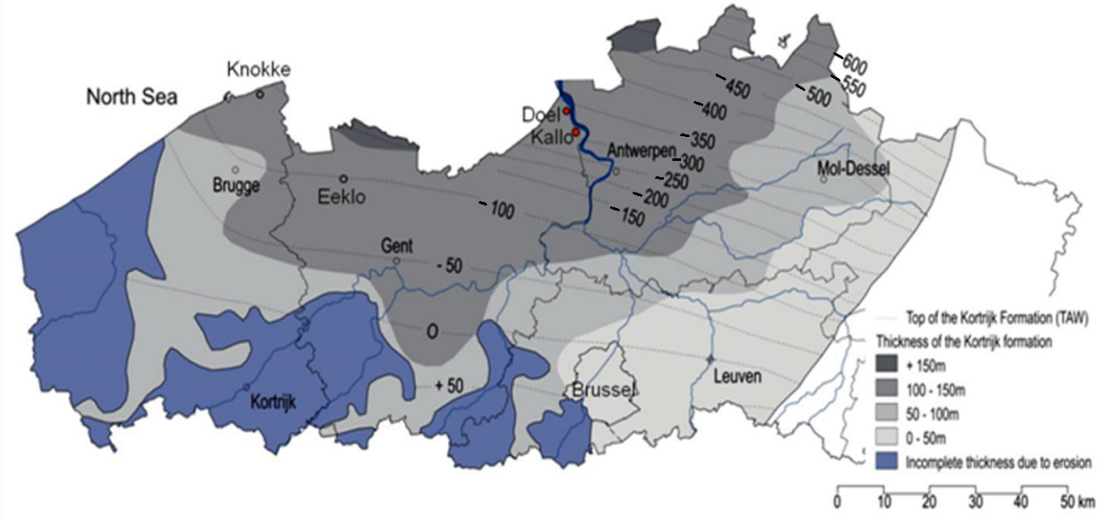

Source: from ONDRAF/NIRAS (2001).

Queenston and Georgian Bay Formations – Canada

The argillaceous Queenston and Georgian Bay shale formations are located within the Michigan Basin, consisting primarily of marine sediments of Cambrian to Devonian age (Armstrong and Carter 2010) that unconformably overlie Precambrian Grenville basement rock along the southern edge of the Canadian Shield (see Figure 4). The shale formations are of Late Ordovician age (~458-443 Ma old). At the Bruce Site (southwestern Ontario), the low-permeability massive Ordovician shale sequence occurs at reference depths between ~448 and 660 metres below ground surface, consisting of the Queenston, Georgian Bay and Blue Mountain shales, as well as the Collingwood Member shale of the Cobourg Formation. In the region surrounding the Bruce Site, the Paleozoic strata dip gently between 0.28° and 1.0° towards the centre of the Michigan Basin (west) and to the south-west.

The Queenston Formation consists of red to maroon, non-calcareous to calcareous shale, with minor amounts of green shale, siltstone, sandstone and limestone. Gypsum occurs as locally abundant nodules and thin, sub-horizontal fracture infillings. The Georgian Bay Formation consists of greenish- to bluish-grey shale, interbedded with limestone, siltstone and sandstone. The upper 30 m is dark grey-green shale with grey, fine- to medium-grained, occasionally fossiliferous limestone, siltstone and sandstone layers or hardbeds. The lower 60 m is dark grey-green shale with occasional layers and laminations of fossiliferous limestone, siltstone and sandstone, the frequency of which decreases with depth. The lowest hardbed is fossiliferous limestone. The clay fractions of the Queenston and Georgian Bay formations are approximately 40 wt.% and 50 wt.%, respectively. The clay minerals identified in the shales are predominantly illite and mica (typically > 50% of all clay minerals), chlorite (20 to 45%), and minor kaolinite and interstratified illite-smectite. Typically, the shales contain about 20-30 wt.% quartz, as well as highly variable amounts of carbonate minerals. Halite is commonly observed infilling mm-scale to hairline thickness fractures throughout the shale sequence. The primary iron mineral in the

Queenston Formation is hematite, while the primary iron mineral in the Georgian Bay Formation is pyrite. The presence and traceability in multiple boreholes of small-scale lithological variation (i.e. mm- to cm-thick hardbeds of limestone, siltstone and sandstone within m-scale horizons) provides evidence that the stratigraphy is laterally consistent and predictable.

Figure 4: **Bruce Site lithology**

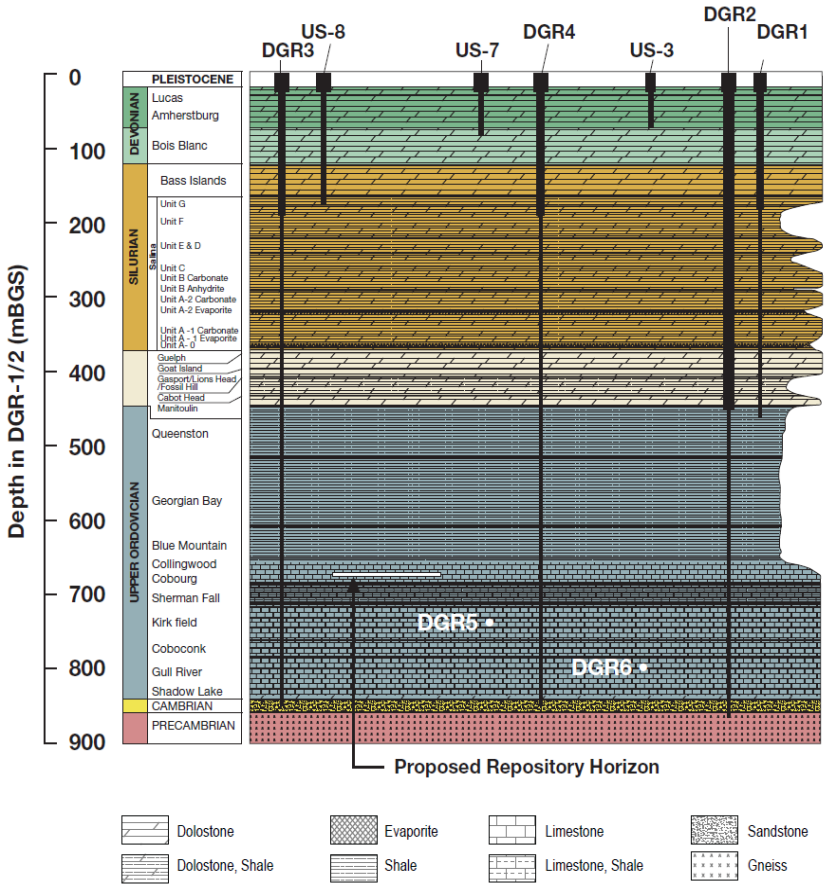

Source: modified from NWMO (2011).

Core logging suggests the Ordovician shales are unfractured to sparsely fractured. Fracture data exhibit an orthogonal geometry, consisting of two major sub-vertical joint sets oriented east-northeast and north-northwest, and the region surrounding the Bruce Site is characterised as undeformed and tectonically quiescent. The estimated peak burial depths for the top of formations are ~1 446 and 1 518 m for the Queenston and Georgian Bay, respectively, with peak burial temperatures approximating 70°C.

Toarcian-Domerian Formation – France

The argillaceous Toarcian-Domerian Formation of Jurassic age is located in the north-south oriented Causses Basin, containing Permian to late Jurassic sediments, and is delineated by basement massifs (Rouire and Rousset, 1980; Constantin et al., 2002; Constantin et al., 2004). The bedding planes at the site generally are sub-horizontal, with dip orientation ranging between 5° and 10° to the north. The argillaceous formation is sandwiched between two karstified carbonate aquifers (refer to Figure 5) and is overlain by approximately 200 to 250 m of limestone and dolomite (Aalenian to Bathonian) and underlain by a lower Liassic series (Carixian to Hettangian) mainly composed of karstified carbonates (> 300 m).

From a mineralogical point of view, the clay fraction of the formation ranges between 20 and 50 wt.% of the bulk rock, and is composed mainly of illite (5-15%), illite/smectite mixed-layer minerals (5-10% with a smectitic proportion of about 10%), chlorite (1-5%) and kaolinite (15-20%). The claystone contains 10 to 20% quartz (grains), 10 to 40% carbonates (mainly composed of calcite, with traces of dolomite and siderite) and 2 to 7% pyrite (Boisson et al. 2001; Savoye et al., 2006).

The study area is bound by two east-west trending reverse faults, ~5 km apart and with several hundreds of metres offset. The Pyrenean compression phase created most of the local faults, and reactivated others at the regional scale and is assumed to have been responsible for the karstification of the bounding aquifers (Ambert et al., 1995; Constantin et al., 2004). Based on fission track analyses (Peyaud, 2002) the formation is interpreted to have been buried under an additional 1 300 ± 400 m of sediment, which would account for the over-consolidated state of the clay formation. Due to this deep burial and intense diagenetic cementation, the studied shales and marls of the Toarcian-Domerian are highly consolidated, relatively massive rocks and exhibit brittle deformation behaviour (Constantin et al., 2002).

Figure 5: **Triassic and Jurassic Stratigraphy at the Tournemire site**

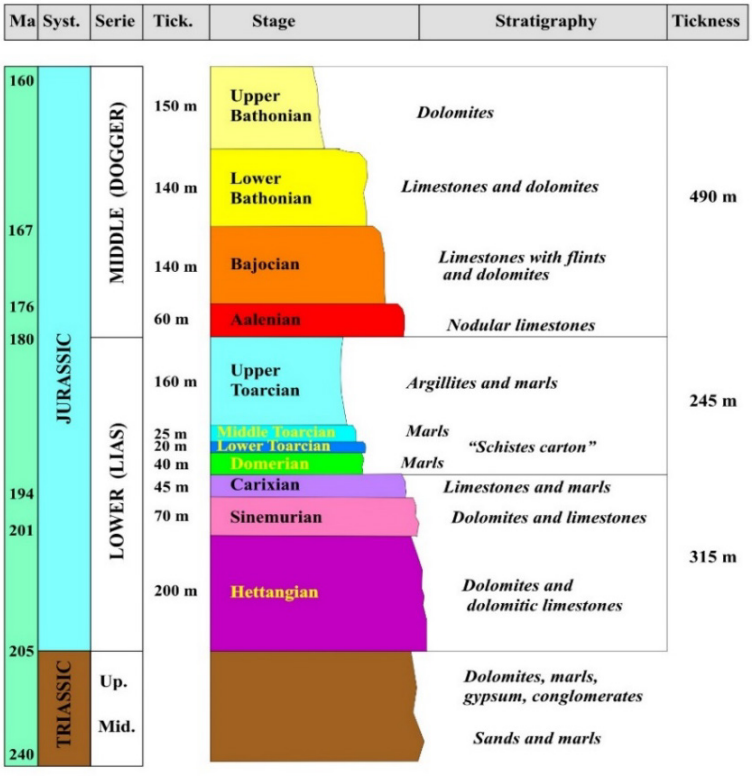

Source: adapted from Cabrera et al. (2001).

Callovo-Oxfordian – France

The Meuse/Haute-Marne site is located in the east Paris Basin. In this region, the Paris Basin is composed of alternating sedimentary (predominantly argillaceous) and limestone layers, deposited in a stable marine environment during the Jurassic (165-135 Ma). These layers have a simple and regular geometric structure, and slope slightly towards the north-west (1.5 to 2 degrees). The Callovo-Oxfordian layer is at least 130 metres thick, argillaceous and laterally homogeneous, with low porosity (15% to 18%; see Figure 6).

The rock consists of argillaceous mineral phases (e.g. smectites, illites and illite/smectite interlayers), representing up to 60 wt.% of the total rock mass, as well as silts (fine quartzes) and carbonates. The top of the Callovo-Oxfordian is between 340 and 520 m in depth and its base is between 490 and 660 m, for a total thickness from 142 to 162 m. The middle and upper Callovian, and the base of the Upper Oxfordian, are of homogeneous mineralogical composition, with clay content > 35 wt.%.

The structural framework is stable and the site is located away from large regional faults, such as the Marne Fault to the south-west.

Figure 6: **Geological cross-section at the location of the Underground Research Laboratory**

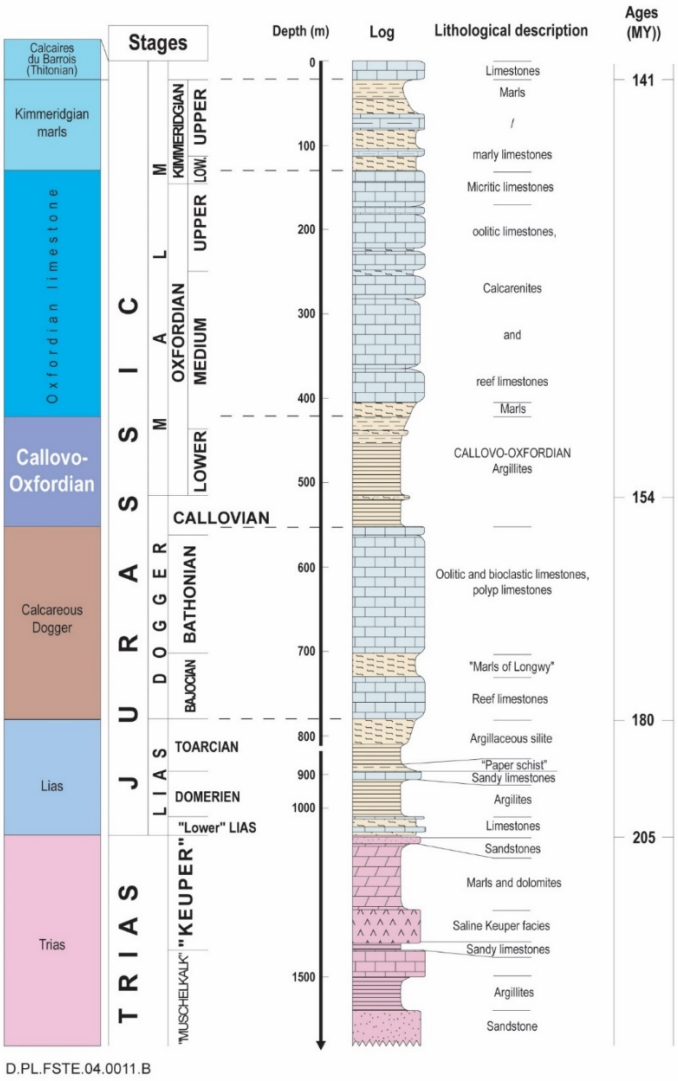

Source: Andra (2005).

Boda Claystone Formation – Hungary

The Boda Claystone Formation (BCF) is located in southwestern Hungary. The ~265 Ma old (Middle Permian [Guadalupian] age) formation is known to cover an area larger than 150 km^2. The lithofacies represent an intermittent, saline playa lake in a desert to semi-desert environment.

The presence of an extremely high proportion of sedimentary albite in the rock is a defining characteristic of the BCF, as well as a lack of organic material and pyrite. On the basis of mineralogical investigation (X-ray diffraction, differential thermal analysis, electron microprobe), the main rock-forming minerals of the BCF are: clay minerals (dominant are illite-muscovite and chlorite; smectite, kaolinite, vermiculite and mixed-layer clay minerals were identified in inconsiderable amounts), authigenic albite, quartz, carbonate minerals (calcite and dolomite) and hematite. Barite, anhydrite, authigenic K-feldspar and detrital constituents (muscovite, biotite, chlorite, zircon, rutile, apatite, ilmenite, Ca-bearing plagioclase, K-feldspar) are also identified in trace amounts. The dominant rock type in the formation is albitic claystone.

Figure 7: **Detailed geological column of Boda Claystone Formation**

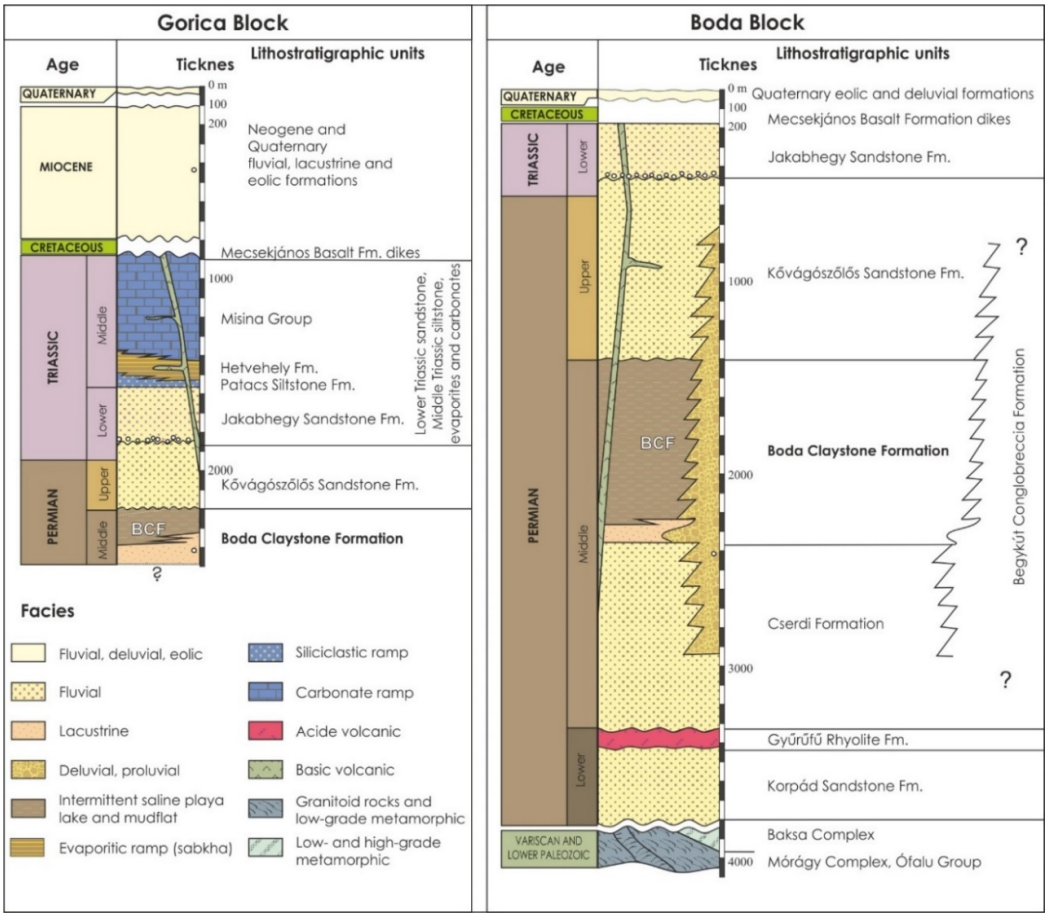

Source: modified from Konrád et al. (2010).

The formation is divided into two distinct blocks (see Figure 7), separated by the Hetvehely-Magyarszék Fault Zone. The thickness of the BCF, the mineralogical composition and the degrees of diagenesis are different in the two blocks. The Gorica Block is located north of the fault zone, overlain by Permian, Triassic and Miocene sediments, and the beds dip to the NE. The Boda Block is part of an anticline structure, the axis of which plunges to the east; the formation has been significantly or completely eroded in the west. Its depth increases towards the north, east and south. In this block, the maximum thickness of the BCF varies between 700 and 1 000 metres. During sedimentation, the catagenetic stage was reached under conditions of high temperature (200-250°C) and pressure (120-150 MPa). The BCF beds are interpreted to have been covered by sediments of up to 3.5-4.5 km thickness during the Cretaceous Period. The over-consolidated, highly indurated character of BCF is a result of this burial and compaction.

Koetoi and Wakkanai Formations – Japan

The study site is located in an active Quaternary-aged foreland fold-and-thrust belt near the boundary between the Okhotsk and Amurian plates (e.g. Yamamoto, 1979; Wei and Seno, 1998; Ikeda, 2002) on the eastern margin of a Neogene- to Quaternary-aged sedimentary basin on the western side of northern Hokkaido. The basin sediments consist of the Wakkanai Formation (siliceous mudstones with opal-CT – i.e. microcrystalline opal), the Koetoi Formation (diatomaceous mudstones with opal-A – i.e. noncrystalline opal), the Yuchi Formation (fine to medium-grained sandstones) and the Sarabetsu Formation (alternating beds of conglomerate, sandstone and mudstone, intercalated with coal seams); see Figure 8. The Koetoi Formation can be found at depths between ~20 m and 230 m, and the Wakkanai Formation is observed at depths greater than ~230 m. The boundary between the Koetoi and Wakkanai formations generally strikes northwest-southeast and dips moderately westward (e.g. Tokiwa et al., 2014).

Figure 8: **Schematic columnar section of the Horonobe Area**

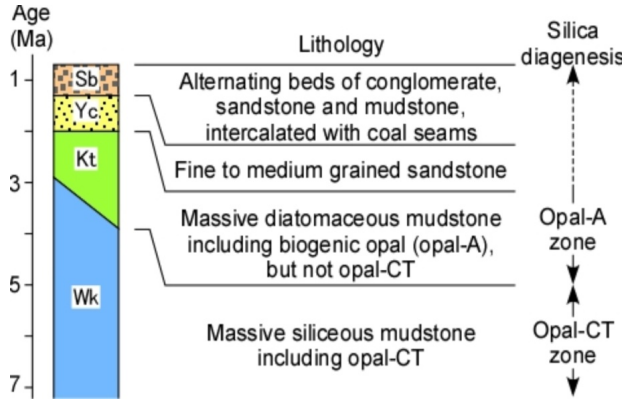

Sb – Sarabetsu Formation, Yc – Yuchi Formation, Kt – Koetoi Formation and Wk – Wakkanai Formation

Source: modified from Ota et al. (2011).

The Koetoi and Wakkanai formations consist mainly of amorphous materials (principally opal-A and/or opal-CT) in addition to trace amounts of quartz, K-feldspar, clay minerals (kaolinite, illite, smectite and chlorite), pyrite and carbonate (calcite, siderite) (Ota et al., 2011). The upper part of the Wakkanai Formation is thought to be a diagenetic transition zone, separating biogenic sediments consisting mainly of opal-A in the overlying Koetoi Formation from deeper zones in the Wakkanai Formation where opal-CT dominates.

Burial and subsidence of the Wakkanai and Koetoi formations occurred during the Neogene to Quaternary. The siliceous mudstone was buried to a depth of more than 1 km at the time of maximum burial (Ishii et al., 2008; Kai and Maekawa, 2009), with uplift and denudation initiated approximately 1.0 Ma ago.

Opalinus Clay – Switzerland

Two separate datasets have been compiled for the Opalinus Clay: one is based on data from the Mont Terri URL, representative of shallow depth occurrences of the formation (250-300 metres below ground surface) and showing a strong tectonic overprint; the second, representative of the candidate repository regions, is based mainly on data from the boreholes at Benken (approximately 600 m depth) and Schlattingen (900 m depth). The Opalinus Clay is an over-consolidated Jurassic claystone with a typical thickness of approximately 100 m across northern Switzerland (112-120 m in the potential siting regions).

Clay mineral contents are typically 60 ±15 wt.%, consisting predominantly of non-swelling clays such as kaolinite, illite and chlorite, and approximately 10 wt.% of swelling illite-smectite mixed layers. Carbonates (20 ±15 wt.%) and quartz/feldspars (20 ±10 wt.%) are the other main constituents. Compared to other Mesozoic sedimentary rocks in the area, the Opalinus Clay is a homogeneous formation with only minor vertical and lateral lithological variability (Figure 9). At a metre scale, some coarsening-upward cycles are observed with characteristic changes in grain size from clay to silt-/sand particles. At the decimetre to millimetre scale, the preferred alignment of platy clay particles is responsible for a distinct fabric (bedding) in the formation. The macro- to microscopic bedding is an important characteristic of the Opalinus Clay and is responsible for the observed anisotropy in both mechanical and transport properties.

Figure 9: **Illustration of the Lithological variability of Opalinus Clay at different scales**

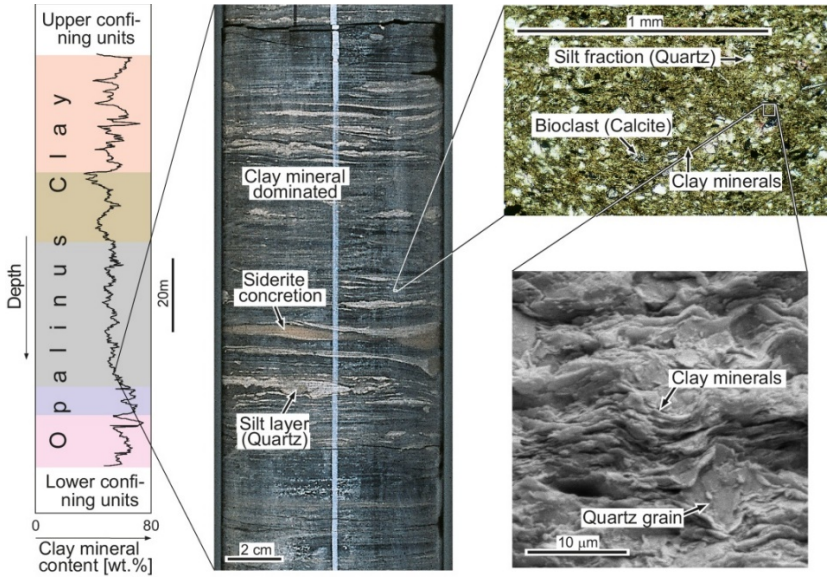

Note: Coloured depth intervals on the left distinguish different sub-units (facies).

Source: Nagra (2014).

The tectonic overprint of the Opalinus Clay is different at the Mont Terri URL when compared with the candidate regions in northern Switzerland. The URL is located in the south-eastern limb of the Mont Terri anticline and tectonically belongs to the Folded Jura of the detached Alpine foreland. The Folded Jura is the zone with the most intense deformation of the Jura fold-and-thrust belt, which developed during late Miocene north-south shortening. In contrast, the candidate regions are located within the deformed Tabular Jura and the Subjurassic Zone, which experienced significantly less internal deformation during Miocene shortening. The Mesozoic sedimentary rocks in northern Switzerland experienced two major burial phases. A first, continent-scale, long-lasting phase occurred during Cretaceous times, when the Opalinus Clay was buried to a depth of about 1 100 m, after which about 600 m of Cretaceous and upper Malm were eroded during late Cretaceous and early Tertiary times. In the late Tertiary the sedimentary pile was buried again, below the Molasse (erosional debris of the rising Alpine mountain chain), and the Opalinus Clay at Benken reached a depth of about 1 650 m ~10 Ma before present. At the Mont Terri URL in north-western Switzerland, burial is thought to have reached a maximum depth of roughly 1 350 m.

The following two remarks from Nagra relate to data quality and, in particular, the geomechanical properties. 1) In 2018, as data compilation for this catalogue was being finalised, a benchmarking study was initiated on undrained triaxial testing of Opalinus Clay from Mont Terri. The study provided its conclusions in late 2018 and improved significantly the database on hydromechanical properties of Opalinus Clay for Mont Terri. 2) Nagra's deep drilling programme

has begun early in 2019. Extensive new core characterisation and testing data were thus expected to enter the database for the Opalinus Clay in north-east Switzerland, which up to that time was represented by data from the boreholes at Benken and Schlattingen.

4.2. General observations from figures

The following general observations are derived from the Master Dataset and Figures (Annexes I-III):

1. Hydraulic conductivities (K_h) measured in situ for clay-rich formations typically range between 10^{-11} and 10^{-14} m/s.
2. Hydraulic conductivities measured in the laboratory also range between 10^{-11} and 10^{-14} m/s, with slightly larger values measured parallel to bedding when compared to values measured perpendicular to bedding.
3. There is a wide range of porosity values for the included formations, ranging from ~2% to 62%. The determinations of porosity from different methods for the same formation are observed to be generally quite consistent.
4. The total clay mineral(s) content of the formations average between 30 and 60 wt.%; nine of the twelve included formations have clay mineral(s) contents in the range of 40-60 wt.%.
5. There is a notable range in chloride concentrations between the various formations included, and somewhat less variability with respect to salinity (TDS). Chloride concentrations, on average, are between 100-10 000 mg/L, with values above and below this range observed for three of the included formations. For TDS, all values are ≥ 1 000 mg/L.
6. Average values for water content are typically less than 30 wt.%, with 8 of the 12 included formations plotting in the range of < 10 wt.%.
7. Values measured for Young's modulus typically are higher when measured perpendicular to bedding versus parallel to bedding.
8. Average values of uniaxial compressive strength are < 50 MPa, the only exception being the Hungarian Boda Formation.
9. Diffusion coefficients of I^-, Cl^- and HTO are higher when measured parallel to bedding versus perpendicular to bedding in the laboratory; normal to bedding laboratory tests using HTO are lower than measurements made both parallel to bedding in the laboratory and parallel to bedding in situ.
10. A general relationship correlating porosity with in situ hydraulic conductivity can be observed.
11. For all porewaters included in the database, Na^+ chemistry dominates, with fluids of Na or Na-Ca composition for major cations. Anion compositions vary more substantially, but the majority of the fluids are still dominated by Cl^- (and a few by SO_4^{2-} or HCO_3^-).
12. There appears to be an almost linear relationship between porosity and D_e HTO both parallel and perpendicular to bedding. Values measured in the laboratory using different methods are typically similar/consistent for the respective formations.
13. There is no clear linear relationship for D_e I^- and D_e Cl^- perpendicular to bedding with respect to porosity; however, there does appear to be more linearity in the relationship when measured parallel to bedding. Again, values measured using different methods are quite consistent for both parallel and perpendicular orientations. The difference observed in the relationships perpendicular to bedding versus parallel to bedding may be related to the nature of the clay materials in the respective formations and the anion-accessible porosity in the normal direction for Cl^- and I^-.
14. Correlation can be observed between the total carbonate(s) content and in situ hydraulic conductivity.
15. Moderate to high densities are observed for the formation rock; almost all have densities above 2 200 kg/m^3.

Chapter 5. **Conclusions**

The formations included in this compilation are of varied lithology, water content, porosity and argillaceous content. The majority of the formations included are classified as clays or shales, with clay fractions averaging 40-60% by weight. Some key properties of all of the included formations are highlighted in Table 3. As highlighted in Section 4.2, there are differences between the various formations included in this report, but what is most significant are the numerous similarities in the framework of fluid and solute longevity and transport.

The limitations of the catalogue, detailed in Chapter 3, must be kept in mind when evaluating or using the data for any specific purpose. The scales of measurement and scales of observation are important, especially when considering the formations at scales larger than those that were measured. There is potential for heterogeneity across both short and long lateral distances; inferences about formation scale properties must therefore be carefully balanced in light of the scales of measurement indicated by the contributors.

The data and information contained in the annexes provide clear indications of the capacity of argillaceous rock, in the proper context, to retain dissolved solutes and maintain integrity in spite of external changes. As noted throughout the report, the purpose of this updated catalogue is not to compare sites and promote a ranking of locations, but instead it is to depict the range of values for various properties from one formation to another, and to highlight key similarities and/or consistent traits observed across all formations. When combined, these consistent traits demonstrate the suitability of natural argillaceous rock formations to host and contain spent fuel, as well as low- and intermediate-level waste associated with nuclear power activities, over long time frames.

Table 3: **Formation properties – Overview**

Property/parameter	Boom Clay (at Mol)	Ypresian Clay (at Kallo/Doel)	Queenston Shale (at Tiverton)	Georgian Bay Shale (at Tiverton)	Boda Clay (Gorica Block)	Boda Clay (Boda Block)	Callovo-Oxfordian (at Bure)	Toarcian-Domerian (at Tournemire)	Wakkanai (at Horonobe)	Koetoi (at Horonobe)	Opalinus Clay (at Mont Terri)	Opalinus Clay (NE)
Age (Ma)	32-28	55-51	450	450	260-265	260-265	163-158	180	7-3	4-2	172	172
Maximum temperature during diagenesis (°C)	20	-	70	70	140-180	160	47-52	-	45-60	30-45	85	85
Present burial depth (top) (m)	190	289-329	450	520	350-600	0-600	490	250	230-350	0-20	220	540-830
Maximum burial depth (m)	215	450	1450	1520	3500-4500	3500-4500	645-1045	1300	1200	1000	1350	1650
Thickness (m)	102	110	70	90	350	800	153	250	600-1000	350	90-160	110
Clay content (weight %)	51.5	50	41.5	48.5	40	41.5	29-49	29.5	26	21	59	54
Organic carbon (weight %)	1.0	1.0	0.1	0.2	0.1	0.1	1.0	0.7-1.6	1.0	1.1	0.7	0.5
Pore water type	Na-HCO_3	Na-Cl	Na-Cl	Na-Cl	Na-HCO_3-SO_4 & Na-SO_4-HCO_3	Na-HCO_3-SO_4	-	Na-HCO_3-Cl	Na-Cl	Na-Cl	Na-Cl-(SO_4)	Na-Cl-(SO_4)
Mineralisation/TDS (mg/L)	1360	13810	285420	295020	1350	3500	4100	1980	10000	9600	15350	12810
Eh (mV)	-274	-	-150	-150	-100	-50	-200	-	-	-	-175	-170
Physical porosity (based on water content)	34.3	43.0	8.4	9.4	2.0	1.4	14.9-15.9	10.5	35.6	61.6	13.7	10.9
Diffusion effective coeff. D_e (HTO) ($\perp$, m^2/s)	9.4E-11	3.0E-10	1.8E-12	1.0E-12	-	-	2.2-2.5E-11	7.5E-12	8.8E-11	-	1.4E-11	6.4E-12
Hydraulic conductivity, K (in situ, m/s)	4.7E-12	-	3.0E-14	3.0E-14	1.0E-12	1.0E-12	1.9E-13	1.0E-14	1.0E-09	5.2E-09	3.1E-13	8.0E-14
UCS, ($\perp$, MPa)	2	1.3	48	32	70	110	26±6	13	16.9	7.6	7-16	31

References

Ambert, M. and P. Ambert (1995), "Karstification des plateaux et encaissement des vallées au cours du Néogène et du Quaternaire dans les Grands Causses méridionaux" (Larzac, Blandas), *Géologie de la France*, Vol. 4, pp. 37-50.

Andra (2005), "Dossier 2005 Argile – Tome Architecture and management of a geological repository", C.RP.ADP.04.0001.

Armstrong, D. K. and T.R. Carter (2010), *The Subsurface Paleozoic Stratigraphy of Southern Ontario*, Ontario Geological Survey, Special Volume 7.

Boisson, J.-Y. et al. (2001), "In situ and laboratory investigations of fluid flow through an argillaceous formation at different scales of space and time, Tournemire tunnel, southern France", Special issue on "Confining units" Springer Verlag, *Hydrogeology Journal*, Vol. 9(1), pp. 108-123.

Cabrera, J. et al., (2001), "Le projet Tournemire comme support de l'expertise sur le stockage profond en milieu argileux : synthèse des programmes de recherché", Rapport IRSN / SERGD 01-19.

Constantin, J. et al. (2004), "Evolution of the structural fault permeability in argillaceous rocks in a polyphased tectonic context", *Physics and Chemistry of the Earth*, Parts A/B/C, Vol. 29(1), pp. 25-41, Elsevier.

Constantin, J., P. Vergély and J. Cabrera (2002), "Tectonique et fracturation associée dans le bassin des Causses (Aveyron, France): le cas du secteur de Tournemire. SGF Séance Spécialisée Industrie minérale et environnement", *Bulletin de la Société Géologique de France*, Vol. 173, No. 3, pp. 229-243, Société Géologique de France.

Ikeda, Y. (2002), "The origin and mechanism of active folding in Japan", *Active Fault Research*, Vol. 22, pp. 67-70 (in Japanese).

Ishii, E. et al. (2008), "Inception of anticline growth near the Omagari Fault, northern Hokkaido, Japan", *The Journal of the Geological Society of Japan*, Vol. 114, pp. 286-299.

Kai, K. and K. Maekawa (2009), "Oxygen and hydrogen isotopic ratios and Cl^- concentration of saline water in the Neogene siliceous sediments of Horonobe, Hokkaido, Japan", *Journal of the Japanese Association of Petroleum Technologists*, Vol. 74, pp. 96-106 (in Japanese).

Konrád, G. et al. (2010), "Sedimentology of a Permian playa lake: the Boda Claystone Formation, Hungary", *Geologos*, Vol. 16(1), pp. 27-41.

Mazurek, M. et al. (2011), "Natural tracer profiles across argillaceous formations", *Applied Geochemistry*, Vol. 26, Issue 7, pp. 1035-1064, Elsevier, doi:10.1016/j.apgeochem.2011.03.124.

Nagra (2014), "SGT Etappe 2: Vorschlag weiter zu untersuchender geologischer Standortgebiete mit zugehörigen Standortarealen für die Oberflächenanlage. Geologische Grundlagen", Nagra Tech. Ber. NTB 14-02, Nagra, Wettingen, Switzerland.

NEA (2005), *Clay Club Catalogue of Characteristics of Argillaceous Rocks*, compiled by J.-Y. Boisson, OECD, Paris.

NEA (2003), *Features, Events and Processes Evaluation Catalogue for Argillaceous Media*, compiled by M. Mazurek, F.J. Pearson, G. Volckaert and H. Bock, OECD, Paris.

NWMO (2011), "Geosynthesis", Nuclear Waste Management Organization Report NWMO DGR TR-2011-11 R000. Toronto, Canada.

ONDRAF/NIRAS (2001), Safety Assessment and Feasibility Interim Report 2 (SAFIR2), *NIROND 2001-06E*.

Ota, K., H. Abe, and T. Kunimaru (Eds.) (2011), "Horonobe Underground Research Laboratory Project Synthesis of Phase I Investigation 2001-2005", Volume Geoscienctific Research, JAEA-Research 2010-068.

Peyaud, J.-B. (2002), *Diagenèse et transferts en milieu argileux fracturé: l'argilite de Tournemire (Aveyron, France)*, Thèse Docteur en Sciences Université Paris XI Paris Sud-Orsay (France).

Rouire, J. and C. Rousset (1980), *Causses, Cévennes, Aubrac,* Guide Géologiques Régionaux, Masson Eds., Paris p. 190.

Savoye, S. et al. (2006), "Contribution of the diffusive exchange method to the characterisation of pore-water in consolidated argillaceous rocks", *Journal of Contaminant Hydrology*, Vol. 86(1-2), pp. 87-104.

Tokiwa, T. et al. (2014), "Fracture characterisation around a gallery in soft sedimentary rock in Horonobe URL of Japan", *International Journal of Rock Mechanics & Mining Science*, Vol. 65, pp. 1-7.

Vandenberghe, N. et al. (2004), "Stratigraphic architecture of the Upper Cretaceous and Cenozoic along the southern border of the North Sea Basin in Belgium", *Netherlands Journal of Geosciences / Geologie en Mijnbouw*, Vol. 83.

Vandenberghe, N., M. De Craen, and L. Wouters (2014), "The Boom Clay geology from sedimentation to present-day occurrence: A review", *Memoirs of the Geological Survey of Belgium*, Vol. 60.

Wei, D. and T. Seno (1998), "Determination of the Amurian plate motion", *In*: Flower, M., S.L. Chung, C.H. Lo and T.Y. Lee (Eds.), Mantle Dynamics and Plate Interactions in East Asia, Geodynamics Series 27, American Geophysical Union, Washington, DC., pp. 337-346.

Yamamoto, H. (1979), "The geologic structure and the sedimentary basin off northern part of the Hokkaido Island", *Journal of the Japanese Association of Petroleum Technologists*, Vol. 44, pp. 260-267 (in Japanese).

Database illustrations

Annexes I and II illustrate some potential utilisations of the Master Database compiled in Annex III: Table 1.

Figures are presented for a selection of parameters considered relevant in evaluating the capacity of a given argillaceous rock mass to contain and isolate radioactive waste from the environment on safety-relevant time frames (i.e. Level 1 ranked features, events and processes). These figures illustrate: 1) the variety in nature of the clay formations included, and 2) the similarities between different argillaceous rock formations that are considered representative of potential repository host rocks in various countries around the world.

The database affords the potential for performing comparisons of ranges in the data seen between formations (i.e. from one location to another) in order to gain understanding of the numerous, favourable properties of argillaceous formations; however, as mentioned previously in Chapters 3 and 4, any comparison for the purpose of assessing a given site/formation, or assessing one rock formation versus another, is not appropriate and is not the intended purpose of this report. Any comparisons that are made based on the information presented in this report must be interpreted with caution and with the understanding that differences may, and often do, exist with respect to scales of measurement, measurement methods and the number of samples evaluated for any given parameter.

Figure A1-1 to Figure A1-18 (see Annex I) illustrate some key parameters that are generally considered to be relevant for assessing long-term rock mass and groundwater system stability. Figures A2-1 to A2-25 (see Annex II) display a selection of correlations that may be of use in the context of clarifying/demonstrating relationships between key parameters in argillaceous media – relationships that lend support to the utility of such formations as potential long-term storage solutions.

Abbreviations in the figures for each country and formation (including different lithological units within the Callovo-Oxfordian) are indicated below for reference:

BEL_Boom: Belgium, Boom Clay

BEL_Ypresian: Belgium, Ypresian Clay

CAN_Georgian Bay: Canada, Georgian Bay Formation

CAN_Queenston: Canada, Queenston Formation

HUN_Boda-Gorica: Hungary, Boda Claystone Formation – Gorica Block

HUN_Boda-Boda: Hungary, Boda Claystone Formation – Boda Block

JAP_Koetoi: Japan, Koetoi Formation

JAP_Wakkanai: Japan, Wakkanai Formation

FRA_Callovo-Oxfordian (USC): France, Callovo-Oxfordian (silto-carbonated unit)

FRA_Callovo-Oxfordian (UA): France, Callovo-Oxfordian (argillaceous unit)

FRA_Callovo-Oxfordian: France, Callovo-Oxfordian (USC or UA not indicated)

FRA_Toarcian-Domerian: France, Toarcian-Domerian

CHE_Opalinus-MTerri: Switzerland, Opalinus Clay at Mont Terri (Mont Terri URL)

CHE_Opalinus-NE: Switzerland, Opalinus Clay north-east Switzerland

Annex I: **Some relevant key parameters**

The first set of figures presents some key parameters, usually considered as representative and relevant for geological disposal investigations, which are listed below.

- Figure A1-1: Present-day burial depth (top of formation)
- Figure A1-2: Formation peak burial depth
- Figure A1-3: Formation thickness
- Figure A1-4: Total clay mineral(s) content
- Figure A1-5: Total carbonate(s) content
- Figure A1-6: Chloride concentration
- Figure A1-7: Total dissolved solids (TDS) concentration
- Figure A1-8: Water content
- Figure A1-9: Porosity measured using different methods or calculated by water content and grain density
- Figure A1-10: Hydraulic conductivity measured in situ
- Figure A1-11: Hydraulic conductivities measured in laboratory parallel (//) or perpendicular (⊥) to bedding
- Figure A1-12: Diffusion coefficient of iodide measured in laboratory parallel (//) or perpendicular (⊥) to bedding
- Figure A1-13: Diffusion coefficient of chloride measured in laboratory parallel (//) or perpendicular (⊥) to bedding
- Figure A1-14: Diffusion coefficient of HTO measured in laboratory parallel (//) (PB) or perpendicular (⊥) (NB) to bedding
- Figure A1-15: Seismic velocity (Vp and Vs; best-estimate values)
- Figure A1-16: Laboratory uniaxial compressive strength (UCS) laboratory tests parallel (//) or perpendicular (⊥) to bedding
- Figure A1-17: Young's modulus static laboratory tests parallel (//) or perpendicular (⊥) to bedding
- Figure A1-18: Young's modulus dynamic laboratory tests parallel (//) or perpendicular (⊥) to bedding and dynamic in situ tests

Each formation is presented adjacent to all others in a column-style plot format, allowing for quick and easy identification and simple comparison/assessment of the ranges of data observed for each parameter at various locations around the globe.

- Figures A1-1 to A1-2 illustrate the present-day burial depths (top of the formation) and maximum burial depths for all formations included in the Master Database. These two parameters provide an overall picture of the geological history of the formations in terms of subsidence, uplift and the potential state of consolidation of the material.

- Figure A1-3 illustrates the formation thicknesses, and also shows complementary information on that subject in the form of minimum, maximum and best-estimate values.
- Figures A1-4 to A1-5 depict the total clay minerals and total carbonate(s) content, respectively. The mineralogical parameters help to define the nature of the argillaceous formations (clay-rich, carbonate-rich, mixed lithology, etc.). Maximum and minimum values provide a reasonable idea of the possible variability of these parameters at various depths and locations within the formation.
- Figures A1-6 to A1-7 depict the porewater (or groundwater) chloride concentrations and total dissolved solids (TDS), respectively. It can be observed that there is variation in both chloride concentration and TDS between the various locations around the world. In general, chloride concentration and TDS typically correlate well, particularly in those formations for which Cl^- is the dominant anion in the porewater. TDS values within the included formations range between 10^3 to 10^6 mg/L (i.e. relatively high salinities).
- Flow and solute transport properties are typically related to key petrophysical and hydraulic parameters, including water content (Figure A1-8), porosity (Figure A1-9), hydraulic conductivities measured in situ (Figure A1-10) and in laboratory (Figures A1-11 to A1-12), effective diffusion coefficients of iodide, chloride and HTO measured in laboratory (Figures A1-13 to A1-15, respectively), all of which provide an overall picture of the current (and possible) physical states of the considered clay material.
- Numerous types of porosity measurements are considered by the different contributing organisations: classic mercury (Hg) injection, nuclear magnetic resonance, pulse tests (HTO), pycnometry, as well as porosity deduced from water content (at 105-110°C) and density. Porosity values determined by these various methods can be directly compared in Figure 9 for the included formations, and show clear correlation with values determined for water content (Figure 8).
- The low hydraulic conductivity values (typically $<10^{-11}$ m/s) of the different formations can both be seen in Figure A1-10 (in situ) and in Figure A1-11 (in laboratory, parallel and perpendicular).
- Figures A1-12 to A1-14 illustrate the effective diffusion coefficients (measured in laboratory both parallel and perpendicular to bedding) for iodide, chloride and HTO, respectively. Where data are available for both orientations, it is possible to highlight the differences in the D_e values due to the orientation towards stratigraphy. Based on the available data, it may be reasonably inferred that HTO diffusion coefficients typically are higher than those from tests using anionic species such as I^- or Cl^-.
- Petrophysical and mechanical characteristics of the different formations are illustrated with the following parameters: laboratory seismic velocities (Vp and Vs, Figure A1-15), laboratory uniaxial compressive strength (Figure A1-16) and Young's modulus (static and dynamic, Figures A1-17 to A1-18).

Figure A1-1: **Present-day burial depth (top of formation)**

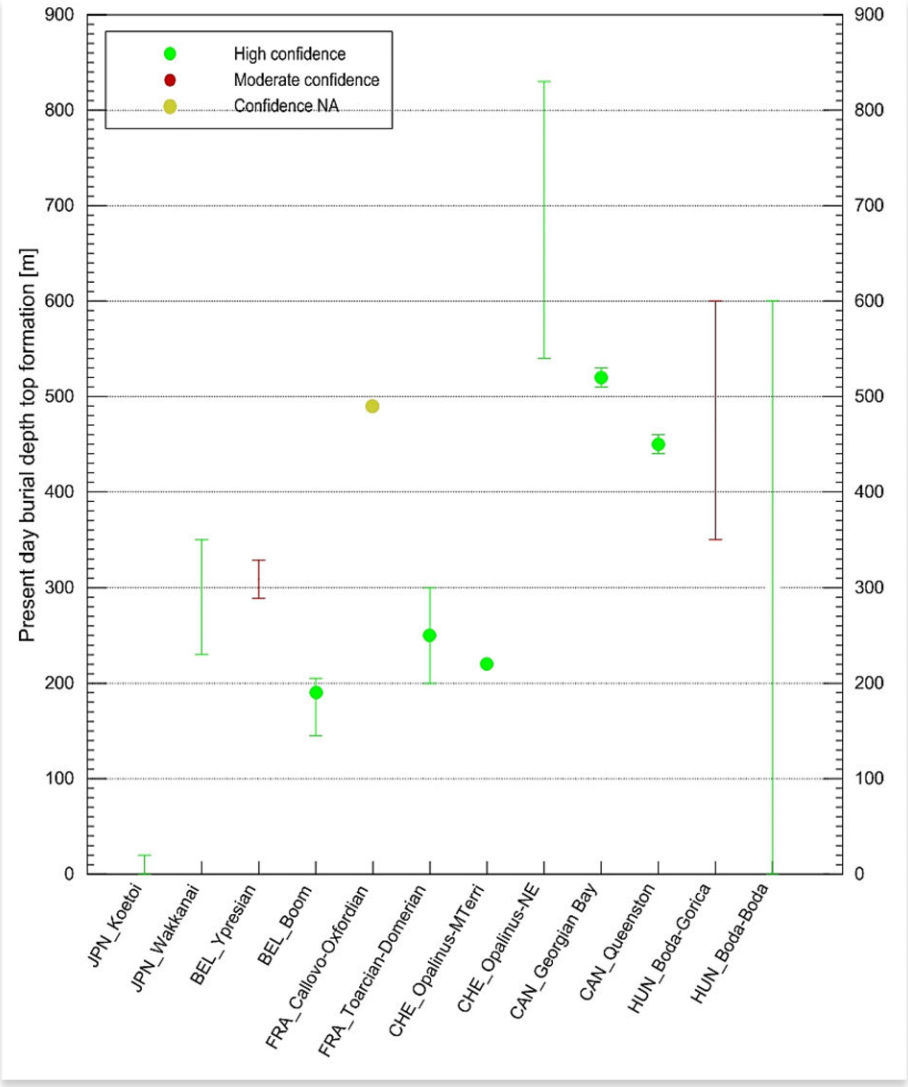

Notes: Lines represent the range of values measured (minimum to maximum). Dots represent best-estimate values.

Source: NEA CCC Master Database.

Figure A1-2: **Formation peak burial depth**

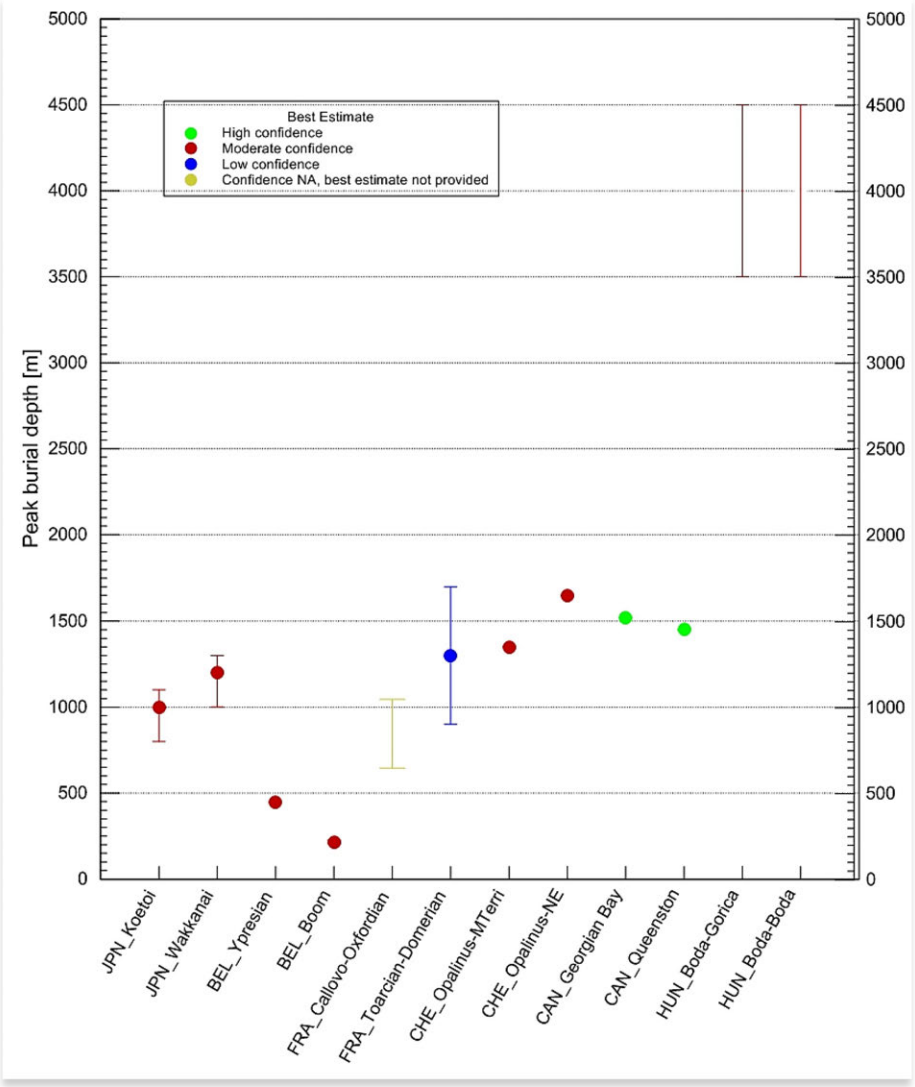

Notes: Lines represent the range of values measured (minimum to maximum). Dots represent best-estimate values.

Source: NEA CCC Master Database.

Figure A1-3: **Formation thickness**

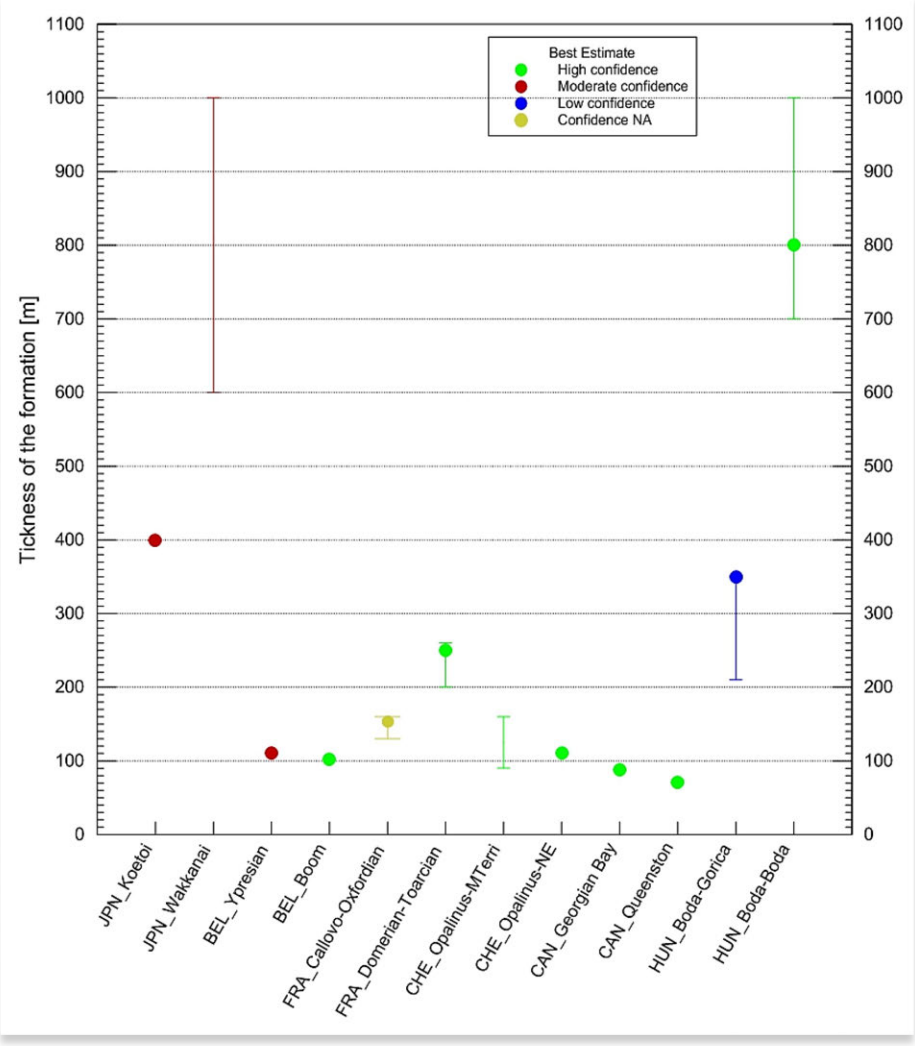

Notes: Lines represent the range of values measured (minimum to maximum). Dots represent best-estimate values.

Source: NEA CCC Master Database.

Figure A1-4: **Total clay mineral(s) content (presented in wt.%)**

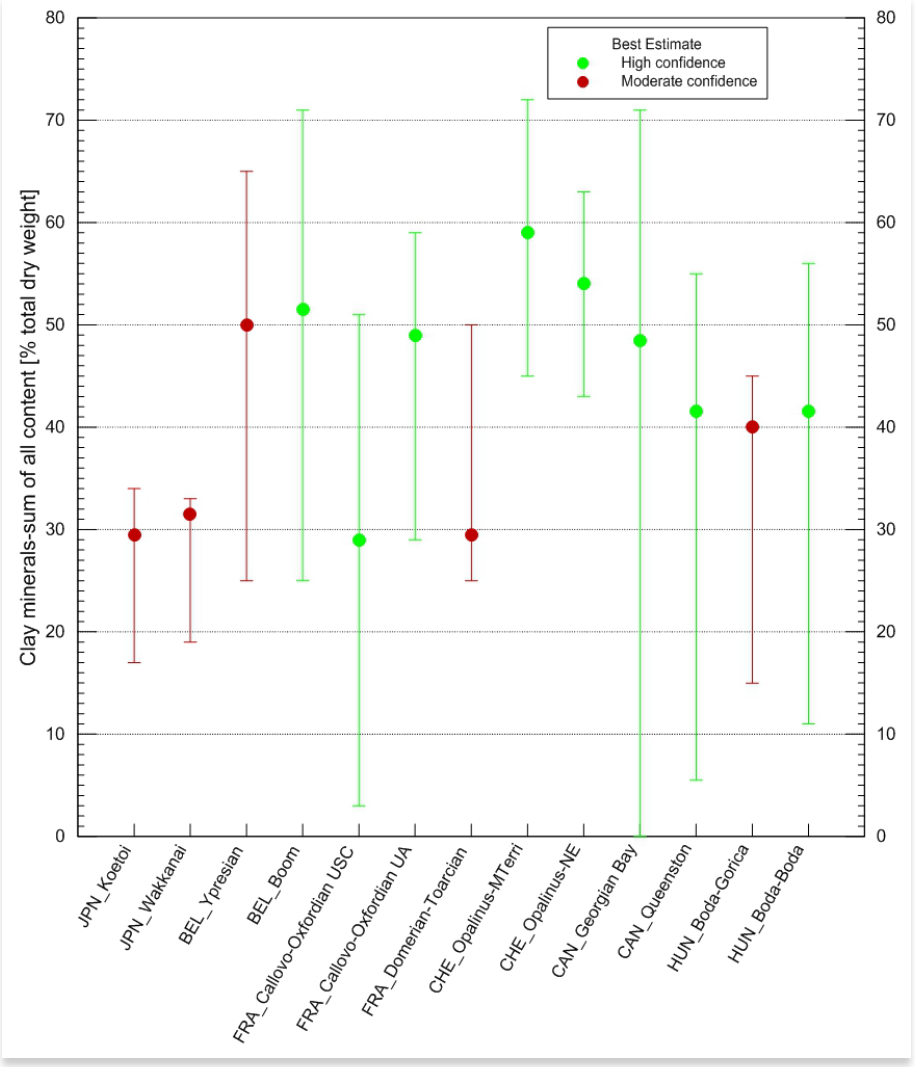

Notes: Lines represent the range of values measured (minimum to maximum). Dots represent best-estimate values.

Source: NEA CCC Master Database.

Figure A1-5: **Total carbonate(s) content (presented in wt.%)**

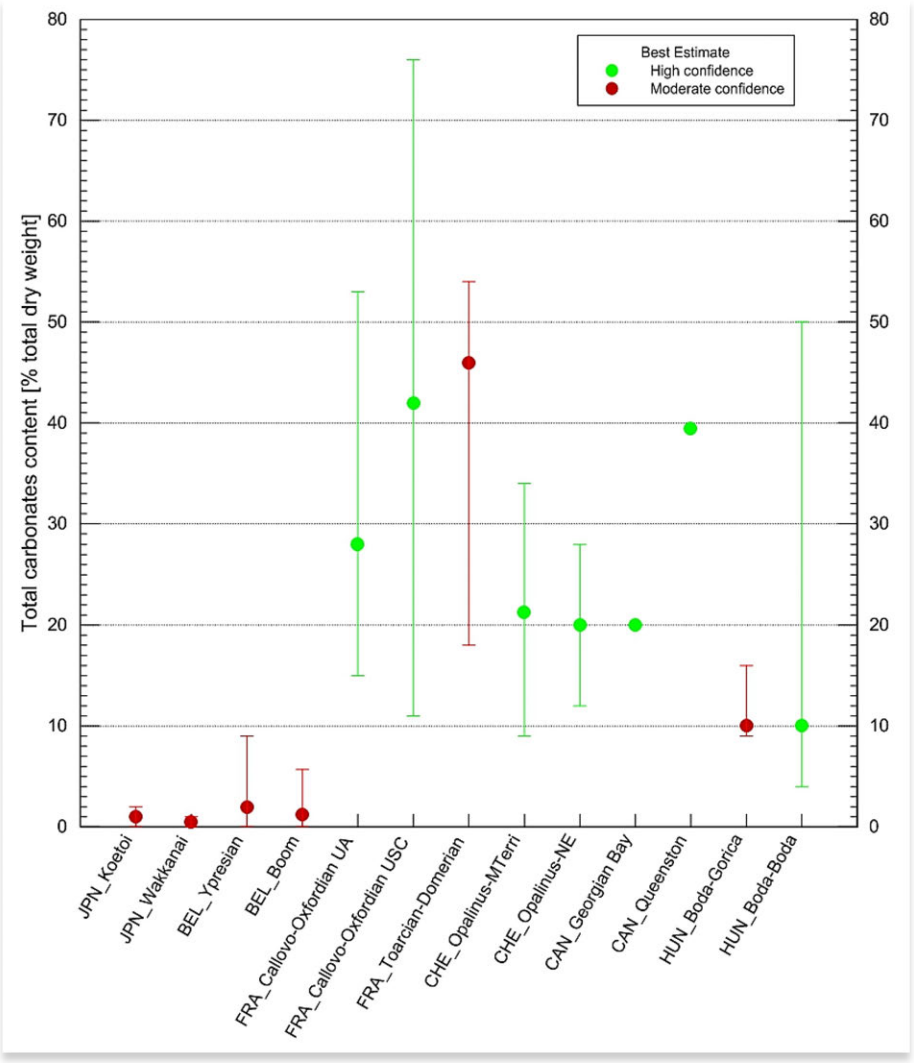

Notes: Lines represent the range of values measured (minimum to maximum). Dots represent best-estimate values.

Source: NEA CCC Master Database.

Figure A1-6: **Chloride concentration**

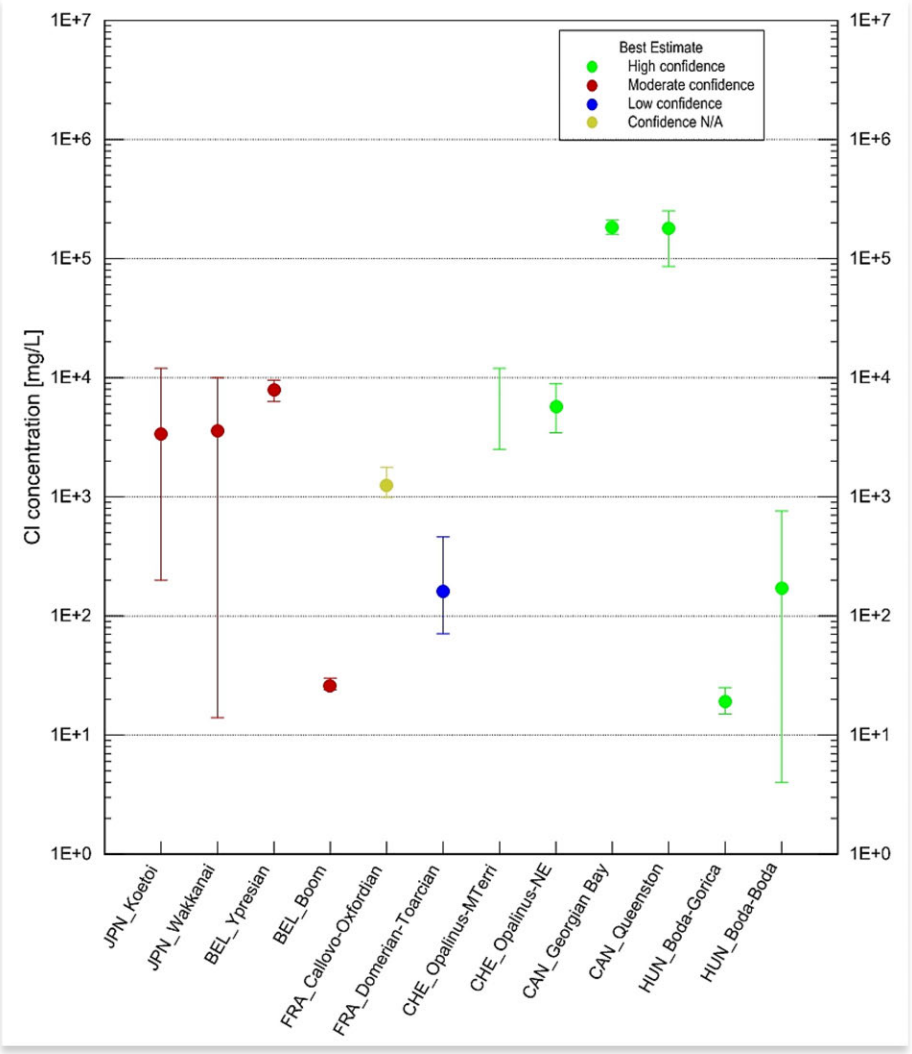

Notes: Lines represent the range of values measured (minimum to maximum). Dots represent best-estimate values. HUN_Boda-Gorica block and HUN_Boda-Boda block formations data originated from groundwater.

Source: NEA CCC Master Database.

Figure A1-7: **Total dissolved solids (TDS) concentration**

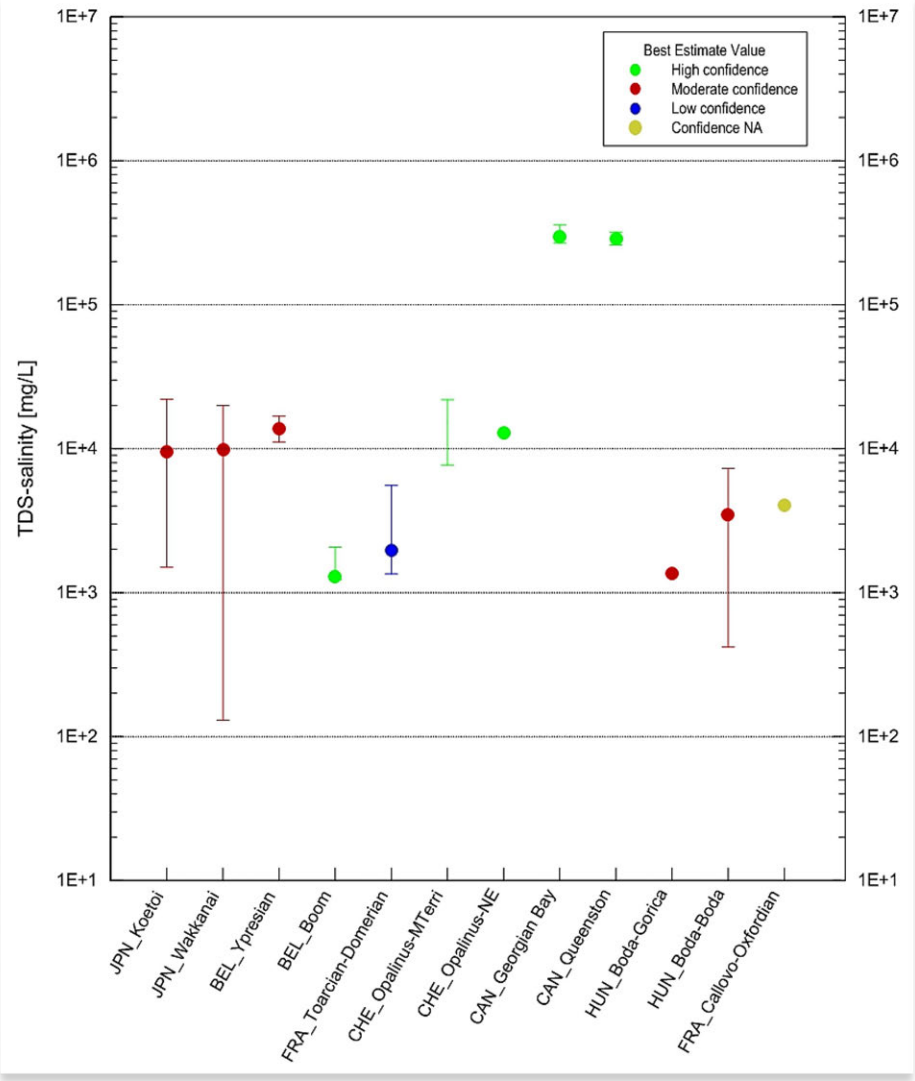

Notes: Lines represent the range of values measured (minimum to maximum). Dots represent best-estimate values. HUN_Boda-Gorica block and HUN_Boda-Boda block formations data originated from groundwater.

Source: NEA CCC Master Database.

Figure A1-8: **Water content (presented in wt.%)**

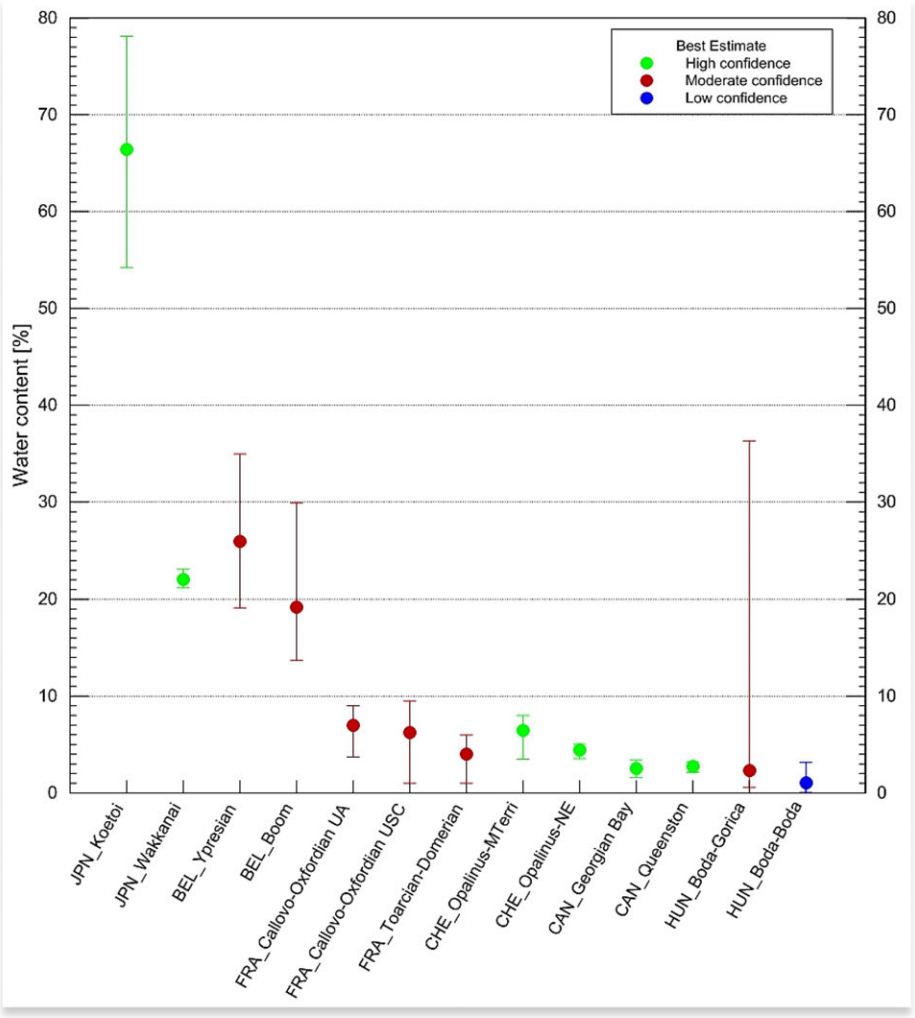

Notes: Lines represent the range of values measured (minimum to maximum). Dots represent best-estimate values.

Source: NEA CCC Master Database.

Figure A1-9: **Porosity measured using different methods or calculated by water content and grain density**

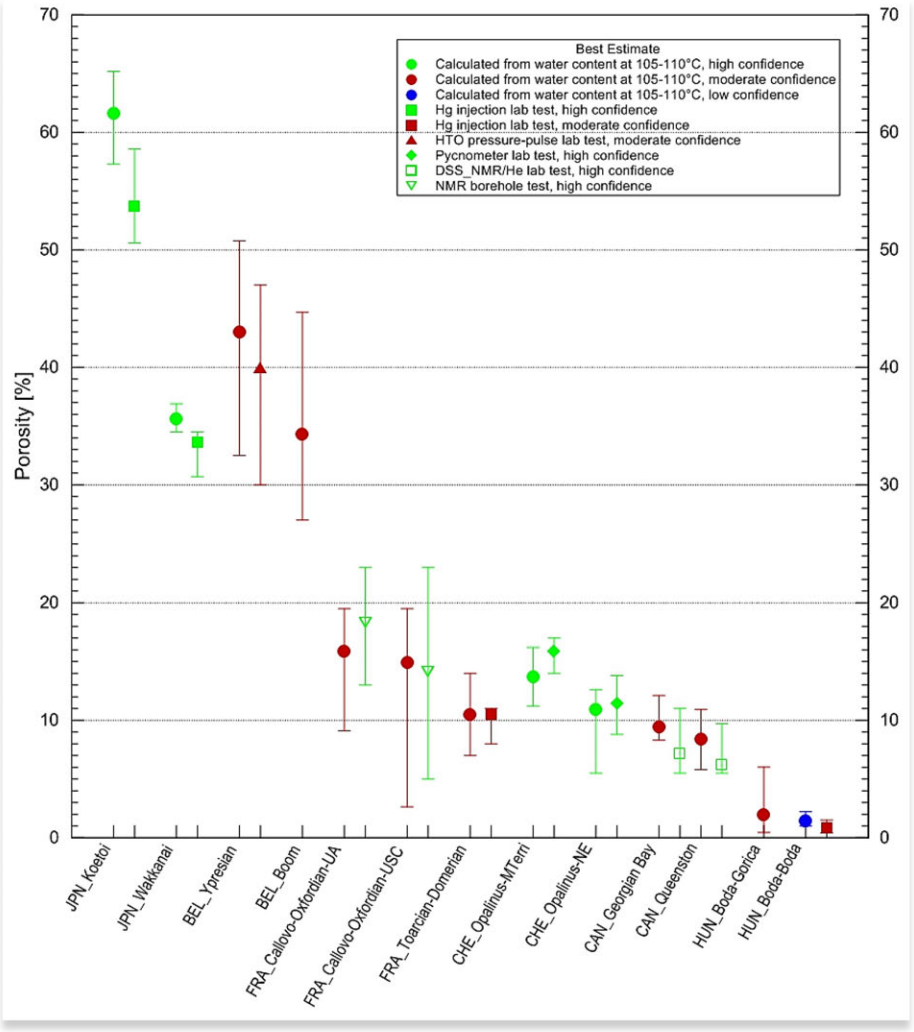

Notes: Lines represent the range of values measured (minimum to maximum). Symbols represent best-estimate values (DSS_NWR/He: dean stark fluid saturation and nuclear magnetic resonance/He gas expansion).

Source: NEA CCC Master Database.

Figure A1-10: **Hydraulic conductivity measured in situ**

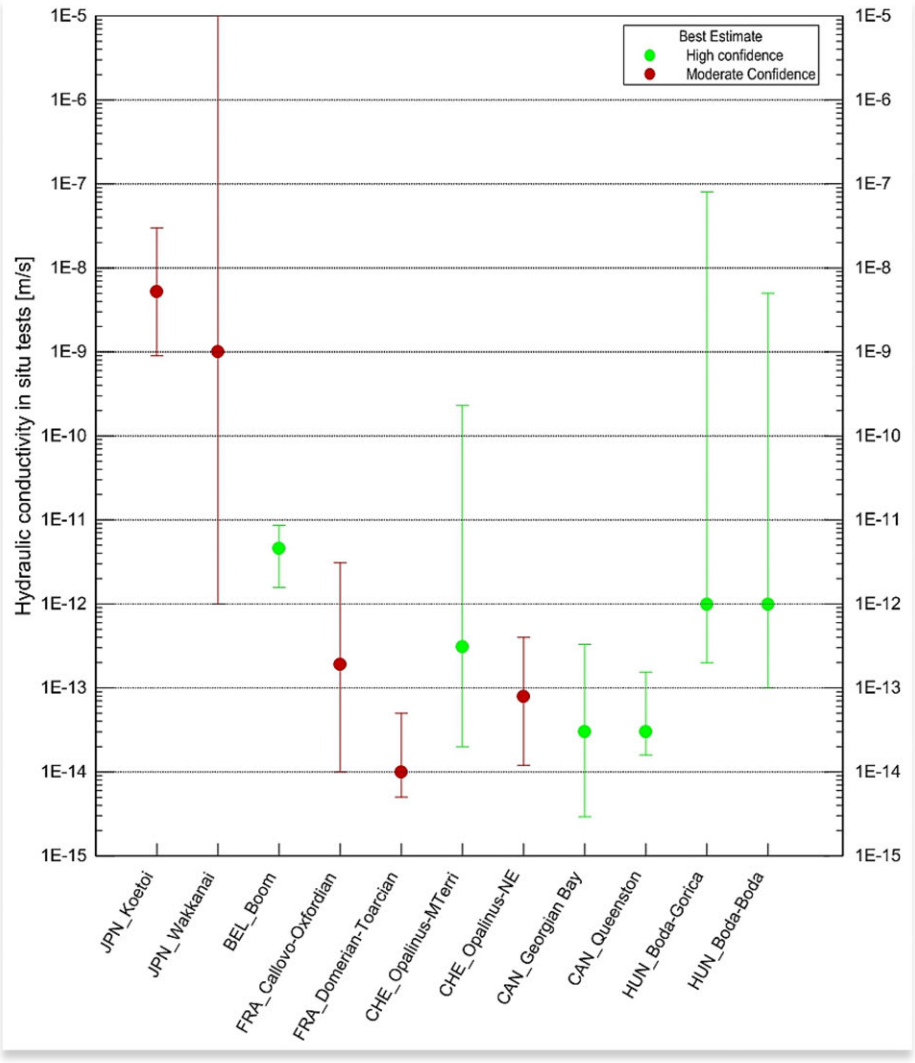

Notes: Lines represent the range of values measured (minimum to maximum). Dots represent best-estimate values

Source: NEA CCC Master Database.

Figure A1-11: **Hydraulic conductivities measured in laboratory parallel (//) or perpendicular (⊥) to bedding**

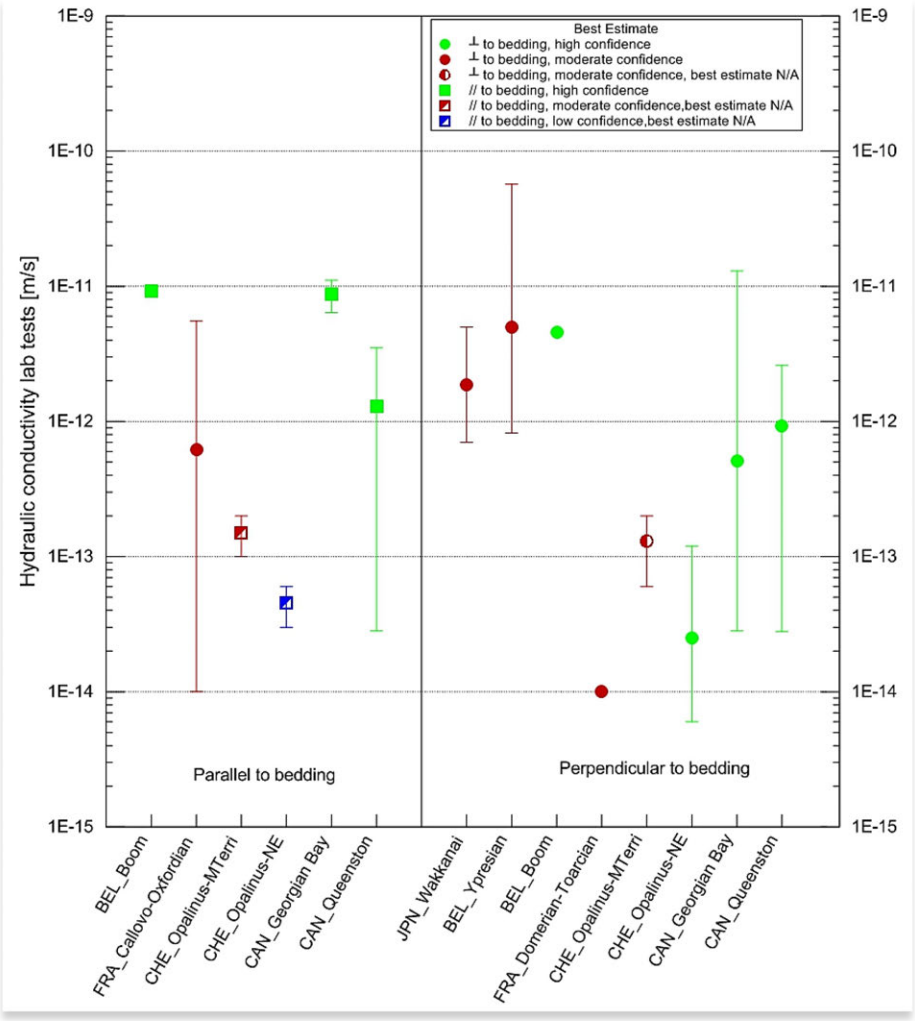

Notes: Lines represent the range of values measured (minimum to maximum). Symbols represent best-estimate values

Source: NEA CCC Master Database.

Figure A1-12: **Diffusion coefficient of iodide measured in laboratory parallel (//) or perpendicular (⊥) to bedding**

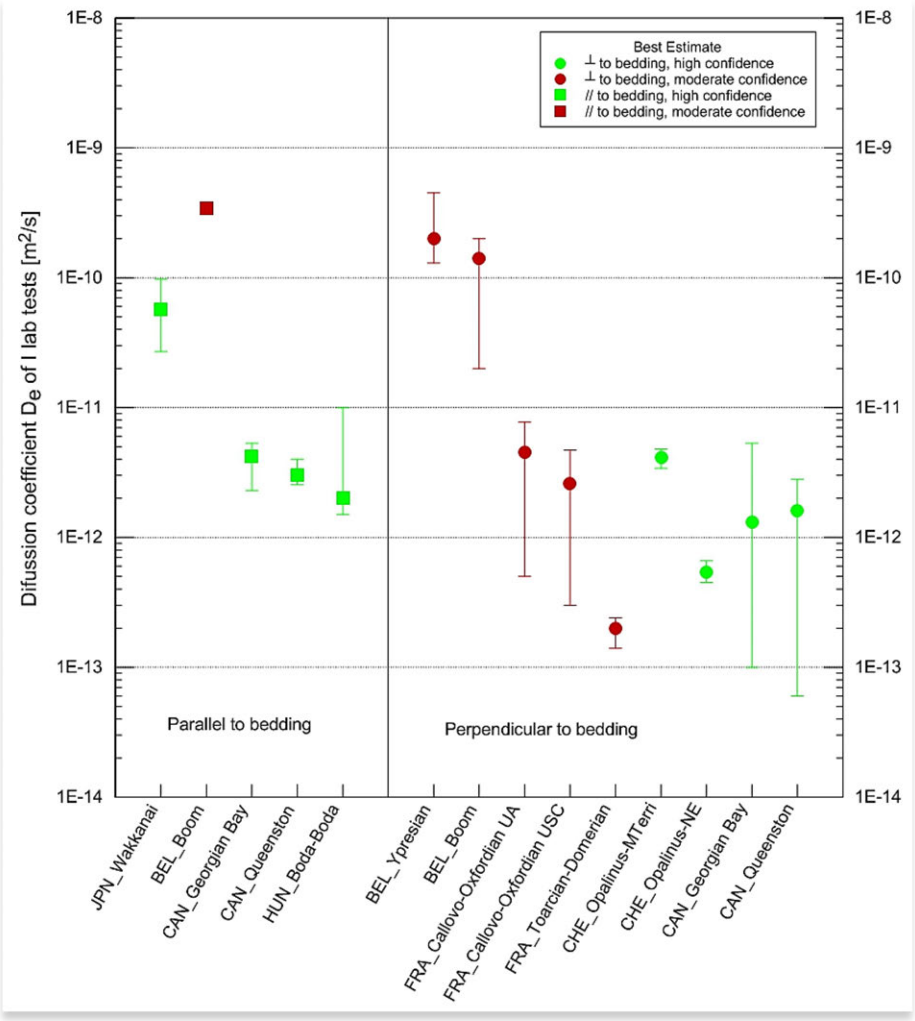

Notes: Lines represent the range of values measured (minimum to maximum). Symbols represent best-estimate values

Source: NEA CCC Master Database.

Figure A1-13: **Diffusion coefficient of chloride measured in laboratory parallel (//) or perpendicular (⊥) to bedding**

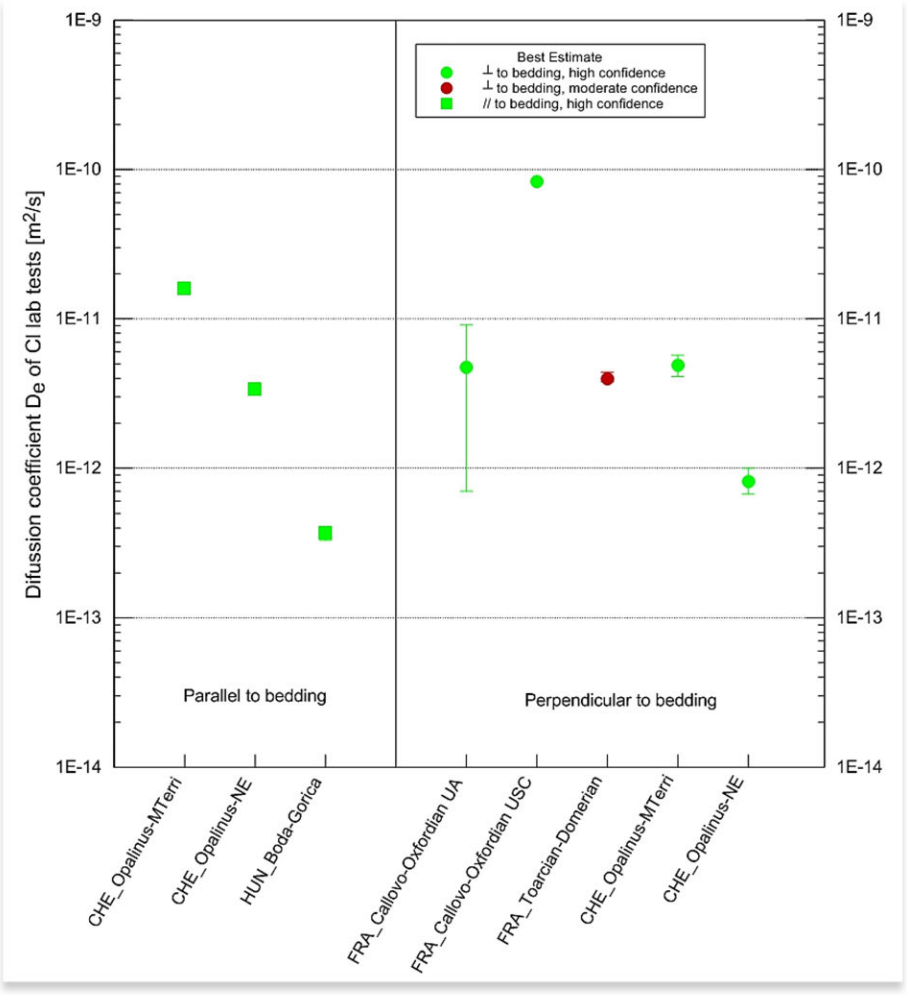

Notes: Lines represent the range of values measured (minimum to maximum). Symbols represent best-estimate values.

Source: NEA CCC Master Database.

Figure A1-14: **Diffusion coefficient of HTO measured in laboratory parallel (//) (PB) or perpendicular (⊥) (NB) to bedding**

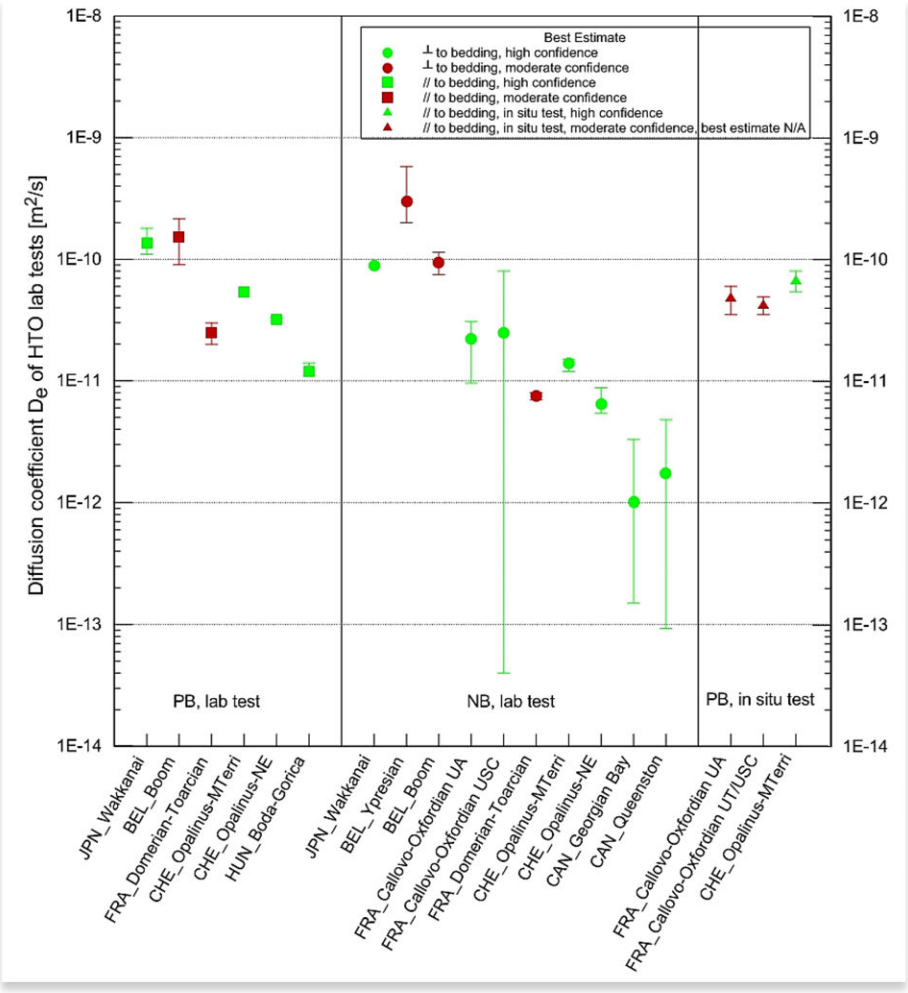

Notes: Lines represent the range of values measured (minimum to maximum). Symbols represent best-estimate values.

Source: NEA CCC Master Database.

Figure A1-15: **Seismic velocity (Vp and Vs; best-estimate values)**

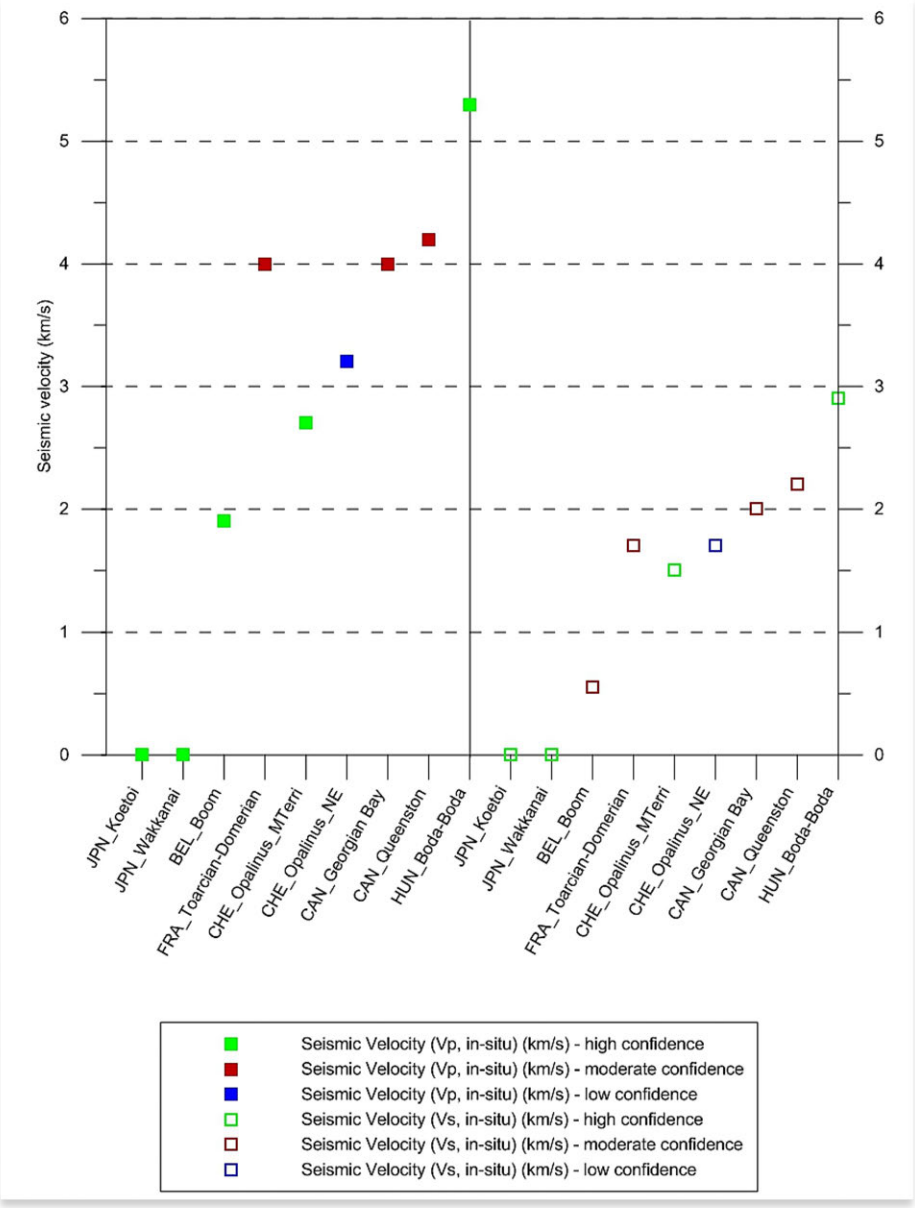

Source: NEA CCC Master Database.

Figure A1-16: **Laboratory uniaxial compressive strength (UCS) tests parallel (//) or perpendicular (⊥) to bedding**

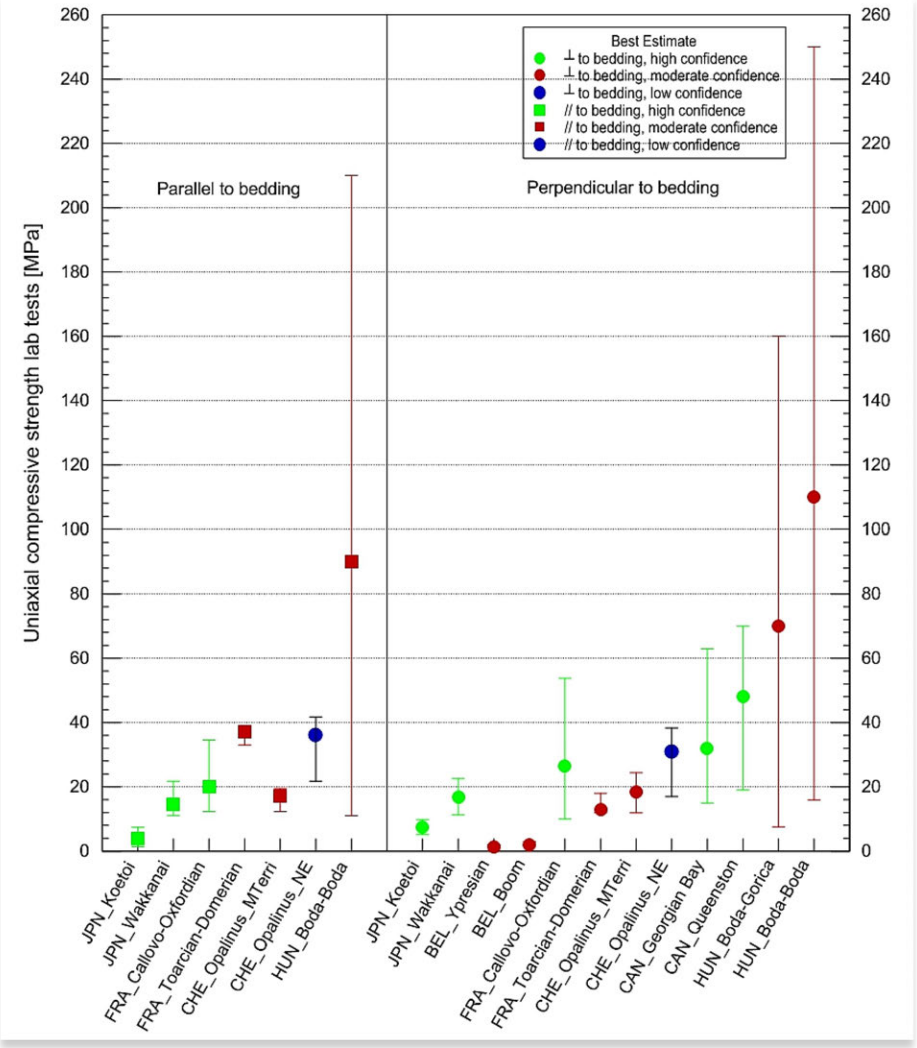

Notes: Lines represent the range of values measured (minimum to maximum). Symbols represent best-estimate values

Source: NEA CCC Master Database.

Figure A1-17: **Young's modulus static laboratory tests parallel (//) or perpendicular (⊥) to bedding**

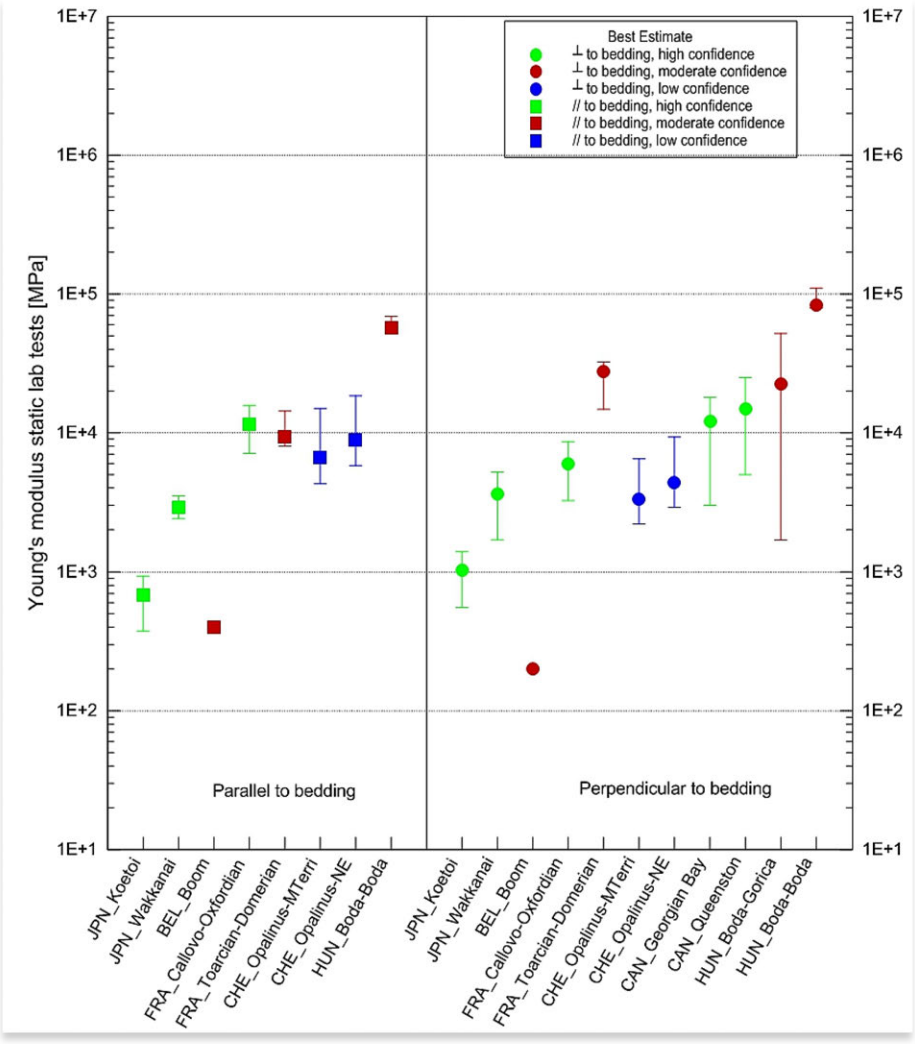

Notes: Lines represent the range of values measured (minimum to maximum). Symbols represent best-estimate values.

Source: NEA CCC Master Database.

Figure A1-18: **Young's modulus dynamic laboratory tests parallel (//) or perpendicular (⊥) to bedding and dynamic in situ tests**

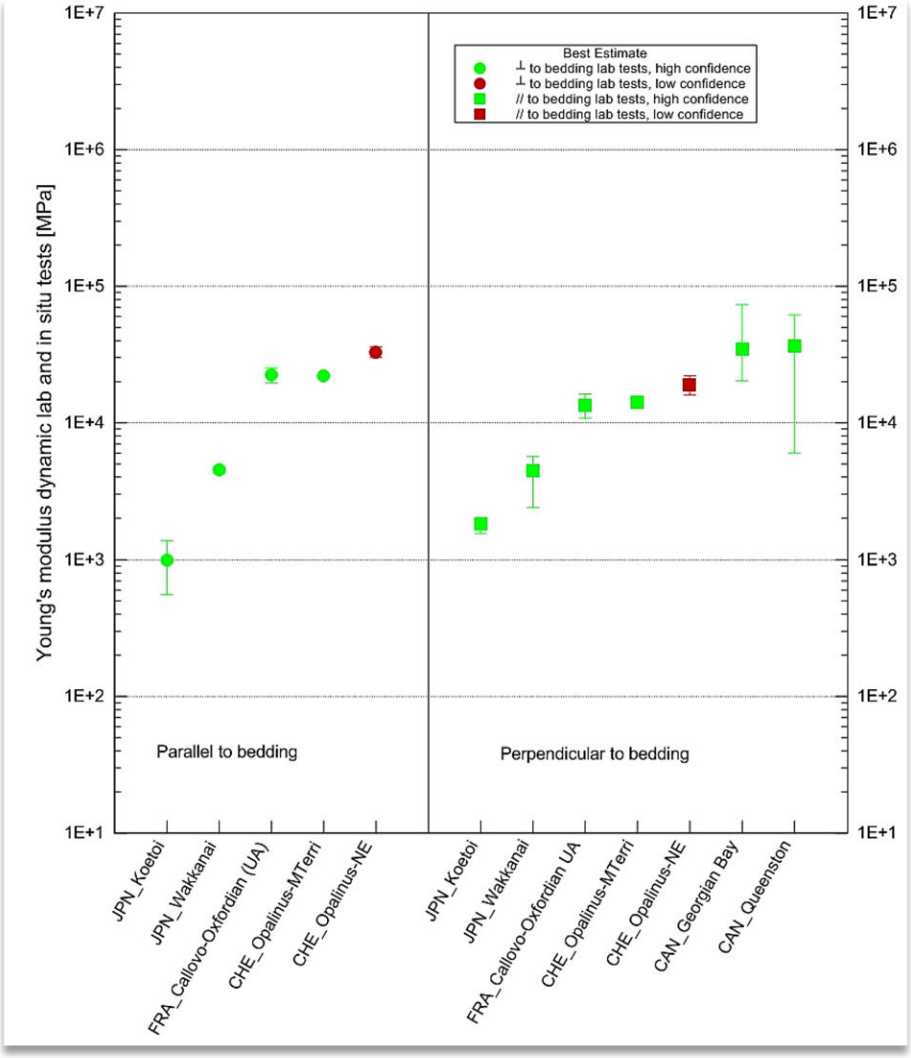

Notes: Lines represent the range of values measured (minimum to maximum). Symbols represent best-estimate values.

Source: NEA CCC Master Database.

Annex II: **Some relevant correlations**

Figures 19-43 present a series of correlation diagrams, many of which depict observed relationships in the database, based only on the "best-estimate" value provided. The correlations presented are intended to highlight key relationships observed in, and typical of, argillaceous media.

- Figure A2-1: Correlation between porosity and peak burial depth
- Figure A2-2: Correlation between present-day burial depth and salinity of formations
- Figure A2-3: Ternary diagram for porewater major ion chemistry – cations
- Figure A2-4: Ternary diagram for porewater major ion chemistry – anions
- Figure A2-5: Ternary diagram for total clay mineral(s) content, total carbonate(s), sum of other minerals content
- Figure A2-6: Correlation between hydraulic conductivity and density
- Figure A2-7: Correlation between porosity and in situ hydraulic conductivity
- Figure A2-8: Correlation between porosity and HTO diffusion coefficient perpendicular to bedding
- Figure A2-9: Correlation between porosity and HTO diffusion coefficient parallel to bedding
- Figure A2-10: Correlation between porosity and chloride + iodide diffusion coefficient perpendicular to bedding
- Figure A2-11: Correlation between porosity and chloride + iodide diffusion coefficient parallel to bedding
- Figure A2-12: Correlation between total carbonate(s) content and in situ hydraulic conductivity
- Figure A2-13: Correlation between total carbonate(s) content and porosity
- Figure A2-14: Correlation between total carbonate(s) content and water content
- Figure A2-15: Correlation between total carbonate(s) content and diffusion coefficient of iodide
- Figure A2-16: Correlation between total carbonate(s) content and diffusion coefficient of HTO
- Figure A2-17: Correlation between total clay content and in situ hydraulic conductivity
- Figure A2-18: Correlation between total clay content and porosity
- Figure A2-19: Correlation between total clay content and water content
- Figure A2-20: Correlation between total clay mineral(s) content and diffusion coefficient of iodide
- Figure A2-21: Correlation between total clay mineral(s) content and diffusion coefficient of HTO
- Figure A2-22: Correlation between total clay mineral(s) content and density
- Figure 42-23: Correlation between diffusion coefficient of HTO and water content
- Figure A2-24: Correlation between uniaxial compressive strength (UCS) and water content
- Figure A2-25: Correlation between uniaxial compressive strength (UCS) and young's modulus static laboratory tests

- Figure A2-1 presents the correlation between porosity and peak burial depth (only "best estimates" of porosity from all methods are included); in general, a trend can be recognised between the two parameters of decreasing porosity with increasing peak burial depth.
- Figure A2-2 presents a cross-plot of salinity and present-day burial depth of the formations. No obvious correlation is apparent between these two parameters.
- Figures A2-3 to A2-4 present ternary diagrams for the major ions (cations and anions, respectively) measured in the formation porewaters (or groundwaters).
- Figure A2-5 presents the relative position of the various clay formations in a ternary diagram [clay minerals – carbonates – other minerals]. The diagram confirms that, typically, none of the formations are "purely clay", and that some of their characteristics, and consequently behaviour, may be influenced more or less by the amount of carbonates or others minerals present.
- Figure A2-6 presents the correlation between hydraulic conductivity and formation density.
- Figure A2-7 presents the correlation between porosities (from different types of measurements) and in situ hydraulic conductivities.
- Figures A2-8 to A2-9 confirm the direct correlation between the various measured porosities and HTO effective diffusion coefficients (both parallel and perpendicular to bedding). For those formations with measurements in both orientations, it is observed that effective diffusion coefficients of HTO parallel to bedding are typically larger than those measured perpendicular to bedding.
- Figures A2-10 to A2-11 show the correlation between porosity and effective diffusion coefficients for chloride and iodide (both parallel and perpendicular to bedding). For those formations with measurements in both orientations, it is observed that anion effective diffusion coefficients parallel to bedding are typically larger than those measured perpendicular to bedding.
- Figures A2-12 to A2-16 show key correlations related to total carbonate(s) contents (wt.%) including: in situ hydraulic conductivity, porosity, water content, and effective diffusion coefficients of iodide and HTO.
- Figures A2-17 to A2-22 show key correlations related to total clay content (wt.%), including: in situ hydraulic conductivity, porosity, water content (wt.%), effective diffusion coefficients of iodide and HTO, and density.
- Figure A2-23 illustrates the correlation between effective diffusion coefficient of HTO and water content (wt.%) of the formation.
- Figures A2-24 to A2-25 present the correlations between uniaxial compressive strength (UCS) and water content (wt.%), and uniaxial compressive strength and Young's modulus, respectively. The figure illustrates the typical hydromechanical coupling between such parameters in clay formations.

Figure A2-1: **Correlation between porosity and peak burial depth (best-estimate values)**

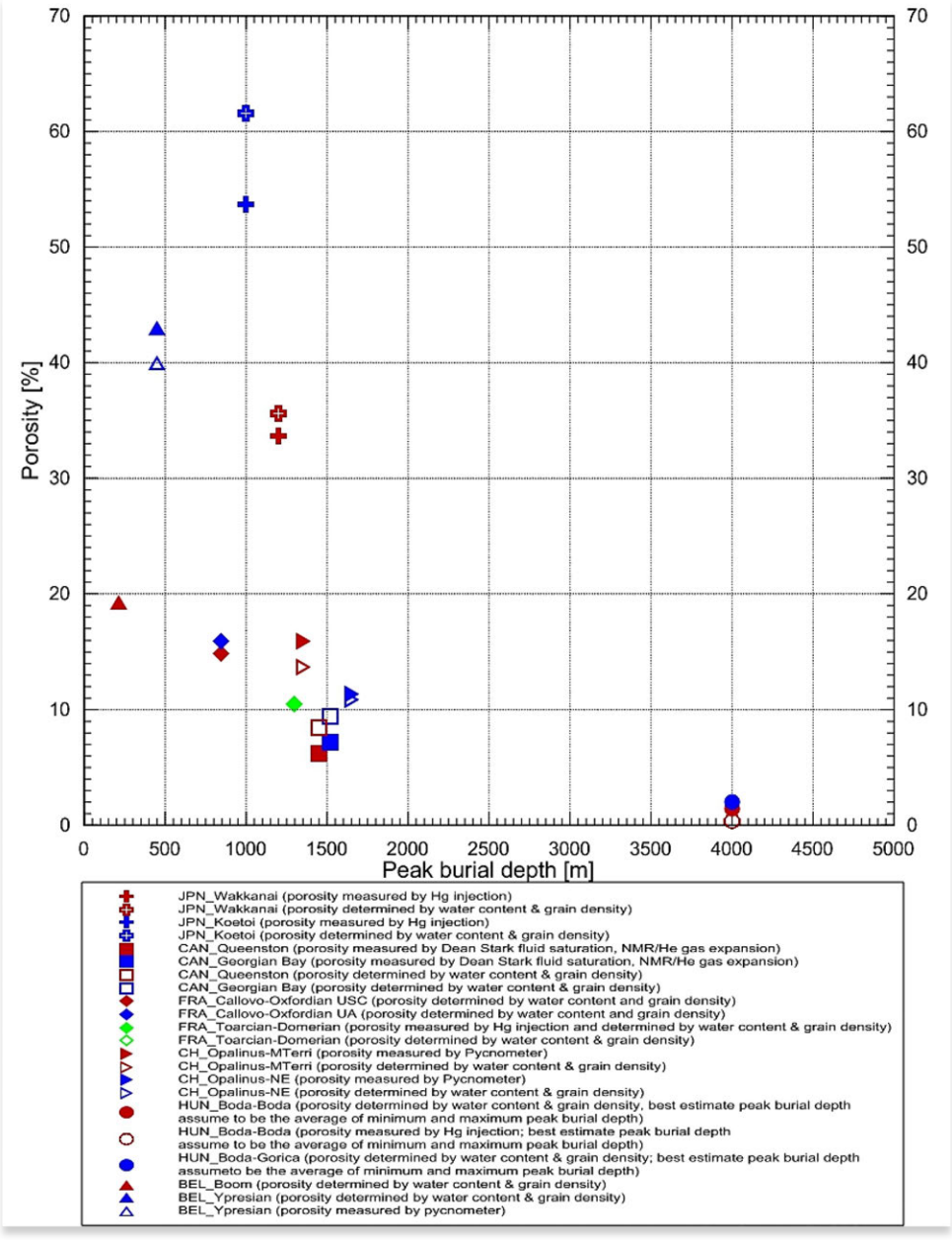

Source: NEA CCC Master Database.

Figure A2-2: **Correlation between present-day burial depth and salinity of formations**

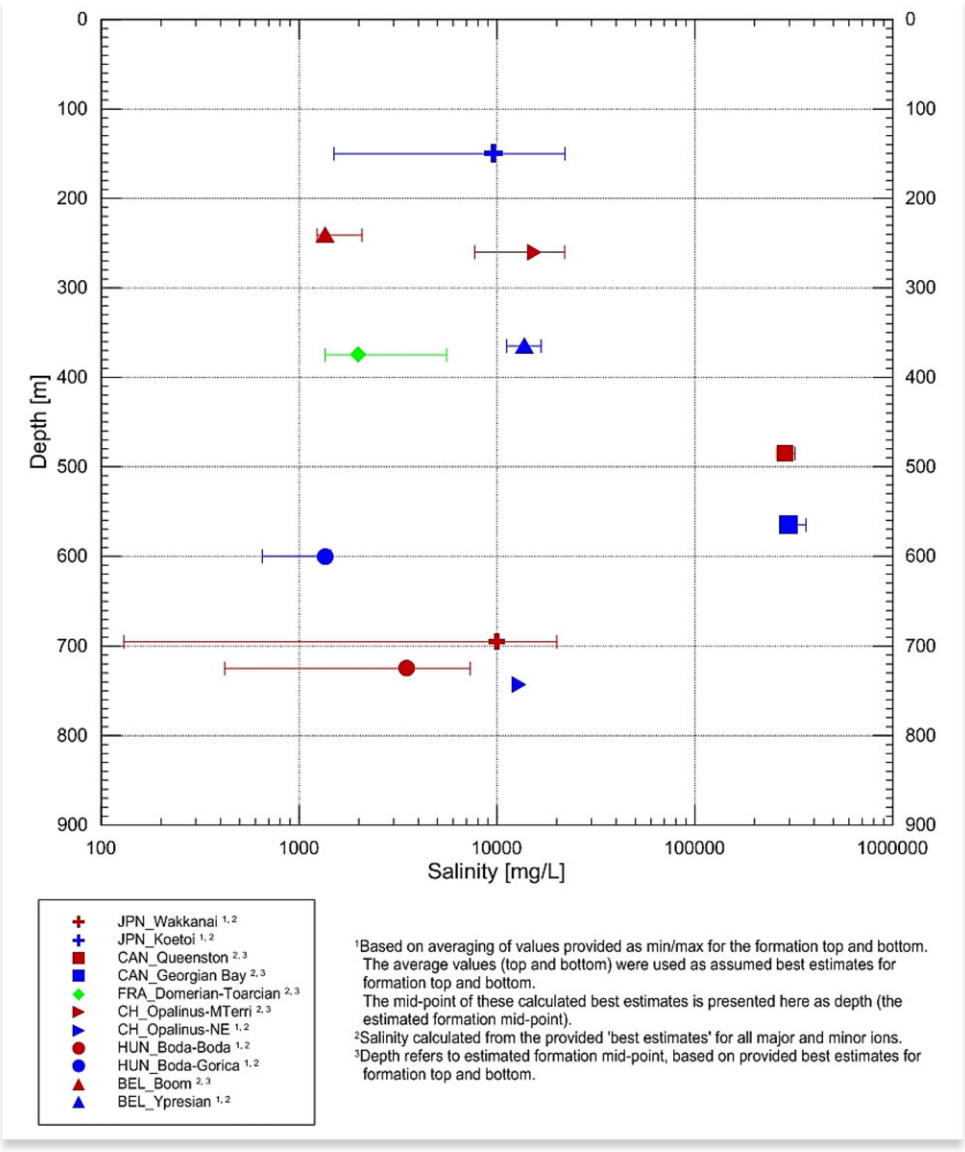

Note: Lines represent the range of values measured (minimum to maximum). Symbols represent best-estimate values.

Source: NEA CCC Master Database.

Figure A2-3: **Ternary diagram for porewater major ion chemistry – cations (best-estimate values)**

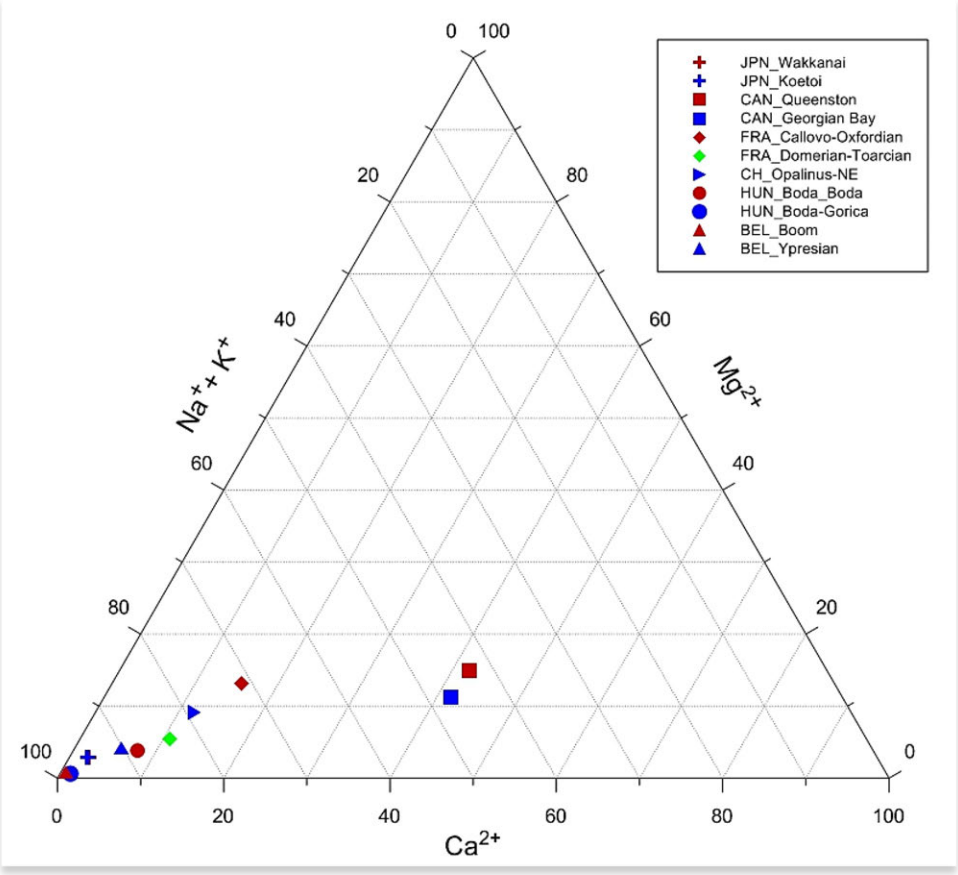

Note: HUN_Boda-Boda block and HUN_Boda-Gorica block formation data originated from groundwater.
Source: NEA CCC Master Database.

Figure A2-4: **Ternary diagram for porewater major ion chemistry – anions (best-estimate values)**

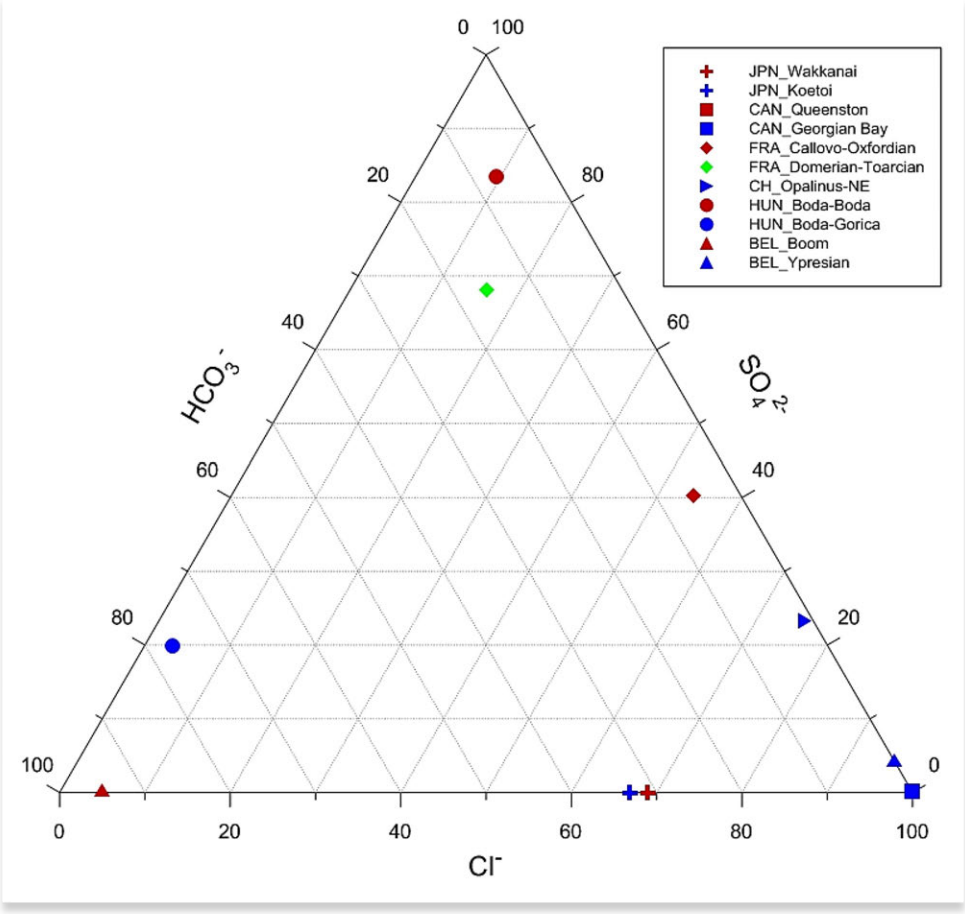

Note: HUN_Boda-Boda block and HUN_Boda-Gorica block formation data originated from groundwater.
Source: NEA CCC Master Database.

Figure A2-5: **Ternary diagram for total clay mineral(s), total carbonate(s), and sum of other minerals content, presented in wt.% (best-estimate values)**

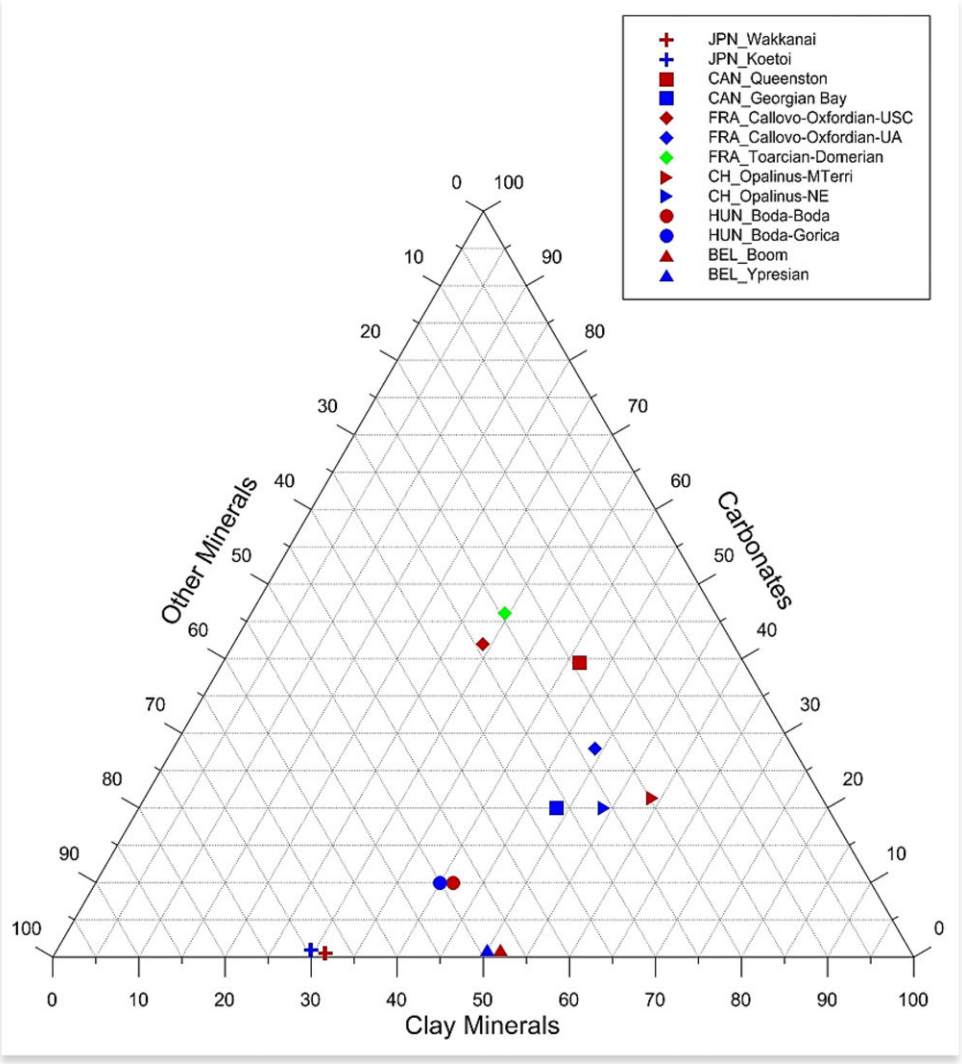

Source: NEA CCC Master Database.

Figure A2-6: **Correlation between hydraulic conductivity and density (best-estimate values)**

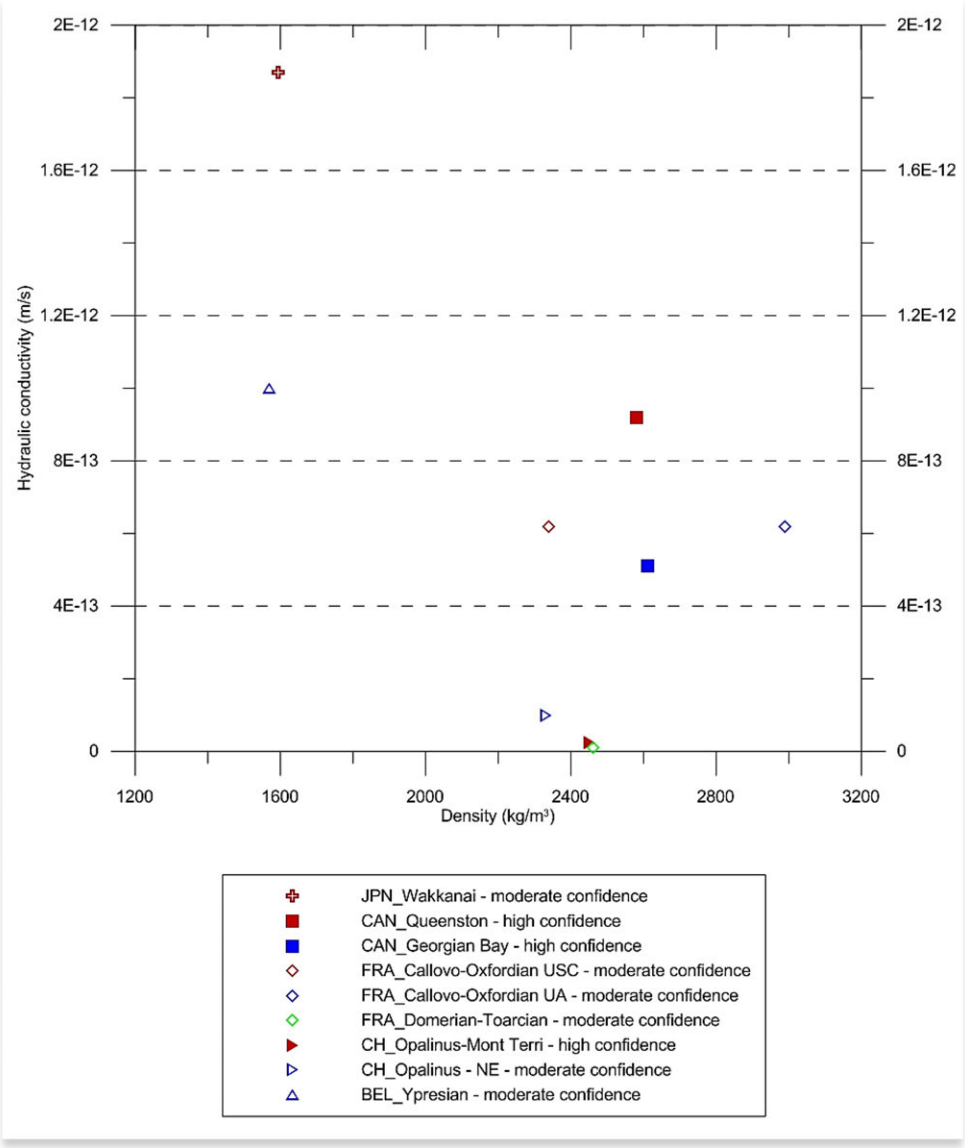

Source: NEA CCC Master Database.

Figure A2-7: **Correlation between porosity and in situ hydraulic conductivity (best-estimate values)**

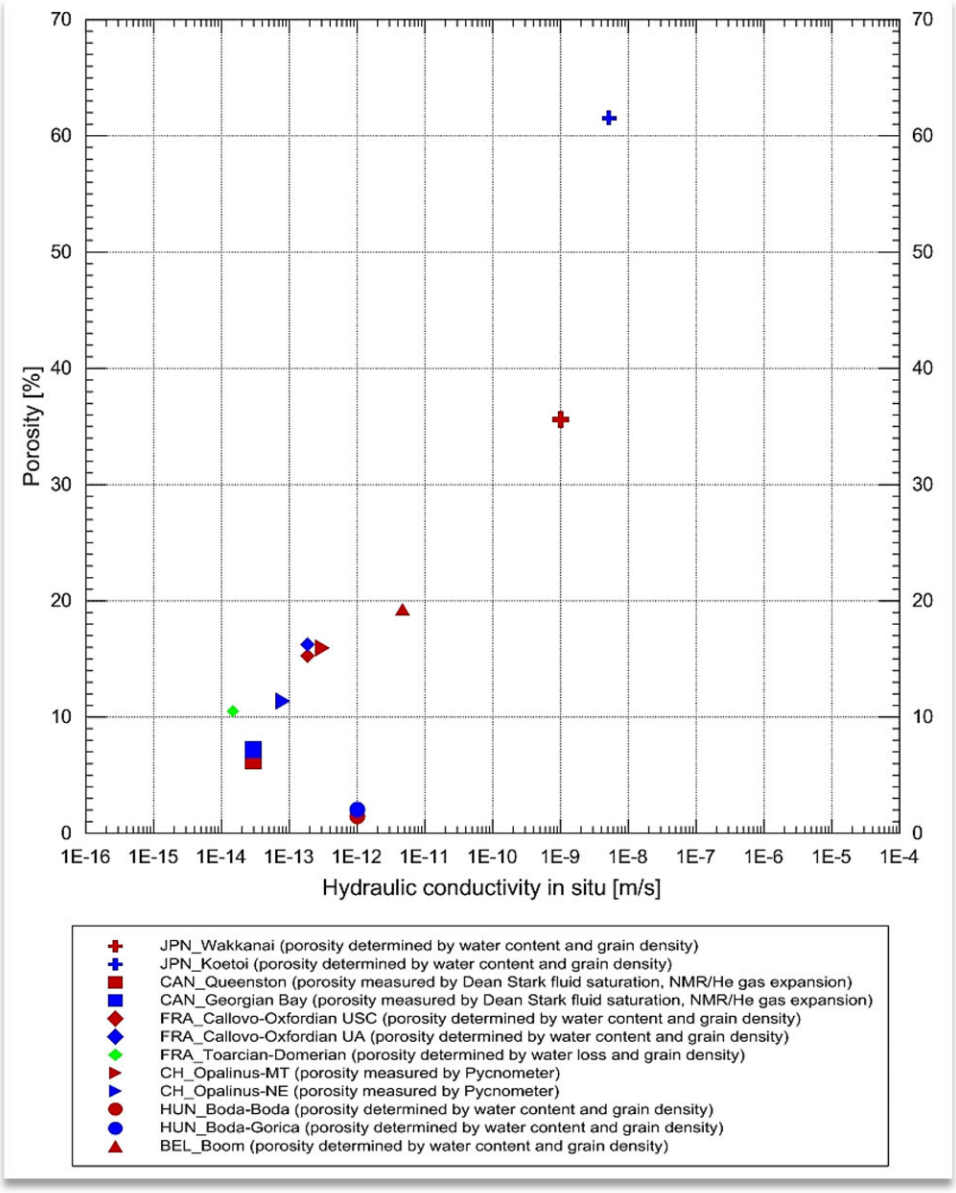

Source: NEA CCC Master Database.

Figure A2-8: **Correlation between porosity and HTO diffusion coefficient perpendicular to bedding (best-estimate values)**

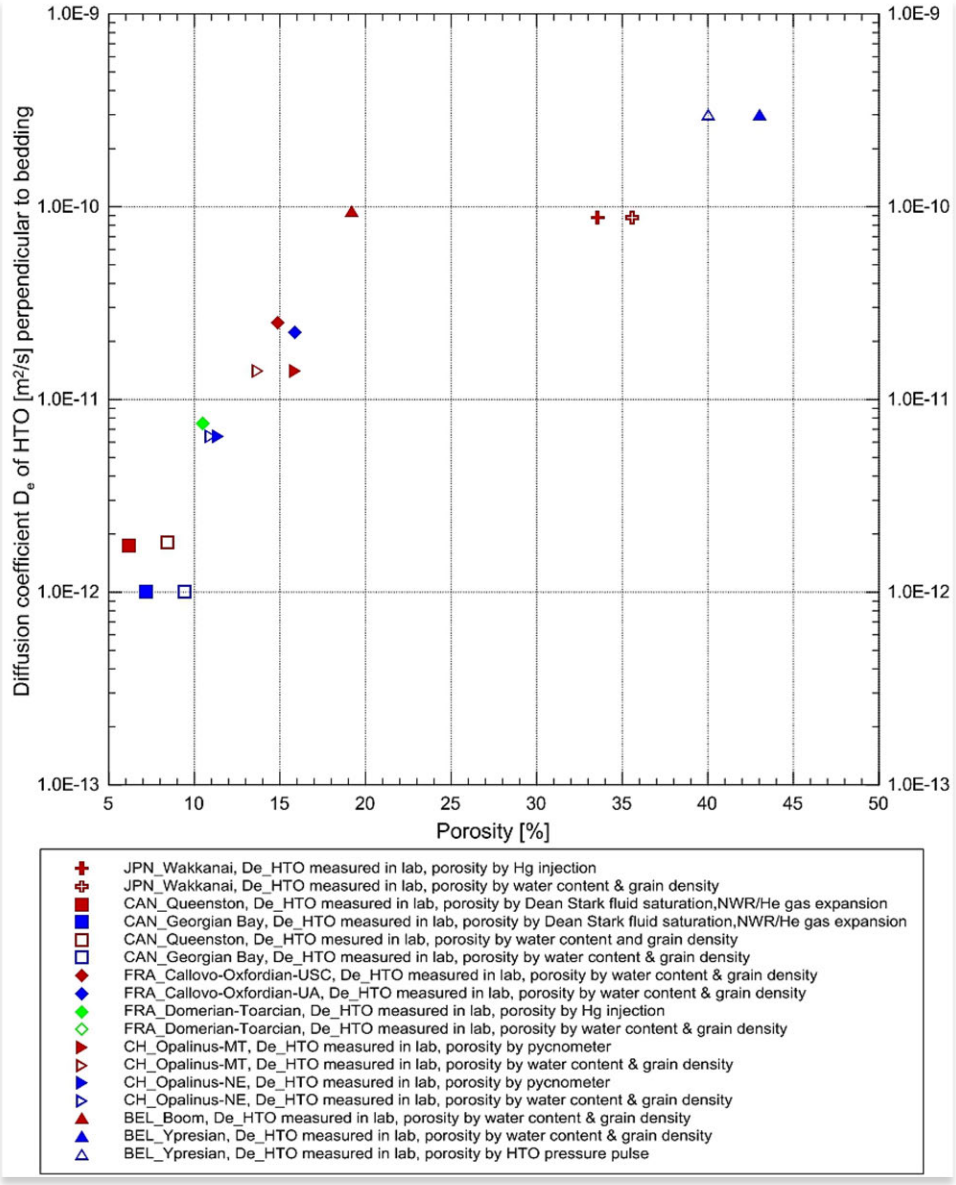

Source: NEA CCC Master Database.

Figure A2-9: **Correlation between porosity and HTO diffusion coefficient parallel to bedding (best-estimate values)**

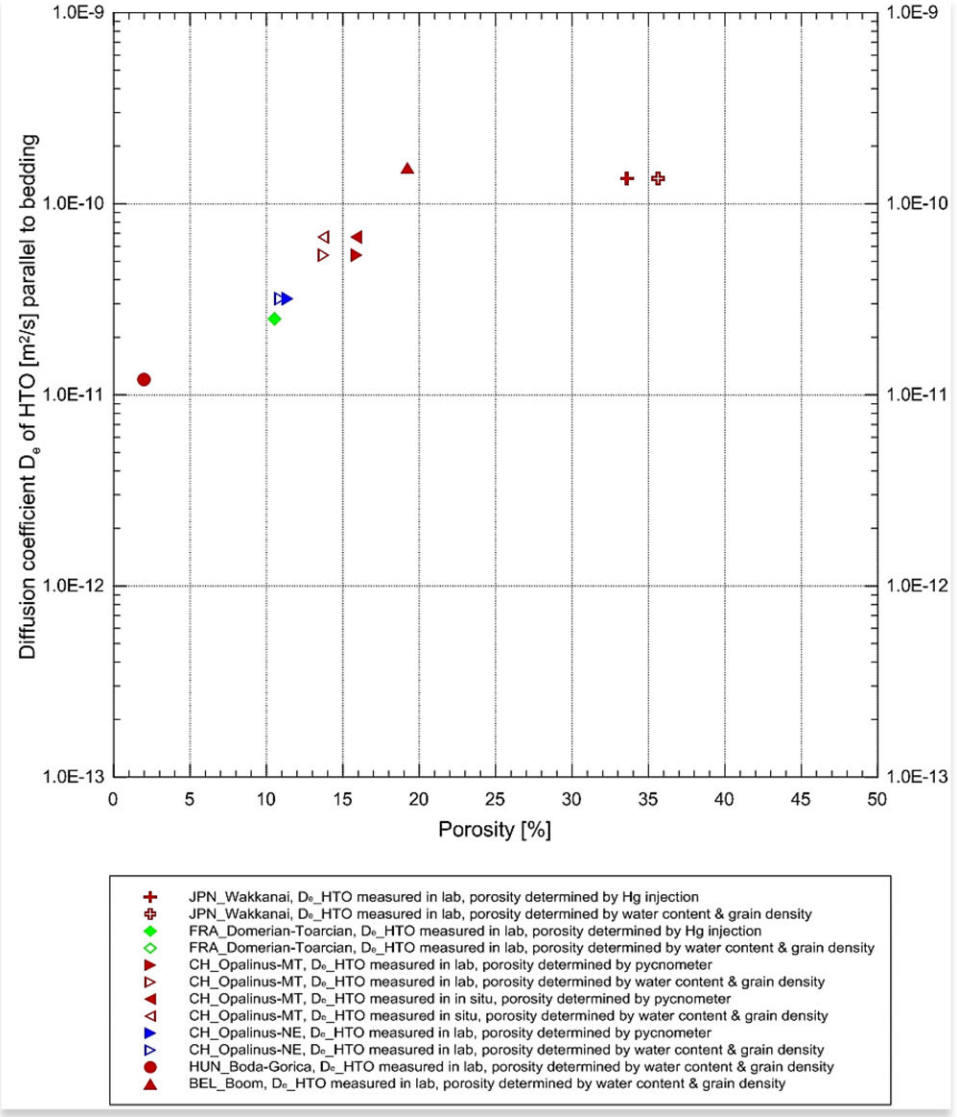

Source: NEA CCC Master Database.

Figure A2-10: **Correlation between porosity and chloride + iodide diffusion coefficient perpendicular to bedding (best-estimate values)**

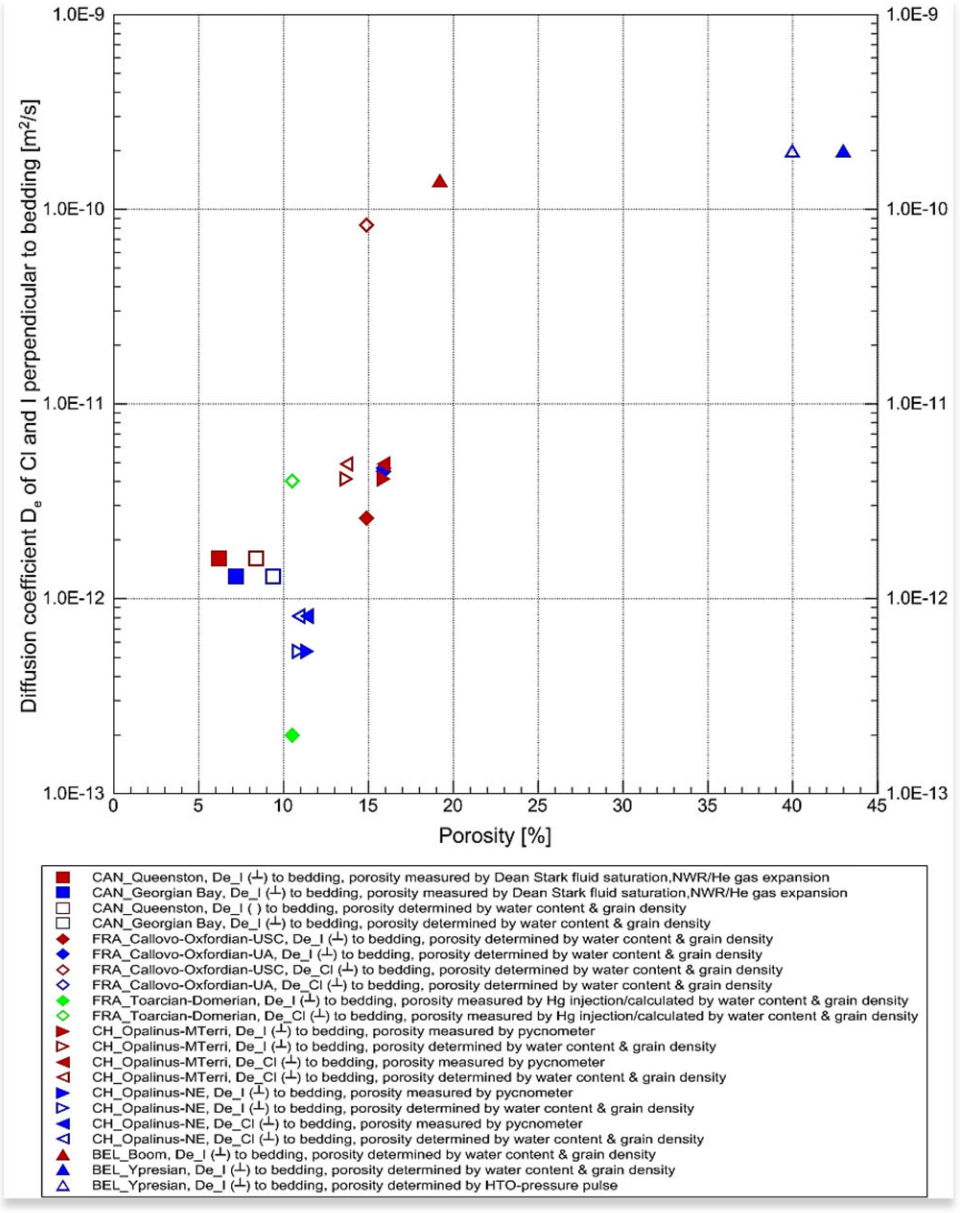

Source: NEA CCC Master Database.

Figure A2-11: **Correlation between porosity and chloride + iodide diffusion coefficient parallel to bedding (best-estimate values)**

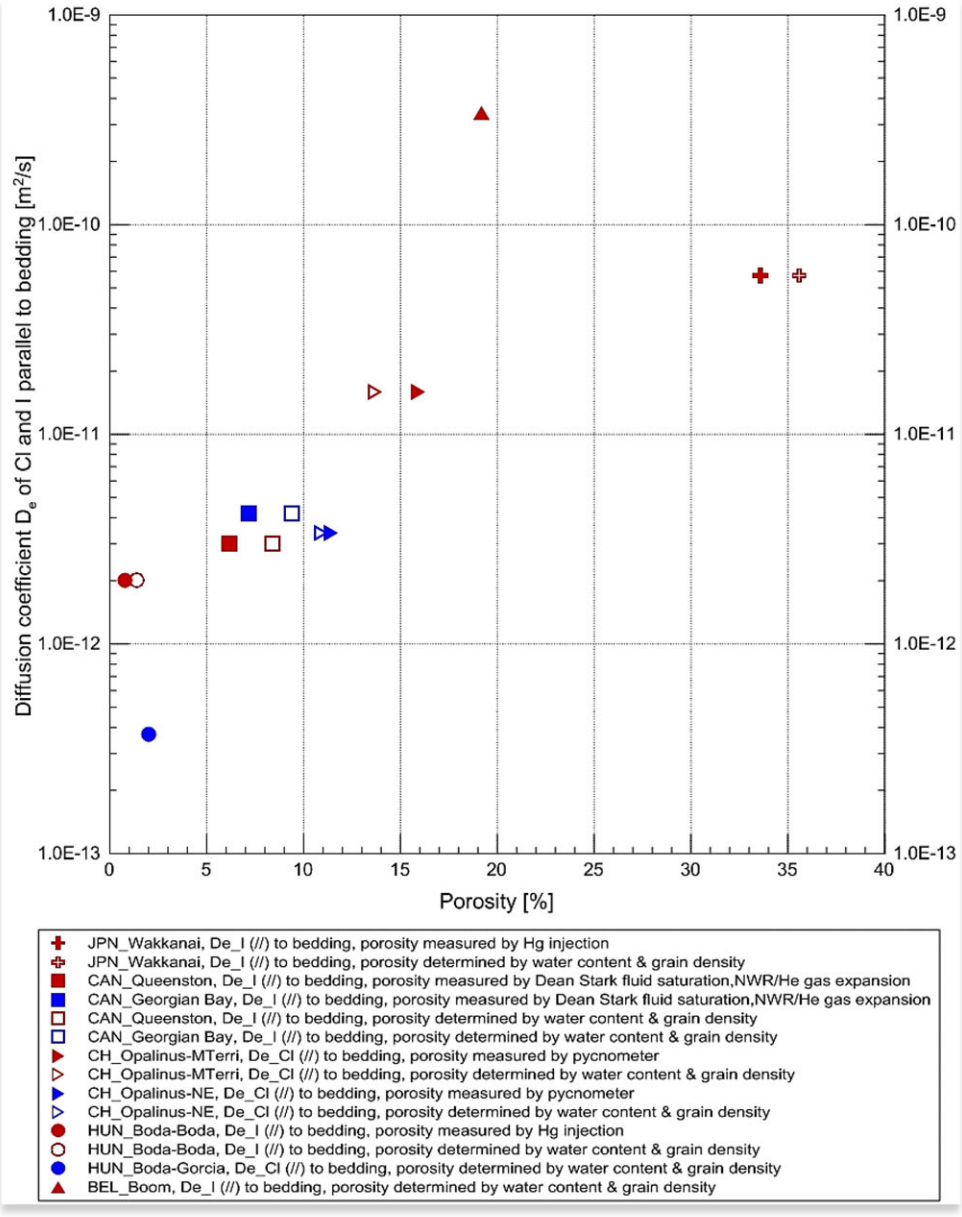

Source: NEA CCC Master Database.

Figure A2-12: **Correlation between total carbonate(s) content (presented in wt.%) and in situ hydraulic conductivity (best-estimate values)**

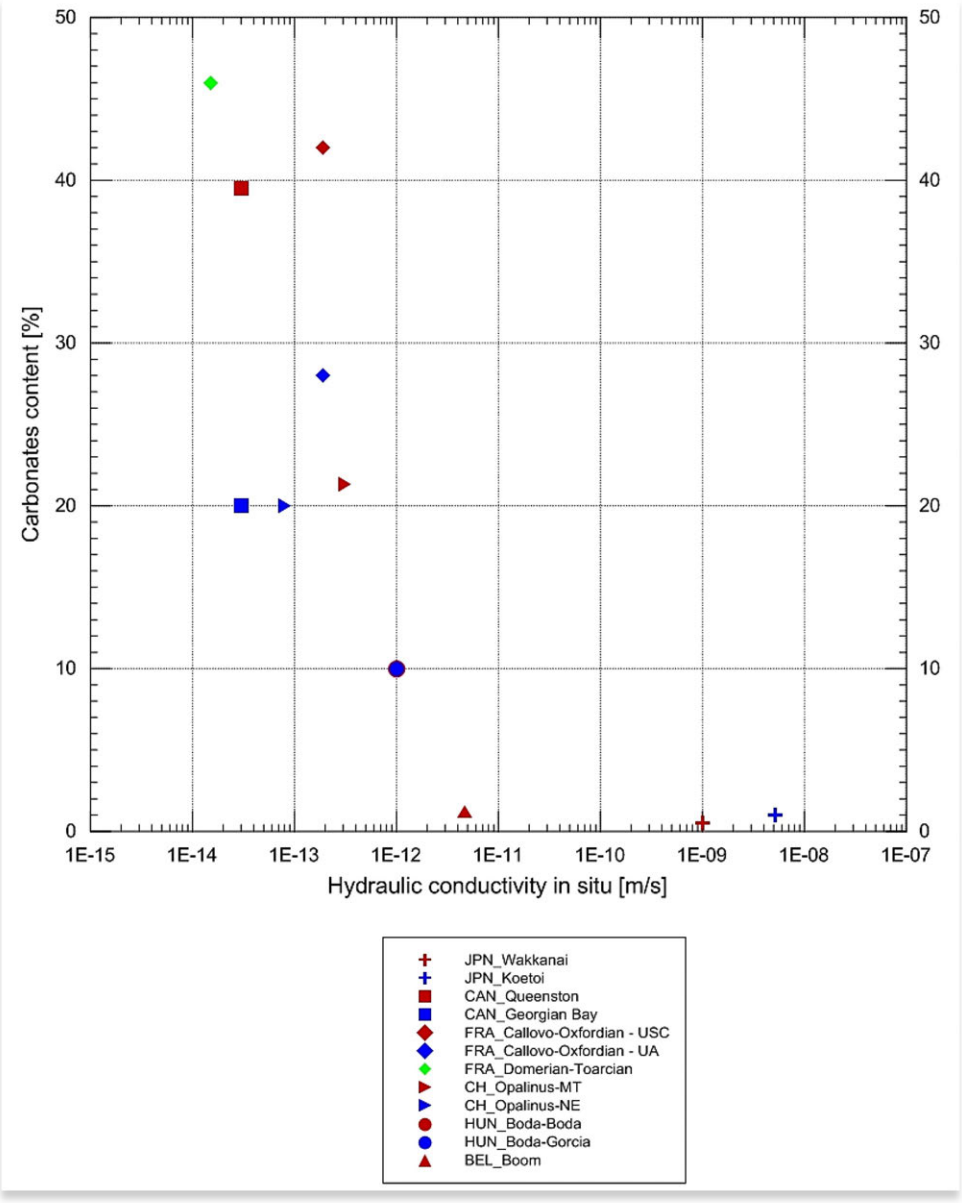

Source: NEA CCC Master Database.

Figure A2-13: **Correlation between total carbonate(s) content (presented in wt.%) and porosity (best-estimate values)**

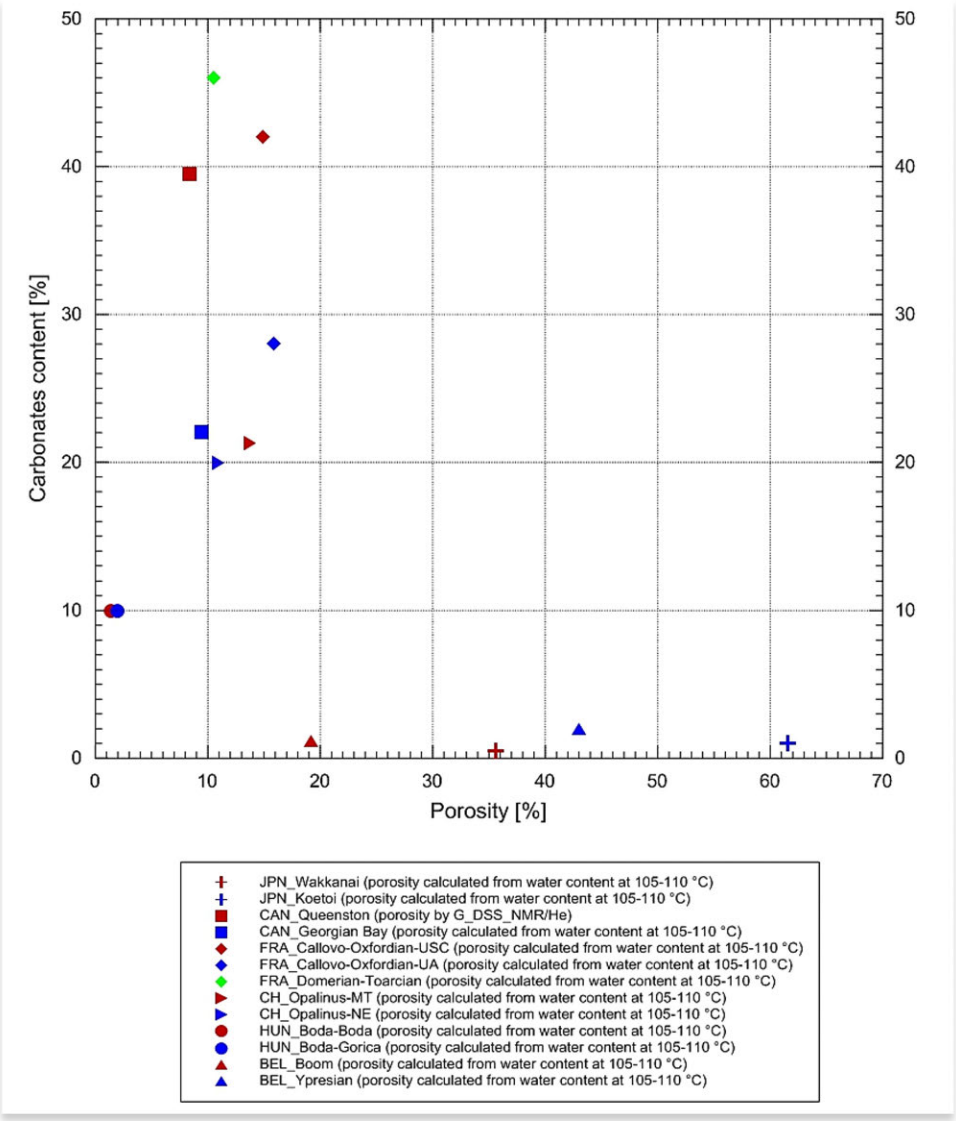

Source: NEA CCC Master Database.

Figure A2-14: **Correlation between total carbonate(s) content (presented in wt.%) and water content (presented in wt.%)(best-estimate values)**

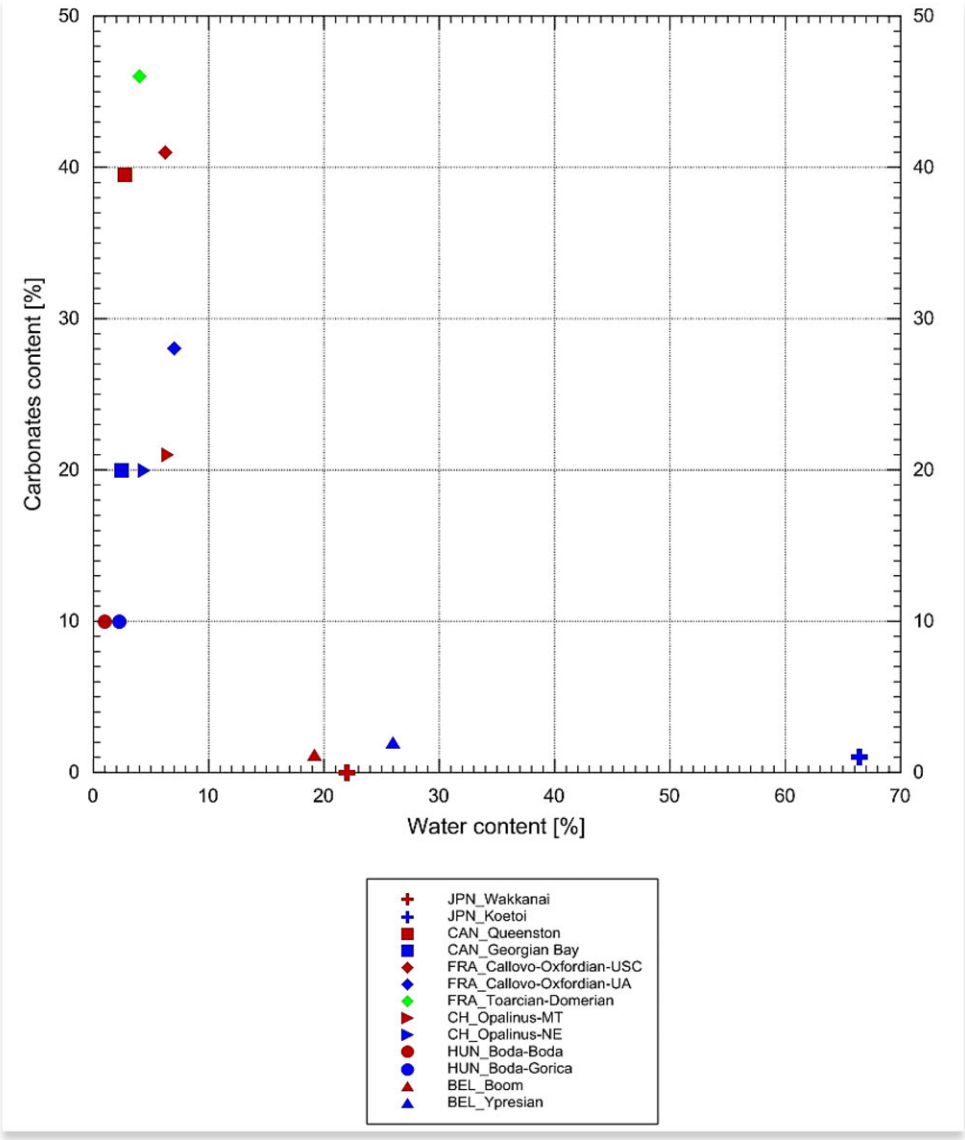

Source: NEA CCC Master Database.

Figure A2-15: **Correlation between total carbonate(s) content (presented in wt.%) and diffusion coefficient of iodide (best-estimate values)**

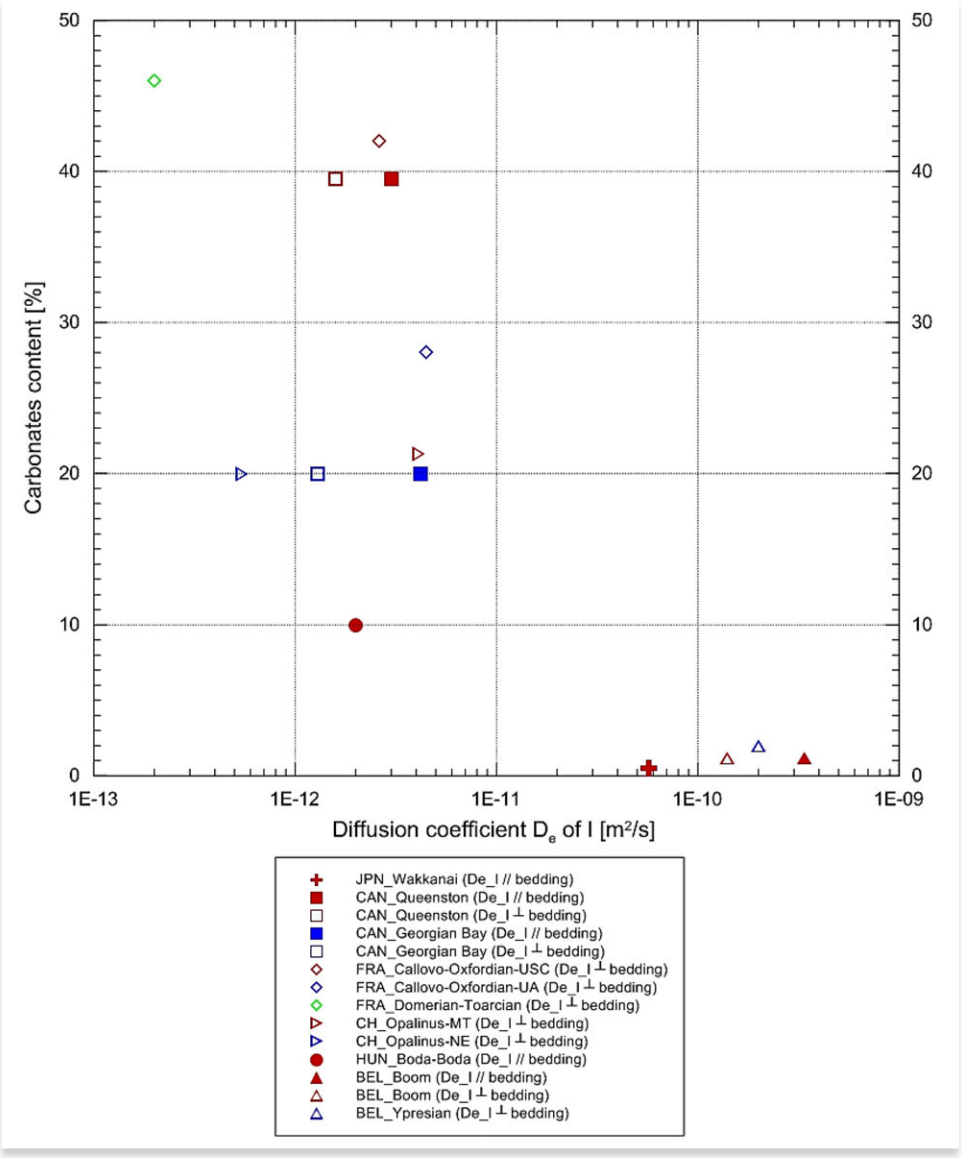

Note: Hollow symbols – measurements oriented perpendicular to bedding; filled symbols – measurements oriented parallel to bedding.

Source: NEA CCC Master Database.

Figure A2-16: **Correlation between total carbonate(s) content (presented in wt.%) and diffusion coefficient of HTO (best-estimate values)**

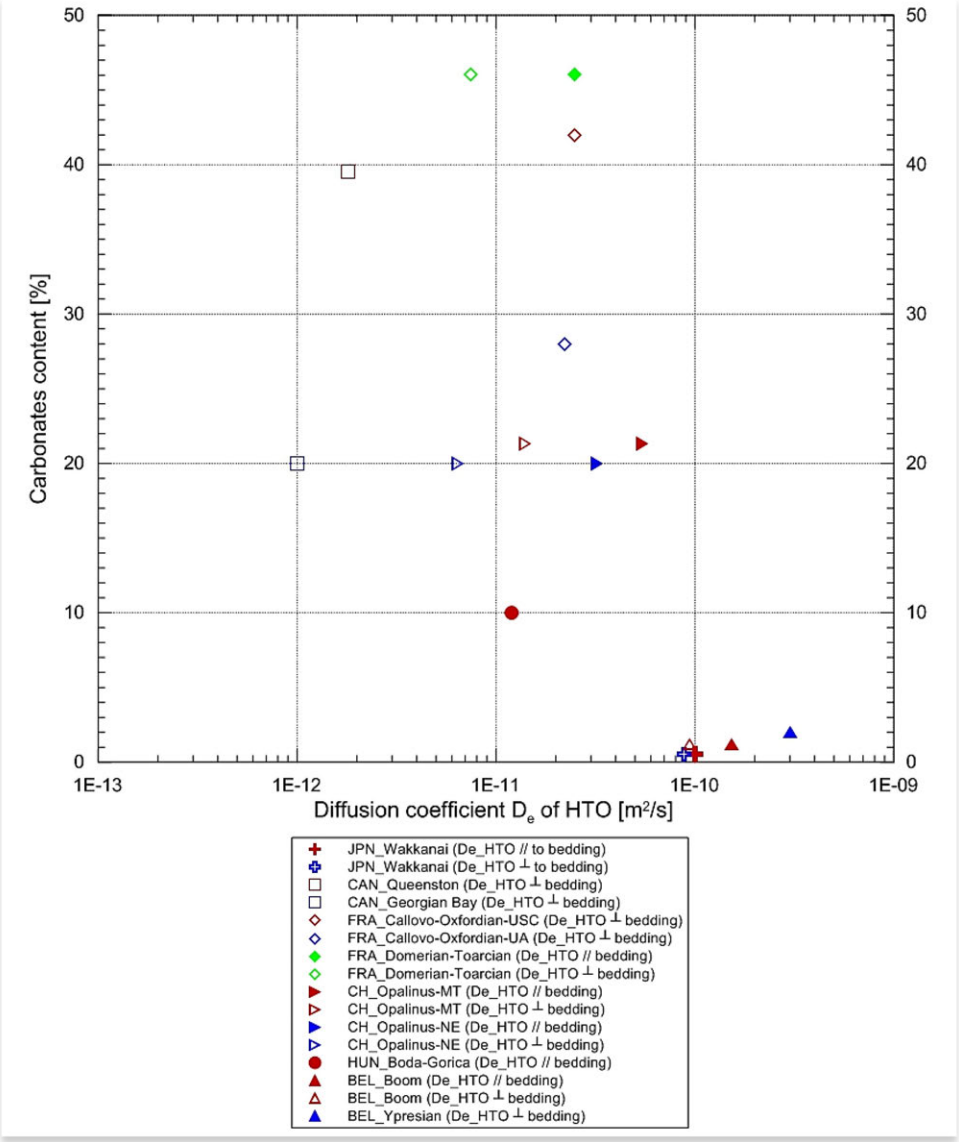

Note: Hollow symbols – measurements oriented perpendicular to bedding; filled symbols – measurements oriented parallel to bedding.

Source: NEA CCC Master Database.

Figure A2-17: **Correlation between total clay mineral(s) content (presented in wt.%) and in situ hydraulic conductivity (best-estimate values)**

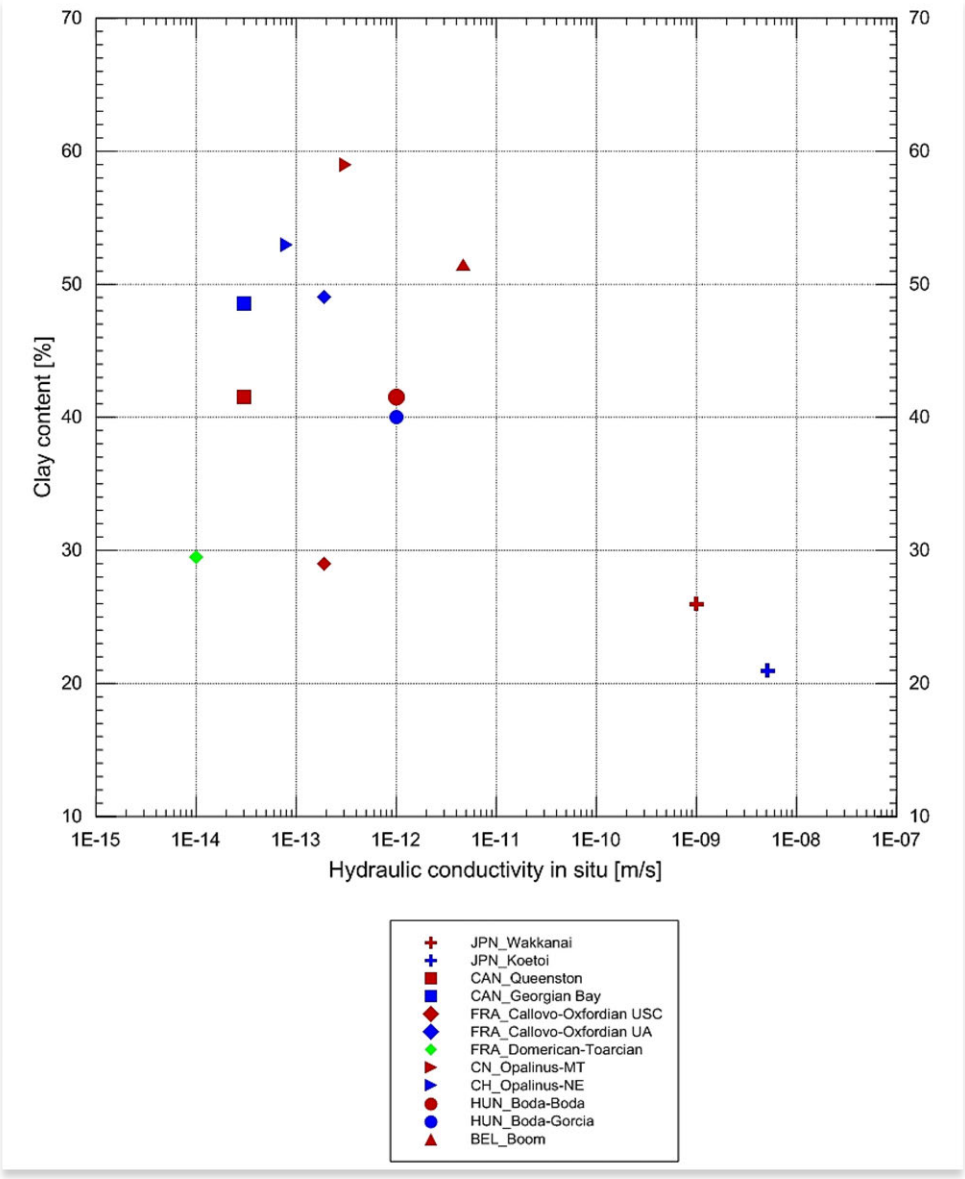

Source: NEA CCC Master Database.

Figure A2-18: **Correlation between total clay mineral(s) content (presented in wt.%) and porosity (best-estimate values)**

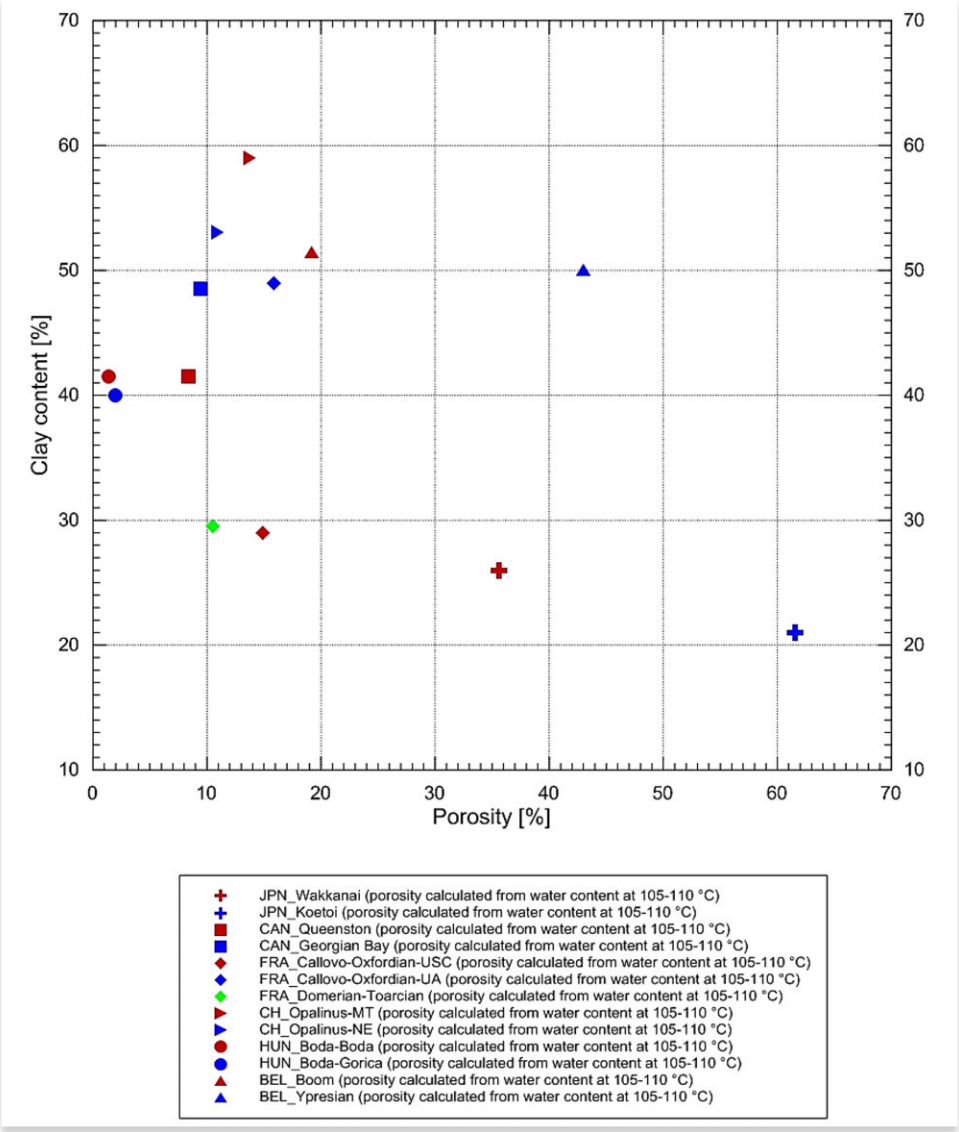

Source: NEA CCC Master Database.

Figure A2-19: **Correlation between total clay mineral(s) content (presented in wt.%) and water content (presented in wt.%) (best-estimate values)**

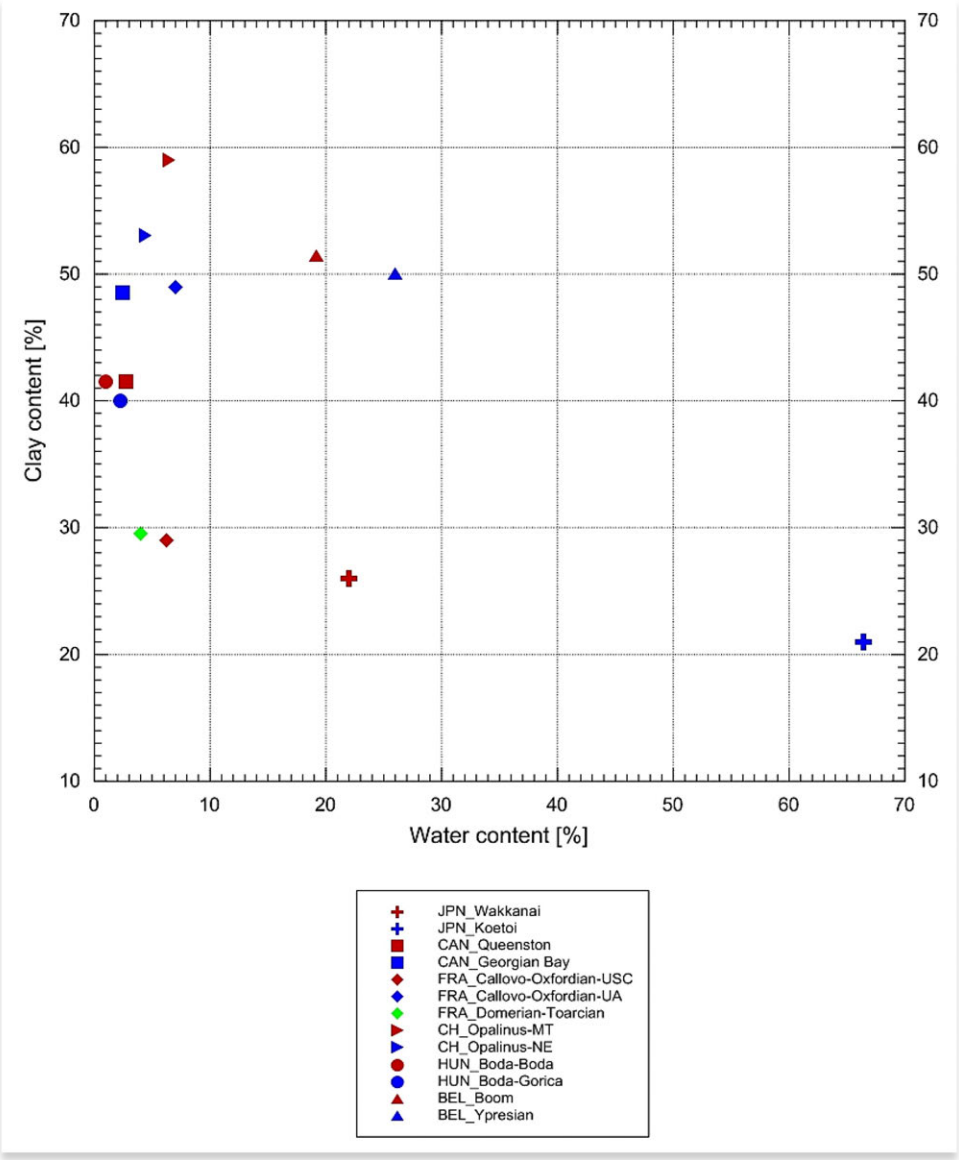

Source: NEA CCC Master Database.

Figure A2-20: **Correlation between total clay mineral(s) content (presented in wt.%) and diffusion coefficient of iodide (best-estimate values)**

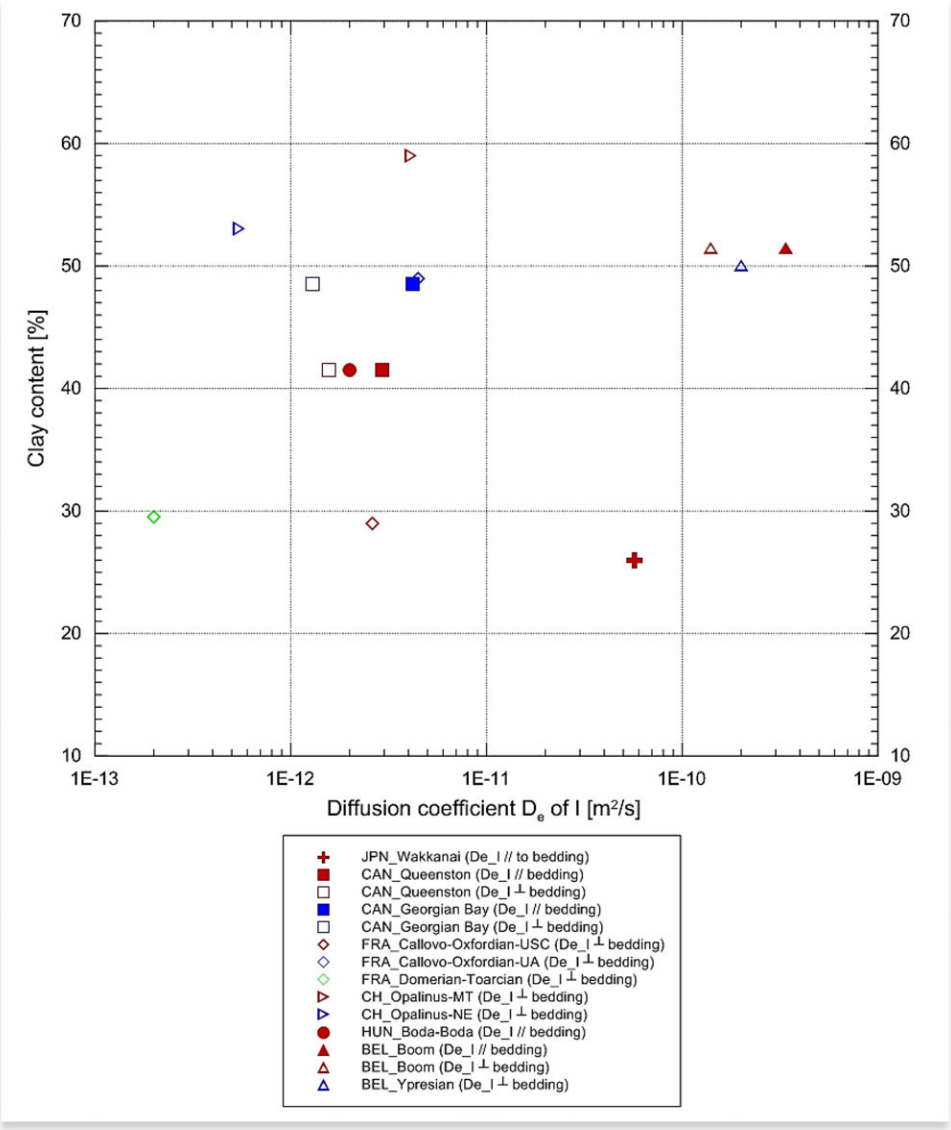

Note: Hollow symbols – measurements oriented perpendicular to bedding; filled symbols – measurements oriented parallel to bedding.

Source: NEA CCC Master Database.

Figure A2-21: **Correlation between total clay mineral(s) content (presented in wt.%) and diffusion coefficient of HTO (best-estimate values)**

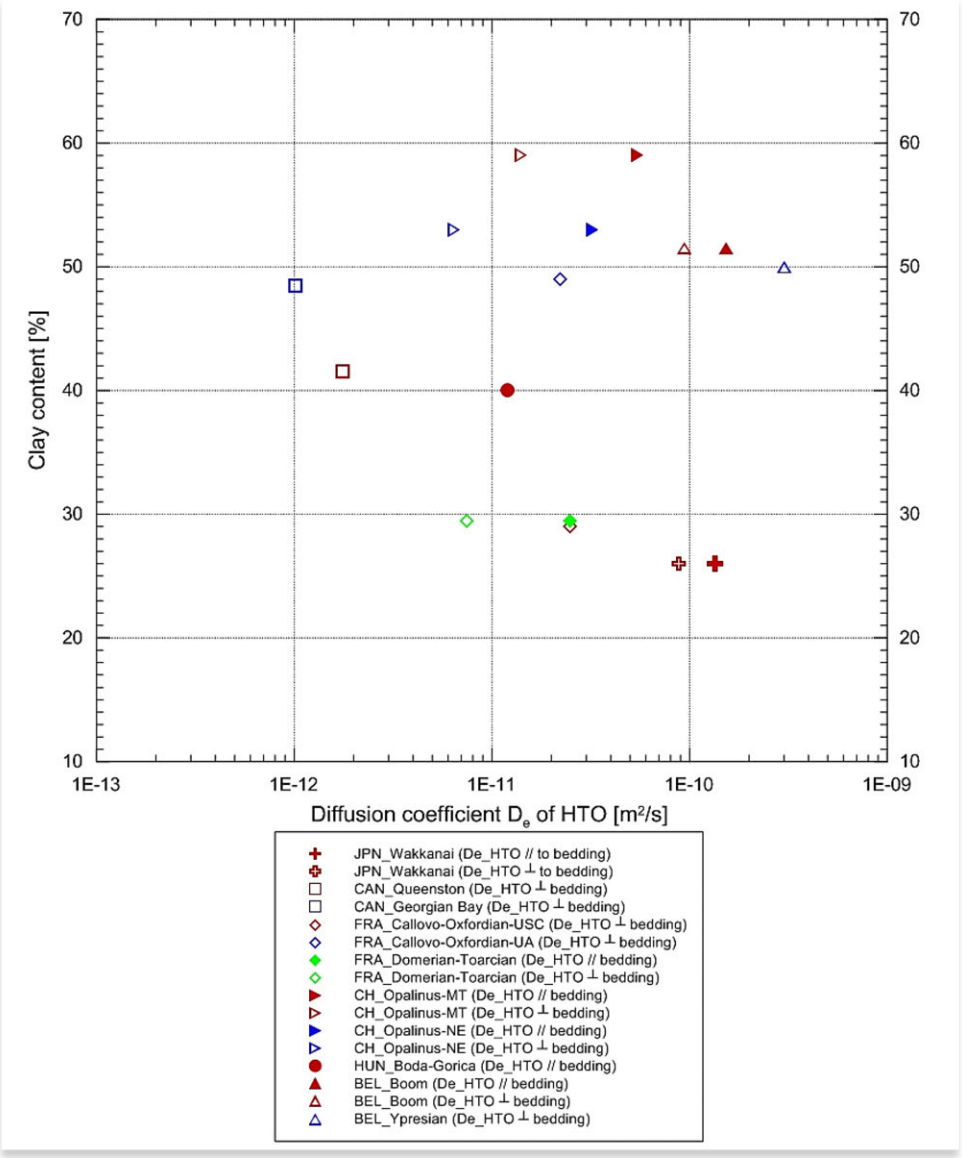

Source: NEA CCC Master Database.

Figure A2-22: **Correlation between total clay mineral(s) content (presented in wt.%) and density (best-estimate values)**

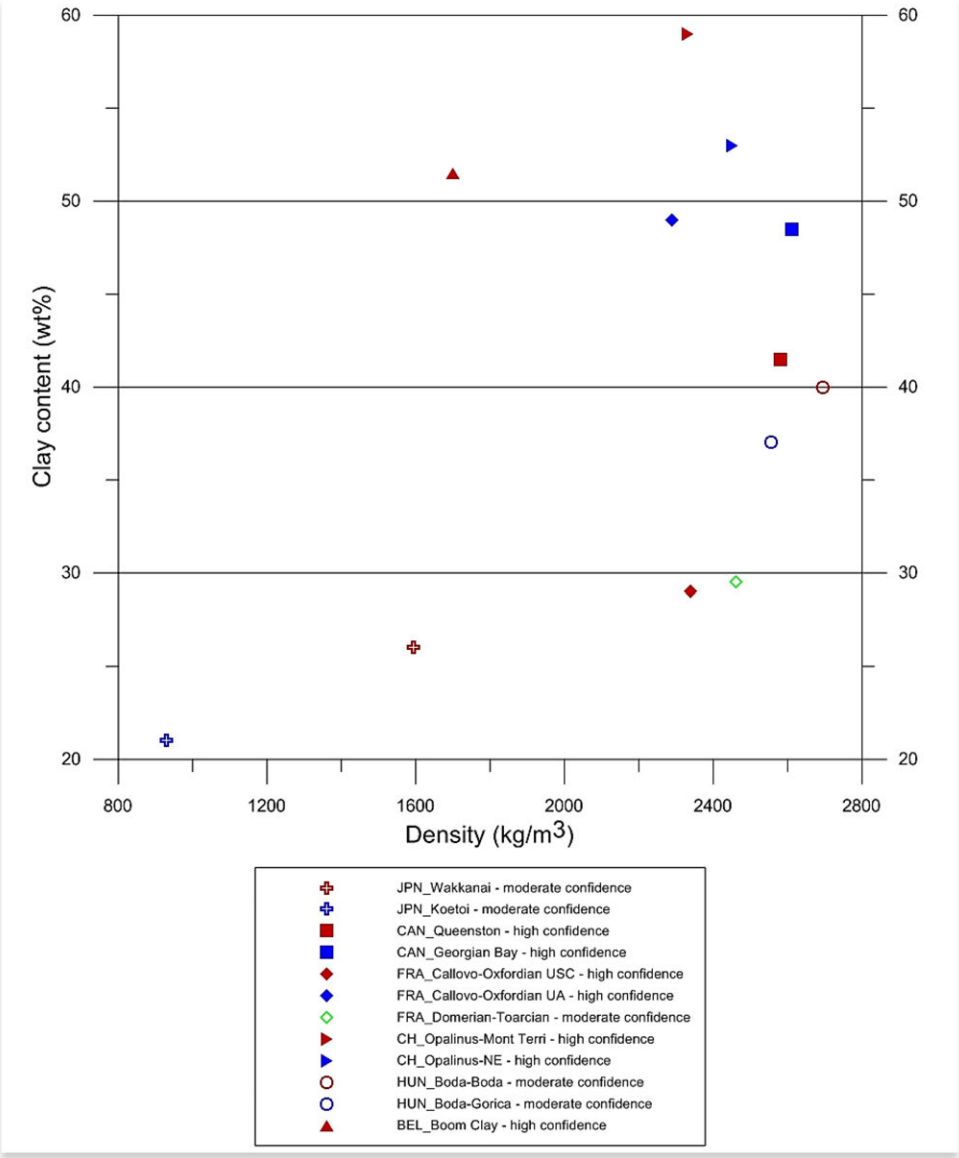

Source: NEA CCC Master Database.

Figure A2-23: **Correlation between diffusion coefficient of HTO and water content (presented in wt.%) (best-estimate values)**

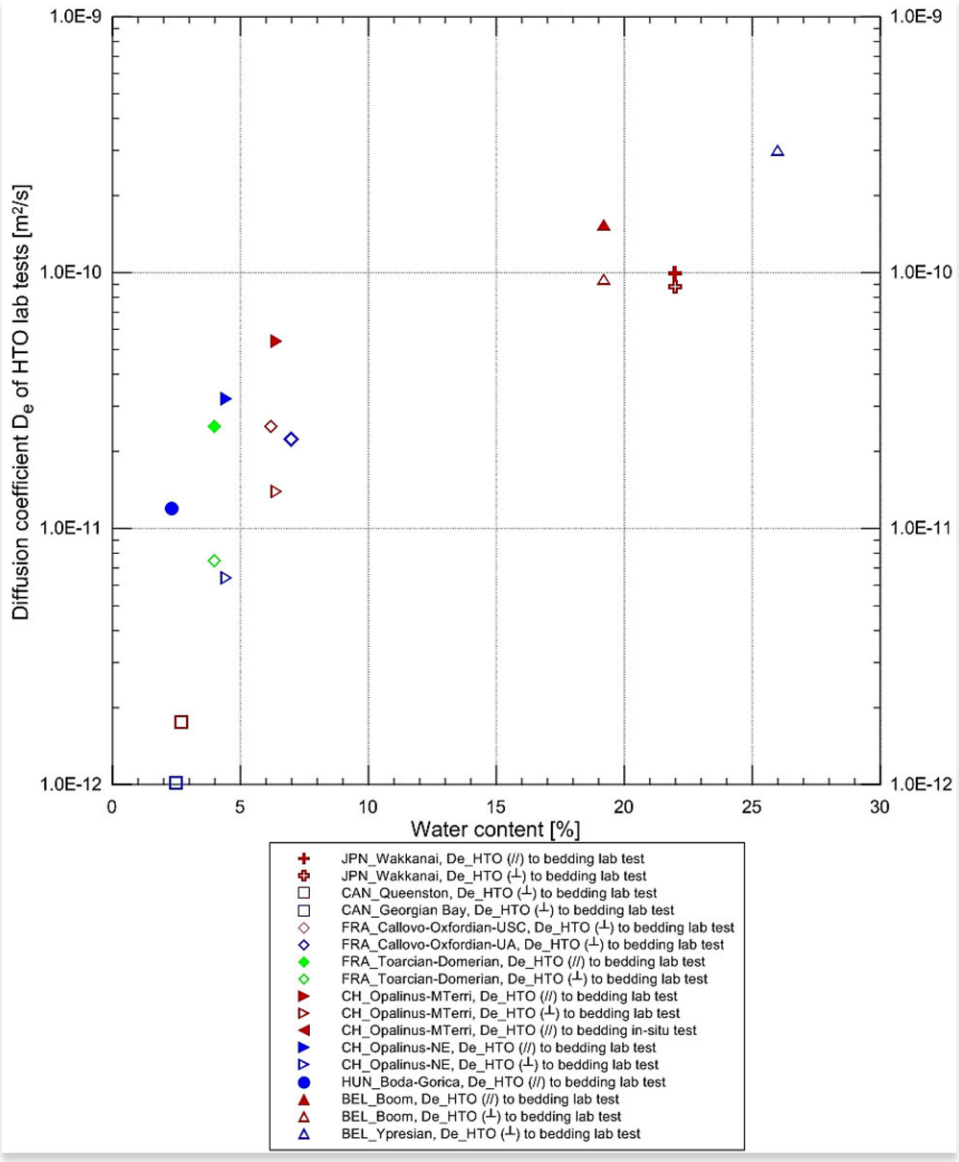

Note: Hollow symbols – measurements oriented perpendicular to bedding; filled symbols – measurements oriented parallel to bedding.

Source: NEA CCC Master Database.

Figure A2-24: **Correlation between uniaxial compressive strength (UCS) and water content (presented in wt.%) (best-estimate values)**

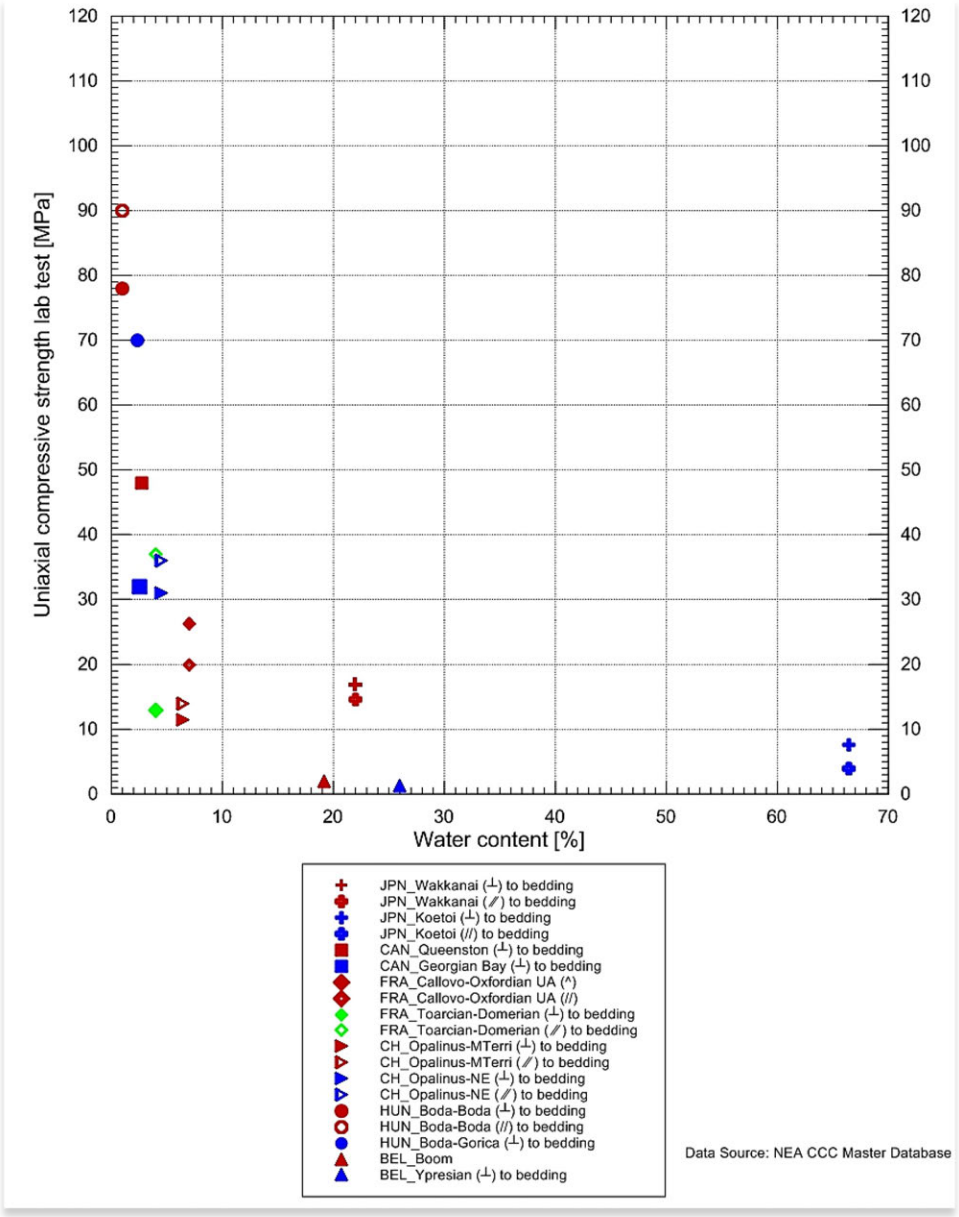

Source: NEA CCC Master Database.

Figure A2-25: **Correlation between uniaxial compressive strength (UCS) and Young's modulus static laboratory tests (best-estimate values)**

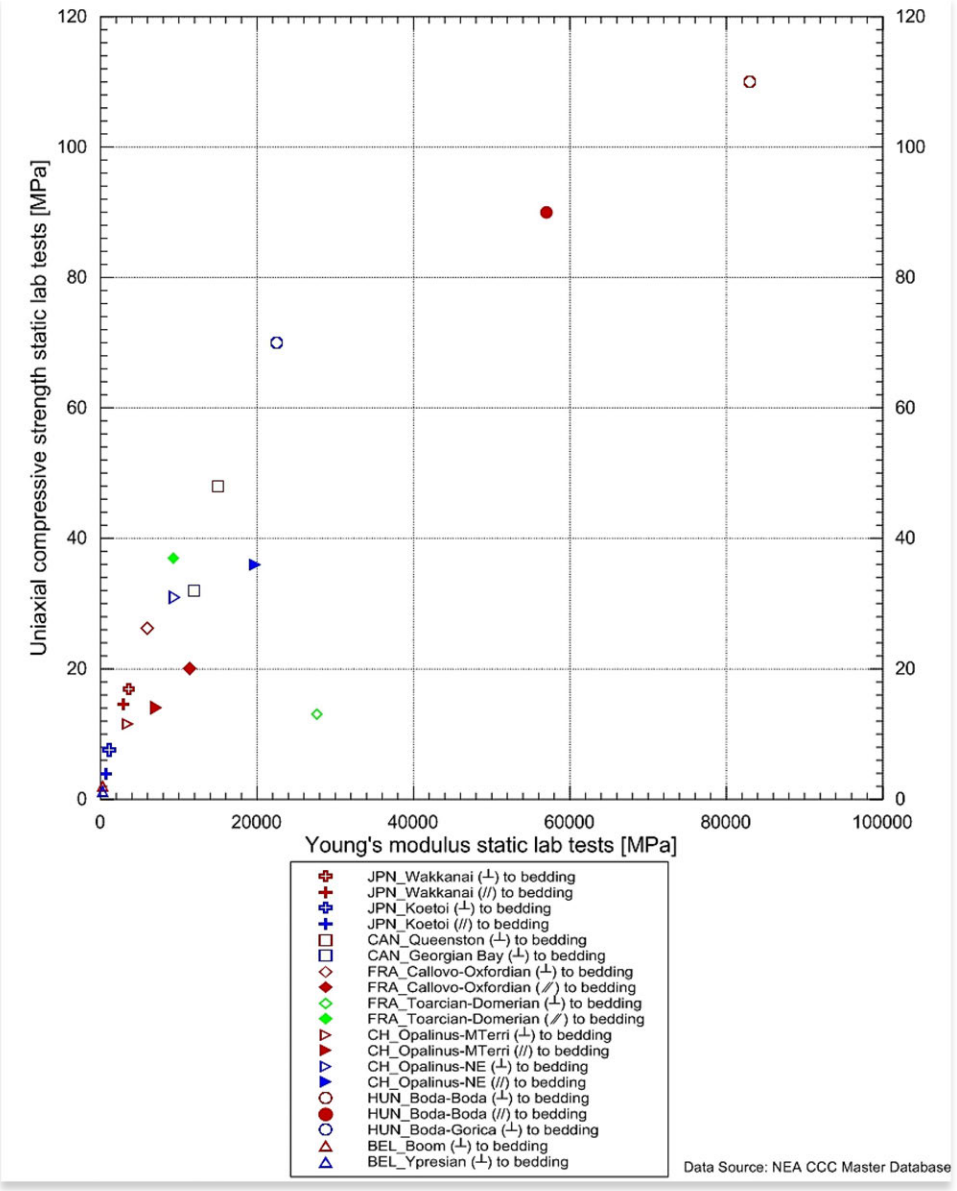

Note: Hollow symbols – measurements oriented perpendicular to bedding; filled symbols – measurements oriented parallel to bedding.

Source: NEA CCC Master Database.

Annex III: Argillaceous rock formations description[1]

Boom Clay – Belgium

Introduction

The Boom Clay, a non-indurated clay unit, has been studied for almost 40 years in Belgium in the context of the long-term management of radioactive waste (ONDRAF/NIRAS, 1990; ONDRAF/NIRAS, 2001; ONDRAF/NIRAS, 2013). Research began in the 1970s at SCK CEN (Nuclear Research Institute), situated in Mol, with exploratory drilling and the construction of the underground research facility (URF), HADES. The URF is presently managed by the EIG EURIDICE (ONDRAF/NIRAS and SCK CEN). Since its establishment in 1980, ONDRAF/NIRAS, the Belgian Agency for Radioactive Waste and Enriched Fissile Materials, has been responsible for radioactive waste management in Belgium. The agency considers geological disposal in poorly indurated clay as the reference solution for the long-term management of high-level waste (classified as category C waste) and long-lived intermediate and low-level waste (classified as category B waste). ONDRAF/NIRAS is also responsible for the research, development and design programmes related to geological disposal.

Disposal concept

The disposal concept includes the post-conditioning of the waste in disposal packages and the subsequent disposal of these packages in an underground repository. Before being transported and disposed of in the repository, the primary waste packages, in which wastes are currently contained, will be post-conditioned in disposal packages: so-called "super-containers" for category C waste (high-level long-lived heat-emitting waste) and monoliths for category B (medium-level long-lived waste). These disposal packages must provide radiological protection to workers, to enable safe handling of the waste without requiring additional protection. Apart from radiological shielding, the disposal package for the category C waste, the super-container, also has to assure complete waste containment during the thermal phase. This is the phase during which the host rock is at elevated temperature (i.e. higher than 25°C) due to the heat generated by the waste.

The super-containers and monoliths are then transported to an underground repository. The reference design for a repository, as considered in ONDRAF/NIRAS' Research, Design and Development (RD&D) programme on geological disposal, consists of a disposal facility constructed in poorly indurated clay. The disposal packages are transferred to the repository along a large waste shaft, which separates the repository into category B and category C waste sections. Two smaller shafts are built at each end of the respective sections for personnel and material transfer, and to allow the repository to be ventilated. The shafts are connected by access galleries, perpendicular to which the actual disposal galleries are constructed. The disposal galleries are dead-end structures.

As waste disposal progresses, the repository is progressively closed by backfilling and sealing of the disposal galleries. After completion of all disposal operations, the repository is closed by backfilling and sealing of the access galleries and shafts.

1. The summaries were published as provided by the countries with minimal editorial input from the NEA.

Formation properties

Present in the north-eastern part of Belgium, the Boom Clay has a long history of being studied by geologists, soil engineers and industrial users. Study of the Boom Clay began in the 19th century in its outcrop area along the Rupel River. This river has also given its name to the Early Oligocene age and stage, the Rupelian.

Geology/structure

Boom Clay is the name given to a thick plastic clay unit of (Early) Oligocene age, present in the Campine Basin in the North-east of Belgium, in the Netherlands (Rupel Clay Member), under the North Sea (Lark Formation), and in the Lower Rhine area and Northern Germany (Septarienton/ Rupelton).

The Boom Clay Formation is, from base to top, subdivided into four members (Figure A3-1): Belsele-Waas Member, Terhagen Member, Putte Member and Boeretang Member (Vandenberghe et al., 2014). The Boeretang Member is absent in the outcrop area of the formation and is only recognised in drill core/cuttings. To the east, the Belsele-Waas Member extends laterally into the Berg Sand, and the lower part of the Terhagen Member extends into the Kleine Spouwen Clay and the Kerniel Sands. The Boom Clay is covered by glauconitic and clayey sands of the Eigenbilzen Formation. In the northern part of Belgium, the distinction between the Boeretang Member and the Eigenbilzen Formation is difficult to discern. In this case, the Eigenbilzen Formation is incorporated into the Boom Formation, forming a thick clay layer.

Figure A3-1: **Sequence stratigraphic data and interpretation for the Rupelian**

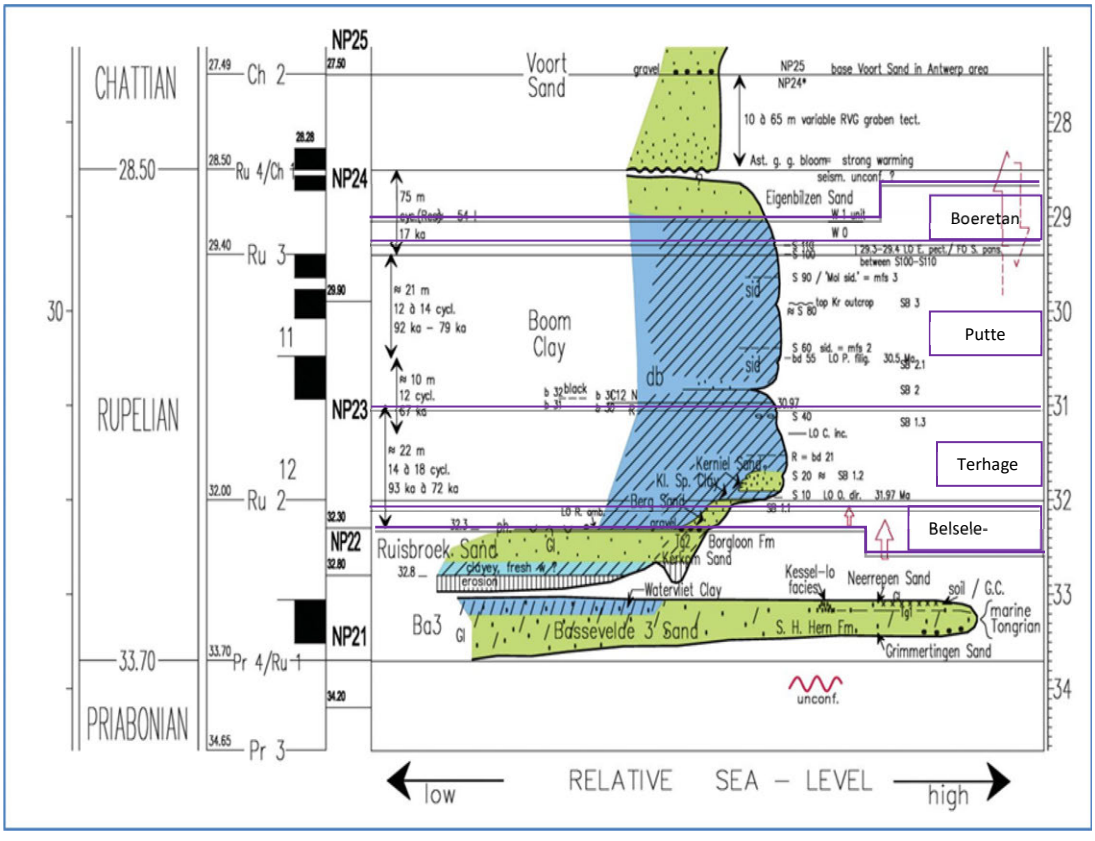

Source: Modified from Vandenberghe et al., 2004.

Note: In green are shallow marine and coastal deposits; in blue are deep marine clays. Lithostratigraphic Subdivisions are shown in purple.

The occurrence area of the Boom Clay is shown in Figure A3-2. The clay deepens to the northeast and to the east due to the presence of the Roer Valley Graben, with formation dip of approximately 1° to 2°. In subcrop, the thickness of the clay is on the order of 80 to 100 m. When the clayey silt sediments of the Eigenbilzen Formation are included, the maximum thickness of the formation is ~140 m. The outcrop zone of the Boom Clay forms a 5 to 15 km wide belt along a west-east line (roughly from the south of Antwerp, via Aarschot to Hasselt), which is interrupted in the Hageland by a deeply eroded channel filled with Diest Sands (Upper Miocene). The western outcrop zone is bounded by the Scheldt estuary and both the Rupel and Demer rivers. The Eastern outcrop is located in the Hageland and the Demer region in Limburg. At Mol, the Boom Clay is present at a depth of approximately 185 to 285 m below ground surface (b.g.s.).

The most striking characteristic of the Boom Clay, directly visible in outcrop, is its horizontal layering, which is the result of variations in grain size, organic matter content and carbonate content (Figure A3-3). Within this layering, several marker horizons (i.e. layers with distinct characteristics) are recognised. These horizons are labelled, or shown, in Figure A3-3 and Figure A3-4 (as indicated below).

Examples of such markers are the “pink horizon” (“R”), the boundary between the grey clay (Terhagen Member) and the black clay (Putte Member), the “double band” (“db”), and all septaria horizons. Septaria are carbonate concretions with similar characteristics (size, composition and mineral precipitates on their septae) within one single horizon. Their size can vary from a few tens of centimetres up to almost 2 m, and their height is confined to 40 cm. These marker horizons are recognised in outcrops and in boreholes and enable study of the lateral continuity of the Boom Clay over very long lateral distances.

The basal member of the Boom Clay (Belsele-Waas) is comprised of two thick silt layers. It is overlain by the Terhagen Member, a grey clay with a small number of distinct black stained layers. This unit contains dispersed carbonate in its lower part and three septaria horizons. It also contains the pink horizon (“R”), a reddish- to brown-coloured band, depending on humidity conditions of the clay surface, which corresponds to a maximum flooding surface (“mfs”). The top of the member is defined by the sudden and systematic occurrence of black bands in the overlying clay. This clay, the Putte Member, is rich in vegetal organic matter. A large amount of pyrite is associated with the organic matter as well. In this member, the coarse-grained silty double band (“db”) occurs, and also the typical sideritic septaria level S60, the latter corresponding to another maximum flooding surface. The top unit or Boeretang Member is defined on the basis of geophysical loggings. It was formerly noted as a “Transition zone” or “10-WIG zone” (due to its ten characteristic resistivity peaks). This member gradually becomes coarser, with silty clay layers and clayey silt to fine sand.

The Boom Clay belongs to a series of Paleogene deposits formed in the North Sea Basin. The structural features of the North Sea qualify it as an epicontinental sea. Tectonically, the Rupelian represents a time interval of intense Alpine deformation. The geographical extension of the Boom Clay and other Rupelian clays – over what could be considered the northern European branch of the Paratethys – involved significant subsidence of that area. Sedimentation initiated under sub-tropical to warm temperature climate conditions, and evolved to colder and drier conditions towards the Late Rupelian. A sudden cooling, caused by the tectonic separation of the continental land masses of Antarctica, South America and Australia, marked the start of the Oligocene.

The Boom Clay has been subjected consistently to subsidence, with the exception of a short period of uplift during the Chattian (27-24 Ma, see Figure A3-4). New findings indicate that the Central Campine experienced large-scale erosion and denudation over the last 1 Ma. The Boom Clay at Mol may have been buried as much as 20 to 30 metres deeper than its present depth (not shown in Figure A3-4).

Figure A3-2: **Isohypse map of the top of the Boom Clay**

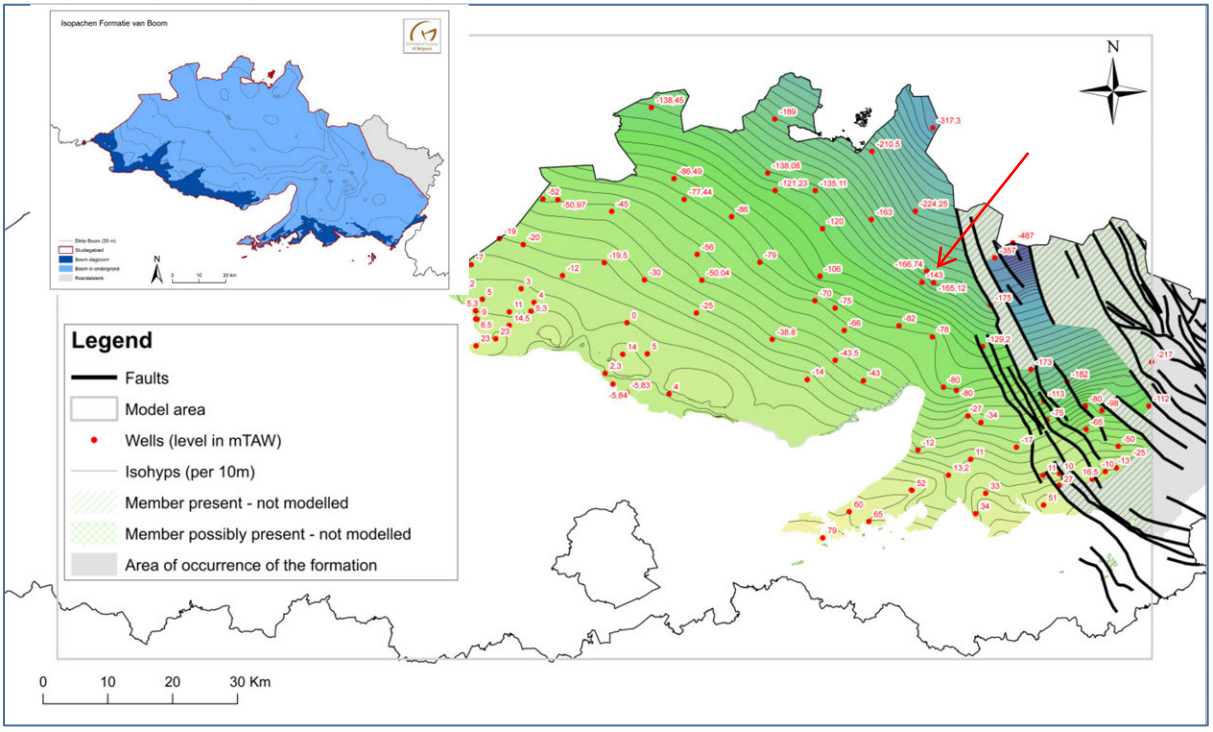

Source: Welkenhuysen et al., 2012; courtesy of Geological Survey of Belgium.

Note: The Red Arrow Points to the Nuclear Zone of Mol-Dessel. Inset is an Isopach Map of the Boom Clay with the Outcrop Zone in Dark Blue.

Figure A3-3: **Geophysical logging, gamma ray and resistivity, through the Boom Clay at herentals with indication of the marker horizons (left); Photograph of the Boom Clay in its outcrop zone with the lighter layers containing more silty material (right)**

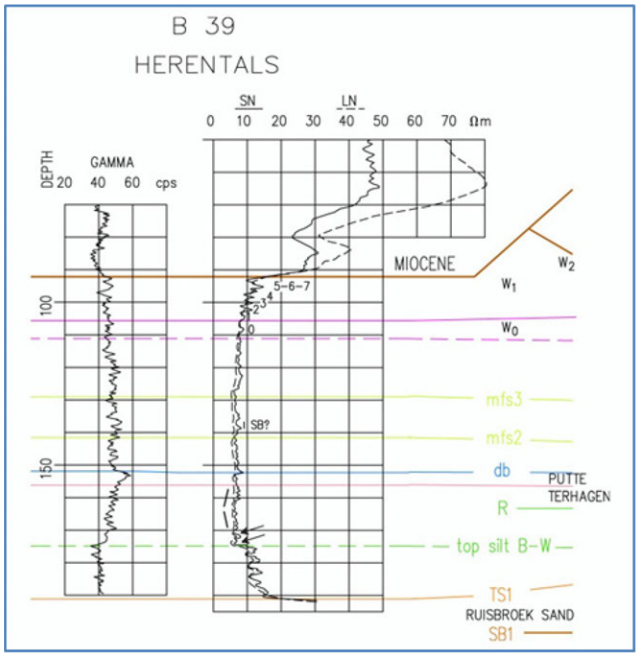

Source: Vandenberghe, 2001.

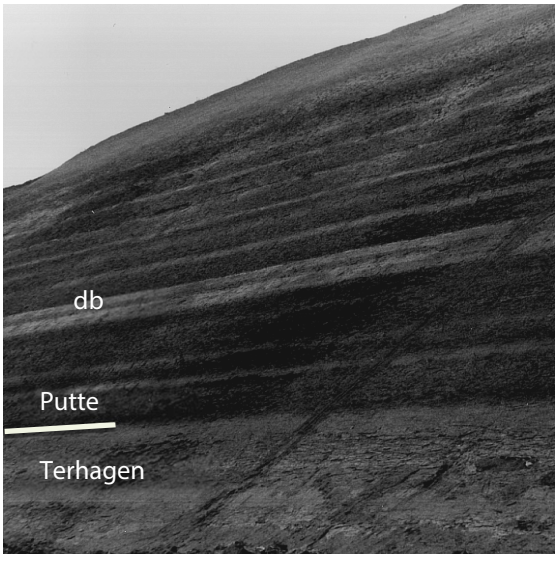

Source: Courtesy of M. De Craen.

Figure A3-4: **Burial history at Mol during the past 37 Ma**

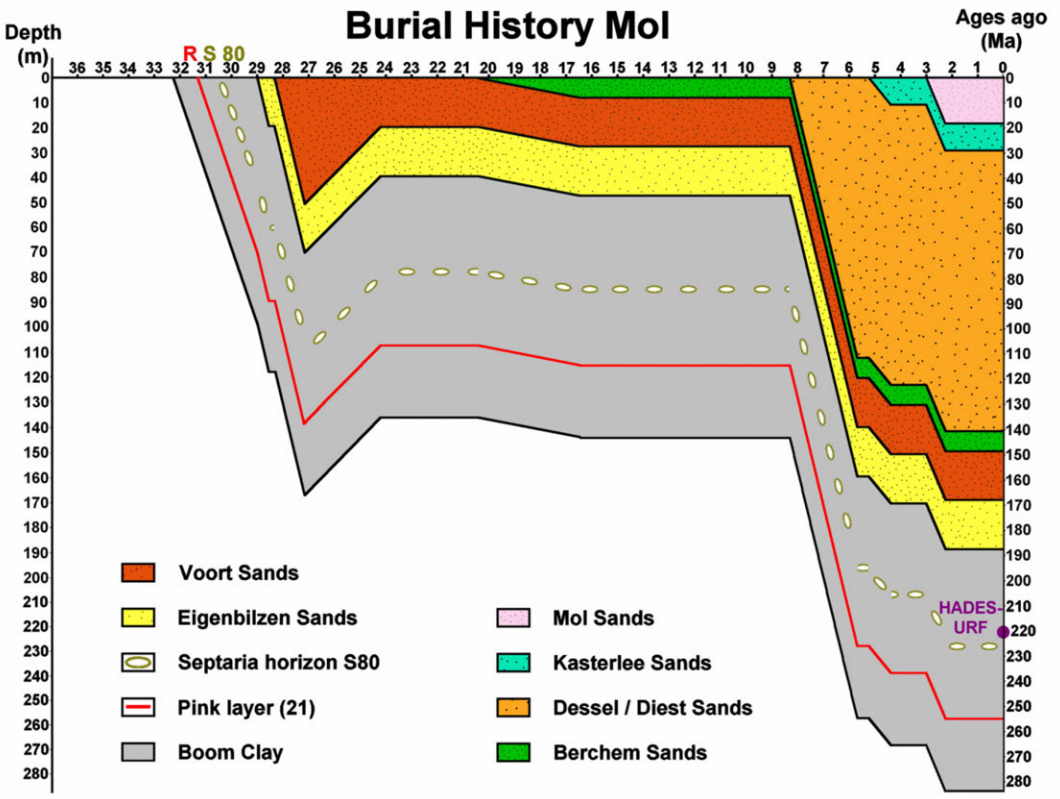

Source: Mertens, 2005.

Observed natural discontinuities in the Boom Clay are composed primarily of sub-vertical joints and slickenside surfaces. Until present, only one normal fault has been found (clay pit of Kruibeke), and its presence is related to minor differential regional tectonic tilting that occurred in the Late Oligocene.

Based on paleo-stress and SEM texture analyses, a comprehensive evolution and relationship between the joints and slickensides has been proposed by Dehandschutter et al. (2005). The low-angle slickensides form as shear bands in the plastic domain, at the maximum burial depth of the clay deposit, which was reached during the Rupelian (see Figure A3-4). The orientation of the slickensides is governed by the NE-trending extension that occurred during the Oligocene, which was related to the formation of the Roer Valley Graben. As a result of ongoing uplift associated with this process, the tectonic anisotropy increased and the fault planes developed perpendicular to the north-east extensional direction. With uplift, lower effective stress levels were reached, approaching the tensile regime where joints develop. At first, the joints were hybrid, tensional and shear (bending of clay-grain shear bands can be observed at the boundary with the joint surface). With further reduction in stress levels, the total effective stress became so low that pure tensile joints developed.

Plastic diapir-like deformations (valley bulging) are observed where the Scheldt River eroded down into the top of the Boom Clay; valley bulging is noted to occur when a local decrease in the overburden load is caused due to denudation and river incision. The horizontal stress inherited from past burial conditions largely exceeds the (reduced) vertical stress after the local removal of the overburden (river incision and erosion), which results in the vertical upward movement of the clay by several metres (Shaw et al., 2011).

Geochemistry, hydrogeology and transport properties

Geochemistry

Porewater chemistry controls the speciation of radionuclides and, hence, their mobility. It also plays an important role in the evolution of the geologic disposal system. The present Boom Clay porewater at Mol is a Na-HCO_3 solution, but it evolves to a more saline composition to the northwest. Main cations are Na, Ca, K, Mg, Si and Fe, and major anions are Cl^-, Br^-, SO_4^{2-} and HCO_3^-. Boom Clay porewater contains between 50 to 150 mg C/litre of dissolved natural organic matter, composed of humics and fulvics. In the Mol area, the Boom Clay is a reducing, slightly alkaline environment with a redox potential (Eh) lower than -270 mV and a pH of 8.3. The specific water composition is calculated with a geochemical model based on the assumption of a chemical equilibrium between the porewater and the Boom Clay rock-forming minerals. The current model assumes equilibrium conditions for calcite, siderite, pyrite and kaolinite, and cation exchange between Ca, Na, K, Mg and the porewater (De Craen et al., 2004). For the Safety and Feasibility Case 1 (SFC1), ONDRAF/NIRAS requires the building of a single internally-consistent thermo-chemical database to be used as a reference for geochemical modelling and reactive transport calculations, referred to as MOLDATA.

Hydrogeology and transport properties

In NE-Belgium, a shallow aquifer system (unconfined and semi-confined) and a deep aquifer system (confined) are considered. The shallow system comprises the hydrogeological system above the Boom Clay, while the deep aquifer system refers to the confined hydrogeological system below the Boom Clay (Figure A3-5). This subdivision is based on modelling and conceptual knowledge of groundwater flow in the region (Vandersteen et al., 2013).

The shallow system is the main source of water supply for Flanders (Northern part of Belgium). The regional groundwater flow direction is primarily from to the northwest, from a major recharge area on the Campine Plateau in the east.

For the deep aquifers, regional pumping near the outcrop zones in the south results in a decrease in the water levels at great distances to the north, inducing hydraulic gradients which effect both the magnitude of the groundwater velocities and the groundwater flow direction (as indicated by groundwater modelling results). Under natural conditions, the groundwater flow in these aquifers is west to north-west, and water balance calculations show a large influence of pumping activities on groundwater flow dynamics.

The assumed natural conditions correspond to a closed hydraulic system. The lack of an outlet for groundwater in the deep aquifer system causes almost all groundwater that enters the deep aquifer system through the Boom Clay to return to the shallow aquifer system. Under current conditions (influence of pumping), the hydraulic system is considered to be open, where the pumping wells remove water that infiltrates the deep groundwater circulation domain. Additional recharge occurs through aquifer outcrops. The determination of the hydraulic conductivity of the Boom Clay has been ongoing for more than 30 years, and experiments have been conducted on different scales: permeameter cells, percolation experiments, piezometers around the HADES URF, macro-permeameter experiments, radial hydraulic potential profiles, and in situ tests in boreholes (MDT and Dual Packer tests). The hydraulic conductivity in the Terhagen and Putte members is fairly constant at the regional scale and is in the order of 10^{-12} m/s, although it does increase to the west. The anisotropy is approximately 2.5, with a geometric mean for K_v of 1.7 x 10^{-12} m/s and for K_h of 4.4 x 10^{-12} m/s at Mol (Yu et al., 2011).

The dominance of diffusion in comparison with advection is demonstrated by large-scale and long-lasting (several decades) experiments in the HADES URF. Uptake of cations may occur through two main sorption mechanisms, including cation exchange and surface complexation. The former represents sorption sinks for metal cations and the cation-exchange capacity is roughly proportional to the smectite content of the Boom Clay. Surface complexation takes place between hydrolysed metals and functional groups on the solid phase. The solutes also may react with colloids present in the porewater. Migration experiments are conducted as pure diffusion tests and percolation tests (both diffusion and advection are possible in this case). The behaviour of the solutes of interest are categorised and four groups are identified: neutral and

non-sorbing species (HTO), solutes subjected to anion exclusion (I^-), solutes influenced by cation exchange (Cs), and solutes interacting with natural organic matter (Tc).

Figure A3-5: **(A) Conceptual sketch of the shallow and deep aquifer system and its boundaries; (B) Detailed overview of the hydrogeology incorporated in the deep aquifer pumping model; (C) Extension of the DAP Model (black line) in relation to the occurrence of the Boom Clay and the asse/ursel clay (grey) and the Roer Valley Graben Fault System**

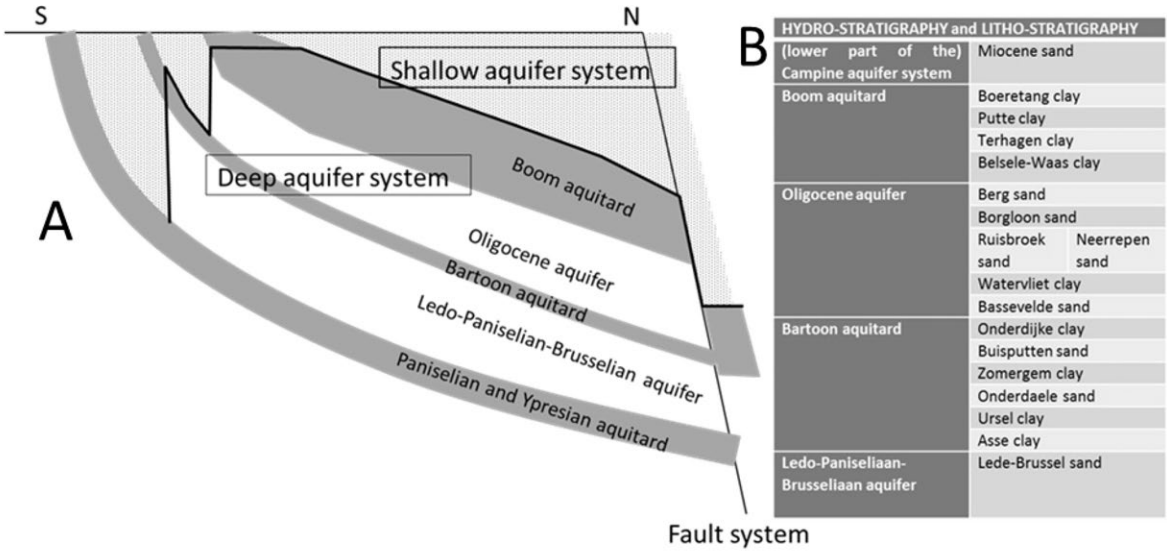

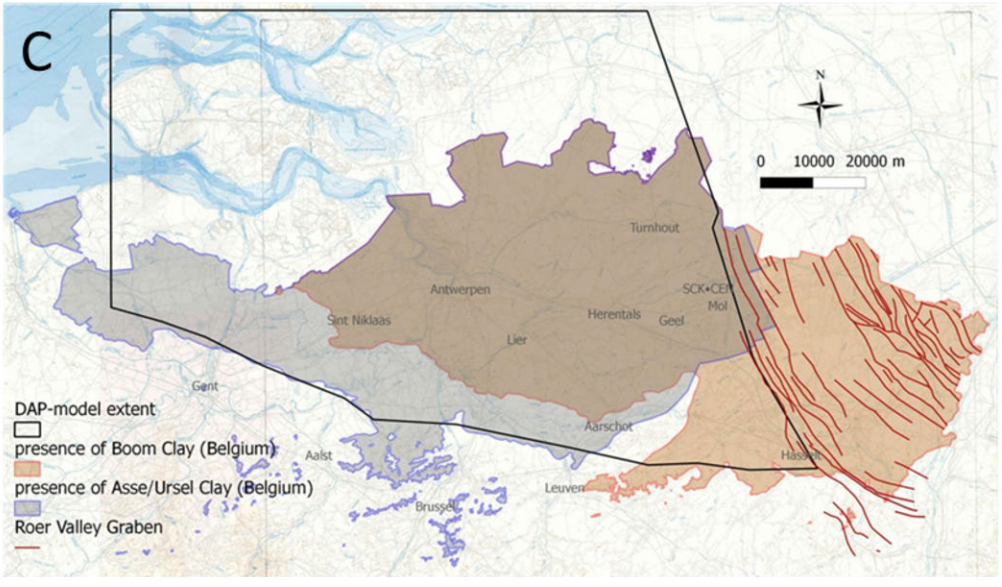

Source: Vandersteen et al., 2013.

Favourable formation attributes

Figure A3-6 depicts summary arguments developed in support of the capacity of the Boom Clay to contain and isolate nuclear waste. Key safety case arguments, detailing properties of the formation, are presented below (ONDRAF/NIRAS, 2013).

The areal extent and thickness of the lithological units allow for predictability at scales relevant to establishing safety

The geological barrier and the environment can be characterised

- From several drilling operations dispersed over the Campine area, the Boom Clay is well characterised both in vertical and lateral orientations (Vandenberghe et al., 2014).
- The key horizons of the Boom Clay, and even the clay/silt alternations and septaria horizons, recognised in outcrop (clay pits) can be identified consistently throughout the basin by means of geophysical logging tools (Vandenberghe and Mertens, 2013), demonstrating the lateral extent of the formations and marker horizons.

The presence of natural barriers (host and enclosing formations) acts to isolate the host rock and contain solutes for safety-relevant time frames

Isolation of the system is ensured during the period of concern

- The geodynamic evolution of the Campine over the next million years can be partly evaluated based on the understanding of its past evolution. Although the geodynamics of the region are closely related to the evolution of the Roer Valley Graben, the Boom Clay will roughly remain at the same depth as it is today.
- Tectonic activity is not anticipated to create major faults in this part of the Campine.
- Climate change will occur in the future, and global warming and an associated sea level rise – resulting in flooding of a large area of the Campine – cannot be excluded from considerations of future system behaviour.
  - Models show that glaciations will again occur after 400 ka from present. However, a simulated future glacial maximum (at 890 ka after present) would not result in the extension of an ice sheet into Belgium. Permafrost penetration could potentially reach a depth of 200 m b.g.s.
- Human actions in the Campine include exploration and exploitation of underground resources for economic reasons, such as drinking water, geothermy and gas storage. Therefore, drilling is one of the main human actions that can be expected to happen in the region in the future. Although such actions cannot be excluded totally, it is considered fairly unlikely that a drilling would traverse the disposal system.

Stability of the geosphere on safety-relevant time frames supported by multiple lines of geoscientific evidence/reasoning

Transport processes are anticipated to remain diffusion-dominated over geologic time frames (hundreds of thousands to millions of years)

- The dominance of diffusion over advection has been demonstrated in decades-long experiments in the HADES URF.
- Tests show that temperature increase does not influence the intrinsic permeability of the clay, although hydraulic conductivity can increase due to the decrease of water viscosity.

Water flow is limited and transport is retarded for many radionuclides

- Transport is diffusion dominated and migration is further delayed by retention processes (sorption). After the slow transport via diffusion through the Boom Clay, during which a large fraction of the radionuclides will have decayed, only a minor fraction will reach the biosphere.

Geochemical stability of the groundwater-porewater system over geologic time frames

- The Boom Clay displays a significant buffer capacity with regard to chemical perturbation. The potential chemical perturbations affecting the pH, redox potential and pCO_2 can be buffered by the minerals present, primarily by the pyrite (Eh), carbonates (pH and pCO_2) and organic matter (Eh).
- The heating of the Boom Clay leads to degradation of the organic matter, where large molecules are broken into smaller ones, increasing the hydro-soluble fraction and resulting in the production of CO_2. CO_2 production can potentially perturb the chemistry of the porewater. This perturbation will depend on the quantity of produced CO_2, the buffering capacity of the components (such as carbonates) and the diffusive transport of species whose concentrations are locally increased due to the generation/presence of CO_2.

Geomechanical stability of the formations to natural perturbations

- The Boom Clay has a remarkable self-sealing capacity.
  - Fractures induced by excavation works seal within weeks.
  - Evidence is shown by the spontaneous closure of the clay around borehole casings and underground liners.
  - In situ experiments using porewater pressure distribution in piezometers and seismic parameter measurements, as well as laboratory experiments (X-ray computed tomography), show the self-sealing capacity of the clay.
- The sealing capacity of the clay is linked, in part, to its swelling capacity (based on the clay mineralogy – especially the smectite content), which is not expected to be significantly modified due to the excavation, operations and long-term presence of a repository.

Summary and future work

ONDRAF/NIRAS intends to develop its geological disposal facility for category B and C waste in a step-wise process, punctuated by the submission of key documents to the relevant authorities. One of these documents is the Safety and Feasibility Case (SFC), a synthesis of evidence, analyses and arguments that quantify and substantiate the claim that the repository can be constructed and will be safe. The first SFC is intended to ask the competent authorities to launch the siting process. In this context, roadmaps were identified that will lead to the development and compilation of the SFC1 (ONDRAF/NIRAS, 2013).

The SFC1 should focus on, among other items, the testing of safety assessment methodologies, the refinement of the design of the disposal facility, and further characterisation of the geological barrier. The latter includes developing state-of-the-art investigation techniques to be used during a future siting process. The transferability of geotechnical properties to other locations in the Boom Clay, and to greater depths in particular, is an ongoing research topic in preparation for the siting process. Methodologies and procedures will be defined, to allow for the successful application of the preferred techniques during future siting/reconnaissance campaigns.

The recently cored drilling of ON-Mol-2 will provide additional characterisation opportunities, both of the Boom Clay and of the surrounding formations.

Figure A3-6: **Key safety summary arguments for the Boom Clay**

We have confidence in the long-term safety

- Indeed, **The system is known**
  - Indeed, The system components can be characterised
    - Indeed, The conditioned wastes can be characterised
    - and, The other parts of the engineered barrier system can be characterised
    - and, The geological barrier can be characterised
    - and, The environment can be characterised
  - and, The evolution can be bounded
    - Indeed, Siting and design favour stability
      - Indeed, Limited number of drivers
      - and Robust features
    - and For those drivers than cannot be avoided, the changes in properties and conditions can be bounded
      - indeed The evolution of the disposal system due to changes in its environment can be bounded
      - and The evolution of Boom Clay due to repository excavation, operation and closure can be bounded
      - and The evolution of the EBS with time can be bounded
- and, **The safety functions that have been defined are relied upon**
  - Indeed, Isolation of the system is ensured during the period of concern
    - Indeed, Overburden above the system remains sufficient
    - and, Human intrusion is unlikely
  - and, Containment is ensured during at least the thermal phase
    - Indeed, No loss of integrity
  - and, Rate of radionuclides transport is low and some radionuclides are delayed
    - Indeed, The release rates from the waste forms are limited
      - Indeed, Waste forms have a limited degradation rate
      - and The solubility of many radionuclides is limited
    - and, Water flow is limited
      - Indeed, No permanent bypass
      - and Limited driving forces
      - and Limited availability of mobile water
    - and, Transport is retarded for many radionuclides
      - Indeed, Host formation displays sorption capacity for many radionuclides
      - and Dissolved NOM does not excessively reduce the retardation
- and, **The performance of the disposal system meets the requirements**
  - Indeed, The radiological impact meets the regulatory requirements
  - and, The environmental impact meets the regulatory requirements
  - and, The disposal system meets conditions arising from the consultations and included in the technical solution
- and, **The remaining/residual uncertainties are identified and manageable (by RD&D, conservative assumptions, scenarios, etc.). The irreducible uncertainties do not impact the overall knowledge, understanding and safety of the disposal system.**

References

De Craen, M., L.Wang, M. Van Geet and H.Moors (2004), "Geochemistry of Boom Clay pore water at the Mol site – status 2004", Report of SCK CEN BLG-990.

Dehandschutter, B. et al. (2005), "Brittle fractures and ductile shear bands in argillaceous sediments: inferences from Oligocene Boom Clay (Belgium)", *Journal of Structural Geology*, 27(6), pp. 1095-1112.

Mertens, J. (2005), "Burial history of the two potential host formations (Boom Clay; Ypresian clays)", ONDRAF/NIRAS, note 2005-0062 (rev. 0).

ONDRAF/NIRAS (1990), "Safety Assessment and Feasibility Interim Report (SAFIR)", Report submitted to the Secretary of State for Energy (22 May 1990).

ONDRAF/NIRAS (2001), "Safety Assessment and Feasibility Interim Report 2", NIROND 2001 - 06E.

ONDRAF/NIRAS (2013), "ONDRAF/NIRAS Research, Development and Demonstration Plan. State of the Art Report as of December 2012", NIROND-TR 2013-12.

Shaw, R. et al. (2011), "Desk based study and literature review of diapirism in plastic clays and an analysis of the critical state of Boom Clay", British Geological Survey, Minerals & Waste, Commercial Report CR/11/012.

Vandenberghe, N. et al. (2004), "Stratigraphic architecture of the Upper Cretaceous and Cenozoic along the Southern Border of the North Sea Basin in Belgium", *Netherlands Journal for Geosciences*, 83(3): pp. 155-171.

Vandenberghe, N. and J. Mertens (2013), "Differentiating between tectonic and eustatic signals in the Rupelian Boom Clay cycles (Lower Oligocene, Southern North Sea Basin)", *Newsletters on Stratigraphy*, 46(3): pp. 319-337.

Vandenberghe, N., M. De Craen and L. Wouters (2014), "The Boom Clay Geology: from sedimentation to present-day occurrence. A review", *Memoirs of the Geological Survey of Belgium*, No. 60.

Vandenberghe, N. et al. (2001), "Stratigraphical correlation by calibrated well logs in the rupel group between north Belgium, the lower-rhine area in Germany and southern limburg and the achterhoek in the Netherlands", *Aardkundige Mededelingen*, 11: pp. 69-84.

Welkenhuysen, K., P. Vancampenhout and M. De Ceukelaire (2012.), "Quasi-3D model van de Formatie van Maldegem, de Groep van Tongeren en de Groep van de Rupel", *Geological Survey of Belgium*, Professional Paper, 311, 46p.

Yu, L. et al. (2011), "Boom Clay Hydraulic Conductivity, A synthesis of 30 years of research", External report of the Belgian Nuclear Research Centre, SCK•CEN-ER-122.

Ypresian Clays – Belgium

Introduction

Since the first Safety Assessment and Feasibility Interim Report (ONDRAF/NIRAS, 1990), the Ypresian clays, a non-indurated clay unit in Belgium, have been proposed as an alternative host rock to the Boom Clay (Secretary of State for Energy, 1990; ONDRAF/NIRAS, 2001). Today, the Ypresian clays are considered to be a potential host rock formation for a deep geologic repository (DGR). For these clays, the degree of knowledge is currently at the level of parameter characterisation.

The Ypresian clays, which are present in the northwest part of Belgium, have geological characteristics similar to those of the Boom Clay. Therefore, it is likely that any development and/or considerations of a disposal system in the Ypresian clays could benefit from the knowledge acquired in the characterisation activities performed on the Boom Clay. ONDRAF/NIRAS has carried out several studies and exploratory boreholes in the Doel-Kallo area, the reference zone for RD&D (research, design and development) in the Ypresian clays. The first drilling campaign took place in Doel in 1998, and the second one in Kallo in 2009, both of which were followed by a thorough programme of laboratory experiments on the collected core samples. The information presented here is based primarily on the data acquired during the Doel-Kallo drilling campaigns.

Disposal concept

At present, ONDRAF/NIRAS assumes that the same disposal concept for the Ypresian clays as that developed for the Boom Clay.

Formation properties

Geology/structure

The term “Ypresian clays” is an informal name for a relatively thick sequence of dominantly fine-grained sediments deposited early in the Eocene (about 54 to 51 Ma ago). These clayey units belong to the Kortrijk and Tielt formations (ONDRAF/NIRAS, 2001). The lithostratigraphic subdivision of the Ypresian clays was recently subject to revision by the Belgian Stratigraphical Commission, in order to clarify and pinpoint the boundaries of the various members based on geophysical borehole loggings.

The Kortrijk Formation is, from bottom to top, subdivided into the following members (Figure A3-7): the few metres thick Mont-Héribu Member – forms a transgressive transition layer (not shown in the figure), along with the Orchies Member, the Roubaix Member and the Aalbeke Member. The local and typical “Zoute” Member is restricted to the north-west extremity of Belgium (Knokke). Laterally, the Roubaix Member passes into the sandy Mons-en-Pévèle Formation. The Tielt Formation is like the Kortrijk Formation, characterised by a clayey sedimentation, and is nowadays composed of the Kortemark silt at the base and the Egemkapel clay on top. Higher up in the stratigraphy, the sandy sediments (members of Egem, Bois-la-Haut and Mont-Panisel) are now grouped into the Hyon Formation. The occurrence of the Kortrijk Formation, and its lateral equivalent the Mons-en-Pévèle Formation, corresponds to the coloured areas in Figure A3-8. The two drilling sites, Doel (in 1998) and Kallo (in 2009), are indicated by red dots.

The area of occurrence of the Ypresian clays is delineated in the southeast by roughly a straight line, grossly retracing the original paleo-coastline. The sandy Mons-en-Pévèle Formation, which is not considered for geological disposal of radioactive waste, was deposited directly northwest of this line, in the broad area around Mol-Leuven-Brussels, where the thickness of the deposits is less than 100 metres (lightest grey shades on Figure A3-8). The sedimentary rocks considered as potentially suitable hosts are situated northwest of this rim of shallow-marine sediments in deeper sections of the basin. In outcrop areas, the Ypresian clays were subjected to erosion and the sequence is only partly preserved (blue areas in Figure A3-8). The Ypresian clays dip towards the north and, in northern Belgium, they are unaffected by erosion and are covered by sediments of younger age. The northerly dip angle increases slightly from west to east, and towards the north. Between the ON-Doel and ON-Kallo boreholes, an apparent dip of 0.4° is calculated, corresponding to a true dip of about 0.5°–0.6° to the north-northeast. De Ceukelaire et al. (2012) recently produced contour maps from borehole data for the base and/or top of individual members of the Ypresian clays. As a result, the depth distribution of the different members, and their thickness, is fairly well known; though the scarcity of borehole data in the northern part of the area of occurrence must be considered. No important thickness variations, or sudden depth variations, have been reported to-date. When the entire sequence of Ypresian clays are considered, the total thickness usually is ~100 metres.

Figure A3-7: **Lithostratigraphic subdivision of the Ypresian; The 'Ypresian Clays' includes the Orchies, Roubaix, Aalbeke, Kortemark and Egemkapel Members**

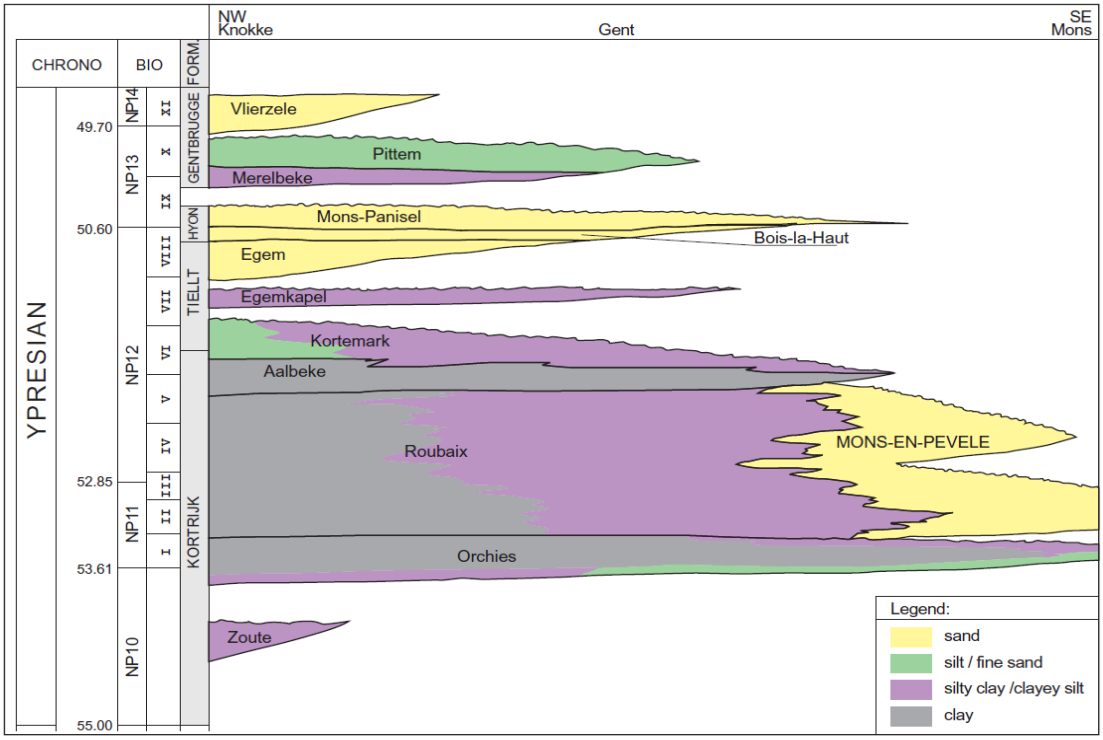

Note: *Since 2017, the Mons-en-Pévèle sand has become a formation on its own and the Tielt Formation is restricted to the clayey Kortemark and Egemkapel Members. The Hyon Formation now encompasses all sandy members (Egem, Bois-la-Haut and Mont-Panisel)*

Source: ONDRAF/NIRAS, 2001.

As a consequence of the early Eocene basin configuration, and possibly due to tectonic activity, the Ypresian clays progressively grade into near-coastal, coarser-grained deposits to the southeast (e.g. the Mons-en-Pévèle Formation). Five zones, sub-parallel to the paleo-coastline and isobaths of the early Eocene basin, have been identified, representing this gradual coarsening to the southeast. The area of interest is situated within the two westernmost zones, namely zone 1

(Knokke), where the Ypresian clays are homogeneous and the different members cannot be distinguished, and zone 2 (Eeklo-Antwerpen), where the Roubaix Member becomes differentiated – with fine silty and easterly sandy layers interbedded in the clay. The lateral continuity of the coarser-grained layers is unknown, and any systematic layering has not been reported to-date. Coarsening- and fining-upward trends at the scale of the members appears to be continuous, even across the borders of different zones, which suggests lateral continuity of the Ypresian clays (geophysical log correlation).

Figure A3-8: **Map of Northern Belgium, showing the depth below sea level for the top of the Kortrijk Formation and thickness of the Kortrijk Formation**

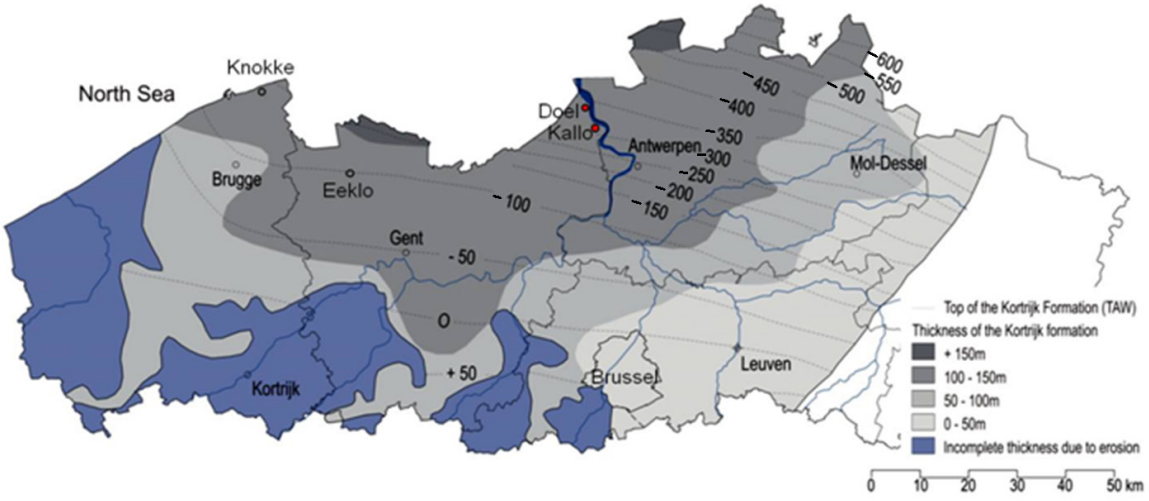

Source: ONDRAF/NIRAS, 2001.

By the end of the Cretaceous, rifting of the North Sea Basin ceased in response to opening of the North Atlantic Ocean, resulting in basin subsidence and concomitant Cenozoic sedimentation. During the latest Eocene – earliest Oligocene, the Pyrenean and Alpine collisions renewed subsidence in the basin, particularly in NE-Belgium (especially significant for the Roer Valley Graben). The Southern Bight of the North Sea Basin, where the zones of interest are located, was a shallow sedimentary basin throughout this time, and sensitive to tectonic and eustatic relative sea level changes. Mertens (2005) reconstructed a burial/erosion curve for the Doel area (Figure A3-9). This curve shows that the Ypresian clays at Doel underwent progressive burial, with only minor erosion events, and that these clays are currently, more or less, at their maximum burial depth. An important component of the progressive subsidence at Doel can be attributed to northward tilting of the basin.

There is little evidence of major tectonic faults cross-cutting the Ypresian clays in the study area. The presence of faults with large throws likely can be assumed absent. However, based on the present knowledge, which is of relatively low resolution, the presence of small-scale faults cannot be ruled out.

A number of intra-formational features, observed on seismic surveys performed in the North Sea and Scheldt Estuary, have been indicated as diapirs (or valley bulging); onshore, in quarries, sedimentary dikes have been described. Neither the nature of these structures, nor their origin, is clear at present. Intra-formational faults have been detected, however, in the Ypresian clays in the North Sea. Possibly, these structures correspond to onshore examples of intra-formational features found in some clay pits. Different models have been proposed to explain their development, but there is no consensus to-date (Dehandschutter et al., 2005). In the study area, there is a lack of knowledge as to whether or not these features are present at depth. Because controversy exists about the (chemo-hydromechanical) mechanism(s) of development of these features, their presence cannot be sufficiently predicted at this time.

Figure A3-9: **Burial History at Doel Over the Past 55 Ma**

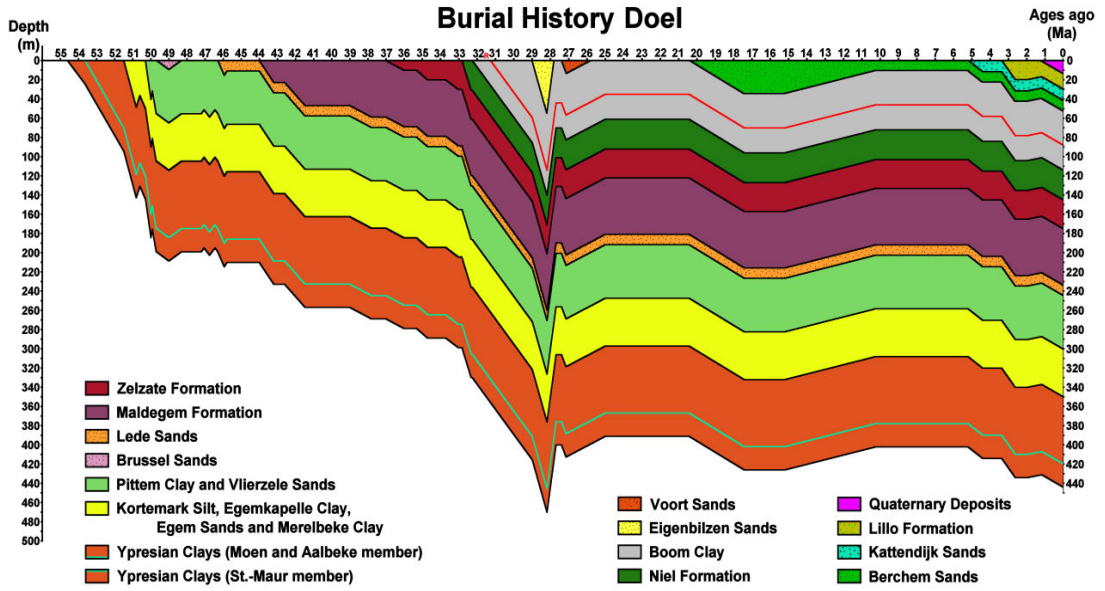

Source: Mertens, 2005.

In outcrop, where the Ypresian clays are exposed, an orthogonal system of two sets of vertical joints has been observed in the same orientation as the sub-vertical joint system observed in outcrop areas of the Boom Clay (Dehandschutter, 2004); such fracture patterns also are recognised in northern France in the London Clay, the lateral equivalent of the Ypresian clays. No observations or estimations are available for the Ypresian clays that might provide insight into the penetration depth of these joints, and/or indicate whether or not they are present at depth. In analogy with the Boom Clay, it is likely reasonable to assume that the clays in the study area are not at conditions of extensional failure at present. However, the evolution of the formations through time, including changes in burial depth, fluid pressure, horizontal stress and geomechanical parameters, are not sufficiently known to allow evaluation of whether or not the Ypresian clays in the study area were ever subjected to conditions conducive to joint formation.

Geochemistry, hydrogeology and transport properties

The hydrogeological regime in northern Belgium is characterised by alternating layers of slightly north-dipping sedimentary rock – bands of high and low hydraulic conductivities – deposited on top of the generally low-permeability, possibly fissured, solid rock of the Brabant massif.

In the western part of Belgium, the Ypresian aquitard system, corresponding to the Ypresian clays, acts as an important hydrogeological barrier, separating two main groundwater systems above and below. In the eastern part of northern Belgium, a similar role can be attributed to the Boom Clay, while the Ypresian clays wedge out and become coarser-grained, such that its character as an aquitard dissipates in that direction. The hydrogeological framework at Doel and Kallo is somewhat transitional – the Ypresian clays can still be considered as an important aquitard, and, in addition, the overlying groundwater system is further compartmentalised by the Boom Clay (among others), which act to separate distinct aquifer systems. Water-conducting layers in this area are primarily recharged in their outcrop locations to the south.

Because the infiltration/recharge areas of the different aquifers are situated at higher topographic elevations, water pressure in the aquifers is typically artesian towards the north, where the aquifers are overlain by aquitard units. Present-day hydraulic heads are influenced significantly by human groundwater extraction activities. For example, groundwater flow, which is upward in natural conditions in northern Belgium, is locally downward due to over-

exploitation. The hydraulic gradients calculated from modelled hydraulic heads in a broad zone around Doel and Kallo illustrate this local inversion of the hydraulic gradient. Tidal fluctuations have been observed in all aquifers at Doel and Kallo.

The porewater composition in the Ypresian clays (and adjacent aquifers) in the area of interest is being analysed in ongoing projects. Despite large differences in results between the Doel and Kallo boreholes, and of high vertical variability within one borehole, it appears that the ionic strength (or total mineralisation) of the porewater is relatively high. A suspected gradual increase of chloride with depth seems to be obscured by effects of pyrite oxidation (and consequential re-equilibration processes) and/or by analytical problems linked to the squeezing procedure (see Clay Conference – Fernandez et al., 2015). The most probable source of the elevated concentrations of chloride and other ions in the present setting is seawater – due to potential inputs from salty to brackish sea/estuary water intrusion, fossil intruded seawater, or connate seawater.

Favourable formation attributes

The evaluation of the Ypresian clays is currently in the stage of basic property characterisation. Safety- and feasibility-related issues will progressively be incorporated into the programme, primarily consisting of the analysis of the transferability of knowledge from Boom Clay to the Ypresian clays, based on comparison of their basic properties. A subsequent step is the development of a large-scale hydrogeological model, built to act as the basis for a simplified block model that adequately represents present-day observations and will be used, in the future, to study the effect of changing boundary conditions (long-term evolution, like erosion etc.).

ONDRAF/NIRAS considers that its safety approach is valid for disposal in poorly indurated clays, both for the Boom Clay and for the Ypresian clays. The disposal system must fulfil the long-term safety functions of containment, delay and attenuation of radionuclide release, and isolation. It is currently premature to launch safety calculations to evaluate whether a disposal system in the Ypresian clays would meet these safety functions. The following bullet points highlight some of the known properties of this argillaceous formation in the context, as much as is possible, of the three key hypotheses presented in Chapter 1.

The areal extent and thickness of the lithological units allow for predictability at scales relevant to establishing safety

- No significant thickness variations, or sudden depth variations, have been observed to-date in the early evaluations of the Ypresian clay.
- The combined thickness of the Kortrijk and Tielt formations is typically ~100 metres (or more).

The presence of natural barriers (host and enclosing formations) acts to isolate the host rock and contain solutes for safety-relevant time frames

- In northern Belgium, the Ypresian clays are unaffected by erosion and are covered by sediments of younger age.
- In western Belgium, the Ypresian aquitard (clays) system acts as an important hydrogeological barrier, separating two groundwater systems.
- The hydrogeological framework at Doel and Kallo is transitional – the Ypresian clays are an important aquitard – and the overlying groundwater system is further compartmentalised by the Boom Clay, which separates distinct aquifer systems.

Stability of the geosphere on safety-relevant time frames supported by multiple lines of geoscientific evidence/reasoning

Transport processes are anticipated to remain diffusion-dominated over geologic time frames (hundreds of thousands to millions of years)

- The hydrogeological regime in northern Belgium is characterised by alternating layers of low-dip sedimentary rock – including bands of high and low hydraulic conductivities – deposited on top of the low-permeability solid rock of the Brabant Massif. Transport properties will be further assessed as characterisation activities continue.

Geochemical stability of the groundwater-porewater system over geologic time frames

- Ionic strength (i.e. total mineralisation) of the porewater is relatively high.

Geomechanical stability of the formations to natural perturbations

- Little evidence exists to-date of major tectonic faults cross-cutting the Ypresian clays in the study area, however, the evolutionary history of the Ypresian clays in the study area is not sufficiently known to allow determination of whether or not these particular clays were ever subjected to conditions conducive to joint formation.

Summary and future work

Pending a policy decision on the long-term management of waste (i.e. that meant to be disposed of in a geological layer), ONDRAF/NIRAS continues to carry on its RD&D programme. For a first methodological Safety and Feasibility Case, intended to be finalised around 2025, some safety assessment work will be performed considering geological disposal in Ypresian clays, and if required, the safety concept will be adapted from that already developed for the Boom Clay.

References

De Ceukelaire, M. et al. (2012), "Wellbore integrity in Ypresian clays in Belgium with reference to geophysical well logs: Report of the Royal Belgian Institute of Natural Sciences", Geological Survey of Belgium, commissioned by ONDRAF/NIRAS, co-ordinated by Faninbel.

Dehandschutter, B. (2004), "Faulting and Jointing in Clay – A Geological and Geotechnical Approach. Report of investigation 2002-2004", KULeuven, commissioned by ONDRAF/NIRAS, 156p.

Dehandschutter, B. et al. (2005), "Brittle fractures and ductile shear bands in argillaceous sediments: inferences from Oligocene Boom Clay (Belgium)", *Journal of Structural Geology*, No. 27, pp. 1095-1112.

Fernandez, A.M. et al. (2015), "Characterizing Clay Pore Water Composition of Ypresian Clays from Doel and Kallo Sites, Belgium", 6th Meeting on Clays in Natural & Engineered Barriers for Radioactive Waste Confinement, Book of Abstracts, pp. 202-203.

Mertens, J. (2005), "Burial history of the two potential host formations (Boom Clay; Ypresian clays)", ONDRAF/NIRAS note 2005-0062 (rev. 0).

ONDRAF/NIRAS (1990), "Safety Assessment and Feasibility Interim Report (SAFIR)", Report submitted to the Secretary of state for Energy (22 May 1990).

ONDRAF/NIRAS (2001), "Safety Assessment and Feasibility Interim Report 2", NIROND 2001 - 06E, 2001, Secretary of State for Energy, SAFIR Evaluation Commission, Final report, Report finalized in February 1990.

ONDRAF/NIRAS (2013), "Research, Development and Demonstration (RD&D) Plan for the geological disposal of high-level and/or long-lived radioactive waste including irradiated fuel if considered as waste. State-of-the-art report as of December 2012", NIROND-TR 2013-12E.

Queenston and Georgian Bay Shale formations – Canada

Introduction

The Nuclear Waste Management Organization (NWMO) is responsible for the development, siting and implementation of the deep geologic repository (DGR) concept in Canada. Part of NWMO's mandate is to ensure that the technical expertise required to perform site characterisation activities in both sedimentary and crystalline rock is developed and maintained.

Six deep boreholes (4 vertical – DGR-1 to DGR-4; 2 inclined – DGR-5 and DGR-6) were drilled at the Bruce nuclear site (Bruce Site) in southwestern Ontario as part of site characterisation activities (2006-2010) for a formerly proposed low- and intermediate-level waste (L&ILW) DGR. The work performed allowed for detailed characterisation of the Queenston and Georgian Bay shale formations in terms of geology, geomechanics, geochemistry and hydrogeology. Shaft investigation boreholes were drilled at the former site in 2011 and the results of the geologic and geophysical analyses confirmed key parameters determined from the site characterisation activities between 2008 and 2011 (Geofirma Engineering Ltd., 2012). Though the Bruce Site is no longer being considered for radioactive waste disposal, geoscience research and development (R&D) programmes continue to be enhanced at the NWMO for both low-permeability sedimentary and crystalline rock environs.

The Queenston and Georgian Bay shales are Late Ordovician (~450 Ma) in age and are thick, near-horizontal argillaceous formations found within the Michigan Basin in southern Ontario, Canada (see Figure A3-10 and Figure A3-11).

Figure A3-10: **Bruce site location and structural geology**

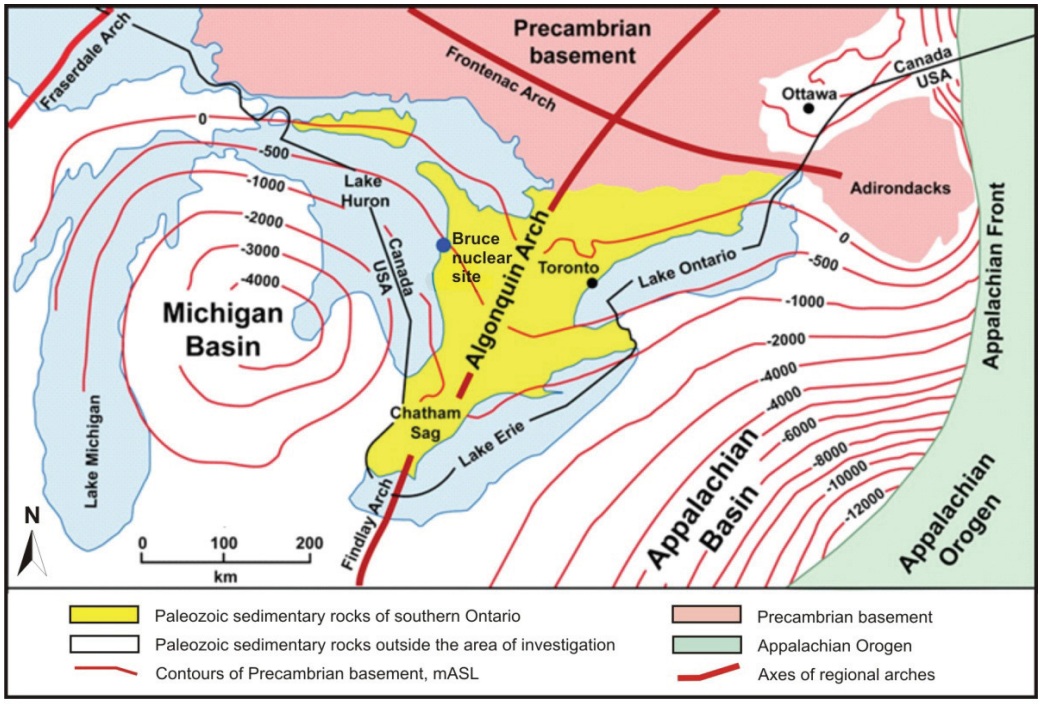

Source: NWMO, 2011b.

Figure A3-11: **Michigan Basin cross-section. Bruce Site is indicated on cross-section by DGR-2 borehole location. 3DGF defines the regional-scale model boundaries**

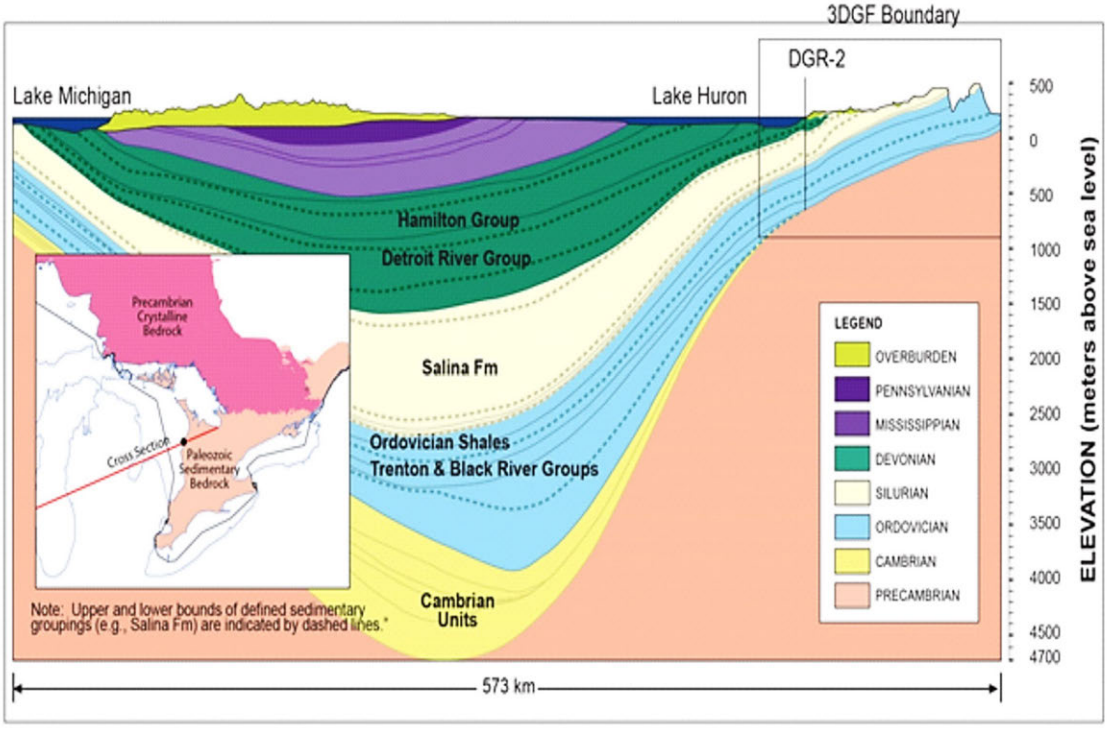

Source: Modified from NWMO, 2011b.

Disposal concept

The former design concept for a L&ILW repository at the Bruce Site is illustrated in Figures A3-12 and A3-13. For L&ILW, the disposal concept has been documented in detail in NWMO (2011a). Low-level waste (LLW) consists of non-fuel waste in which the concentration or quantity of radionuclides is above the clearance levels and exemption quantities established by the Nuclear Substances and Radiation Devices Regulations (SOR/2000-207). LLW contains primarily short-lived radionuclides (half-lives shorter than or equal to 30 years) and normally does not require significant shielding for both handling and storage purposes. LLW typically consists of incinerator ash, compacted waste, low activity ion-exchange resins and system components such as heat exchangers, feeder pipes and steam generators. Intermediate-level waste (ILW) consists of non-fuel waste containing significant quantities of long-lived radionuclides. ILW often requires shielding for worker protection during handling. ILW typically consists of resins and filters, irradiated core components, and wastes from refurbishment activities. ILW resins are stored in steel resin liners. Depending on the dose rates of the resin liners, they would be placed into disposable concrete cylindrical shield overpacks for long-term storage, to ensure that the resulting dose rates do not exceed waste acceptance criteria.

The disposal concept for high-level waste in sedimentary rock has been developed as a part of the NWMO's Adaptive Phased Management (APM) programme, which includes package emplacement and facilities design (see Figure A3-14), in addition to bentonite buffer boxes to house the used fuel waste canister (see Figure A3-15). These concepts will be adapted and/or refined, as needed, as site selection activities advance.

Figure A3-12: **Former proposed repository layout – L&ILW DGR at the Bruce Site**

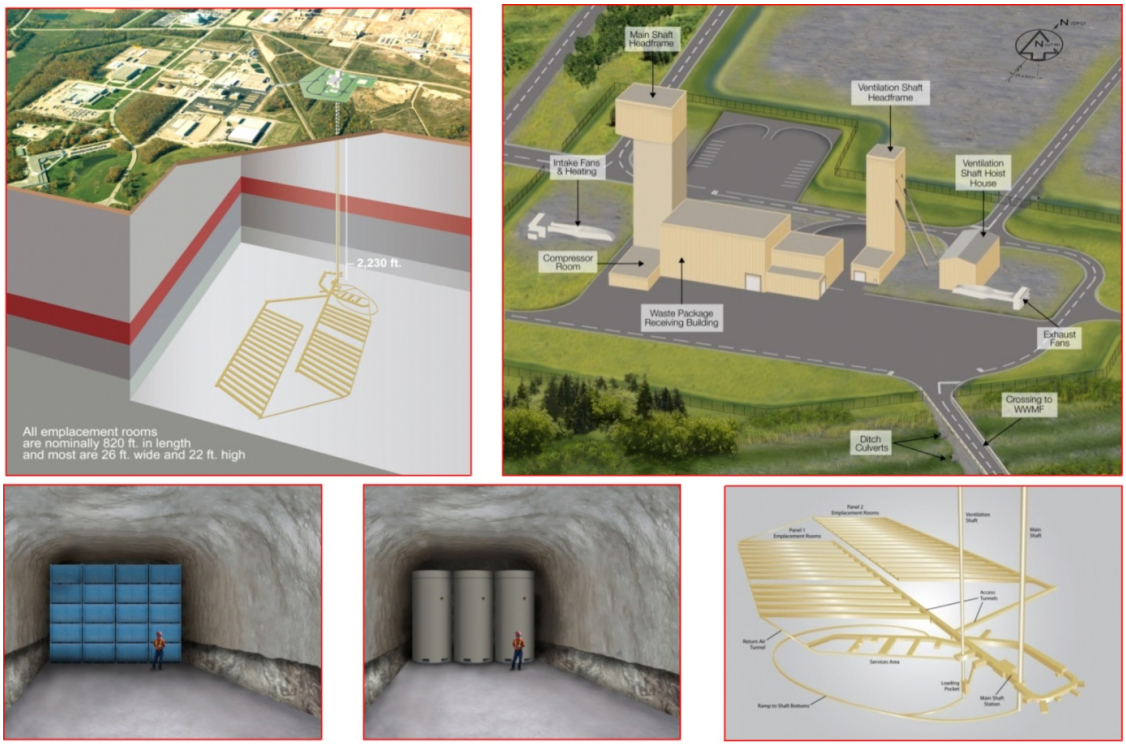

Source: NWMO, 2011a.

Figure A3-13: **Former proposed repository layout – L&ILW DGR at the Bruce Site**

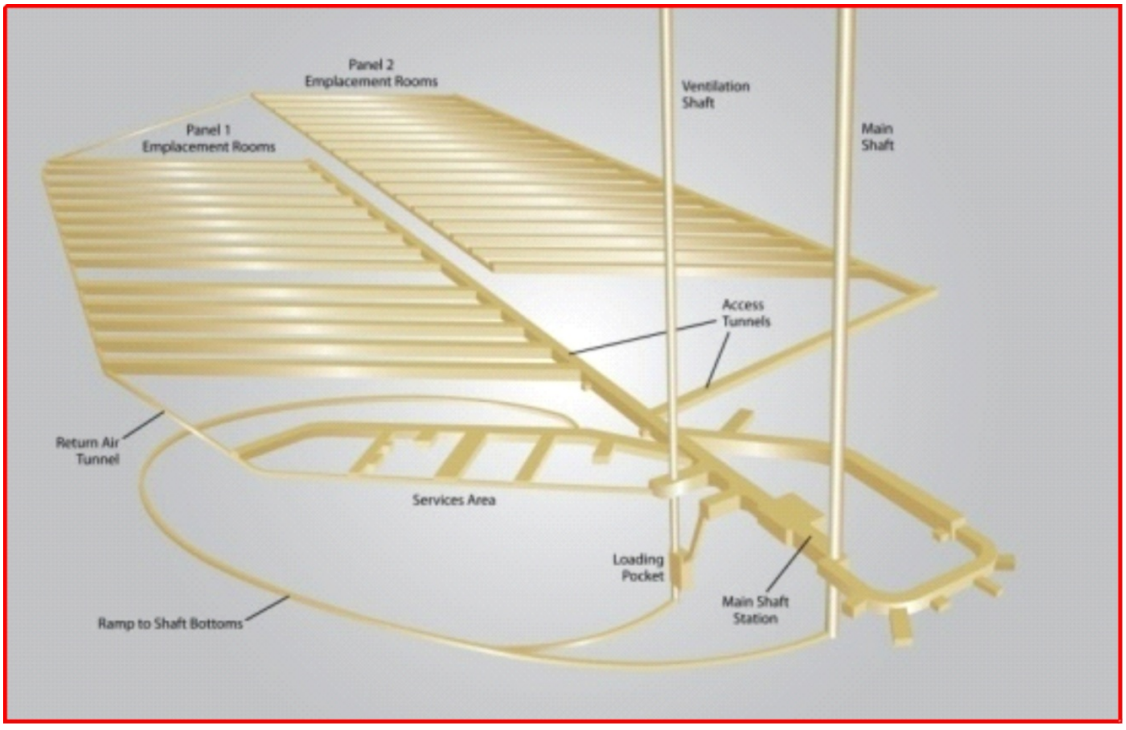

Source: NWMO, 2011a.

Figure A3-14: **Sedimentary conceptual design – canister emplacement and facilities**

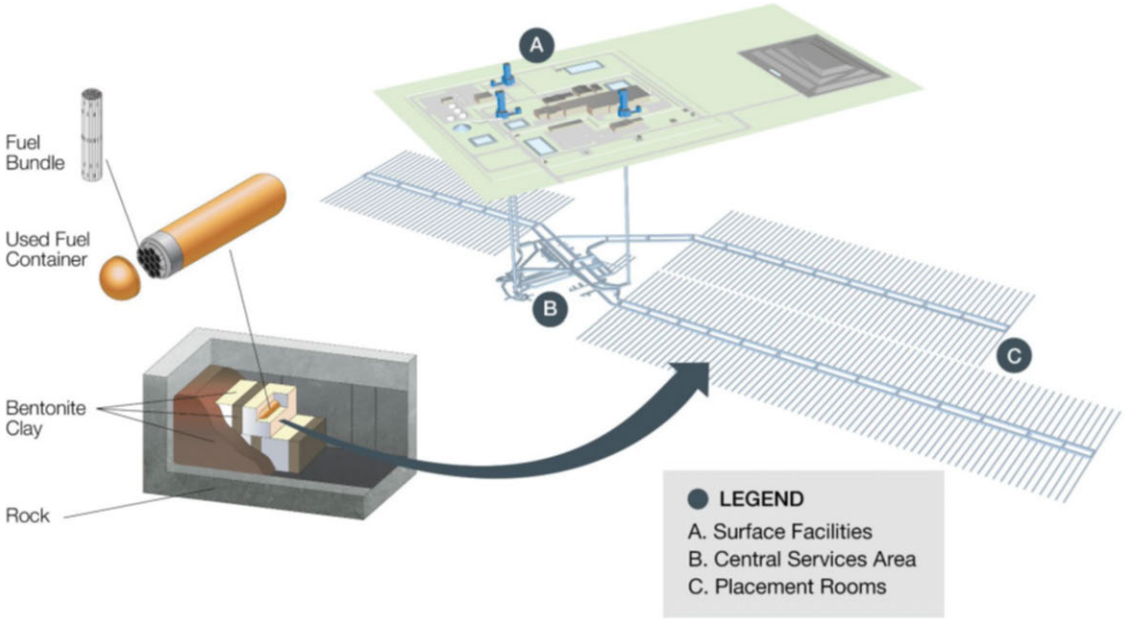

Source: NWMO, 2018.

Figure A3-15: **Fuel canister in bentonite buffer box – conceptual design**

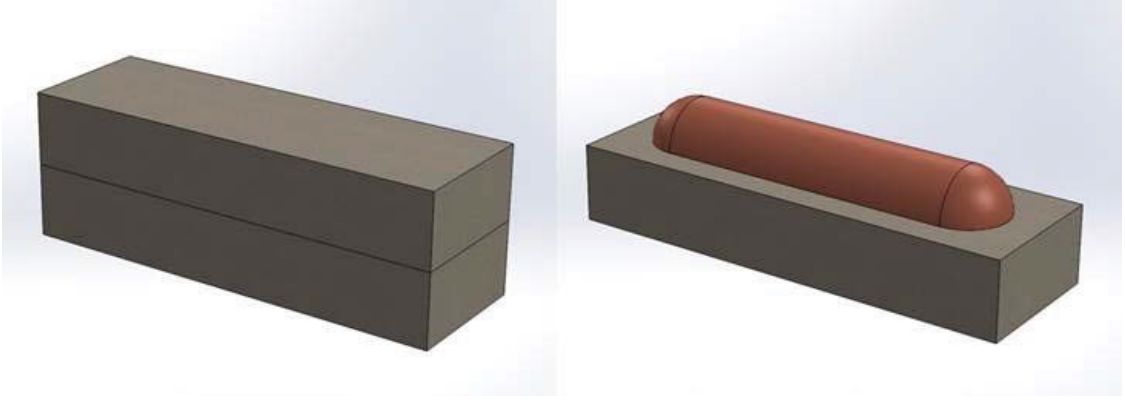

Source: NWMO, 2018.

Formation properties

Geology/structure

The lithology of the Michigan Basin consists largely of marine sediments of Cambrian to Devonian age (Armstrong and Carter, 2010) that unconformably overlie the Precambrian Grenville basement along the southern edge of the Canadian Shield (refer to Figure A3-10 and Figure A3-11). The reference Paleozoic sequence at the Bruce Site consists of 17 m of Cambrian sandstone; 5 m of Ordovician siltstone and sandstone; 179 m of Ordovician argillaceous limestone; 212 m of Ordovician shale; 324 m of Silurian dolostone, argillaceous dolostone, shale and evaporite; and 104 m of Devonian dolostone (see Figure A3-16).

Formation of the intracratonic Michigan Basin initiated with Late Precambrian mid-continental rifting and crustal extension (e.g. Sanford et al., 1985; Van Schmus, 1992), followed by accumulation of over 4.5 km of sandstones, carbonates, shales and evaporites during the Paleozoic. The sedimentary succession at the Bruce Site begins with basal Cambrian sandstone (fine to medium crystalline dolostone, sandy dolostone, argillaceous dolostone, and fine to coarse sandstone) deposited on top of granitic gneiss of the Precambrian shield. The overlying Ordovician Black River Group consists of peritidal lithographic limestones, which grade upward into the Trenton Group argillaceous shelf limestones, reflecting a major marine transgression during this period. Onset of the Taconic Orogeny in the Ordovician resulted in the collapse of platform carbonates of the Trenton Group and the westward inundation of these rocks with orogen-derived marine clastic (shale) sediments, resulting in deposition of the Blue Mountain, Georgian Bay and Queenston formations. The top of the Queenston Formation is a discontinuity associated with a global sea level drop and marks the return to carbonate-forming conditions and deposition of the Early Silurian carbonates. Restricted circulation of shallow seas in the basin – associated with arch uplift and rapid basin subsidence caused by the Late Silurian Acadian Orogeny – produced approximately 200 m of interlayered shale, carbonate and evaporite units of the Salina Formation. At the end of the Silurian, a long period of sediment exposure resulted in the formation of an erosional disconformity. Subsequent to this erosion, Devonian limestones and dolostones of the Bois Blanc, Amherstburg and Lucas formations were deposited in a major marine transgression.

The low-permeability massive Ordovician shale sequence at the Bruce Site occurs at reference depths between ~448 and 660 metres below ground surface, and is comprised of the Queenston, Georgian Bay and Blue Mountain formations, as well as the Collingwood Member shale of the Cobourg Formation.

The Queenston Formation consists of red to maroon, non-calcareous to calcareous shale, with minor amounts of green shale, siltstone, sandstone and limestone. Gypsum occurs as locally abundant nodules and thin, sub-horizontal fracture infillings. The upper 35-36 m of the formation is massive red-maroon calcareous shale with grey-green calcareous shale layers and lenses. Orange fracture infilling minerals (halite with some bounding calcite) are found in the upper 10 to 30 m. The middle ~26 m of the formation is green shale interbedded with medium to light grey, medium- to coarse-grained fossiliferous limestone layers. The bottom 10-11 m of the formation is red-maroon shale interbedded with grey-green shale layers and minor limestone beds. Mineralogically, the upper 36 m consists of: carbonates (40-85%), clays (trace to 50%), calcite fossils (0-40%), dolomite (7-10%), halite (0-10%), quartz (0-12%), gypsum/anhydrite (0-2.5%) and traces of pyrite, hematite, goethite and Fe-oxyhydroxide. The middle 26 m consists of: carbonates (25-85%), fossiliferous carbonates (0-25%), quartz (0-40%) and biotite/dark clays (10-35%), with accessory minerals of pyrite, chalcopyrite, anhydrite and celestite. The lower 11 m consists of: carbonates (3-53%), Fe-oxide/hydroxides (0-50%), illite (15-20%), and quartz (5%), with accessory minerals of pyrite and anhydrite.

The Georgian Bay Formation consists of greenish to bluish-grey shale, interbedded with limestone, siltstone and sandstone. The upper 30 m is dark grey-green shale with grey, fine- to medium-grained, occasionally fossiliferous limestone, siltstone and sandstone layers or hardbeds. The lower 60 m is dark grey-green shale with occasional layers and laminations of fossiliferous limestone, siltstone and sandstone, the frequency of which decreases with depth. The lowest hardbed is fossiliferous limestone. Mineralogically, the upper 30 m consists of: carbonates (20-75%), fossil fragments (10-35%), clays (20-40%), quartz (10-40%), anhydrite and halite (0-2.0%), and traces of pyrite, biotite, sericite and celestite. The lower 60 m consists of: carbonates (5-40%), fossil fragments (0-35%), clays (25-70%), quartz (0-10%), anhydrite and halite (0-2.0%), and traces of pyrite, sericite and celestite.

The clay minerals identified in the shales are predominantly illite and mica (typically > 50% of all clay minerals), chlorite (20-45%), and minor kaolinite and interstratified illite-smectite. The interstratified illite-smectite is predominantly illite, with only 5-10% smectite. Typically, the shales contain about 20-30% quartz, highly variable amounts of carbonate minerals, and halite is commonly observed infilling mm-scale to hairline thickness fractures throughout the shale sequence. The primary iron mineral in the Queenston Formation is hematite, while the primary iron mineral in the Georgian Bay Formation is pyrite.

Figure A3-16: **Bruce site bedrock lithology**

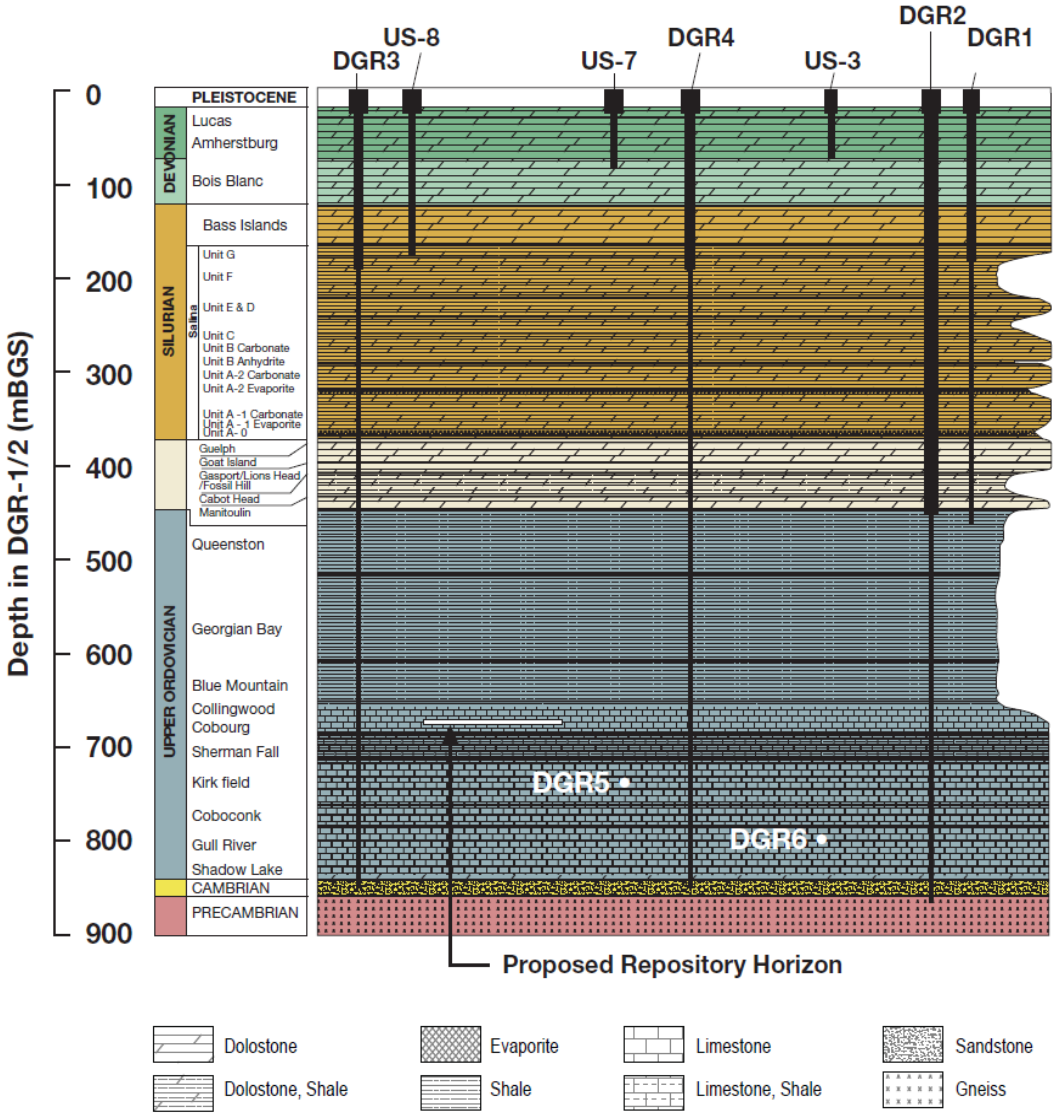

Source: Modified from NWMO, 2011b.

Based on core logging, the Ordovician shales are unfractured to sparsely fractured, with excellent core quality (INTERA, 2011). Measured averages for rock quality designation (RQD) and fracture frequency were 94% and 0.3 m^{-1}, respectively. The sparse number of measured fractures is consistent with an estimated peak burial temperature of 70-80°C, which would have been too low to stimulate the development of pervasive natural hydraulic fractures (e.g. Engelder, 2011). The temperature range reflects the marginal maturity observed for the Type II and Type III kerogen in shales of the Georgian Bay Formation (INTERA, 2011). The Queenston shales are characterised by Type III kerogen, indicating thermal immaturity (INTERA, 2011). Low total organic carbon (TOC), which averages < 1.0 wt%, is consistent with the low degree of thermal maturity. The estimated peak burial depths for the tops of the formations are ~1 446 and ~1 518 m for the Queenston and Georgian Bay, respectively, based on the burial curve developed for the Michigan Basin (Figure A3-17).

Figure A3-17: **Hypothetical burial history curves for the Michigan Basin (southern Ontario)**

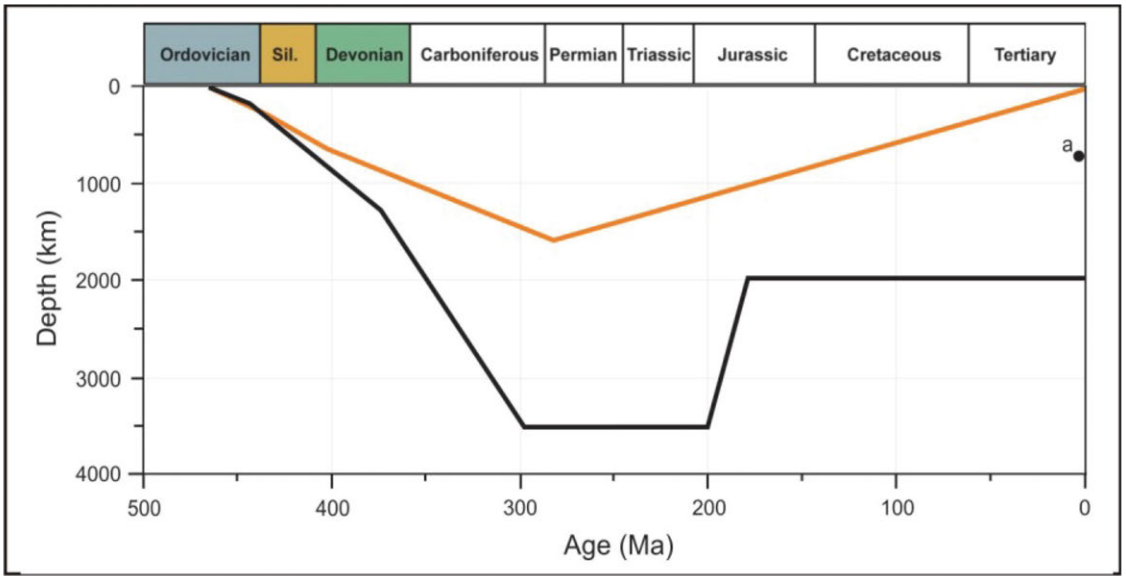

Notes: Interpretations based on Ordovician carbonate rocks – orange curve (Coniglio and Williams-Jones 1992; after Cercone, 1984), black curve (Wang et al., 1994); "a" indicates present-day burial depth (approximately 675 m) for middle of the Ordovician sequence at the Bruce Site. From NWMO, 2011b.

The shales have moderate strength, with an estimated mean uniaxial compressive strength value of 48 and 32 MPa for the Queenston and Georgian Bay formations, respectively. The region surrounding the Bruce Site is characterised as "essentially undeformed and presently tectonically quiescent with no known active faults within the Precambrian basement or overlying Paleozoic sedimentary succession" (NWMO, 2011b). The Paleozoic strata dip gently between 0.28° and 1.0° towards the centre of the Michigan Basin to the southwest. The site is located in a region generally considered to have been tectonically stable since the Paleozoic (e.g. Park and Jaroszewski, 1994; van der Pluijm and Marshak, 2004; Percival and Easton, 2007). Post-Paleozoic tectonic stability throughout southern Ontario is suggested by the relatively undisturbed sequence of Ordovician and younger sedimentary rocks overlying the Precambrian basement, as interpreted from seismic reflection data (Milkereit et al., 1992), and the recognition that the youngest strata transected by basement-seated faults in southern Ontario are Silurian in age (Armstrong and Carter, 2010). Marker bed analysis and inclined-drilling results demonstrate that the site is structurally simple and undeformed, with no significant offsets observed in the Paleozoic strata. Fracture data exhibit an orthogonal geometry, consisting of two major sub-vertical joint sets oriented east-northest and north-northwest. Detailed fracture mapping was able to prescribe a probable late Paleozoic timing for the development of the observed systematic joint and vein sets (Cruden, 2011).

The Michigan Basin is located within the tectonically stable interior of the North American continent, which is characterised by low rates of seismicity. The Queenston, Georgian Bay and Blue Mountain shale formations comprise the majority of the cap rock thickness at the Bruce Site. The presence and traceability of small-scale lithological variation (i.e. mm to cm thick hardbeds of limestone, siltstone and sandstone within m-scale horizons) is important because these features are encountered within the same stratigraphic interval in all six of the DGR boreholes, providing evidence that the stratigraphy is laterally consistent and predictable. Within the study area, enclosing the formerly proposed DGR footprint, information derived from the deep drilling programme confirms that the Ordovician formation thickness variations are on the order of metres only and formation dips are uniformly 0.59° +/- 0.08° (≈10 m/km) to the southwest towards the Michigan Basin.

Geochemistry, hydrogeology and transport properties

Geochemistry

The brines of the Michigan Basin are considered to have originated by evaporation of ancient sea water (Wilson and Long, 1993a, b). The current understanding regarding the origin of brines from the Michigan Basin is that they were formed by evaporation of sea water that was subsequently modified by: i) dilution of brines by lower salinity water; ii) dissolution of halite by lower salinity water; and, iii) diagenetic water-rock reaction processes, particularly dolomitisation. Chemistry data collected from the Bruce Site is consistent with regional-scale observations, suggesting that the brines at both the regional scale and the site-scale are of similar origin.

Porewater chemistry in the Ordovician shales are consistent throughout the entire sequence, in that the fluid compositions are relatively uniform, consisting of Na-Cl brine (average TDS ~300 000 mg/L). A uniform profile is evident in the major ions, ^{18}O and ^{2}H, as well as TDS and fluid density (see Figure A3-18; Cl, $\delta^{18}O$ and TDS). pH and Eh (calculated values) are approximately 5.5 ± 1 (computed from measured pCO_2) and -150 mV, respectively, reflecting iron and/or sulphur-reducing conditions.

The major ion and geochemical data suggest that diffusion is the dominant solute transport mechanism within the Ordovician shales.

Hydrogeology and transport properties

Based on laboratory testing, an average total porosity of ~6-8% is estimated for the Queenston and Georgian Bay formations. Numerous siltstone and argillaceous limestone hardbeds occur within the shale sequence, particularly in the Georgian Bay Formation, and these hardbeds have a lower average total porosity of about 2.5%, resulting in a bimodal porosity distribution.

Borehole straddle-packer testing shows that the average horizontal hydraulic conductivities for the Queenston and Georgian Bay formations ranges from $2.9x10^{-15}$ to $1.2x10^{-12}$ m/s, with a best estimate of $4x10^{-13}$ m/s (Figure A3-19). Based on laboratory petrophysical testing, the horizontal:vertical K anisotropy for the Ordovician shales is assigned a value of 10:1. Specific storage in the formations, based on calculations from lab measurements of rock compressibility and total porosity, is estimated to be in the range of $1x10^{-6}$ to $1x10^{-5}$ m^{-1}. The Ordovician shales are significantly underpressured as well. Although the genesis of these underpressures is ambiguous, the occurrence and persistence of underpressures are indicative of low formation permeabilities.

Laboratory diffusion testing shows vertical effective diffusion coefficients for iodide of about $1x10^{-12}$ m^2/s for the Queenston Formation, and $4x10^{-13}$ m^2/s for the Georgian Bay Formation. The values decrease slightly with depth and have a horizontal:vertical D_e anisotropy of about 2:1. The vertical effective diffusion coefficients for the hardbeds range from $3x10^{-14}$ to $4x10^{-13}$ m^2/s. The estimated iodide diffusion porosity values are 4.5% for the overall shale sequence and 2% for the siltstone/limestone hardbeds within the shales. The data display systematic variability as a function of the tracer used to make the measurements, and D_e values obtained with HTO tracer are, on average, 1.9 times greater (range of 0.8 to 4.9) than D_e values obtained with iodide tracer. This difference is attributed to the influence of anion exclusion in lowering the tracer-accessible porosity for iodide in the shales. There is also a systematic difference in D_e values as a function of the orientation of the measurements with respect to the bedding direction. The D_e values are greatest for diffusion in the orientation parallel to bedding. The anisotropy ratio (D_e parallel/D_e normal) ranges from 1 to 4 for measurements made with the iodide tracer, and from 1 to 7 for measurements made with HTO (Xiang et al., 2009). The Georgian Bay Formation contains over 700 cm-scale hardbed layers (limestone and siltstone; INTERA, 2011) that increase diffusive anisotropy, yielding a formation scale anisotropy ratio of 7.2.

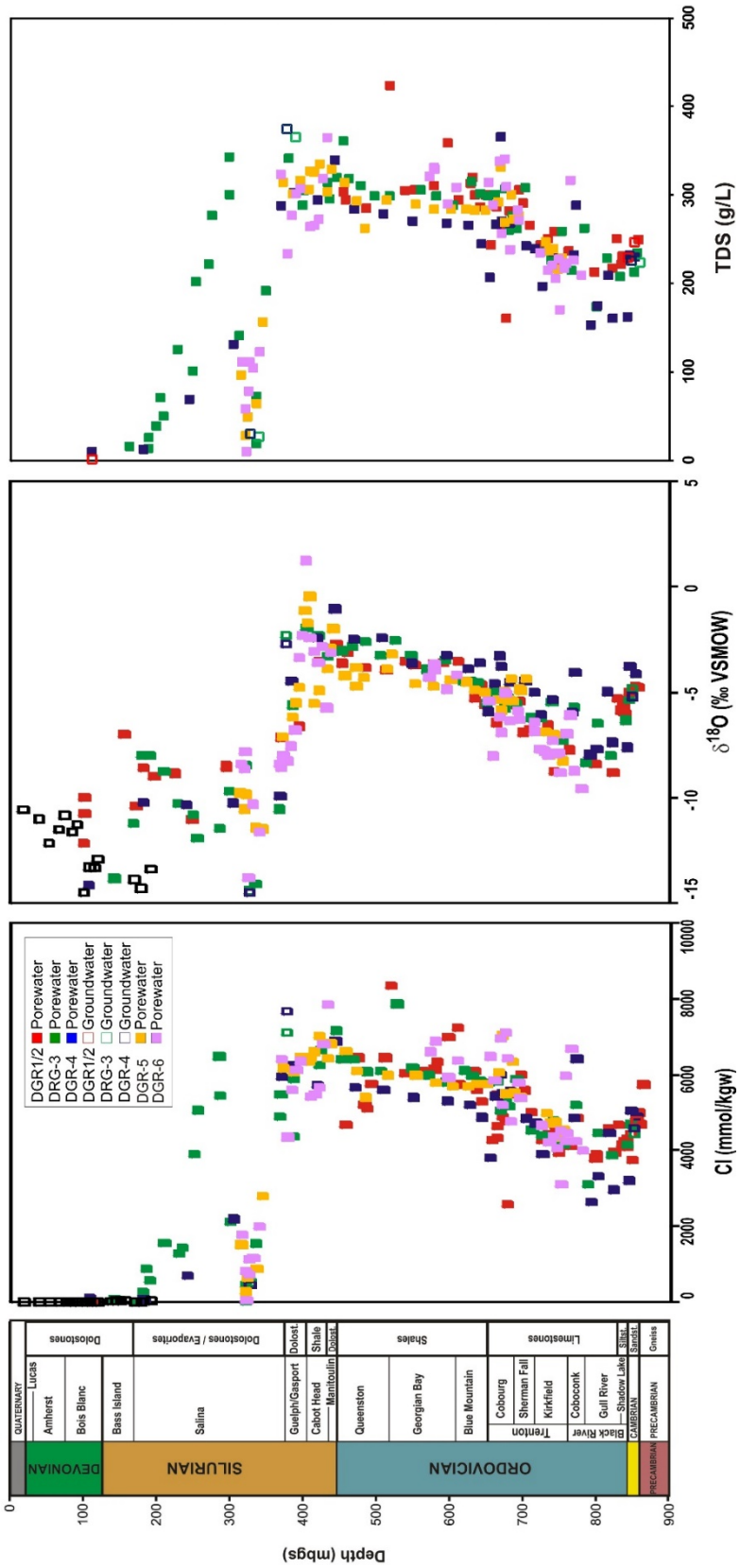

Figure A3-18: Geochemical profiles with depth (Cl, $\delta^{18}O$ and TDS; modified from NWMO, 2011b)

Péclet numbers from hydrogeological modelling simulations indicate that diffusion is the dominant transport mechanism (i.e. values < 0.4).

- Observed abnormal hydraulic heads and vertical gradients in the Ordovician and Silurian sediments at the Bruce Site strongly suggest that significant vertical connectivity across bedrock aquitards/aquicludes does not exist.
- The persistence of low hydraulic heads in the Ordovician and high heads in the Cambrian indicates that they are not connected by conductive vertical features.
- The interpretation that contaminant transport in the Ordovician shales is dominated by diffusion is strongly supported by low hydraulic conductivity values, maintenance of large hydraulic gradients, high porewater salinities, and stable water isotope values typical of deep sedimentary basin brines.

Figure A3-19: **Formation average hydraulic conductivities**

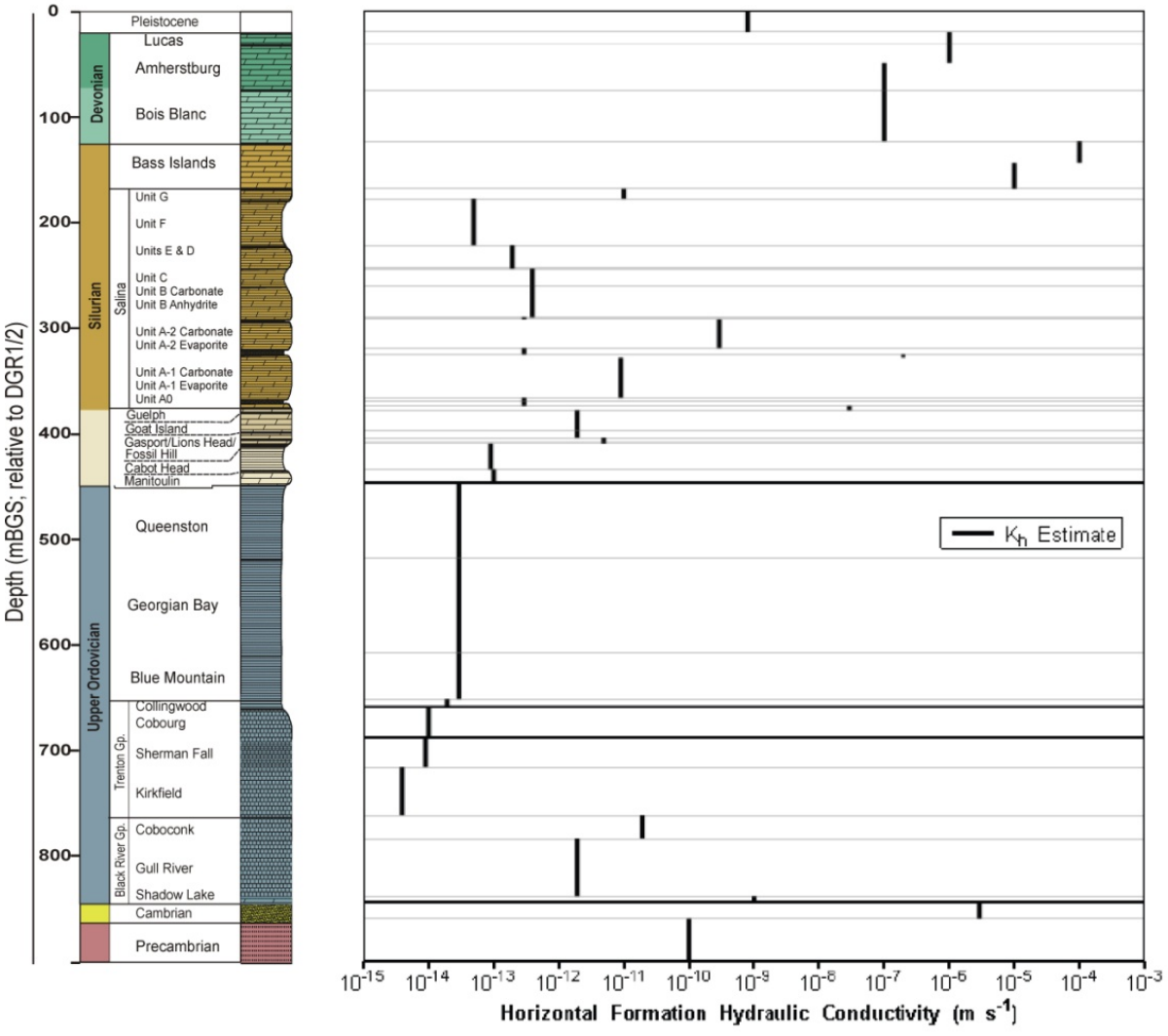

Source: Modified from INTERA, 2011.

Favourable formation attributes

The areal extent and thickness of the lithological units allow for predictability at scales relevant to establishing safety

- Comparison of the Paleozoic bedrock stratigraphy encountered at the Bruce Site to regional information demonstrates traceability of the formations at the local scale.
- A high degree of site-scale predictability, with respect to geometry, stratigraphy and physical properties of the Ordovician shales, is indicated by the uniformity between the datasets from six deep boreholes.
- The deep, horizontally-layered shale and argillaceous limestone sedimentary sequence is geologically stable, geometrically simple and predictable, and of large lateral extent.

The presence of natural barriers (host and enclosing formations) acts to isolate the host rock and contain solutes for safety-relevant time frames

- The deep shale (Queenston, Georgian Bay, Blue Mountain and Collingwood Member formations) and argillaceous limestones are thick and of low permeability.

Stability of the geosphere on safety-relevant time frames supported by multiple lines of geoscientific evidence/reasoning

Transport processes are anticipated to remain diffusion-dominated over geologic time frames (hundreds of thousands to millions of years)

- Mass transport in the Ordovician shales is diffusion-dominated, as demonstrated by the natural tracer profiles ($\delta^{18}O$ and Cl) and supported by numerical modelling (Péclet numbers < 0.4).

Geochemical stability of the groundwater-porewater system over geologic time frames

- The deep groundwater system in the shales and limestones is saline, stable and ancient, and shows no evidence of either glacial perturbations or cross-formational flow or mixing.
- The shallow groundwater system is distinct from the deep system, demonstrating it is hydrogeologically isolated from the deep, saline groundwater system (refer to Figure A3-18).

Geomechanical stability of the formations to natural perturbations

- The investigated site is situated along the north-eastern flank of the Michigan Basin in a region characterised by low seismic activity.
- There is no evidence of active faulting or seismicity at, or near, to the site.

The drilling of two pilot holes at the Bruce Site (DGR-7 and DGR-8) at the proposed location of the L&ILW DGR confirmed the key hypotheses above. No evidence was collected during the shaft investigations to contradict any of the above conclusions with respect to the predictability, stability and confining properties of the sedimentary formations (Geofirma Engineering Ltd., 2012).

Summary and future work

The NWMO R&D programme is continuously striving to improve/enhance and select the best methods and means to characterise a potential repository site in argillaceous sedimentary and crystalline rock. Work programmes are ongoing to evaluate methods for porewater extraction and characterisation, fluid pressure monitoring, hydraulic testing and assessments of mechanical strength, as well as evaluations of upscaling of properties and anisotropy.

References

Armstrong, D.K. and T.R. Carter (2006), "An Updated Guide to the Subsurface Paleozoic Stratigraphy of Southern Ontario", Ontario Geological Survey, Open File Report 6191.

Armstrong, D.K. and T.R. Carter (2010), "The Subsurface Paleozoic Stratigraphy of Southern Ontario", Ontario Geological Survey, Special Volume 7.

Cruden, A. (2011), "Outcrop Fracture Mapping", Nuclear Waste Management Organization Report NWMO DGR-TR-2011-43 R000. Toronto, Canada.

Engelder, T. (2011), "Analogue Study of Shale Cap Rock Barrier Integrity", Nuclear Waste Management Organization Report NWMO DGR-TR-2011-23 R000, Toronto, Canada.

Geofirma Engineering Ltd. (2012), "Geoscientific Characterization of Shaft Investigation Boreholes DGR-7 and DGR-8", Report for the Nuclear Waste Management Organization, NWMO DGR-TR-2012-01, Toronto, Canada.

Howell, P.D. and B.A van der Pluijm (1999), "Structural sequences and styles of subsidence in the Michigan basin", *Geological Society of America Bulletin*, No.111, pp. 974-991.

INTERA (2011), "Descriptive Geosphere Site Model", Intera Engineering Ltd, report for the Nuclear Waste Management Organization, NWMO DGR-TR-2011-24 R000, Toronto, Canada.

Milkereit, B. et al. (1992), "Seismic images of a Grenvillian terrane boundary", *Geology*, No. 20, pp. 1027-1030.

NWMO (2011a), "OPG's Deep Geological Repository for Low and Intermediate Level Waste: Preliminary Safety Report", Nuclear Waste Management Organization Report, Prepared for OPG, 00216-SR-01320-00001 R000, Toronto, Canada.

NWMO (2011b), "Geosynthesis", Nuclear Waste Management Organization Report NWMO DGR TR-2011-11 R000. Toronto, Canada.

NWMO (2018), "Postclosure safety assessment of a used fuel repository in sedimentary rock", Nuclear Waste Management Organization Report NWMO TR-2018-08, Toronto, Canada.

Park, R.G. and W. Jaroszewski (1994), "Craton tectonics, stress and seismicity", *Continental Deformation*, pp. 200-222.

Percival, J.A. and R.M. Easton (2007), "Geology of the Canadian Shield in Ontario: an Update", OPG Report No. 06819-REP-01200-10158-R00, OGS Open File Report 6196, GSC Open File Report 5511.

Sanford, B.V., F.J. Thompson and G.H. McFall (1985), "Plate tectonics – A possible controlling mechanism in the development of hydrocarbon traps in southwestern Ontario", *Bulletin of Canadian Petroleum Geology*, 33: pp. 52-71.

van der Pluijm, B.A. and S. Marshak (2004), *Earth Structure: An Introduction to Structural Geology and Tectonics*, 2nd Edition, WW Norton & Company, New York.

Van Schmus, W.R (1992), "Tectonic setting of the Midcontinent Rift system". *Tectonophysics*, 213: pp. 1-15.

Wilson, T.P. and D.T. Long (1993a), "Geochemistry and isotope chemistry Ca-Na-Cl brines in Silurian strata, Michigan Basin", *U.S.A. Applied Geochemistry*, No. 8, pp. 507-524.

Wilson, T.P. and D.T. Long (1993b), "Geochemistry and isotope chemistry of Michigan Basin brines: Devonian formations", *Applied Geochemistry*, No. 8, pp. 81-100.

Xiang, Y.L., L. Cavé, D. Loomer and T. Al (2009), "Diffusive anisotropy in low-permeability Ordovician sedimentary rocks from the Michigan basin in southwest Ontario", 62nd Canadian Geotechnical Conference and 10th Joint CGS/ IAH-CNC Groundwater Specialty Conference, 20-24 September.

Callovo-Oxfordian Formations – France

Introduction

Andra, the French National Radioactive Waste Management Agency, is responsible for assessing the feasibility of the deep geological disposal of radioactive waste in France. Andra's feasibility research has included an extensive research and development (R&D) programme, as well as the construction and development of an underground research laboratory (URL; Bure, France) in the Meuse/Haute-Marne area – focused on characterisation of the Callovo-Oxfordian clay-rich formations. Based on the results of work performed on the Callovo-Oxfordian formations, Andra now is responsible for conceiving and proposing the implementation of a geologic disposal site (Cigéo) in the vicinity of the URL site.

Andra's R&D activities are regularly assessed by various bodies, including those listed below.

- The National Assessment Board (CNE): the CNE's annual report is submitted to the Government and to Parliament (Parliamentary Office for the Evaluation of Scientific and Technology Choices) and published.
- The French National Safety Authority (ASN), which relies on the scientific and technical expertise of the French Institute for Radiological Protection and Nuclear Safety (IRSN) and advisory committees.
- Andra's Scientific Council, which evaluates the Agency's scientific strategy and the divisions' activities. It is consulted on R&D programmes conducted by the Agency and evaluates the results.
- The Guidance and Monitoring Committee (COS) of the Underground Research Laboratory, which reports to the Scientific Council, is specifically tasked with evaluating the experiments carried out at the URL.
- At the request of the French Government, the major scientific and technical dossiers that Andra submits, as required by law, can be subject to international reviews conducted under the direction of the Nuclear Energy Agency (OECD/NEA).
  - Andra was evaluated in 2012 by the French Agency for the Evaluation of Research and Higher Education (AERES).
  - In addition, the Local Information and Oversight Committee for the URL orders regular expert surveys regarding Andra's large dossiers (or specific topics of interest).

The primary function of a deep geologic repository is to isolate the waste from the surface. The current disposal concept, as developed for the Callovo-Oxfordian (and Cigéo), is described below.

Disposal concept

In concept, the repository will be located approximately 500 metres below ground, as deep disposal would protect the repository (and contents) from natural disturbances, such as erosion or glaciations, over a scale of hundreds of thousands of years (see Figure A3-20). Another function of the repository is to confine the radioactive substances and control the transfer pathways, which may, in the long term, bring radionuclides into contact with the surface environment. These phenomena operate over long time scales, during which the waste becomes less hazardous as a result of radioactive decay. The way in which the underground facility is organised, and the design of the various repository components – such as the waste packages and seals – help to confine the radioactivity and limit water movement/flow(s) within the repository after closure.

The first barrier in the safe geological disposal of radioactive waste is the material(s) used to condition the wastes. These materials are selected for their robustness and ability to prevent or slow down the release of radionuclides. One example is steel, which is used to fabricate the disposal canisters in which the most highly-radioactive waste (HLW) is encapsulated, and which must remain tight for several hundred years. HLW is incorporated into a glass structure that dissolves very slowly as well, delaying the release of radionuclides over a period of several hundred thousand years. Concrete, used for intermediate- and low-level waste (ILLW), helps to slow down the migration of radionuclides.

Confinement in the long term relies on the highly favourable characteristics of the clay layer in which the repository is located. The repository design, therefore, aims to limit any disturbances/damage to the host rock as a result of repository construction. For example, i) using construction methods that limit the extent of damage to the host rock, ii) limiting the volume of residual voids in the repository (backfilling drifts), ii) minimising chemical disturbances related to the selection of the repository materials, and iv) minimising large changes in temperature, are favourable practices to be employed that aim to maintain the original host rock properties in the presence of the repository.

The scientific studies conducted over the past 20 years on the Cigéo URL project have had the primary aim of acquiring the basic information needed to create a strong base for project development, particularly:

- detailed content (chemical and radiological) of waste packages;
- basic parameters relating to radionuclides (e.g. solubility) and repository materials for subsequent assessment of their behaviour under disposal conditions;
- properties of the geologic medium (e.g. permeability, porewater composition, thermal conductivity) on different scales (from a centimetre to ten metres), to ensure that it is suitable for housing a repository and limiting the transfer of radioactivity;
- mechanisms, such as diffusion and convection, by which elements/radionuclides are transferred to/from the materials, geologic medium or biosphere – to learn more about how such elements are dispersed in the geological medium, in what quantities, and on what scales of time and space; and
- dynamics of geological phenomena, such as erosion or hydrogeological flows in the layers of the Paris Basin, to ensure that the repository will remain stable over very long periods of time.

The results of this research have been collected by Andra and its scientific partners within national and international programmes. The work has undergone peer review, has appeared in scientific journals, has been discussed at conferences, and has provided subject matter for student theses. R&D plays a valuable part in steering Cigéo's development and in supporting its operations. The R&D programme is responsible for defining the optimum geometry (e.g. size, orientation) of repository structures, selecting design dimensions, and ensuring that construction will not impair the confinement properties of the host rock.

Thermal criteria

Maximum temperature of 90°C in the rock for the HLW repository zone

HLW is characterised by significant heat release. At this stage of the studies, in order to remain within a temperature domain that is currently well understood in terms of i) the evolution of the materials, ii) knowledge and modelling of the involved phenomena, and iii) limited or negligible impact on the properties of the repository components and Callovo-Oxfordian layer, it has been decided to define a maximum temperature of 100°C within the repository, particularly for clays (argillites and swelling clays). A margin of 10°C (i.e. a maximum admissible temperature of 90°C) has been adopted so as to take into account the uncertainties regarding the thermal properties and models associated with the thermal dimensioning of the repository.

Maximum temperature of 70°C for cementitious components, in particular for ILLW

For ILLW, because the chemical behaviour of the cement-based materials is not well understood at temperatures beyond 70-80°C, a maximum temperature of 80°C has been defined for the cement-based materials of cells. A margin of 10°C, corresponding to a maximum admissible temperature of 70°C, has been adopted for the thermal dimensioning of ILLW cells. More specifically, in the case of bituminised sludge packages, a maximum temperature of 30°C has been defined, so as to limit the creep rate and chemical reactivity of the bitumen.

Figure A3-20: **Illustrative diagram of the underground Cigéo facilities in the Callovo-Oxfordian Formation (in red : IL-LLW disposal zone ; in orange : HLW disposal zone) – Image may differ from the completed site**

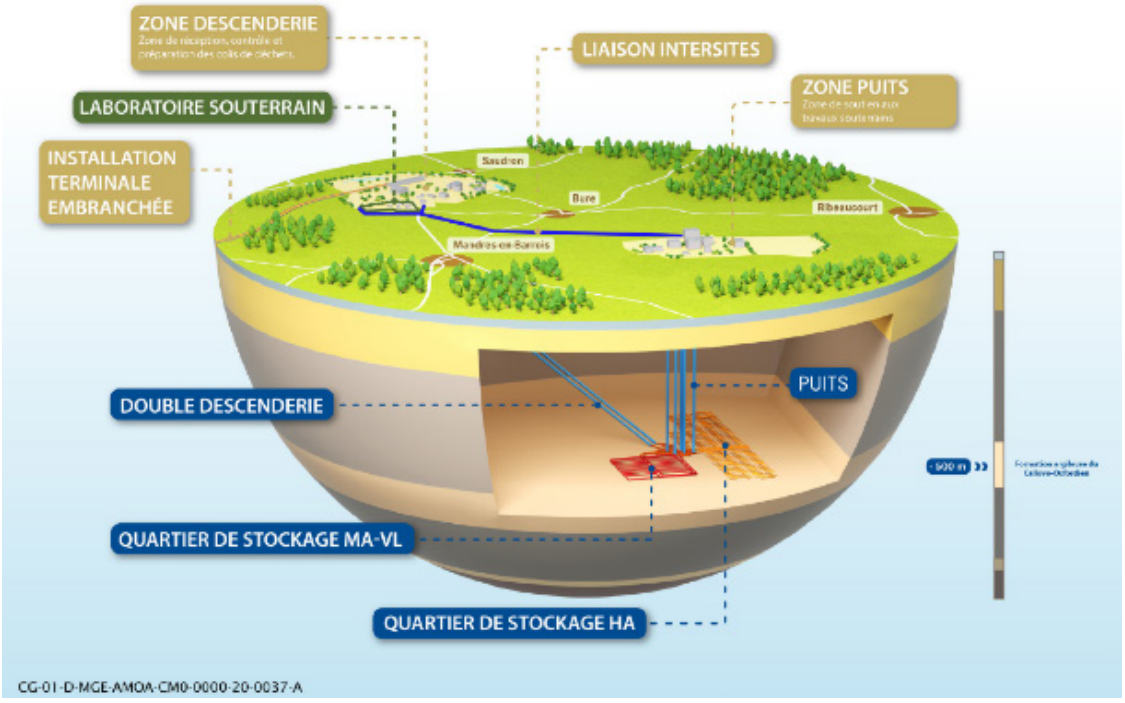

Source: Andra, 2020.

Repository zones

The repository consists of distinct zones separated by distances of several hundreds of metres from one another (e.g. the connecting drifts, connecting to the surface, and the dedicated waste disposal zones for ILLW and HLW are not adjacent to one another). A network of connecting drifts will link the repository zones and the access shafts. By its 100th year of operation, the Cigéo footprint will be somewhere between 15 km² and 25 km².

Robots will emplace waste packages in horizontal tunnels (Figure A3-21), known as cells, excavated into the clay layer. HLW will be emplaced in metal-lined cells measuring a few hundred metres in length and around 70 cm in diameter. ILLW will be emplaced in horizontal disposal cells measuring a few hundred metres in length and some ten metres in diameter. The disposal zones will be modular in design to allow waste disposal tunnels to be built over time.

Figure A3-21: **Overview of a disposal cell for HLW disposal packages**

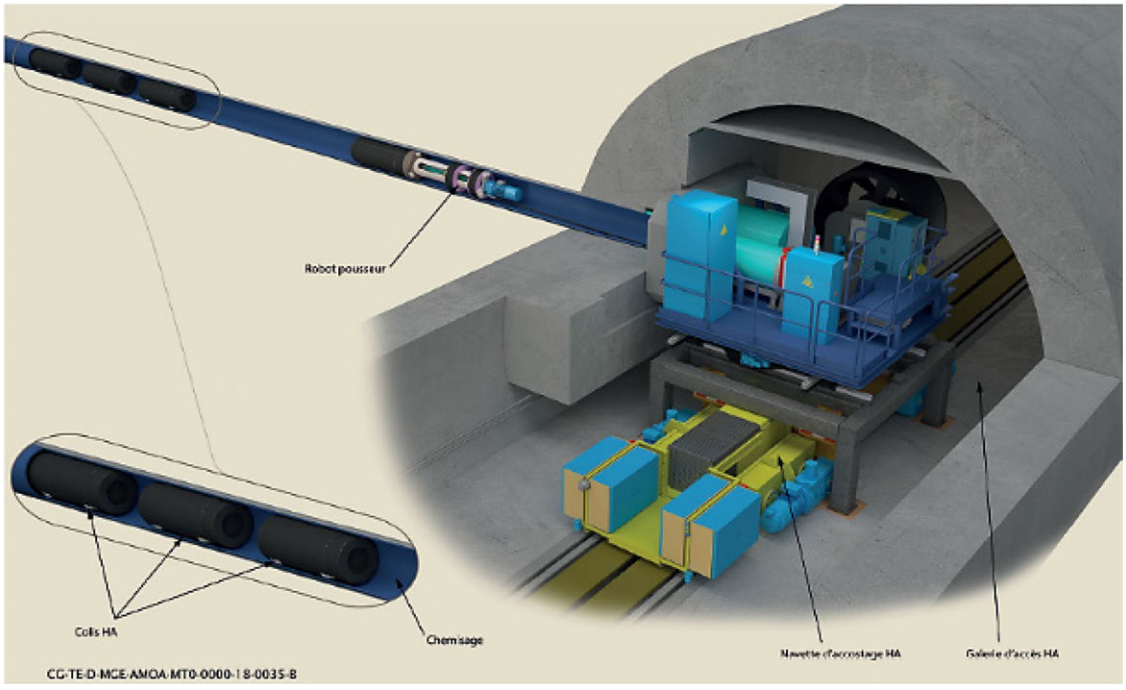

Source: Andra, 2020.

Connection infrastructure

Two types of infrastructure (Figure A3-22) will connect Cigéo's surface facilities with the underground facility. Vertical shafts will be used for ventilation, and to transfer personnel, construction equipment and materials to the underground installations. Waste packages should be transferred via a funicular along a tube known as an access ramp.

Figure A3-22: **Example of waste packages being conveyed down-ramp (left) and example of shaft head configuration for the building equipment and materials shaft (right)**

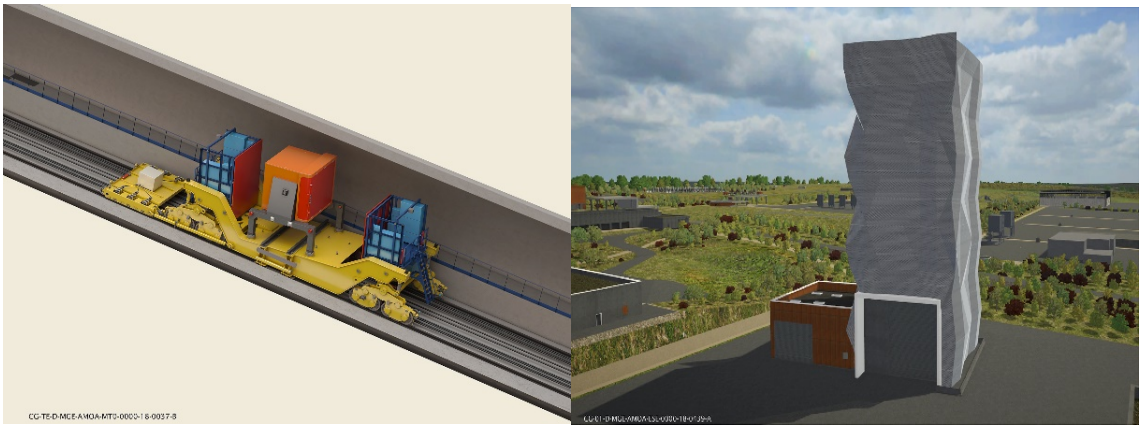

Source: Andra, 2020.

Geological formation properties

Geology/structure

Geologically, the Meuse/Haute-Marne site corresponds to a part of the eastern region of the Paris Basin (Figure A3-23). In this region, the Paris Basin is composed of alternating sedimentary layers, predominantly argillaceous and limestone, deposited in a stable marine environment during the Jurassic (165-135 Ma) (Boulila et al., 2008; Gradstein et al., 2012). These layers have a simple and regular geometric structure, and slope slightly towards the northwest (1 degree) in accordance with the general structure of the Paris Basin (bowl-shaped structure centred in the Paris area).

Figure A3-23: **3D geological block diagram of Meuse/Haute-Marne site**

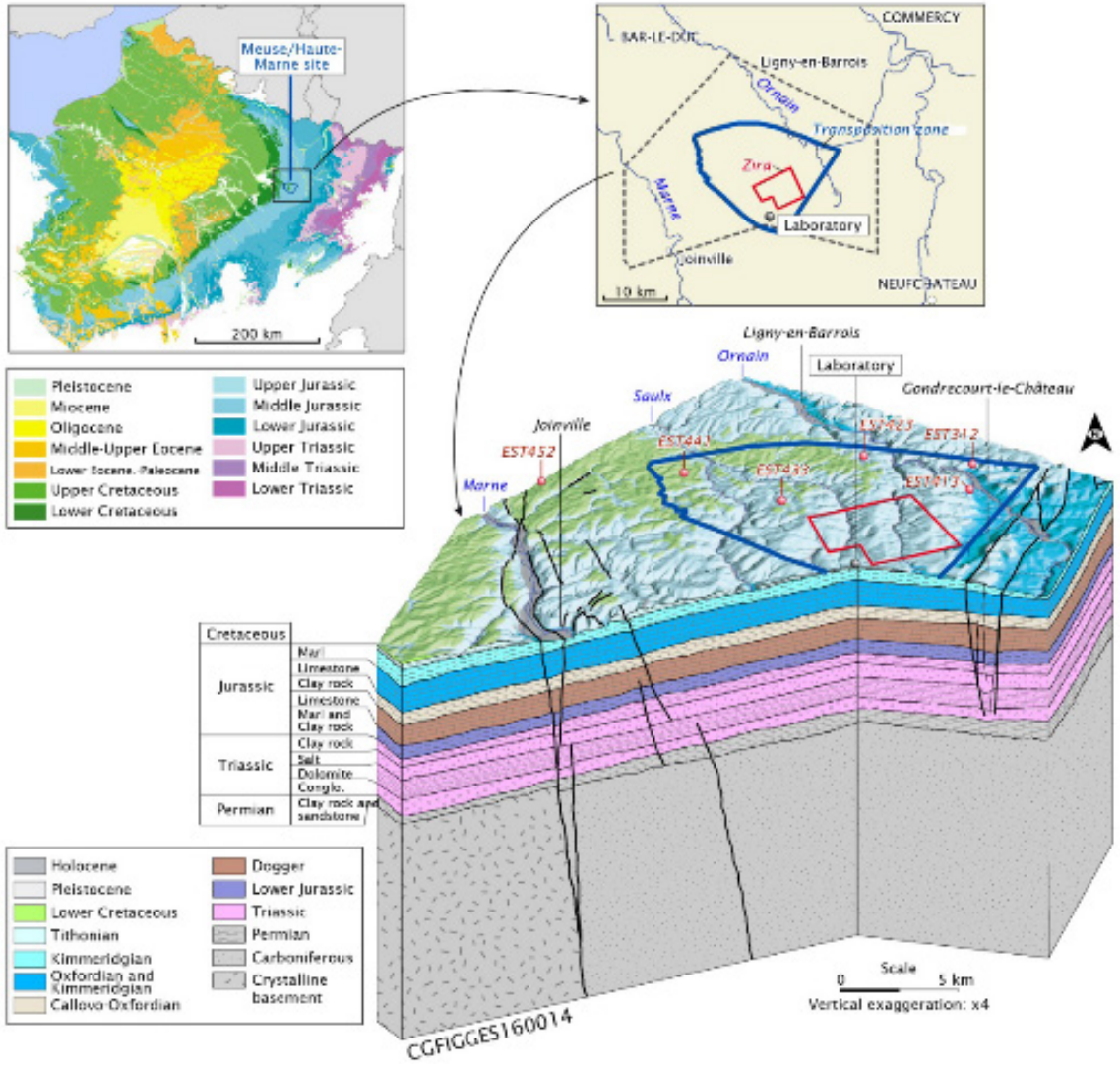

Source: Andra, 2016.

Within the sedimentary sequence, the Callovo-Oxfordian layer has been selected for hosting a deep geologic repository. This layer is dated by ammonites from the Jason zone (middle Callovian) to the Plicatilis zone (Middle Oxfordian) (Thierry et al., 2006). It is surrounded by two calcareous formations (underlying Dogger and overlying Oxfordian) containing several aquifer-type sedimentary horizons characterised by slow runoffs (approximately one kilometre per one hundred thousand years for the Darcy water velocity) (refer to Figure A3-24).

Figure A3-24: **Lithological column for the Callovo-Oxfordian Formation at the Meuse/Haute-Marne site**

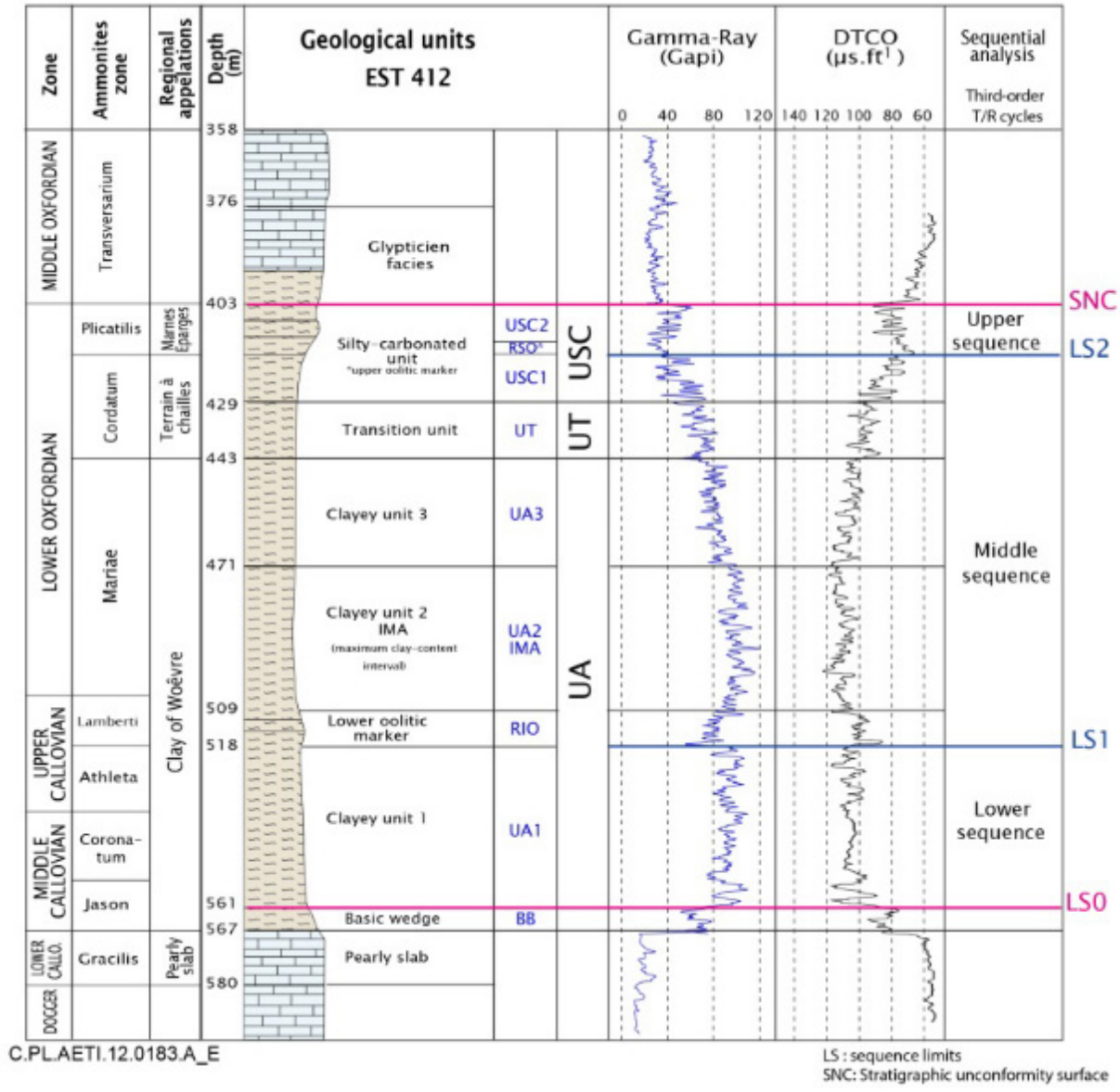

Source: Andra, 2016.

The structural framework is stable, with natural mechanical stresses oriented in the same direction for the past 20 Ma. The site is located away from large regional faults, such as the Marne Fault towards the southwest (refer to Figure A3-23). From a seismic-tectonic perspective, the Paris Basin is a stable zone with very low seismicity, remote from active zones such as the "Fossé Rhénan" (east), the Alps (southeast), the Massif Central (south) and the Massif Armoricain (west). There is no detectable neo-tectonic activity or significant local seismic activity in the Meuse/Haute-Marne region, as indicated by the national seismic monitoring network and the local monitoring network implemented by Andra. The magnitude of the maximum physically possible seismic hazard is estimated at 6.1 ± 0.4, with an epicentre conventionally located on the nearest fault ~6 km away from the URL site (Andra Dossier 2005, Référentiel du site de Meuse/Haute-Marne, Vol. 3). The 3D seismic data produced by Andra shows that no faults are present within the layer with a vertical throw exceeding 2 metres (Mari and Yven, 2014). Directional boreholes confirm the absence of secondary (sub-seismic) faults.

A one-dimensional model of burial history and thermal maturity was developed using data from the EST433 well (see Figure A3-25). Thermal modelling based on several independent geo-thermometers (apatite fission-track thermoschronology, fluid inclusion micro-thermometry, clay mineralogy and sedimentary organic matter evolution) indicates that the Callovian-Oxfordian experienced a maximum burial temperature of 50 +/- 5°C, about 25°C higher than present-day (Blaise et al., 2014). Maximum temperature was reached at the end of Upper Cretaceous. Depending on the thermal flux and conductivity considered, maximum burial depth is estimated at about 850 m ± 200 m for top of the formation.

Figure A3-25: **Burial history diagram with colour-scale temperatures**

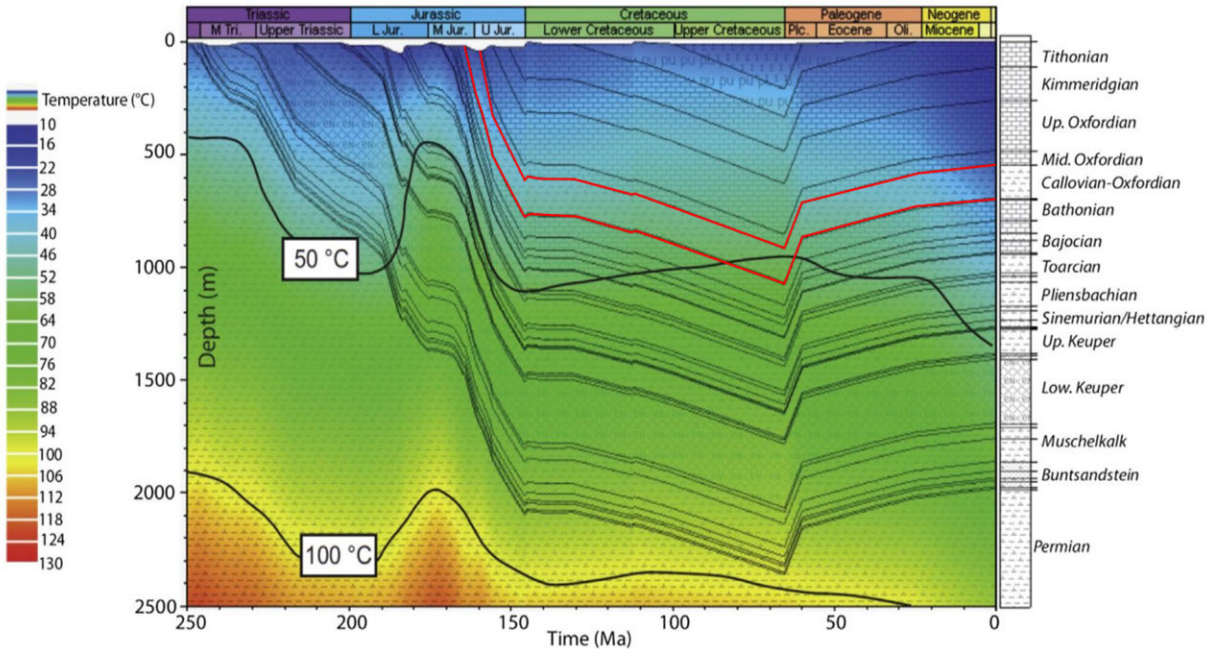

Source: Blaise et al., 2014.

Note: Reconstruction of Low Temperature (< 100 °C) Burial in Sedimentary Basins – A Comparison of Geo-thermometers in the Intracontinental Paris Basin, Marine and Petroleum Geology

The Callovo-Oxfordian formation is a sedimentary clay-rich formation. It consists primarily of clay minerals (e.g. mainly illite and illite/smectite interlayered phases), representing up to 60% of the total rock mass, as well as silts (fine quartz) and carbonates (Gaucher et al., 2004; Pellenard and Deconinck, 2006). Due to the presence of clays, the rock is featured by a nanoporous microstructure and low porosity values (15% to 18%) (Yven et al., 2007). The pore

size distribution is characterised by a median diameter of 10-20 nm (Sammartino et al., 2003; Yven et al., 2007). Built directly in the Callovo-Oxfordian formation, the Underground Research Laboratory (URL) is an exceptional facility for conducting scientific studies and characterising the combined thermal, hydro, mechanical and chemical properties of the clay rock over time.

The lower part of the Callovo-Oxfordian layer is characterised by a relative homogeneity of its mineralogical composition. This part is defined as a clayey unit (UA), subdivided into 3 zones (UA1, UA2, UA3; refer to Figure A3-24). These units have clay content > 35%. The unit UA2 is the stratigraphic level where the clay content is higher than in the rest of the formation (mean around 50%). It represents the highest-surveyed stratigraphic level in the URL.

The top of the Callovo-Oxfordian layer is characterised by units with a mineralogical composition more varied and heterogeneous, defined as the silto-carbonated units (USC). They are characterised by alternating carbonate siltstones and marls. The enrichment in carbonate content in the USC marks the progressive installation of carbonate platforms during the Upper Oxfordian. This consistent layering of the homogeneous units allows the study of the spatial (vertical and lateral) variability of physical properties of the argillite layers, properties that are known from well-logs and core measurements (Garcia et al., 2011).

Between the clayey unit and the silto-carbonated unit, there is a transition unit with intermediate properties. It consists of argillites, with interbedded thin layers of clay enriched in carbonates and siltstones.

A large zone of study for the characterisation of the geological medium was defined in 2005 by Andra, within which the Callovo-Oxfordian layer has physical and chemical properties similar to those observed at the URL. This zone is called the transposition zone (ZT). The argillites have mechanical and thermal properties favouring the feasibility of underground engineered structures at the depth of the Callovo-Oxfordian layer in the ZT (simple compression resistance > 21 MPa; thermal conductivity between 1.3 and 2.5 $W.m^{-1}.K^{-1}$, depending on the orientation of the sample with the stratigraphy). Based on the complementary studies developed on the transposition zone and in the URL, Andra proposed a 30 km^2 zone of interest for detailed survey (ZIRA) to obtain more precise information for the implementation of a future repository in 2009 (see Figure A3-26). In the ZIRA area, the depth to the top of the Callovo-Oxfordian across this zone varies from 340 m to over 530 m, and the thickness of the layer itself varies from 140 m to 160 m (Mari and Yven, 2014).

Geochemistry, hydrogeology and transport properties

The characteristics of the Callovo-Oxfordian layer were acquired shortly after deposition and have remained undisturbed since early diagenesis (< 10 Ma), as indicated by $^{87}Sr/^{86}Sr$, $\delta^{18}O$ and $\delta^{13}C$ isotopic markers, geological thermometers and the near-absence of minerals formed at a later date.

The presence of clay minerals and its associated nanoporous microstructure gives the layer high retention capabilities, combined with low diffusion coefficient values. The diffusion of anionic solutes is minimal or very slow due to the occurrence of anion exclusion phenomena (electrostatic repulsion of anions from the negatively charged clay mineral surfaces; refer to Descostes et al., 2008; Altmann et al., 2012). As a consequence, approximately half of the total porosity is accessible for anion diffusion.

The Callovo-Oxfordian formation is also characterised by low hydraulic conductivities (Delay et al., 2006) (Darcy water velocity of approximately 3 centimetres after 100 000 years), consistent with the low porosity values and the nanoporous microstructure.

The natural tracer profiles (Cl^-, Br^-, He), and marked differences in chloride concentration between the base of the Oxfordian and the top of the Callovo-Oxfordian, confirm slow solute transport dominated by diffusion (Mazurek et al., 2009; Mazurek et al., 2011).

Figure A3-26: **Perimeter of studied zones around Meuse/Haute-Marne site and position of boreholes drilled by Andra (blue: zone where the feasibility of repository was established in 2005; red: zone for the emplacement of underground facilities of Cigéo project chosen in 2009)**

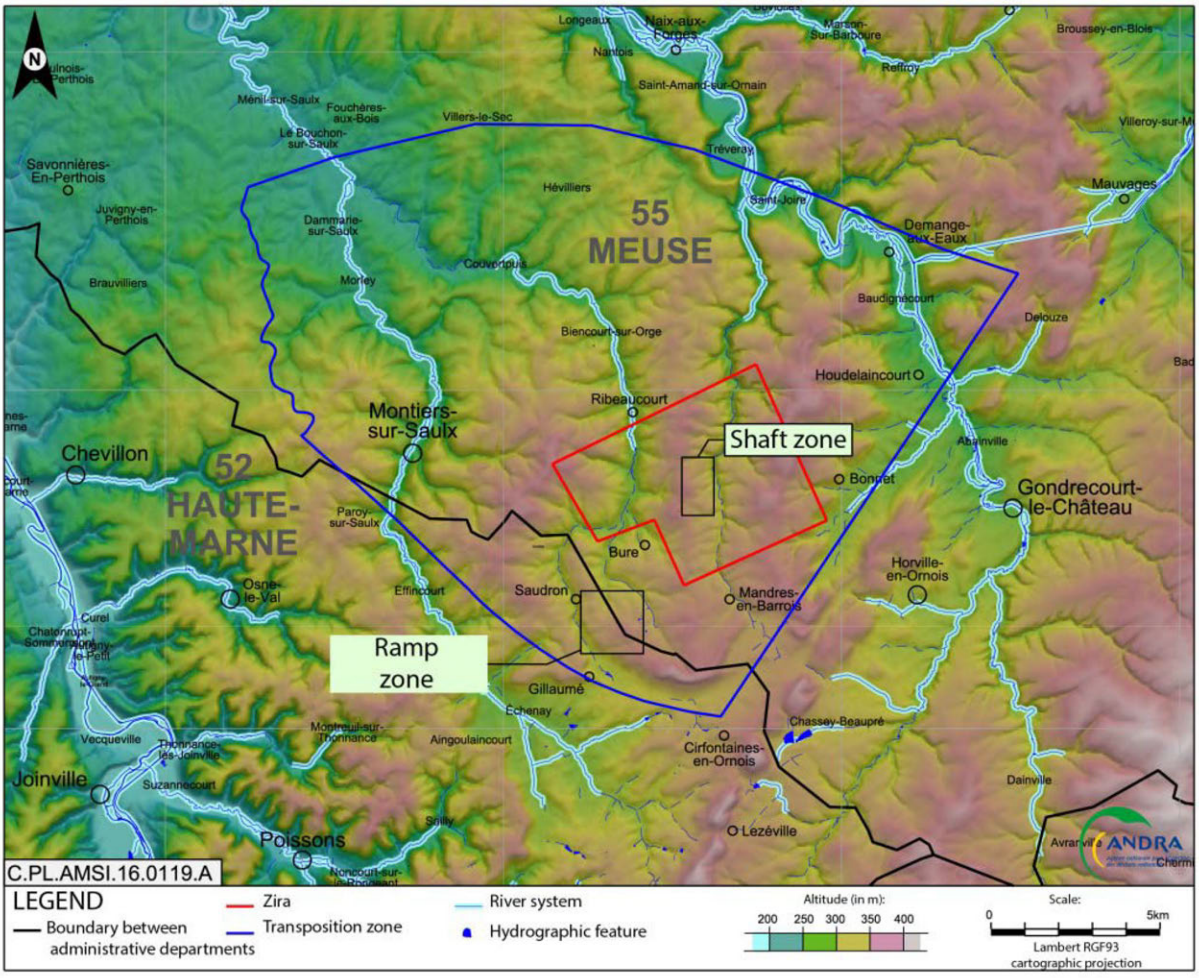

Source: Andra, 2016.

Favourable formation attributes

The following key lines of evidence are used to support the key safety hypotheses in the context of the Cigéo project and the knowledge gained from studies at the URL.

The areal extent and thickness of the lithological units allow predictability at scales relevant to establishing safety

- The modality for development of the geological formations in the Paris Basin (i.e. stable marine environment during the Jurassic, 165-135 Ma), and the stratigraphic analysis based on all drillings of the transposition zone, made it possible to predict the thickness of the formation with an uncertainty of only a few metres. The 3D seismic survey on the zone of interest for detailed investigation (ZIRA) confirmed the results (Mari and Yven, 2014).
  - The comments from different reviewers (National Evaluation Commission, IRSN, French National Safety Authority [ASN]) indicate that seismicity does not reveal/present unacceptable structures for the implementation of the deep geologic repository concept. Identified uncertainties, due to the complexity of seismic data

processing and interpretation, do not compromise the quality of knowledge acquired through the 3D seismic survey of 2010, confirming the favourable nature of ZIRA for the implementation of geologic disposal.

– The National Evaluation Commission considers that knowledge cannot be increased on the properties of ZIRA before digging direct access to the Callovo-Oxfordian by shafts and galleries during the first phase of Cigéo construction. Excavations will be an opportunity to confirm the geological model of the ZIRA.

The presence of natural barriers (host and enclosing formations) acts to isolate the host rock and contain solutes for safety-relevant time frames

- Shallow groundwater resources in the region are rare. Groundwaters are found primarily within porous horizons in the Oxfordian and Dogger sediments, in which slow water circulation occurs (Regnet et al., 2015; Brigaud et al., 2014).
- The aquifer zones show a lower percentage of smectite, with higher transport and transfer properties than in the inter-porous levels and Callovo-Oxfordian. Water productivity levels in boreholes are low for all of the porous horizons and aquifer drainage has been monitored in the laboratory shafts.

Stability of the geosphere on safety-relevant time frames supported by multiple lines of geoscientific evidence/reasoning

Transport processes are anticipated to remain diffusion-dominated over geologic time frames (hundreds of thousands to millions of years)

- Low permeabilities in the Callovo-Oxfordian formation (Delay et al., 2006; Vinsot et al., 2011), as measured on samples and in situ (more than two hundred data from pulse tests, 20 analyses from steady state and long-term in situ tests), as well as low diffusion coefficients (Descostes et al., 2008; Savoye et al., 2010) associated with load gradients of about 0.1 m/m, indicate diffusion is the dominant transport mechanism (Péclet < 0.1). Geodynamic evolution of the region over time is unlikely to change the characteristics of Callovo-Oxfordian (permeability and diffusion coefficient).
- The numerical evaluations of the geodynamic evolution of the Meuse/Haute-Marne region over the next million years show very small variations of the hydraulic gradient. Transport processes are anticipated to remain diffusion dominant over geologic time frames.

Geochemical stability of the groundwater-porewater system over geologic time frames

- The porewater composition was determined on the basis of analyses of samples from the Callovo-Oxfordian and on geochemical models (Gaucher et al., 2009). Results from the PAC experimental programme in the URL (porewater sampling for chemical and isotopic analysis) allowed precise determination of the porewater composition, including significant parameters: ionic strength, chloride, major anion concentration and total cation concentration (Appelo et al., 2008; Vinsot et al., 2008; Tournassat et al., 2015).
- The vertical profiles of stable isotopes and chloride concentrations in the water throughout the formation are interpreted to result from (low) diffusion. Minimum evolution times of about 10-25 Ma can be calculated, assuming that the initial Cl^- concentration was similar to that observed today in the Dogger aquifer (or higher).
- Water circulation in the Dogger aquifer, which was locally triggered near the end of the Jurassic (first retreat of the sea), is related to the emersion of the Paris Basin between the end of the Cretaceous, ~65 Ma ago, and the Tertiary. This emersion, related to the raising of the basin edges, caused outcropping of the major argillaceous carbonate units of the Jurassic, mainly in the entire eastern part of the Paris Basin and enabling meteoric water to circulate within aquifer formations. Isotopic data and modelling confirm the slow transfer velocities already revealed in this medium.

Geomechanical stability of the formations to natural perturbations

- The state of natural mechanical stress should remain stable over the next million years. If stress values change gradually as superficial layers are eroded, the general orientation of the stress field will stay the same for single formations. The fact that the region is more than 350 kilometres from the Alpine front, as well as slow plate velocities, explains the stability of this stress regime.
- During glacial periods, the sector is in a permafrost zone, based on observation, so there is no accumulation of ice and there is no overstressing from overlying ice. Observation has shown that fossil periglacial structures, indicative of continuous permafrost during the last glacial climate periods, are present everywhere on the site and in the surrounding region. Moraine deposits present at the regional scale indicate that the extent of the last glacial front(s) was very far from the zone of interest for detailed survey (ZIRA) (the nearest glaciers during glacial periods are localised on the Vosges mountains) (Antoine et al., 1999).
- Finally, this region of Meuse/Haute-Marne is a very stable zone from a seismic-tectonic point of view, with respect to both historic seismicity and recent geological periods. No quaternary evidence of tectonic activity has been found along the major faults surrounding the area. The maximum possible earthquake intensity is estimated at 6.1 ± 0.4 along the regional faults (Gondrecourt graben, Marne faults), with return periods of between 100 000 and 1 000 000 years (Andra Dossier 2005, Référentiel du site de Meuse/Haute-Marne, Vol. 3).

Summary and future work

Twenty years of characterisation of the geological medium – based on regional studies, boreholes, geophysical measurements, various methods and observations made in the underground laboratory – has provided detailed knowledge of the formations in terms of geometry, structure, stability, uniformity and continuity at various scales.

For the application for Cigéo creation expected in 2022, reconnaissance work continues, in addition to characterisation of the Callovo-Oxfordian at the scale of the storage area, in order to confirm and consolidate the scientific knowledge on the geometry and the vertical and lateral variability of some formation properties (hydro-dispersive, mechanical parameters).

References

Altmann, S. et al. (2012), "Diffusion-driven transport in clayrock formations", *Applied Geochemistry*, No. 27(2), pp. 463-478.

Andra (2020), "Public enquiry dossier prior to the declaration of public utility of the disposal facility Cigéo", www.andra.fr/publications?f%5B0%5D=facet_doc_cat%3A232.

Andra (2016), "Safety Options Report – Operating Part (DoS-Expl)", https://international.andra.fr/documents-and-visual-ressources.

Andra (2005), "Dossier 2005 Argile – Tome Architecture and management of a geological repository", C.RP.ADP.04.0001.

Antoine, P. et al. (1999), "La France pendant les deux derniers extrêmes climatiques, Variabilité naturelle des environnements (2 cartes au 1/1000000 et notice)", co-publication CNF-INQUA/Andra 92298 Châtenay-Malabry, France.

Appelo, C.A.J. et al. (2008), "Obtaining the porewater composition of a clay rock by modeling the in- and out-diffusion of anions and cations from an in-situ experiment", *Journal of Contaminant Hydrology*, No. 101, pp. 67-76.

Blaise, T. et al. (2014), "Reconstruction of low temperature (< 100 C) burial in sedimentary basins: A comparison of geothermometer in the intracontinental Paris Basin", *Marine and Petroleum Geology*, No. 53, pp. 71-87.

Boulila, S. et al. (2008), "Astronomical calibration of the Early Oxfordian (Vocontian and Paris basins): Consequences of revising the Late Jurassic Time scale", *Earth and Planetary Sciences Letters*, No. 276, pp. 40-51.

Brigaud, B. et al. (2014), "Characterization and origin of permeability-porosity heterogeneity in shallow-marine carbonates: From core scale to 3D reservoir dimension (Middle Jurassic, Paris Basin, France)", *Marine and Petroleum Geology*, No. 57, pp. 631-651.

Delay, J., A. Trouillerand and J.M. Lavanchy (2006), "Propriétés hydrodynamiques du Callovo-Oxfordien dans l'Est du bassin de Paris: comparaison des résultats obtenus selon différentes approches", *Comptes Rendus Geoscience*, No. 338(12), pp. 892-907.

Descostes, M. et al. (2008), "Diffusion of anionic species in Callovo-oxfordian argillites and oxfordian limestones (Meuse-Haute-Marne, France)", *Applied Geochemistry,* No. 23, pp. 655-677.

Garcia, M.H. et al. (2011), "Multivariate and spatial statistical analysis of Callovo-Oxfordian physical properties from lab and borehole logs data: Towards a characterization of lateral and vertical spatial trends in the Meuse/Haute-Marne Transposition Zone", *Physics and Chemistry of the Earth*, No. 36(17-18), pp. 1469-1485.

Gaucher, E. et al. (2004), "ANDRA Underground Research Laboratory interpretation of the mineralogical and geochemical data acquired in the Callovo-Oxfordian formation by investigative drilling", *Physics and Chemistry of the Earth* A/B/C, No. 29, pp. 55-77.

Gaucher, É.C. et al. (2006), "Modelling the porewater chemistry of the Callovian–Oxfordian formation at a regional scale", *Comptes Rendus Geoscience*, No. 338(12), pp. 917-930.

Gaucher, E.C. et al. (2009), "A robust model for pore-water chemistry of clayrock", *Geochimica et Cosmochimica Acta*, No. 73, pp. 6470-6487.

Gradstein, F.M. et al. (2012), "The geologic Time Scale 2012", DOI: 10.1016/B978-0-444-59425-9.00019-6.

Mari, J.L. and B. Yven (2014), "The application of high-resolution 3D seismic data to model the distribution of mechanical and hydrogeological properties of a potential host rock for the deep storage of radioactive waste in France", *Marine and Petroleum Geology*, No. 53, pp. 133-153.

NEA (2009), *Natural tracer profiles across argillaceous formations: The CLAYTRAC project*, NEA No. 6253, OECD Publishing, Paris.

Mazurek, M. et al. (2011), "Natural tracer profiles across argillaceous formations", *Applied Geochemistry*, No. 26(7), pp. 1035-1064.

Regnet, J.B. et al. (2015), "Acoustic and reservoir properties of microporous carbonate rocks: Implication of micrite particle size and morphology", *Journal of Geophysical Research: Solid Earth*, No. 120(2), pp. 790-811.

Robinet, J.C. et al. (2015), "Upscaling the porosity of the Callovo-Oxfordian mudstone from the pore scale to the formation scale; insights from the 3H-PMMA autoradiography technique and SEM BSE imaging", *Sedimentary Geology*, No. 321, pp. 1-10.

Sammartino, S. et al. (2003), "Spatial distribution of porosity and minerals in clay rocks from the Callovo-Oxfordian formation (Meuse/Haute-Marne, Eastern France)—implications on ionic species diffusion and rock sorption capability", *Applied Clay Science*, No. 23(1), pp. 157-166.

Savoye, S. et al. (2010), "New experimental approach for studying diffusion through an intact and unsaturated medium: a case study with Callovo-Oxfordian argillite", *Environmental Science & Technology*, No. 44(10), pp. 3698-3704.

Thierry, J. et al. (2006), "Les ammonites du Callovien-Oxfordien des sondages ANDRA dans l'Est du Bassin de Paris : Synthèse biochronostratigraphique, intérêts paléoécologique et paléobiogéographique", *Comptes Rendus Geoscience*, No. 338, pp. 834-853.

Tournassat, C. et al. (2015), "Chapter 3. Chemical conditions in clay-rocks", *in*: C. Tournassat, C. I. Steefel, I. C. Bourg, F. Bergaya (Eds.), *Natural and Engineered Clay Barriers, Developments in Clay Science,* Vol. 6, Elsevier, ISBN 9780081000274.

Vinsot, A., S. Mettler and S. Wechner (2008), "In situ characterization of the Callovo-Oxfordian pore water composition", *Physics and Chemistry of the Earth*, Parts A/B/C, 33: S75-S86.

Vinsot, A. et al. (2011), "Pumping tests in a low-permeability rock: Results and interpretation of a four-year long monitoring of water production flow rates in the Callovo-Oxfordian argillaceous rock", *Physics and Chemistry of the Earth,* Parts A/B/C, 36: pp. 1679-1687.

Yven, B. et al. (2007), "Mineralogy, texture and porosity of Callovo-Oxfordian argillites of the Meuse/Haute-Marne region (eastern Paris Basin)", *Mémoires de la Société Géologique de France*, 178: pp. 73-90.

Domerian and Toarcian Marls (rock units) – IRSN Tournemire Tunnel, France

Introduction

Andra, the French National Radioactive Waste Management Agency, is responsible for assessing the feasibility of the deep geological disposal of radioactive waste in France. Andra's feasibility research has included an extensive research and development (R&D) programme, as well as the construction and development of an Underground Research Laboratory (URL; Bure, France) in the Meuse/Haute-Marne area – focused on characterisation of the Callovo-Oxfordian argillaceous formations. Since June, 2006, Andra has been responsible for the conception, proposal and implementation of a deep disposal site in this region (i.e. the Cigéo project), which was subject to a public debate/hearing in 2013.

Andra's R&D activities are regularly assessed by various bodies, including those listed below.

- Andra's Scientific Council, which evaluates the Agency's scientific strategy and the divisions' activities. It is consulted on R&D programmes conducted by the Agency and evaluates the results.
- The Guidance and Monitoring Committee (COS) of the URL, which reports to the Scientific Council, is specifically tasked with evaluating the experiments carried out at the URL.
- The French National Safety Authority (ASN), which relies on the scientific and technical expertise of the French Institute for Radiological Protection and Nuclear Safety (IRSN) and the advisory committees.

IRSN is responsible for the technical soundness and technical expertise presented in any safety analysis that would be developed for a deep geologic repository site in France. Within this framework, IRSN has developed research and development programmes with focus on safety, in situ research, the confining properties of geological formations, and, more specifically, on deep geological disposal in clay media. Based on an evaluation of the level of knowledge and understanding with respect to the properties/nature of deep impervious argillaceous formations in the late 1980s, IRSN initiated in situ research (1989) within a former railway tunnel at Tournemire (Aveyron, south of France; see Figure A3-27), with direct access to a series of indurated clay stones and marls (Toarcian and Domerian rock units), in order to better understand the various transport and mechanical properties of such clay rocks (Barbreau and Boisson, 1994).

The Tournemire railway tunnel site is not under consideration for radioactive waste disposal, but it does support a number of IRSN's studies focused on ensuring readiness for site selection/evaluation in argillaceous media. The main objective of the Tournemire tunnel project was to develop generic studies that could be applicable to other argillaceous formations that may be considered for radioactive waste disposal in the future. The research programme has been focused on hydrogeological, geochemical and geomechanical properties in order to recognise and better understand fluid transfers possibilities through argillaceous formations. The URL design is shown in Figure A3-28.

The database included here is an update of the previous OECD/NEA Clay Club Catalogue of Characteristics of Argillaceous Rocks (Boisson, 2005), taking into account additional data collected since 2005.

Figure A3-27: **Simplified geological map of the Tournemire Area (Aveyron, France) with location of the IRSN site**

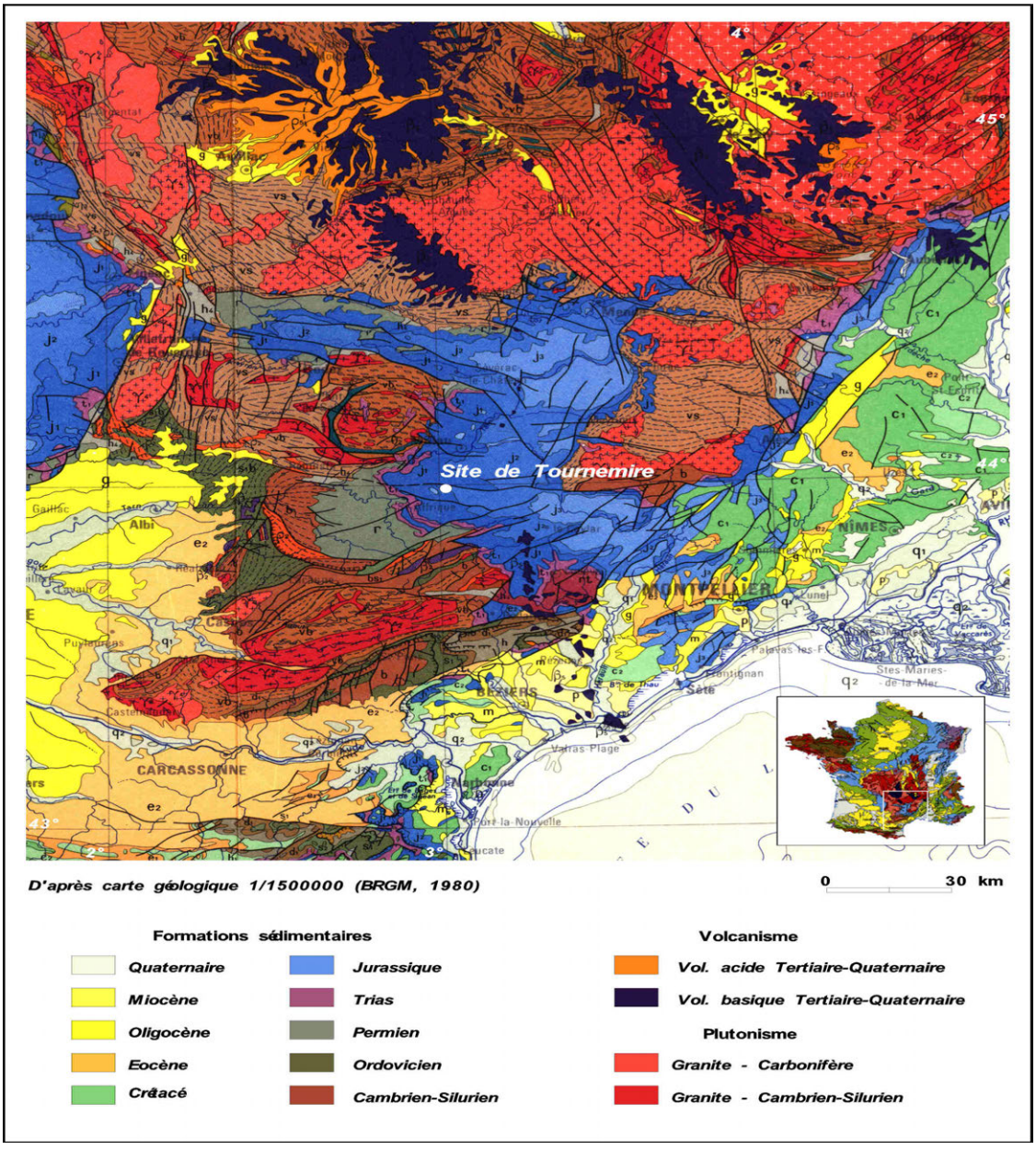

Source: Adapted from Cabrera et al., 2001.

Disposal concept

There is no disposal concept for the Tournemire experimental site, as the location is not being considered for a deep geological repository. The French conceptual design for deep geological disposal in France can be found in the summary on the Callovo-Oxfordian formations.

Formation properties

Geology/structure

The site (La Boutinenque), located close to the village of Tournemire in the South of Aveyron, France, and operated by IRSN, is situated in the Mesozoic marine Causses du Larzac Basin (see Figure A3-29) on the southern border of the French Massif Central (Debelmas 1974). It has been selected because of its geological simplicity and because a former railway tunnel (excavated between 1 882 and 1 888, and totalling 1 885 metres long) provides direct access to the centre of the argillaceous Toarcian-Domerian Formation.

The Causses Basin is an north-south oriented basin, containing Permian to late Jurassic sediments, and is delineated by basement massifs (Rouire and Rousset, 1980; Constantin et al., 2002; Constantin et al., 2004). The study area consists of a sub-horizontal monoclinal structure affected by a major east-west trending reverse fault. The bedding planes at the site generally are sub-horizontal, with dip orientation ranging between 5° and 10° to the north.

The sedimentary formations that have been evaluated represent three major sedimentary layers of Jurassic age (Boisson et al., 1998). The argillaceous formation at tunnel level is ~250 m thick and corresponds to a sub-horizontal argillaceous and marl layer of Domerian age (~188-183 Ma), and thinly bedded clay stones and marls of Toarcian age (~184-175 Ma).

Figure A3-28: **Schematic view of the tunnel, galleries and boreholes at the Tournemire experimental site**

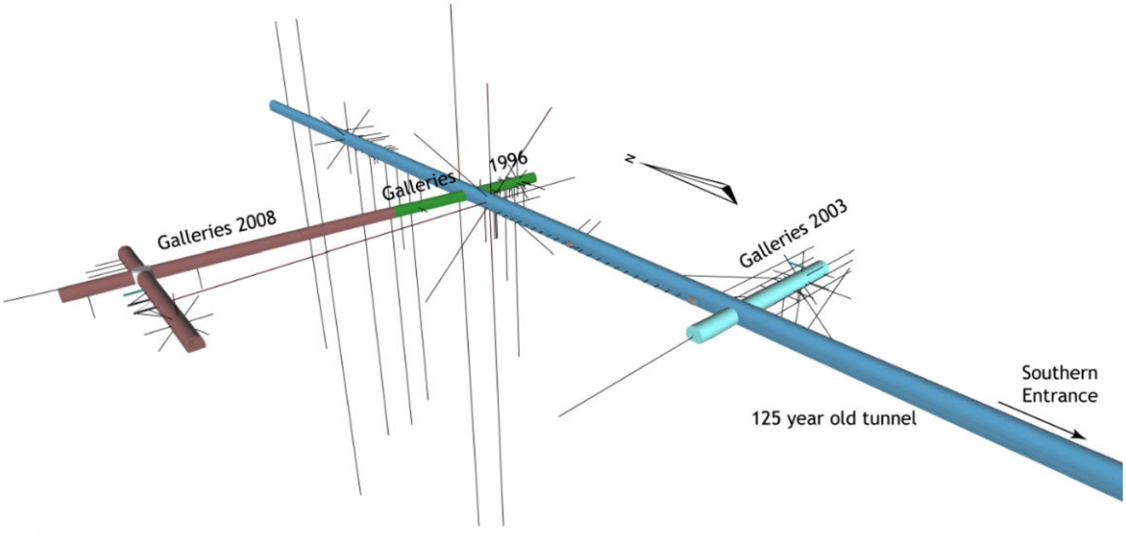

Source: adapted from Wittebroodt, 2011.

The Domerian rock unit consists of ~40 m of marl and indurate clay. The Lower Toarcian, the Middle Toarcian and the Upper Toarcian units consist of 25 m of organic-rich marl, 20 m of marl, and 160 m of clay, respectively (Boisson et al., 1998). This argillaceous formation is sandwiched between two karstified carbonate aquifers (refer to Figure A3-30 and Figure A3-31; Boisson et al., 2001; Patriarche et al., 2004a, b, c). The formation is overlain by approximately 200 to 250 m of limestone and dolomite (Aalenian to Bathonian), characterised by a well-developed karstic system, and underlain by a lower Liassic series (Carixian to Hettangian) mainly composed of karstified carbonates (> 300 m).

From a mineralogical point of view, the clay fraction of the formation ranges between 20 and 50% of the bulk rock, and is mainly composed of illite (5-15%), illite/smectite mixed-layer minerals (5-10%, with a smectitic proportion of about 10%), chlorite (1-5%) and kaolinite (15-20%). The claystone contains 10-20% quartz (grains), 10-40% carbonates (mainly composed of calcite, with traces of dolomite and siderite), and 2-7% pyrite (Boisson et al., 2001; Savoye et al., 2006b).

A number of boreholes have been drilled from the tunnel. Lithologically, the shale-marl sequence shows some heterogeneity in the vertical dimension. A number of sub-units, with somewhat different properties, are distinguished: Middle and Upper Toarcian shale unit (carbonate content 10-25 wt.%), Lower Toarcian carbonate (carbonate content generally > 30 wt.%), Upper Domerian shale unit (carbonate content ~10 wt.%) and Lower Domerian carbonate (carbonate content decreasing from bottom, ~70 wt.%, to top, ~10 wt.%).

Figure A3-29: **Triassic and Jurassic stratigraphy at the Tournemire tunnel experimental site**

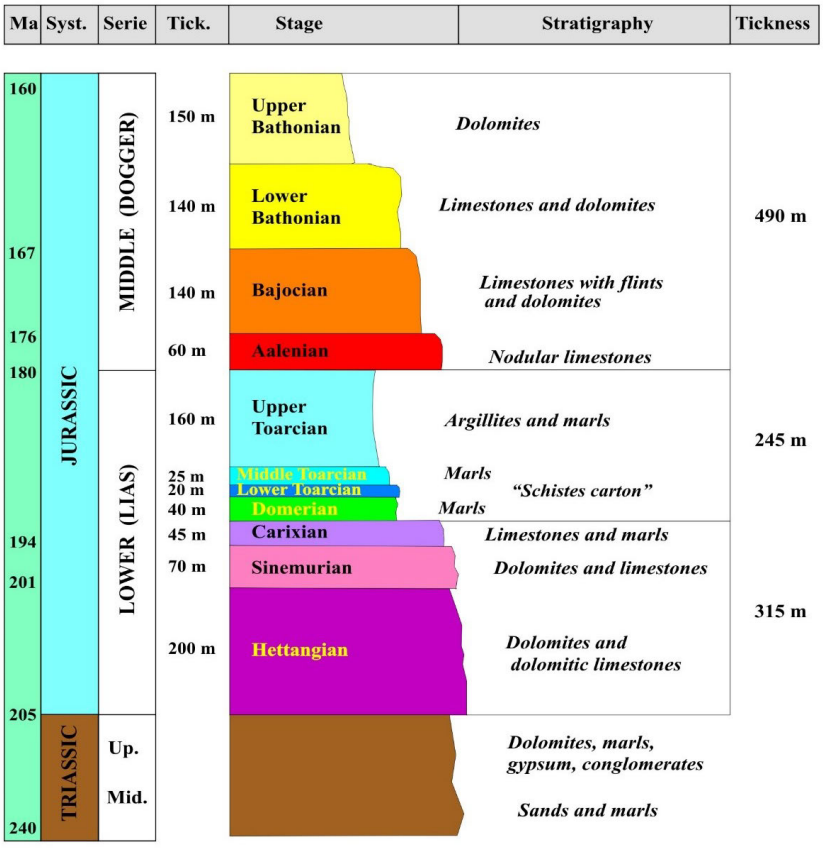

Source: Adapted from Cabrera et al., 2001.

Based on fission track analyses (Peyaud, 2002), it is suggested (Barbarand et al., 2001) that the argillaceous formation was buried under 1 300 ± 400 m additional sediments than currently observed, which would account for the currently over-consolidated state of the clay formation. Due to this deep burial and intense diagenetic cementation, the studied shales and marls of the Toarcian-Domerian are highly consolidated and relatively massive rocks, and exhibit more brittle deformation behaviour (Constantin et al., 2002) than many of the other formations described in this report. These characteristics are demonstrated by the mean mechanical parameter values of the rock: elastic modulus (E1 = 27 680 MPa, E_2 = 9 270 MPa), Poisson's coefficients (ν_1 = 0.17, ν_2 = 0.20), shear modulus (G_1 = 3 940 MPa, G_2 = 3 940 MPa) and uniaxial compressive strengths (σ_1 = 32 MPa, σ_2 = 13 MPa), where 1 and 2 refer to parallel and normal to the bedding, respectively (Maßmann et al., 2009).

Several fault types affect the massif of Tournemire. Faulting in the area is the result of two main tectonic events in the geologic past: i) an extension during the Jurassic; and ii) a compression during the Eocene (from 53 to 33 Ma), as a consequence of the Pyrenean Orogeny (Constantin et al., 2002).

Figure A3-30: **Geological profile across the Toarcian-Domerian at the Tournemire tunnel level**

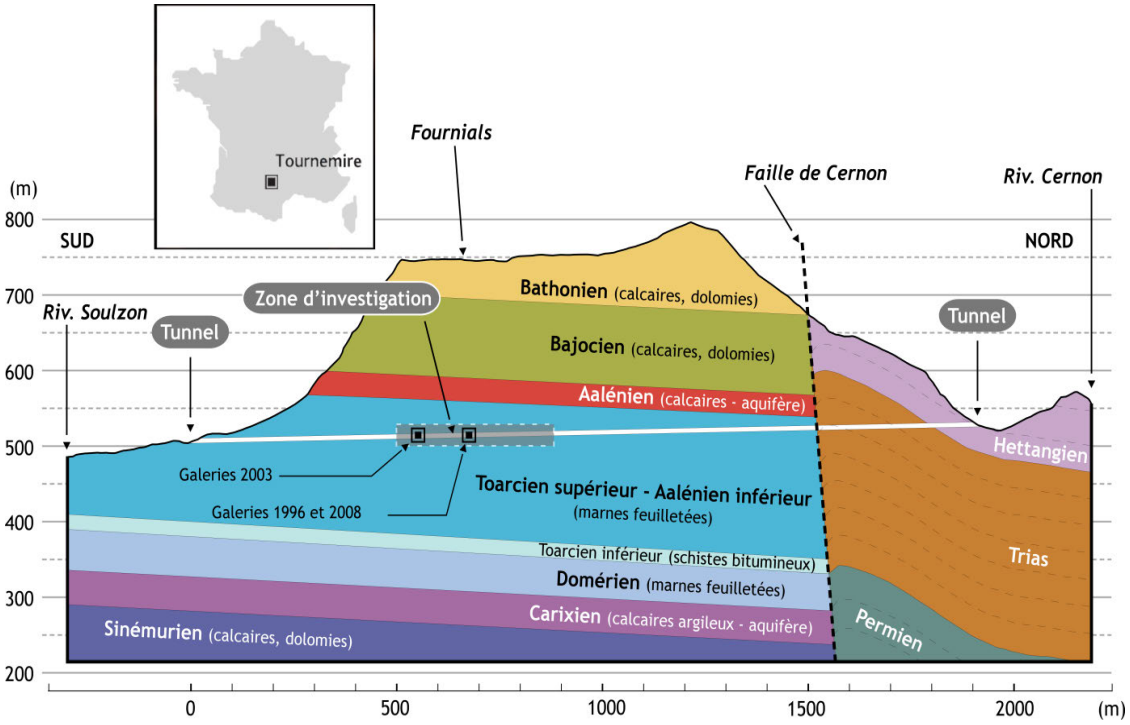

Source: Adapted from Cabrera et al., 2001.

Two east-west trending reverse faults, ~5 km apart and with several hundreds of metres offset, bound the area of interest (Cernon fault in the north, St-Jean-d'Alcapies fault to the south). The reverse Cernon fault, located 1 550 m from the southern tunnel entrance and ~80 km in length, is the result of a regional extension and has resulted in direct contact between the Toarcian-Domerian and the underlying Hettangian formation (~199 Ma). This transmissive major structure enables the communication between two surrounding carbonate aquifers, namely the Aalenian limestone above and the Carixian limestone below. The Pyrenean compression phase created most of the local faults, and reactivated others at the regional scale – including the Cernon fault – and is assumed to have been responsible for the karstification of the surrounding aquifers (Ambert et al., 1995; Constantin et al., 2004).

At the tunnel location, in addition to the main Cernon fault (see Figure A3-30), secondary sub-vertical faults of hectometric extension, and oriented N170-180°E, effect the clay rock formation and have been observed in the galleries and identified in several underground boreholes. These sub-vertical fault zones (or fracture network, close to the maximal horizontal stress direction), display mainly sub-horizontal offset (decameter scale) and small vertical offset (metre scale). In the upper limestone and dolomite of Aalenian to Bathonian levels, these fault zones widen and fracturing becomes more scattered. Because most of these faults date from the Pyrenean compression during the Eocene, and because the Cernon fault preceded them, the clays and marls likely acquired their rigidity and subsequent susceptibility to fracturing under mechanical stresses quite early in the massif history (Patriarche et al., 2004a, b, c).

Figure A3-31: **Block diagram of the Tournemire tunnel experimental site**

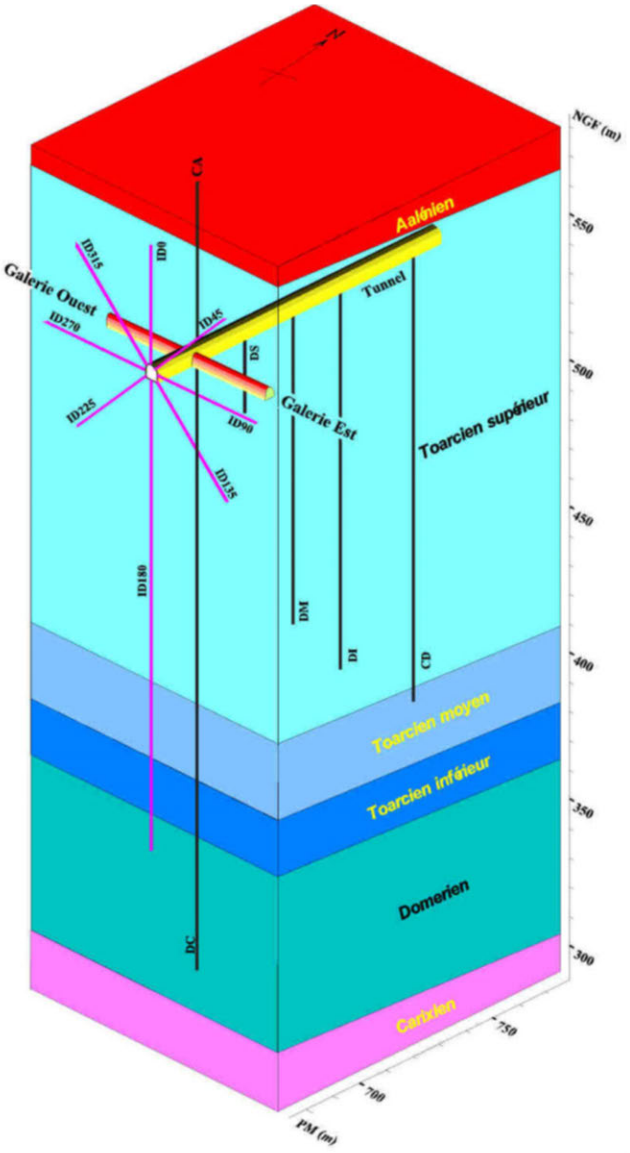

Source: Adapted from Cabrera et al., 2001.

Geochemistry, hydrogeology and transport properties

Geochemistry

Direct assessment of porewater chemistry and water-rock interactions for such rocks is an almost impossible task due to the very low hydraulic conductivity and low water content, leading to difficulties in porewater sampling without inducing perturbations.

Porewater composition of the Toarcian/Domerian argillaceous formation at Tournemire has been developed via an indirect approach (Trémosa et al., 2012) using a geochemical model of water-rock interaction using some properties of the rock and the fluid. It is based on a comprehensive characterisation of the geochemical clay rock system, including mineralogy, petrology, mobile anions, cation exchange properties, accessible porosity and CO_2 partial pressure, and taking into account geochemical characteristics of fluids obtained from old sealed

fractures. The porewater compositions calculated at different elevations across the Tournemire argillaceous formation allow establishment of a vertical profile. The composition profile follows the mobile anions and shows a bell-shaped profile with a maximum concentration in the middle of the formation (salinity of 5.6 g L^{-1}) and a gradual solute decrease towards the bounding aquifers. pH varies between 7.35 and 7.9 across the formation, a typical range of values for a clay rock porewater. The lowest pH values are observed in the Lower Toarcian, where the CO_2 partial pressure is higher. The average temperature of water circulating in fractures is ~15°C. U and Th contents in the Toarcian-Domerian are reasonably homogeneous, with average values of 11 ppm Th and 2.5 ppm U.

Hydrogeology and transport properties

The sequence of shale and marl lithologies is relatively flat-lying and is considered to be an aquitard sandwiched between two limestone aquifers above (Aalenian) and below (Carixian) (see Figure A3-31). The hydrogeological regime for the area is summarised in Trémosa et al. (2012). The lower aquifer (Hettangien and Carixian) outcrops approximately 2 km southwest of the study area and discharges part of its water through the Lauras spring. The recharge zone of this lower aquifer includes the plateau of Saint-Jean d'Alcapiès and Lauras, to the south of Tournemire. The upper aquifer (Aalenian) is composed of Aalenian, Bajocian and Bathonian limestones and is recharged by local precipitation falling onto the Larzac plateau.

At the site, the Aalenian aquifer is known to discharge primarily through the drain of the Cernon fault, which feeds the Cernon River, and, to a minor extent, through springs located at the interface between the aquifer and the impervious argillaceous formation – as drainage can be observed at the interface in some outcrops. Taking into account the hydraulic heads in the two aquifers, with an average hydraulic gradient of slightly less than 0.5 m/m across the low-permeability sequence, calculations of Darcy flux through the aquitard suggest that the flow direction should be downward (Boisson et al., 2001; Matray et al., 2007). Hydraulic pressures have been measured at different depths in boreholes drilled into/through the Toarcian Formation, as well as localised in the unfractured zone of the area with permanently sealed probes and a multipacker system. Hydraulic heads have also been measured in water-bearing fractures by means of a double packer systems.

Different phenomena have been recognised as disturbing the more or less simple hydraulic regime. The obtained profile shows a depression of ~30-40 m around the tunnel with respect to the theoretical hydraulic head profile derived from heads measured in the two aquifers (Bertrand et al., 2002). This level is characterised by the occurrence of sub-atmospheric water pressures, limited to the first metre around the tunnel (de-saturation phenomena), and constitutes a capillary fringe as a consequence of tunnel excavation and natural ventilation. In contrast, the hydraulic head measured in an 80-m high test section in the lower part of the argillaceous formation, isolating a water-bearing fracture, indicates the occurrence of overpressure in the clay formation. In addition, two other fracture networks are observed in the tunnel and drift walls that may have an important role on water flow and the transport of dissolved species. Fracture networks, due to the rock disturbance and de-stressing in response to the excavation of the tunnel and galleries, have been observed, followed by a stress re-distribution and subsequent rock convergence. This mechanical behaviour is highly influenced by the anisotropic character of the shales. Another network consists of sub-horizontal fissures at the drift wall, which developed, more or less, parallel to bedding (several metres deep, each with a millimetre-scale aperture, and a frequency of about 1 per 10 cm), directly linked to seasonal variations in the drifts' atmosphere (hygrometry and temperature), and attributed to variations in the chemical potential of the interstitial solutions under swelling/shrinking cycles (Daupley, 1997; Maßmann et al., 2009).

IRSN has performed a series of in situ and laboratory tests (hydraulic conductivities, diffusion parameters, etc.) for estimating the various transport properties of the Toarcian/Domerian argillaceous formation. Early measurements from in situ hydraulic tests indicated a hydraulic conductivity ranging between 10^{-11} and 10^{-13} m s^{-1}, whereas laboratory tests provided much lower values with an average of 10^{-14} m s^{-1} (Boisson et al., 2001). More recent measurements, from a series of in situ hydraulic pulse tests performed on undisturbed argillite, gave hydraulic conductivities ranging between 10^{-15} and 10^{-14} m s^{-1}, very close to those estimated from laboratory tests. The results were obtained on boreholes equipped with permanent bottom-hole probes installed in a 1-m high test section located at 15 m and 40 m below the tunnel ground level, and isolated from

the surface with epoxy resin and concrete (Bertrand et al., 2002). The difference between the two sets of tests (early versus late) was explained by the occurrence of water-bearing fractures of tectonic origin in the previously-tested intervals (Matray et al., 2007).

Secondary fractures are usually sealed with calcite and give access to unfractured blocks of argillite characterised by small hydraulic conductivities (10^{-14} to 10^{-15} m/s; i.e. 10^{-21} to 10^{-22} m^2 as intrinsic permeabilities) and specific storativity of ~10^{-6} m^{-1} (Boisson et al., 2001). Because the formation is penetrated by systems of brittle fractures, some of these secondary faults are weakly water conducting and sometimes geodic cavities are identified at the junctions of two faults that enable the vertical transfer of fluids. Hydraulic tests performed on these fault junctions have supplied relatively high transmissivities (around 10^{-10} m^2/s), with permeabilities five orders of magnitude higher than those of the unfractured zone for an equivalent-tested height (Savoye et al., 2003). With the Cernon fault, these fractures represent the only conduit(s) for fluids to come in direct contact with the clay formation, which is of importance in the context of collecting information on the clay interstitial fluid geochemistry (De Windt, 1998, 1999; Beaucaire et al., 2005, 2008).

The limited water discharge observed from fractures observed in the Toarcian shale in the Underground Research Laboratory, and the difference between laboratory and in situ measurements of hydraulic conductivity, together indicate that limited fracture flow occurs in the formation. On the other hand, the regular distribution of natural tracers suggests that, on the scale of the formation, advective transport is not of prime importance, probably due to a limited connectivity of the fracture network.

A number of techniques were applied to evaluate porosities of the clay formations (Boisson et al., 1998, 2001; Patriarche et al., 2004a) and diffusion properties of chemical species. Laboratory measurements, primarily concerned with the Upper Toarcian, yielded effective diffusion coefficients parallel to the bedding of 10^{-11} for water (tritium or deuterium) and 10^{-12} m^2/s for anions (chloride or bromide) (Patriarche et al., 2004a, 2004b; Altinier et al., 2007; Savoye et al., 2008). Diffusion coefficients normal to bedding are typically 2-3 times lower than those parallel to bedding. The anisotropy factor (parallel/normal) for pore diffusion coefficients for Cl^- is 2. Table A3-1 provides an overview of the transport parameters for the Toarcian-Domerian marls and indurate clays at Tournemire (after Mazurek et al., 2006).

Table A3-1: **Transport parameters of the Toarcian-Domerian Marls and indurate clays at Tournemire**

Sub-unit	Lithology	Elevation [m a.s.l.]	Pore diffusion coefficient Dp normal to bedding at 20°C [m^2/s]		Effective diffusion coefficient De at 20°C [m^2/s]		Hydraulic conductivity K [m/s]		Accessible porosity n [-]	
			Anions	HTO	Anions	HTO	Normal to bedding	Parallel to bedding	Anions	Water
Aalenian aquifer										
Middle and Upper Toarcian	Shaly unit, carbonate content 10-25 wt.%	377.6-554.3	$2.8.10^{-11}$	$5.6.10^{-11}$	$7.3.10^{-13}$	$4.8.10^{-12}$	$1.0.10^{-12}$	$2.0.10^{-12}$	0.025	0.085
Lower Toarcian	Carbonate content generally >30 wt.%	354.5-377.6	$2.1.10^{-11}$	$4.2.10^{-11}$	$5.7.10^{-13}$	$2.3.10^{-12}$			0.028	0.055
Upper Domerian	Shaly unit, carbonate content ~10 wt.%	325.0-354.5					$1.3.10^{-12}$	$2.6.10^{-12}$		
Lower Domerian	Carbonate content decreasing from bottom (70 wt.%) to top (10 wt.%)	296.9-325.0								
Carixian aquifer										

Source: Adapted after Mazurek et al., 2006.

Calculations of the Péclet number (Patriarche et al., 2004a; Mazurek, 2006), yield values much lower than 1, indicating that mass transport is not controlled by advection. This result

confirms the assumption already proposed that diffusion is the dominant transport process in the Tournemire argillaceous formation (Moreau-le Golvan et al., 1997; Boisson et al., 2001; Savoye et al., 2008). However, major observed fractures could represent local advective flow paths (Constantin et al., 2004).

- Tracer distributions

Tracers in porewaters were studied in core materials from several boreholes drilled from the railway tunnel or adjacent galleries. Anion tracer data are available only from the Toarcian. Cl^- contents in porewater were analysed by aqueous leaching and radial out-diffusion experiments. The spatial distribution of Cl^- in porewater shows that Cl^- contents are highest in the middle Toarcian and decrease towards both aquifers. Cl^- contents from different boreholes show substantial heterogeneities due to lateral variability and the local effects of fractures.

δ^2H and $\delta^{18}O$ values of porewater were measured using vacuum distillation (50 and 60°C) and the isotope exchange method; the latter method currently is preferred, but the use of vacuum distillation data is considered acceptable via an appropriate correction procedure. The spatial distributions of water isotopes shows, for the δ^2H profile, a well-defined curved shape with an apex at ~400 m above sea level (a.s.l.), similar to what was found for Cl^-. The $\delta^{18}O$ profile shows a similar shape, though less well defined.

Groundwaters in the Aalenian and Carixian aquifers, constituting the upper and lower boundaries of the system, have a very low salinity and a stable isotopic composition similar to that of recent recharge.

Cl^- contents in porewaters vary in the range 12-141 mg/L, whereas the groundwater sample yields 6 mg/L. It appears that flushing of the aquifer by fresh water has not completely leached out the salinity in the matrix of the limestones.

The stable isotopic composition of groundwaters from both aquifers is typically characterised by substantially higher δ^2H and $\delta^{18}O$ values than the uncorrected values in the porewaters (Figure A3-32). The corrected porewater values are much more consistent with the groundwater values measured in the surrounding aquifers. The good correspondence in the corrected values adds credibility to the applied correction procedure of the isotope data from vacuum distillation.

Figure A3-32: **Spatial distribution of Cl^-, δ^2H and $\delta^{18}O$ in porewater at Tournemire (data from Patriarche, 2004a; Savoye et al., 2006b; adapted from Mazurek et al., 2006)**

Figure A3-32.1: **Spatial distribution of Cl^- in free porewater at Tournemire**

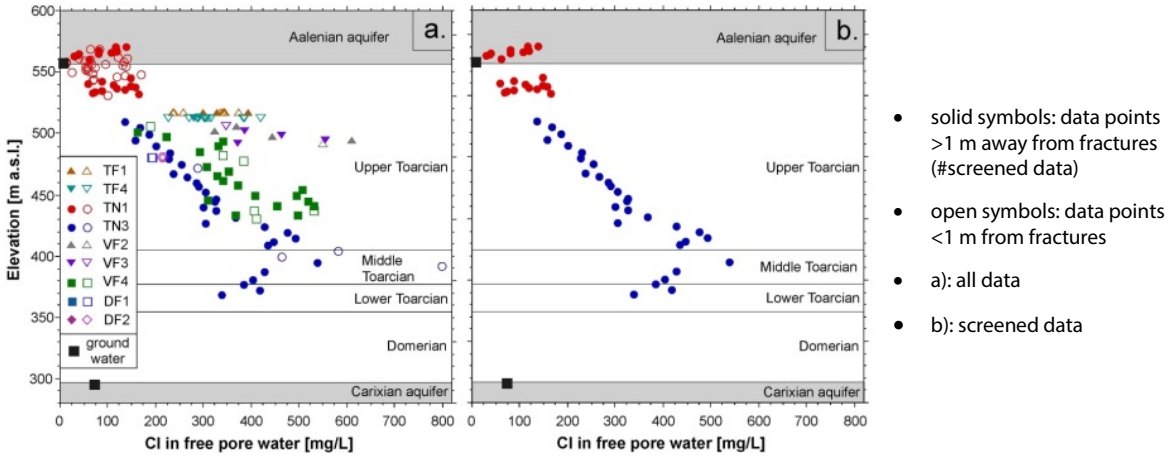

Figure A3.32.2: **Spatial distribution of δ^2H in porewater at Tournemire**

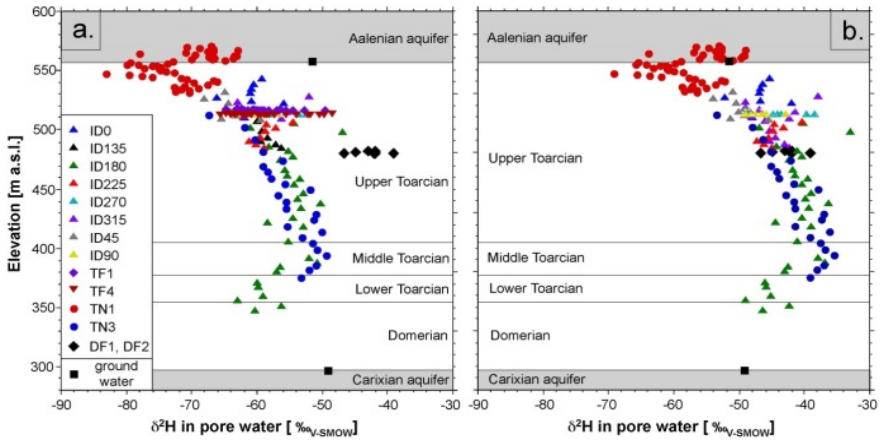

- a: Uncorrected full data set
- b: Screened data set corrected for the effect of incomplete distillation

Figure A3-32.3: **Spatial distribution of $\delta^{18}O$ in porewater at Tournemire**

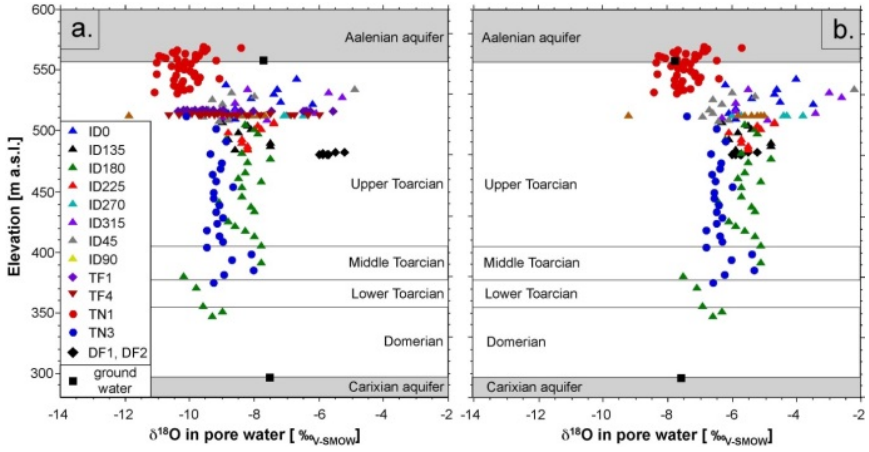

- a: Uncorrected full data set
- b: Screened data corrected for the effect of incomplete distillation

Favourable formation attributes

As already mentioned, the IRSN Tournemire tunnel site is not under consideration for a radioactive waste disposal, but supports a number of IRSN's studies focused on ensuring readiness for site selection/evaluation in argillaceous media.

The main objective of the Tournemire tunnel project was to develop generic studies that could be applicable to other argillaceous formations that may be considered for radioactive waste disposal in the future. The research programme has been focused on hydrogeological, geochemical and geomechanical properties in order to recognise and better understand fluid transfers possibilities through argillaceous formations.

As mentioned, the site has been selected because of its geological simplicity and because a former railway tunnel provides direct access to the centre of the argillaceous Toarcian-Domerian Formation. Considering that the overlying limestone layers are approximately 250 m thick, it has been hypothesised that the physical and hydrogeological conditions (one aquifer above and one below) could be representative of those that would be encountered in the siting of a deep geologic repository.

The research programme, carried out from the tunnel inside the geological formation is supported by both in situ tests from boreholes and galleries, and laboratory studies from core samples. It is demonstrated, in the framework of this specific site and its specific geological history, that primary transport processes through the Toarcian/Domerian argillaceous formation remain diffusion-dominated over geologic time frames (hundreds of thousands to millions of

years), together with long groundwater residence times with geochemical buffering capacity. The following bullet points highlight some of the properties of the formation observed from work at the Tournemire testing facility, organised, as much as is possible, in accordance with the three key hypotheses presented in Chapter 1.

The areal extent and thickness of the lithological units allow for predictability at scales relevant to establishing safety

- The formation is evident over a large lateral distance (> 235 km, as depicted in Figure A3-29, from Tournemire to Mas-Audran).

The presence of natural barriers (host and enclosing formations) acts to isolate the host rock and contain solutes for safety-relevant time frames

- The Causses du Larzac Basin is a north-south oriented basin (Permian- to Jurassic-age sediments), and is delineated by basement massifs – the formation covers a broad area within the southern part of the basin.

Stability of the geosphere on safety-relevant time frames supported by multiple lines of geoscientific evidence/reasoning

Transport processes are anticipated to remain diffusion-dominated over geologic time frames (hundreds of thousands to millions of years)

- Early in situ hydraulic tests indicated a hydraulic conductivity ranging between 10^{-11} and 10^{-13} m s^{-1} and laboratory tests provided lower values with an average of 10^{-14} m s^{-1}. More recent measurements, from a series of in situ hydraulic pulse tests, suggest hydraulic conductivities ranging between 10^{-15} and 10^{-14} m s^{-1}.
- Laboratory measurements, primarily for the Upper Toarcian, yield effective diffusion coefficients parallel to the bedding of 10^{-11} for water (tritium or deuterium) and 10^{-12} m^2/s for anions (chloride or bromide).
- Calculations of the Péclet number yield values much lower than 1, suggesting that mass transport is not controlled by advection, but instead that diffusion is the dominant transport process in the Tournemire Toarcian-Domerian Formation.
- Very low hydraulic conductivity and low water contents have led to difficulties in porewater sampling (without inducing perturbations) due to the measures required to extract fluids from the rock.

Geochemical stability of the groundwater-porewater system over geologic time frames

- Regular distribution of natural tracers suggests that, on the scale of the formation, diffusion is dominant in the context of solute transport, most likely due to limited connectivity of the fracture network.

Geomechanical stability of the formations to natural perturbations

- Fracture networks are observed due to the rock disturbance and de-stressing in response to the excavation of the tunnel and galleries, which were followed by stress re-distribution and subsequent rock convergence; such mechanical behaviour is influenced by the anisotropic character of the shales.
- Secondary fractures are usually sealed with calcite, yielding unfractured blocks of argillite characterised by small hydraulic conductivities (10^{-14} to 10^{-15} m/s; i.e. 10^{-21} to 10^{-22} m^2 as intrinsic permeabilities) and specific storativity values of ~10^{-6} m^{-1}.

Summary and future work

Measuring equipment and observation techniques have been deployed at the IRSN Tournemire tunnel to analyse the clay formation and its behaviour. The main experimental programmes that have been developed to-date are related to: i) mechanisms responsible for the transfer of water and natural substances present in the clay formation; ii) effects of excavation, and of using the underground engineering structures, on the containment properties of the rock; iii) detection of faults and discontinuities using a wide array of geophysical methods; iv) effects related to interaction between the rock and the exogenous materials, such as concrete and metal components; and v) performance of important components relevant to the long-term safety of a geological repository, such as bentonite seals.

The ongoing and planned R&D activities to be performed at the Tournemire URL in the coming years are summarised below.

- Performance of disposal sealing components (SEALEX experiments), including perturbations, and their influence on the confinement properties of the disposal components, together with technical feasibility of seals with respect to their safety functions and their expected performance level;
- Interaction between components (CEMTEX experiments) – looking at the Engineered Barrier System/host rock interactions in saturated conditions at 70°C, with particular attention on chemical evolution (solid and pore solution), microstructure evolution, composite effective diffusion coefficient evolutions and validation of numerical blind simulations;
- Duration of the oxidising transient (OXITRAN experiments), aiming at estimating the duration of the oxidising transient within the steel/clay interfaces based on the host rock oxygen consumption (with and without steel) at different humidity degrees;
- Transport properties within faults (FRACTEX experiment), dealing with water transport properties within a fault zone using in situ hydraulic testing, as well as characterising mineralogical and petrophysical parameters, porewater chemistry, natural tracer profiles and diffusion parameters (through-diffusion and radial diffusion);
- Knowledge on argillite petro-fabric within undisturbed versus fault zones (PFAT experiment), focused particularly on the hydraulic behaviour of faults and fractures via porosity characterisation (nano- to microscopic scales), mineralogical and chemical evolution, and magnetic properties;
- Hydromechanical properties of a fault zone (FF experiment) – in order to evaluate fault seal integrity using i) in situ characterisation of hydraulic, elastic and strength properties, ii) estimation of flow times and lengths within different fault zones, iii) permeability-stress-strain evolution of silty claystones and mudstones, and iv) geophysical imaging of the architecture of a fault zone in clay-rich formations;
- Geophysical survey, with the purpose of assessing the ability to detect natural faults from i) the surface (very high-resolution 3D seismic survey and very high-resolution 2D electric resistivity profile) using advanced interpretation methods, and ii) the existing drifts (very high resolution seismic at drift walls), and by studying the feasibility test on large-scale tomography based on muons flux measurements at surface.

References

Alheid, H.-J. et al. (1999), "Comparison of in situ hydraulic and seismic measurements in the excavation damaged zone of underground drifts", 9th ISRM 1999 International Congress on Rock Mechanics (International Soc. for Rock. Mech.), Paris (France), 25-28 August 1999 [Poster] Vouille & Berest (eds.) A.A. Balkema, Rotterdam, Holland pp. 1263-1266.

Altinier, M.-V. et al. (2007), "The isotopic composition of pore-water from Tournemire argillite (France): an inter-comparaison study", *Physics and Chemistry of the Earth Parts* A/B/C, 32(1), pp. 209-218, DOI: 10.1016/j.pce.2006.02.047.

Ambert, M. and P. Ambert (1995), "Karstification des plateaux et encaissement des vallées au cours du Néogène et du Quaternaire dans les Grands Causses méridionaux (Larzac, Blandas)", *Géologie de la France*, 4: pp. 37-50

Barbarand, J. et al. (2001), "Burial and exhumation history of the south-eastern Massif Central (France) constrained by apatite fission-track thermochronology", *Tectonophysics*, No. 335, pp. 275-290.

Barbreau, A. and J.-Y. Boisson (1994), "Caractérisation d'une formation argileuse. Synthèse des principaux résultats obtenus à partir du tunnel de Tournemire de janvier 1992 à juin 1993", Rapport d'activité 1991-1993. EC Rapport d'avancement n° 1 (contrat CCE-CEA n° FI 2W CT91-0115) EUR 15756 fr CEC Nuclear Science & Technology Series, Euroffice. Luxembourg.

Beaucaire, C. et al. (2008), "Groundwater characterization and modelling of water-rock interaction in an argillaceous formation (Tournemire, France)", *Applied Geochemistry*, No. 23(08), pp. 2182-2197.

Beaucaire, C., F.J. Pearson and A. Gautschi (2005), "Chemical buffering capacity of clay rock", OECD/NEA/RWMC/IGSC Workshop on Stability and buffering capacity of the geosphere for long term isolation of radioactive waste: application to argillaceous media, Braunschweig (Germany), 9-11 Dec 2003, ISBN 92-64-00908-6, OECD, Paris, pp. 147-154.

Bensenouci, F. et al. (2011), "A profile of Helium-4 concentration in pore-water for assessing the transport phenomena through an argillaceous formation (Tournemire, France)", *Physics and Chemistry of the Earth Parts A/B/C*, 36(17), pp. 1521-1530, DOI: 10.1016/j.pce.2011.10.016.

Bertrand, L. et al. (2002), "Instrument for measuring pore pressure and permeability in low-permeability clay/rock", 1st Clays In Natural And Engineered Barriers For Radioactive Waste Confinement International Meet, Reims (France), 9-12 Dec 2002 [Poster] Proc.: Book of abstracts Poster session on Mass transfer n° P-MT-16 Andra Science and Technology Series pp. 321.

Boisson, J.-Y. (2005), "Catalogue of Characteristics of Argillaceous rocks", Introductory brochure + specific databases in a CD-ROM (Excel versions) per formation, OECD/NEA/RWMC/IGSC/Clay Club Report NEA 4436 (Brochure and CD-Rom including data base), ISBN 92-64-01067-X, OECD/NEA Paris, France, 72 pp.

Boisson, J.-Y. et al. (2001), "In situ and laboratory investigations of fluid flow through an argillaceous formation at different scales of space and time, Tournemire tunnel, southern France", *Hydrogeology Journal*, No. 9(1), pp. 108-123.

Boisson, J.-Y., J. Cabrera and L. De Windt (1998), "Etude des écoulements dans un massif argileux: laboratoire souterrain de Tournemire", EC Rapport final (contrat CCE-CEA n° FI 2W CT9-0115 et Avenants 1 et 2) EUR 18338 fr CEC Nuclear Science & Technology Series, Euroffice, Luxembourg, 300 p.

Cabrera, J. et al. (2001), "Le projet Tournemire comme support de l'expertise sur le stockage profond en milieu argileux : synthèse des programmes de recherche", Rapport IRSN/SERGD 01-19.

Constantin, J. et al. (2004), "Evolution of the structural fault permeability in argillaceous rocks in a polyphased tectonic context", *Physics and Chemistry of the Earth Parts A/B/C,* No. 29(1), pp. 25-41.

Constantin, J., P. Vergély and J. Cabrera (2002), "Tectonique et fracturation associée dans le bassin des Causses (Aveyron, France): le cas du secteur de Tournemire", SGF Séance Spécialisée Industrie minérale et environnement, Paris, Ecole Nationale Supérieure des Mines de Paris (France), 5-6 février 2000 Bulletin de la Société Géologique de France, vol. 173 n° 3, Séance spécialisée SGF "Industrie minérale et environnement" pp. 229-243.

Daupley, X. (1997), "Etude du potentiel de l'eau interstitielle d'une roche argileuse et de relations entre ses propriétés hydriques et mécaniques – Application aux argilites du Toarcien de la région de Tournemire (Aveyron)", Thèse Docteur en Sciences (Géologie de l'Ingénieur), Ecole Nationale Supérieure des Mines de Paris.

De Windt, L., J. Cabrera and J.-Y. Boisson (1998), "Hydrochemistry of an indurated argillaceous formation (Tournemire site, France)", 9th WRI '09 International Symp. on Water-Rock Interaction (Int. Assoc. of Geochemistry) Taupo (New Zealand), 30 march-3 april, 1998, Greg B. Arehart and John R. Hulston (eds.) A. A. Balkema, Rotterdam, pp. 145-148.

De Windt, L., J. Cabrera and J.-Y. Boisson (1999), "Radioactive waste containment in indurated claystones: comparison between the chemical containment properties of matrix and fractures", Chemical Containment of Wastes in the Geosphere Geological Society of London, Special Publications, n° SP 157, Metcalfe R. & Rochelle C.A. (eds.) Blackwell Scientific Publications Oxford, pp. 169-181.

Debelmas, J. (1974), *Géologie de la France*, Vol 1 and 2, Doin Editeur, Paris.

Gonçalvès, J. and J. Trémosa (2010), "Estimating thermo-osmotic coefficients in clay-rocks: I – Theoretical insights", *Journal of Colloid and Interface Science*, No. 342(1), pp. 166-174.

Maßmann, J. et al. (2009), "Investigation of desaturation in an old tunnel and new galleries at an argillaceous site", *Environmental Geology*, No. 57(6), pp. 1337-1345.

Matray, J.-M., S. Savoye and J. Cabrera (2007), "Desaturation and structure relationships around drifts excavated in the well-compacted Tournemire's argillite (Aveyron, France)", *Engineering Geology,* No. 90(1-2), pp. 1-16.

Mazurek, M. et al. (2006), "Natural Tracer Profiles across Argillaceous Formations: The CLAYTRAC Project", NEA 6253, ISBN 978 92 64 06047-0, OECD Publishing, Paris, pp. 362.

Moreau-le Golvan, Y., J.-L. Michelot and Boisson J.-Y. (1997), "Stable isotope contents of porewater in a claystone formation (Tournemire, France): assessment of the extraction technique and preliminary results", *Applied Geochemistry*, No. 12, pp. 739-745.

Motellier, S. et al. (2007), "Evaluation of tritiated water diffusion through the Toarcian clayey formation of the Tournemire experimental site (France)", *Journal of Contaminant Hydrology*, No. 94(1-2), pp. 99-108.

Patriarche, D. et al. (2004a), "Diffusion as the main process for mass transport in very low water content argillites: 2. Fluid flow and mass transport modelling", *Water Resources Research*, No. 40, pp. 20-39.

Patriarche, D. et al. (2004b), "Characterization and modelling of diffusion process for mass transport through the Tournemire argillites (Aveyron, France)", *Applied Clay Science*, No. 26(1-4), pp. 109-122, *In* "Clays in Natural and engineered Barriers for Radioactive Waste Confinement".

Patriarche, D. et al. (2004c), "Diffusion as the main process for mass transport in very low water content argillites: 1. Chloride as a natural tracer for mass transport-Diffusion coefficient and concentration measurements in interstitial water", *Water Resources Research*, No. 40, pp. 1-19.

Peyaud, J.-B. (2002), "Diagenèse et transferts en milieu argileux fracturé : l'argilite de Tournemire (Aveyron, France)", Thèse Docteur en Sciences Université Paris XI Paris Sud-Orsay.

Savoye, S., J. Cabrera and J.-M. Matray (2003), "Different hydraulic properties of single fractures in argillaceous medium: the case of the IRSN Tournemire site (France)", International Conference on Groundwater in Fractured Rocks, Praha (Czech Rep.), 15-19 Sept 2003, Groundwater in Fractured Rocks IHP-VI series on Groundwater n° 7 Krasny J., Hrkal Z. and Bruthans J. (eds) pp. 47-50.

Savoye, S., J.-L. Michelot and C. Wittebroodt (2006a), "Evaluation of the reversibility of iodide uptake by argillaceous rocks by the radial diffusion method", *Radiochimica Acta*, No. 94(9-11), pp. 699-704.

Savoye, S. et al. (2008), "Transfers through argillaceous rocks over large space and time scales: insights given by water stable isotopes", *Physics and Chemistry of the Earth Parts A/B/C*, 33 (Supplement 1), pp. S067-S074.

Savoye, S. et al. (2006b), "Contribution of the diffusive exchange method to the characterization of pore-water in consolidated argillaceous rocks", *Journal of Contaminant Hydrology*, No. 86(1-2), pp. 87-104.

Savoye, S. et al. (2005), "Evaluation of damage-induced diffusion parameters in Tournemire argillite using an in situ experiment", 10th MIGRATION'05 International Conference on Chemistry and Migration Behaviour of Actinides and Fission Products in the Geosphere, Avignon (France), 18-23 Sept 2005, [Poster] Proc. PB5-Field and large scale experiments, Abstract No. PB5-11, pp. 207.

Trémosa, J. et al. (2012), "Geochemical characterization and modelling of the Toarcian/Domerian porewater at the Tournemire Underground Research Laboratory", *Applied Geochemistry*, 27(7): 1417-1431. Special issue on "25 years after the Chernobyl power plant explosion : Mechanisms of radionuclide transfer in the environment". 2. Investigation of induced or natural short circuits in a geological barrier of an underground nuclear waste disposal analog at Tournemire (France) L. Aquilina, J.-M. Matray & J. Lancelot (eds) Elsevier Amsterdam (Holland).

Trémosa, J. et al. (2010), "Estimating thermo-osmotic coefficients in clay-rocks: II – In situ experimental approach", *Journal of Colloid and Interface Science*, No. 342 (1), pp. 175-184.

Wittebroodt, C. (2011), "Projet FRACTEX: Caractérisation des mécanismes de transfert dans les discontinuités naturelles", Note Technique IRSN/DEI/SARG/2011-026.

Boda Claystone Formation – Hungary

Introduction

The safe disposal of all types of radioactive waste, the interim storage and the final disposal of spent fuel, as well as the decommissioning of nuclear facilities, is the responsibility of the Public Limited Company for Radioactive Waste Management (PURAM) in Hungary. PURAM is a 100% state owned, non-profit organisation, which was established in 1998. The financial resources for the operation and construction of disposal facilities (including site selection and design) are provided by Hungarian Central Nuclear Financial Fund (CNFF).

The preparations for the disposal of high-level and long-lived radioactive wastes (HLW) began in 1993. In 1994, an exploration tunnel was excavated in the Mecsek Uranium Mine, reaching the Boda Claystone Formation (BCF), and on-site underground data acquisition began at a depth of ~1 100 m. The formation was explored underground by a tunnel extending into the claystone ~500 m. The tunnel was utilised as an Underground Research Laboratory (URL) and a large amount of on-site underground data was collected. In 1998, the mine was flooded, and the opportunity to perform underground investigations was terminated.

In 2000, based on desktop studies, a nationwide screening was carried out that evaluated the potential host rock formations in detail. Thirty-two lithological formations within the territory of Hungary, and potentially suitable for a DGR, were identified. This comprehensive investigation confirmed that the BCF has the highest potential among the suitable host rocks for a HLW repository.

The BCF is explored on the surface and underground in south-west Hungary, in the Western Mecsek Mountains, mainly to the west of the city of Pécs. The known aerial extent of the formation is about 150 km^2. The BCF is part of the Permian-Triassic sedimentary sequence, which makes up the Western Mecsek Anticline. Within the rock there is a unit extending up to 37 km^2 which has been identified as a potential disposal area at depths between 500 and 900 m b.g.s. Based on the geometry (thickness) and level of consolidation, two different areas can be distinguished: one in the formation's central and southern part, which is called the Boda Block; and another north of the Boda Block, called the Gorica Block (Figures A3-33 and A3-34).

The geological investigations, which were carried out in the Western Mecsek region in 2004, were suspended in 2005 and initiated again in 2014. The goals of the ongoing work are to characterise the BCF and to reduce the investigation area to 10–15 km^2. The current geological investigation programme covers surface activities, including geological and geomorphological mapping, hydrogeological (re)mobilisation, trenching, and the drilling of six deep boreholes accompanied by seismic profiling.

Disposal concept

Based on the reference scenario of direct disposal for spent nuclear fuel, the first, and so far the final, conceptual design for the long-term management of spent fuel was developed in 2005 and revised in 2008. Parts of the conceptual design were based on that of the existing interim storage facility, and included a new transfer facility that provides loading services for shipping containers, an encapsulation plant, and the underground disposal site. Initial design of the disposal facility was based on the Swedish concept, in spite of differences in lithology.

In 2005, a preliminary safety assessment was carried out in order to judge the suitability of the host formation. This assessment was based on data gathered during exploration of the area before the year 2000. This assessment confirmed that the BCF is a suitable potential host rock

due to its low porosity, low permeability, and high isotope retardation capability. However, it must be stated that in 2005 the available information on the BCF was not comprehensive and some concepts included in the models were only hypothetical.

The conceptual design of the DGR was developed after the preliminary safety assessment. Assessments of inventory, heat load, packaging information, criticality and radiology were carried out to help design the DGR in the conceptual phase. The final disposal concept (TS-ENRCON Kft, 2004) considered a copper overpack on the canisters and the layout of the repository was based on the assumption that disposal of canisters will take place in vertical disposal holes drilled at the bottom of disposal tunnels, excavated within the BCF. The design of the encapsulation plant was based on the Swedish concept as well. The disposal tunnel system was planned for 500-800 m b.g.s., along with associated surface facilities. In the design, underground construction activities will be undertaken via vertical shafts. The disposal shafts will be connected to one another, and to the service area, by ventilation ducts and utility piping. The construction of the underground space will utilise conventional drill and blast methods. It is assumed that for the large-section underground drifts, rock bolts and sprayed fibrous concrete lining, with an average thickness of 10 cm, will be required, while the small-section drifts (including the disposal drifts), rock bolts, and a 5-cm thick sprayed concrete lining will suffice.

Because there are numerous uncertainties, such as the lack of a defined back-end strategy for the management of spent fuel (impacting estimates of the expected inventory of highly-active residue from nuclear energy production) or of an appropriate repository area, as well as unknowns regarding the main geometry and geological characteristics of the selected site, the disposal concept will be reassessed before each decision point (e.g. narrowing of the research area during siting, location of the repository site, building of the URL and/or DGR, operation of disposal facility, etc.) and any revisions based on the reassessment may result in changes to the original design.

As part of the ongoing conceptualisation, PURAM has initiated work on a Project Development Plan, which aims to determine the decision points and their contexts for future research and development of a DGR. PURAM is committed to the "Do and See" strategy (instead of "Wait and See"). PURAM aims to gather all possible information and move forward, using a phased approach.

Formation properties

Geology/structure

The ~265 Ma old (Middle Permian – Guadalupian age) BCF is known to cover an area larger than 150 km^2. A comprehensive surface- and URL-based characterisation programme was carried out between 1993 and 1999. The URL exploring the BCF was then the world's deepest, at a depth of 1 100 m b.g.s.

The lithofacies represent an intermittent, saline playa lake in a desert to semi-desert environment. The present properties of the BCF have been governed, in part, by the extreme climatic, inflow and geochemical conditions of sedimentation and, in part, by its diagenesis. These conditions resulted in the formation of an extremely high proportion of sedimentary albite in the rock, which is the most characteristic mineral of the BCF. The lack of organic material and pyrite is also remarkable. This fact might be regarded as an unfavourable condition from the aspect of confinement properties, but it also demonstrates maintenance of long-term geochemical stability of the formation. Intensive oxidation processes influencing the rock's mechanical properties are not expected to occur within the lifetime of the repository.

Figure A3-33: **Geological map and cross-sections of the Western Mecsek including the surface outcrop of the BCF**

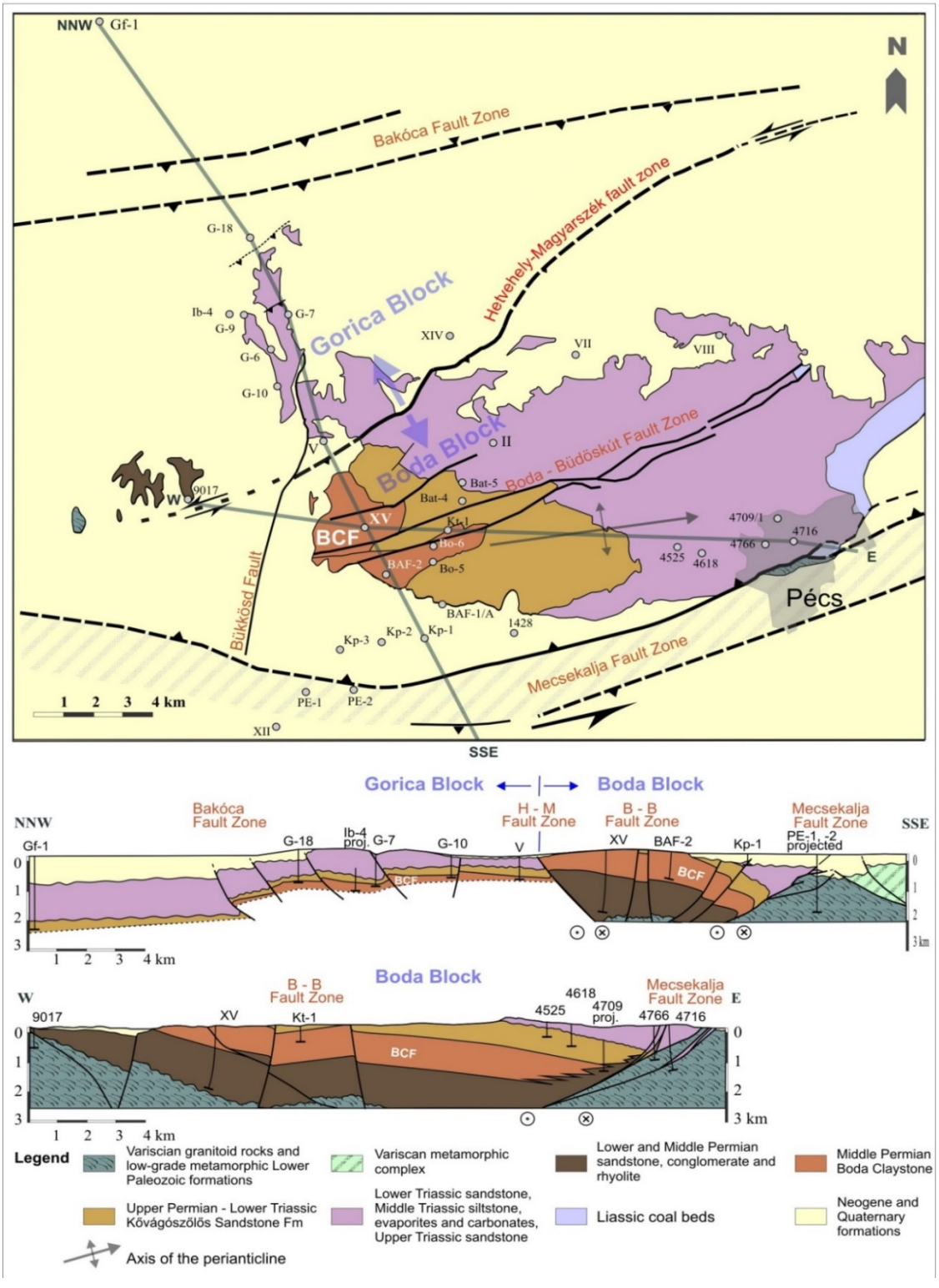

Source: Compiled and modified from Konrád et al., 2010.

Figure A3-34: **Depth contour of the top of the BCF including the surface outcrop of the BCF**

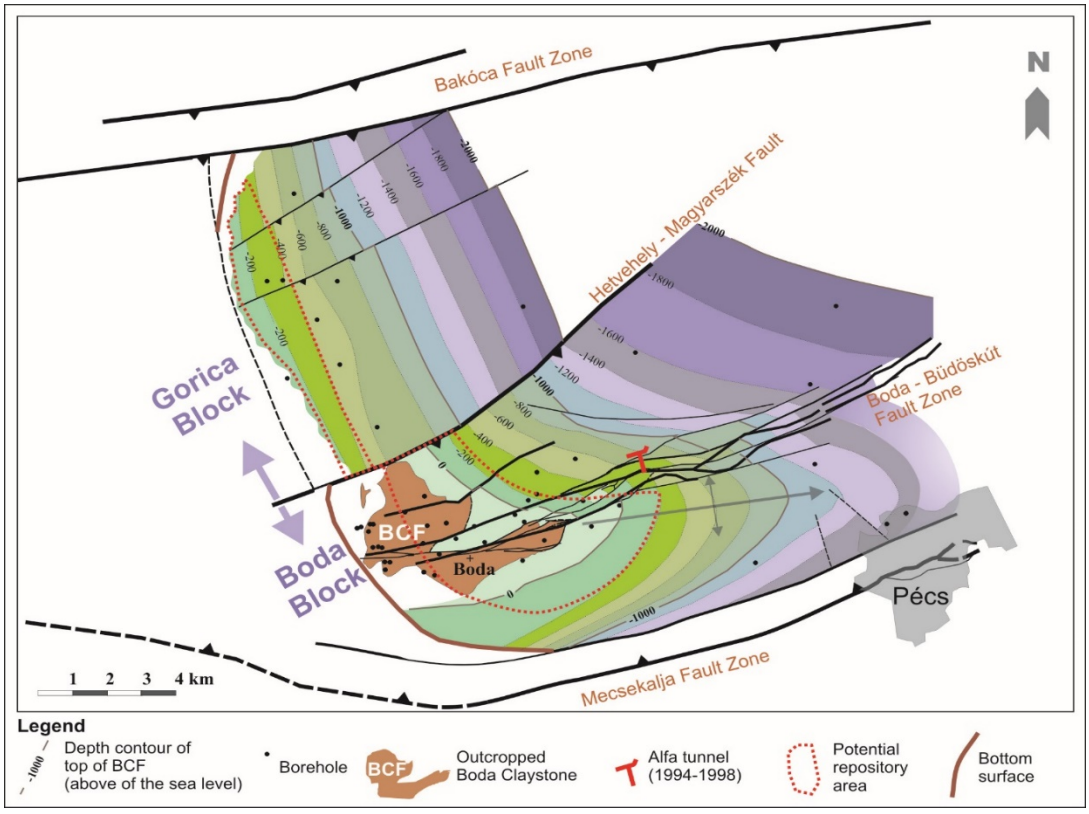

Source: Konrád, 2016.

Because sedimentation conditions were nearly constant for millions of years, an extremely thick quasi-homogeneous sequence was formed. Due to minor, cyclic changes in depositional environment, the formation can be divided into six characteristic rock types, though the main body of the formation (approximately 90%) consists of one rock type, albitic claystone.

The study area of the formation can be divided into two blocks – the Boda and the Gorica – separated by a fault zone. In the two blocks, the thickness of the BCF, the mineralogical composition and the degree of diagenesis is different (Figure A3-35).

The Boda Block is situated within the Western Mecsek Anticline structure and drill core from this block can be seen in Figure A3-36. The axis of the anticline plunges to the east, and, therefore, the Boda Claystone has been eroded in the west. The formation outcrops around the village of Boda where the overlying units have been eroded. Its depth increases with the plunge of the anticline towards the east and with the dipping of strata to both the north and south. The northern and eastern limits of the block are currently unknown. In this block, the maximum thickness of the BCF varies between 700 and 1 000 m in the central region, resulting in considerable freedom when seeking the optimal site for a repository. During sedimentation, the catagenetic stage was reached under high temperature (200-250°C) and pressure (120-150 MPa) conditions. The BCF was covered at one point by sediments as thick as 3.5-4.5 km. The over-consolidated, highly indurated character of the BCF is a result of this diagenetic process.

The Gorica Block is located north of the Hetvehely-Magyarszék Fault Zone. Here, the Boda Claystone is overlain by Permian, Triassic and Miocene sediments and the beds dip to the NE. The overlying Kővágószőlős Sandstone is thinner in the region of the Gorica Block than that of the Boda Block. A total of eight drilled boreholes have reached the BCF in the Gorica Block, but none have drilled completely through the formation. Only the unfinished borehole, Ib-4, suggests that the Boda Claystone may be thinner here, ~250 m, than in the Boda Block. The amount of data available from work performed on this block is limited.

On the basis of mineralogical investigations (X-ray diffraction, differential thermal analysis, electron microprobe), the main rock-forming minerals of the BCF are: clay minerals (dominant are illite-muscovite and chlorite; smectite, kaolinite, vermiculite and mixed-layer clay minerals were identified in minor to trace amounts), authigenic albite, quartz, carbonate minerals (calcite and dolomite) and hematite (Árkai et al., 2011; Mathas, 1998; Varga et al., 2005; Varga et al., 2006). In addition, barite, anhydrite, authigenic K-feldspar and detrital constituents (muscovite, biotite, chlorite, zircon, rutile, apatite, ilmenite, Ca-bearing plagioclase, K-feldspar) were identified in trace amounts. The authigenic albite is present as albite cement (typical of all rock types of the formation), albite and carbonate-lined disseminated irregular white voids (typical of albitic claystone) and albite replacement of detrital feldspars in sandstone beds (Árkai et al., 2011; Mathas, 1998; Varga et al., 2006).

Six main rock types of the BCF can be defined based on mineralogical, geochemical and textural considerations (see Table A3-2): albitic claystone, albitolite, "true" siltstone, dolomite interbeddings, sandstone and conglomerate (Árkai et al., 2011; Barabas and Barabas-Stuhl, 1998; Mathas, 1998; Varga et al., 2006; Konrád et al., 2010). The dominant rock type of the formation is albitic claystone. This mineralogical composition is typical in the perianticlinal structure of the Western Mecsek Mountains. Core recovered in borehole Ib-4 (Gorica Block) is consistent with typical composition of the BCF, though this succession does contain abundant analcime (see Table A3-3). Previous mineralogical investigations show that the amounts of analcime present in the formation can range between 8 and 25 wt.%.

Figure A3-35: **General geological sections for the comparison of lithostratigraphical units in the Boda and in the Gorica blocks**

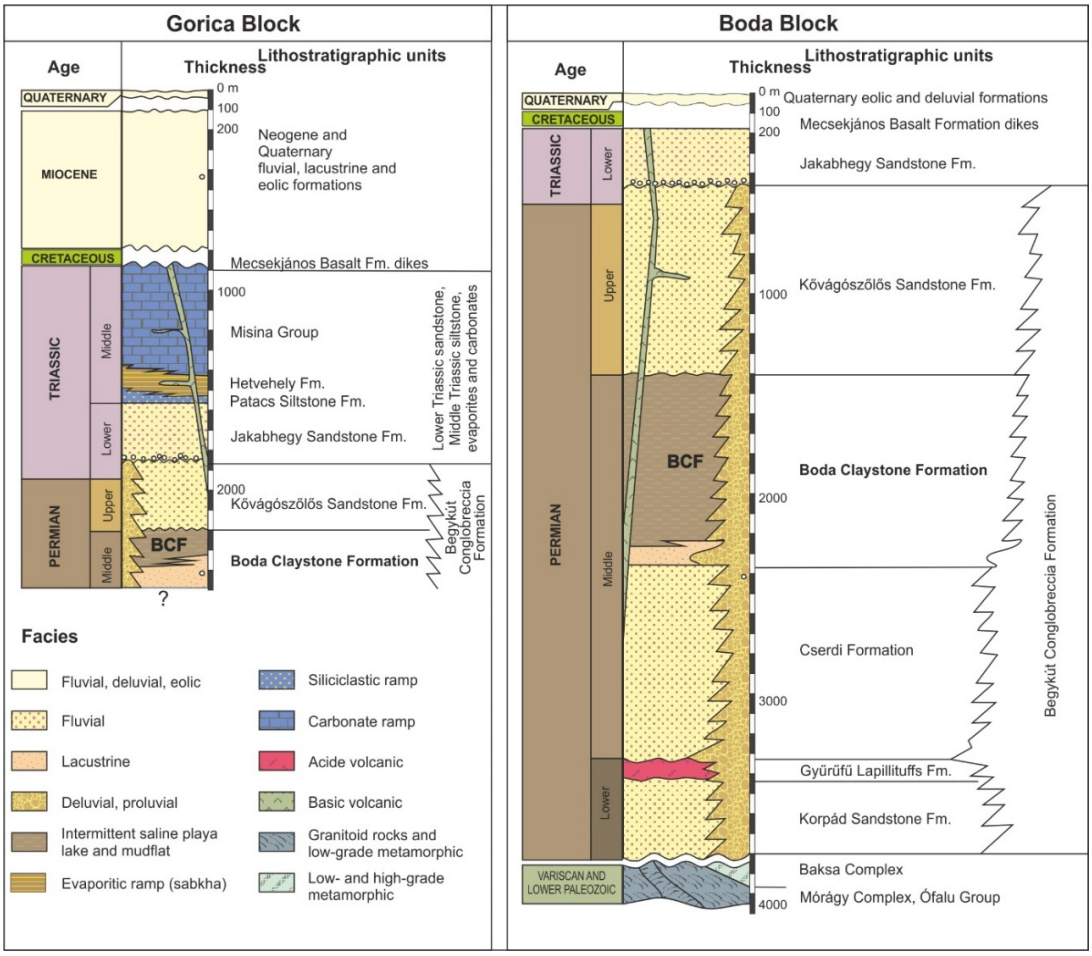

Source: Modified from Konrád, 2010.

Table A3-2: **Main rock types of the BCF**

Rock types	**clay minerals** (wt.%)	**authigenic albite** (wt.%)	**quartz** (wt.%)	**carbonates** (wt.%)	**hematite** (wt.%)
albitic claystone	20-50	20-50	5-10	~10	7-10
Albitolite	<25	>50	<10	10	5-6
"true" siltstone	approx. 10	>35	>25	approx. 10	5
dolomite interbeddings	10	30-40	5	35-50	5
Sandstone	5 (trace)	25-40 (feldspar)	20-30	5-20	5 (trace)

Table A3-3: **Ib-4 borehole mineralogy**

Samples Ib-4	**clay minerals**	**authigenic albite**	**analcime**	**quartz**	**carbonates**	**hematite**
	wt.%					
527.2 m	42	8	12	13	18	6
538.7 m	34	7	16	28	10	5
560.64 m	43	16	20	3	10	8

Figure A3-36: **BCF cores from the BAF-2 borehole (539-544 m), Boda block**

Source: Konrád, 2015.

In the Middle Cretaceous, on the basis of thickness of overlying strata in the perianticlinal structure of the Western Mecsek Mountains, the BCF was located at a burial depth of at least 3.5 to 4.5 km. The illite and chlorite crystallinity, as well as vitrinite reflectance data determined in the area of the perianticlinal structure of the Western Mecsek Mountains, point to maximum diagenetic temperatures of 200-250°C (Árkai et al., 2000). Higher illite and chlorite crystallinity determined in core samples from the deep borehole, Ib-4 (Gorica Block), however, suggest that the BCF in Gorica Block underwent lower-grade diagenesis.

Geochemistry, hydrogeology and transport properties

Bulk porosity and hydraulic conductivity of the intact rock matrix are very low (0.6-1.4%; 10^{-15} m/s) and the average unconfined strength exceeds 100 MPa. Mineral composition of the 35-50% clay content corresponds to burial history. The dominant clay mineral is illite (30-40%), and chlorite content is 5-10%. Smectite content is generally near the detection limit. Smectites occur in larger amounts in the weathered zone of outcrops and inside the deformation zones of faults. Due to the burial (thermal) history of BCF, the possible impact of heat production of HLW (e.g. alteration of clay minerals, thermal softening) is assumed to be rather limited compared to younger argillaceous formations that have not undergone the same thermal stresses.

Due to its eventful tectonic history, the BCF has a discontinuous character. Traces of four different tectonic periods have been recognised by detailed surface and underground geological mapping. Joints and fractures are completely filled by various clay, carbonate or sulphatic materials (see Figure A3-37). Depending on the density, type and orientation of discontinuities, the measurable hydraulic conductivity of the actual rock zone can vary within a relatively broad interval (typically 10^{-9} to 10^{-13} m/s, with values of up to 10^{-8} m/s). Because of its geochemical and geotechnical character, the BCF does not show complete self-healing behaviour, even at the maximum depth of final disposal (1 000 m); however, some partial self-healing effects have been recognised. This aspect of geotechnical stability does not restrict the construction of a repository at depth.

The first measurements on the typical BCF were performed between 1989 and 1993 (Nagykanizsa, 1990; Nagykanizsa, 1991; MÉV, 1993). Porosity, Hg-porosity (up to 2000 bar) and gas permeability measurements were carried out on the rocks. The investigations indicated the rock structure to be microporous and determined the nature of microfracturing. The degree and quality of secondary porosity (Csicsàk, 1999) – openness and frequency of fractures – decisively determines the water storage capacity of the rock, as well as the nature of water flow. During in situ hydrodynamic tests, the permeability of the claystone was measured to be between 10^{-19} and 10^{-15} m^2 (Csicsàk, 1999). The salinity of the Boda Claystone Formation porewater was estimated to be between 1.5 and 7 g/L. Regarding its type, the porewater was considered to be Na^+-SO_4^{2-}-HCO_3-, Na^+-HCO_3^--SO_4^{2-}, and occasionally Na^+-SO_4^{2-}, and frequently mixes with water from the upper sandstone formation, which is mainly of Na^+-HCO_3^- and Na^+-HCO_3^--SO_4^{2-} type (Kovacs, 1998; Kovacs et al., 2000).

A systematic petrophysical analysis (Lakatos et al, 2002; Tóth, 2004) was carried out on some URL samples between 2002 and 2004. The density and porosity of the rock, as well as the diffusion coefficient for Cr^+, were determined. Water and gas permeability measurements under quasi-reservoir conditions ($p_{pore} \approx 80$ bar, $p_{confining} \approx 100$-120 bar, T ≈ 36°C) were carried out using the laboratory prototype of an instrument working according to the pressure-pulse decay (PPD) principle (Szűcs and Fedor, 2007; Fedor et al., 2008). The effective porosity (Lakatos et al., 2002) was found to be higher (1-3%) than estimated from previous measurements. The plugs needed very long time periods to reach a completely dry state and, in this state, the plugs adsorbed the humidity of their environment. Water permeability was one to three orders of magnitude lower than the gas permeability of a given plug. Because of mineralogical inhomogeneity, the plugs rapidly adsorbed different, and occasionally significant, amounts of water (0.1-0.2 cm^3) during the permeability measurements.

Figure A3-37: **Tectonic joints on the wall of the URL exploration tunnel filled with calcite veins**

Source: Hámos, 2015.

A systematic petrophysical investigation on a 1-m long sample from the overlying sandstone, and on a 10-m long BCF sample, was undertaken as part of the investigation of the Gorica Block between 2009 and 2013, mainly for the purpose of method development (Fedor and Somodi, 2010; Fedor et al., 2012; Fedor, 2014). During the project, core scanning and the Laser Induced Pyrolysis System (LIPS), detailed petrographical description, dry and wet computed tomography (CT) on full cores, as well as pore-scale investigations (N_2, CO_2, high-pressure – ~4 100 bar – Hg-porosimetry) and reservoir characterisation (acoustic and electric properties measurements, gas permeability, gas- and water permeability under reservoir conditions) were undertaken, together with mineralogical investigations (microscopy, Inductively Coupled Plasma – Mass Spectrometry [ICP-MS], X-ray diffraction), thermal tests and organic matter content analyses on 44 core sections. The results suggest that the permeability of the BCF from the Gorica Block is controlled primarily by fracturing and is likely to change under varying circumstances (self-healing ability). Two types of fracturing can be distinguished in the rock mass and the predominant type is the result of drying of the rock (5-15 nm range), often causing destruction of the sample. Primary porosity can be connected to micropores (< 2 nm). The water cannot be fully extracted from the sample, even following drying for a very long time period, and the rock is noted to adsorb humidity from the air. Water occurs in its smallest amount as free water, and in larger quantities as adhesive water and in the structure of clay minerals. As a result, a very small amount of swelling clay is fundamentally influencing rock behaviour (Parneix et al., 2008). The flow of free water is limited as well, by the size of capillaries. Diffusion processes are taking place within the rock, even on the

level of fractures. On the basis of the developed laboratory protocol, the water and gas permeability of the rock under reservoir conditions, using pressure-pulse decay (RS-PPD), can be determined in a short time. Experience to-date suggests that the porewater of BCF cannot be fully extracted using current methods. At present, the development of a new method is in progress for the extraction/retrieval of porewater (Fedor et al., 2014).

Favourable formation attributes

The areal extent and thickness of the lithological units allow for predictability at scales relevant to establishing safety

- The horizontal and vertical extension of the BCF, in consideration of a potential disposal area, allows accommodation of a robust (in location) disposal concept in the safety case:
  - thickness: 700-1 000 m (Boda Block) and 200-250 m (Gorica Block);
  - area: 20-25 km^2 (Boda Block) and 15-20 km^2 (Gorica Block); and
  - present-day burial depth : 0-1 600 m (Boda Block) and 350-600 m (Gorica Block).
- The low uplift of Western Mecsek (< 0.5 mm/year) ensures that a disposal facility, which is located > 500 m depth b.g.s., will stay under the surface until the end of safety-relevant time frames (which is assumed to be 1 Ma).

The presence of natural barriers (host and enclosing formations) acts to isolate the host rock and contain solutes for safety-relevant time frames

- There are thick overlying beds at the potential disposal zone and uplift of the Western Mecsek is low; therefore, no major changes in either isolation properties or in solute containment capacity of the host rock are expected for safety-relevant time frames.

Stability of the geosphere on safety-relevant time frames supported by multiple lines of geoscientific evidence/reasoning

- It is proved by geostatistical methods that core samples from different parts of the BCF show no differences in their chemical characteristics and in their mineralogical compositions (Hámos et al., 1998).
- To-date, there is no knowledge/identification of any geoscientific feature/parameter that would have (some/major) influence on the isolation capacity of the BCF, and would be different with respect to physical properties of the BCF in the deeper parts of the potential disposal zone when compared to the near surface (Hámos et al., 1998).
- Because sedimentation conditions of the BCF were nearly constant for millions of years, an extremely thick quasi-homogeneous sequence was formed.
- BCF has some potential for partial self-healing capacity.

Transport processes are anticipated to remain diffusion-dominated over geologic time frames (hundreds of thousands to millions of years)

- Bulk porosity and hydraulic conductivity of the intact rock matrix is very low (0.6-1.4%; 10^{-15} m/s).
- A very small amount of swelling clays are fundamentally influencing rock behaviour.
- The flow of free water is limited by the size of capillaries.
- Diffusion takes place inside the rock, even at the scale of fractures.

Geochemical stability of the groundwater-porewater system over geologic time frames

- The lack of organic material and pyrite helps to maintain the long-term geochemical stability of the formation.
- Intensive oxidation processes, which would influence the rock's mechanical status considerably, are not expected to occur within the lifetime of the repository.
- Due to the burial (thermal) history of the BCF, the possible impact of heat production from the HLW (e.g. alteration of clay minerals, thermal softening) will be limited.

Geomechanical stability of the formations to natural perturbations

- The potential disposal zone is protected from the natural perturbations by the thick overlying beds.

Summary and future work

According to the "Do and See" strategy, the decades-long research for a suitable site has to be maintained without a validated back-end strategy. Based on experiences of countries with well-developed spent fuel/HLW disposal programmes, the Hungarian disposal programme expects an operational licence that would last for about five decades.

There are four planned phases of the programme:

- Siting is planned to last until 2030.
- Building of the URL would be between 2030 and 2038.
- Operation of the URL would last until 2055.
- Installation of the DGR, ~10 years duration, until 2065.

The first phase is divided into three research sub-phases, of which the very first sub-phase is now in progress. Current surface investigation activities – 6 deep boreholes, seismic profiles, hydrogeological (re)mobilisation – have the goal of narrowing the target siting area. PURAM has started examining a 37 km^2 potential siting area, which would have to be reduced to ~10-12 km^2. The second sub-phase of research activities is going to outline the footprint of the URL. In the third sub-phase, siting of the target area will be carried out, which will involve the initial construction of the URL.

It has not yet been decided whether or not the URL will be part of the DGR facility, and this will be decided only when knowledge of the candidate host formation, and the potential layout(s) of the disposal facility, become available.

References

Árkai, P. et al. (2000), "Composition, Diagenetic and Post-diagenetic Alterations of a Possible Radioactive Waste Repository Site: the Boda Albitic Claystone Formation, Southern Hungary", *Acta Geologica Hungarica*, No. 43(4), pp. 351-378.

Barabás, A. and Á. Barabás-Stuhl (1998), "Stratigraphy of the Permian formations in the Mecsek Mountains and its surroundings", In: *Stratigraphy of geological formations of Hungary*, Mol Plc. and Hung. Geol. Institute, Budapest, pp. 187-215 (In Hungarian).

Csicsák, J. (Ed.) (1999), "The short-term program for the qualification of Boda Claystone Formation", Research final report, V. volume, Hydrogeological, hydrochemical investigation program, MECSEKÉRC Inc., Pécs, pp. 1-117 (In Hungarian).

Fedor, F. et al. (2008), "Laboratory Pressure Pulse Decay permeability measurement of Boda Claystone, Mecsek Mts., SW Hungary", *Physics and Chemistry of the Earth,* S45-S53.

Fedor, F. and G. Somodi (2010), "The complex investigation of Boda Claystone Formation for the comparability of laboratory and field measurements – preliminary results", Pál-Molnár E. (Ed): *Basin Development and Geological Resources* (Hungarian Geological Institute, "Vándorgyűlés" abstract volume), Geolitera, Szeged, pp. 49-51.

Fedor, F. et al. (2012), "Interdisciplinary investigation of Boda Claystone Formation – preliminary results", 5th International Meeting on Clays in Natural and Engineered Barriers for Radioactive Waste Confinement, Montpellier, 22-25 October 2012 (poster presentation).

Fedor, F. (Ed.) (2013), "The complex investigation series on samples from the Ib-4 borehole", Research report, MecsekÉrc Rt, Pécs (In Hungarian).

Fedor, F. et al. (2014), "Determination of the BCF pore water content – possibilities and limitations", Research Report, MecsekÉrc Rt, Pécs (In Hungarian).

Geological results of the boreholes BAF-1, -1A and -2: 1. fig. Publication of the BCF investigation conference day, 39-45 pages. ISBN 978-963-8221-60-5

Hámos, G., Z. Máthé, and Z. Nagy (1998), "Homogeneity of Boda Claystone Formation: A Geostatistical Analaysis", Research Report, MecsekÉrc Rt, Pécs (In Hungarian).

Hámos, G. (Ed.) et al. (1998), "Representativity of geoscientific information from URL located in Boda Claystone Formation. A Geostatistical Analysis", Research Report, MecsekÉrc Rt, Pécs (In Hungarian).

Hámos G. (1999), A Bodai Aleurolit Formáció Minősítésének Rövidtávú Programja. Kutatási zárójelentés, 3. kötet: Földtani dokumentációs munkák a BAF megismerésére. Pécs, 1999. március. Kézirat. MECSEKÉRC Zrt., Pécs, Adattár. J-4020

Konrád, G. et al. (2010), "Sedimentology of a Permian playa lake: the Boda Claystone Formation, Hungary", *Geologos*, No. 16(1), pp. 27-41.

Konrád G. (Geológus Kft.), Halász A., Sebe K. (PTE), Bernáth Gy., Gärtner D. (Geo-Log Kft.), Hámos G., Sámson M., Máthé Z., Óbert V. (MECSEKÉRC Zrt.), Benei B. (BIOCENTRUM Kft.), Magyar L. (TIMÓ Bt.) (2016), A BAF-1, -1A és a BAF-2 fúrás földtani eredményei. BAF kutatás szakmai előadói nap kiadványa. 39-45. oldal. ISBN 978-963-8221-60-5

Konrád G. (2012), A Bodai Agyagkő szerkezeti helyzete, litológiája és fáciese, Környezetföldtani megközelítés, Habilitációs pályázat. Structural position, lithology and facies of the Boda Claystone Formation, Environmental geological approach. Habilitation thesis.

Kovács, L. (Ed.) (1998), "Digest on the Results of Short-Term Characterization Programme of Boda Claystone Formation", Special edition of PURAM.

Kovács, L., G. Hámos and J. Csicsák (2000), "Actual State of the Site Characterization Programme of the Boda Siltstone Formation", *Bulletin of the Hungarian Geological Society*, No. 130(2), pp. 197-206.

Lakatos, I., F. Fedor and J. Tóth, (2002), "Hydrodynamic investigations on samples from the Boda Claystone Formation", internal report, Mecsekérc Plc. Pécs (In Hungarian).

Máthé, Z. (Ed.) (1998), "Summary report of the site charachterization program of the Boda Siltstone Formation", Vol. 4. Manuscript, Mecsek Ore Environment Company, Pécs, 76 p.

MÉV (1993), "Report about the results of geological research related to the recommended Mecsek Deep Waste Disposal Site in 1989-1992", Research report. (MÉV, Pécs), MÉV Database (In Hungarian).

MÉV (Mecseki Ércbányászati Vállalat) Berta Zs., Csicsák J., Hámos G., Hideg J., Kovács L., Majoros Gy., Máthé Z., Nagy Z. (1995), ÖSSZEFOGLALÓ JELENTÉS a PA Rt és a MÉV között létrejött, H301M-4-1/93/k, valamint a H301M-4-19/94 rendelési számú Vállalkozási Szerződések keretében elvégzett, a Bodai Aleurolit Formáció minősítését célzó munkálatok eredményeiről. – Kézirat. MECSEKÉRC Zrt. Adattár, Pécs. J-2666.

MÉV (1995), ÖSSZEFOGLALÓ JELENTÉS a PA Rt és a MÉV között létrejött, H301M-4-1/93/k, valamint a H301M-4-19/94 rendelési számú Vállalkozási Szerződések keretében elvégzett, a Bodai Aleurolit Formáció minősítését célzó munkálatok eredményeiről. MÉV Adattár. (Summary report on the results of works for the characterization of Boda Claystone Formation within the scope of Contracts no. H301M-4-1/93/k and H301M-4-19/94 bound between PA Rt. and MÉV.) I.8.2. photo. J-2666

Nagykanizsa (1990), "Determination of the permeability of Lower Permian BCF samples by constant reservoir pressure at changing pore pressure and temperature", Hungarian Hydrocarbon Institute report (In Hungarian).

Nagykanizsa (1991), "Determination of the permeability of Lower Permian BCF samples by constant reservoir pressure at changing pore pressure and temperature", Hungarian Hydrocarbon Institute, part of report (In Hungarian).

Parneix, J.-C., A. Bouchet, A. Mazurier, N. Bétin, S. Ramirez and J.C. Robinet (Eds.) (2008), "Synthesis of the characterization of Callovo-Oxfordian, Opalinus, Boom and Boda clays", Fundamental Processes of Radionuclide Migration (FUNMIG) project PID 3.2.18.

Sámson M. (szerk.), Hámos G., Máthé Z., Mázik J., Mészáros A., Vágó Z. (Mecsekérc Zrt.), Bernáth Gy., Gärtner D., Prohászka A. (Geo-Log Kft.), Kovács At. Cs. (MFGI), Andrássy M., Dankó Gy., Korpai F., Matthäus Zieger (Golder Zrt.), Konrád Gy., Halász A., Sebe K. (Mérce Bt.), Ko-vács L., Zierkelbach-Kovács B., Somodi G. (Kőmérő Kft.), Ács P., Fedor F., Horváth J., Ko-roncz P. J. (GEOCHEM Kft.) (2014), BAF-2 fúrás dokumentáló és értékelő jelentése. — Kézirat. MECSEKÉRC Zrt. Adattár. RHK-K-011/14

Szűcs, I. and F. Fedor (2007), "Spatial Extension and Parameter Integration into the Safety Case – Examples from the Hungarian LLW/ILW and HLW Disposal Project", in *Linkage of Geoscientific Arguments and Evidence in Supporting Safety Case* (workshop proceedings), NEA No. 6119, pp. 163-165, OECD Publishing, Paris.

Tóth, J. (2004), "Porosity of the G-35 and G36 plugs", summary table, internal report.

TS-ENERCON Kft. (2004), "Conception plan and cost estimation for a deep geological repository for the final disposal of high level wastes and spent nuclear fuel assemblies of Hungary", Budapest.

Varga, A. et al. (2005), "Chemical composition, provenance and early diagenetic processes of playa lake deposits from the Boda Siltstone Formation (Upper Permian)", SW Hungary, *Acta Geologica Hungarica*, No. 48, pp. 49-68.

Varga, A. et al. (2006), "Mineralogical, petrological and geochemical characteristics of the siliciclastic rock types of Boda Siltstone Formation", *Bulletin of the Hungarian Geological Society*, No. 136(2), pp. 201-232.

Koetoi and Wakkanai Formations – Japan

Introduction

The Horonobe URL project is a comprehensive research and development (R&D) programme with the overall aim of characterising the sedimentary formations that contain saline groundwater within the region surrounding Horonobe Town in Hokkaido, northern Japan (e.g. Ota et al., 2011). The project involves both geoscientific study and R&D on geological disposal technology in sedimentary formations.

Three major goals of the project include:

1. Establishing/evaluating techniques that will be necessary to ensure adequate characterisation of the deep geological environment;
2. Development/testing of engineering technologies for use in the deep underground; and
3. Confirming/testing the applicability of geological disposal technologies and the disposal concept in a specific geological environment.

The project consists of three phases, extending over a period of approximately 20 years, including: surface-based investigations (Phase I), investigations during tunnel excavation (Phase II), and investigations in the underground facilities (Phase III). Phase I of the Horonobe URL project consisted of preliminary surface investigations undertaken between March 2001 and March 2006. Phases II and III involve detailed sub-surface investigations, were initiated in November 2005, and are ongoing.

Disposal concept

The concept of geological disposal in Japan is based on a multi-barrier system approach, combining the natural, isolating properties of the geologic environment with an engineered barrier system (EBS), as described in the H12 report: Project to Establish the Scientific and Technical Basis for HLW disposal in Japan (JNC, 2000). The approach to develop a disposal system concept has been generic to-date (i.e. has targeted neither a particular rock type nor a particular geographical area). In developing the disposal concept, special consideration is given to evaluating the long-term stability of the geological environment, particularly in Japan, which is located in a tectonically active zone.

Due to Japan's complex geology, an EBS design was developed with sufficient margins in its isolation function(s) to accommodate a wide range of geologic conditions (e.g. JNC, 2000). It is assumed that disruptive events, such as major fault movement and volcanic activity, would lead to exclusion of a particular location/geologic setting as part of the site selection process by the Nuclear Waste Management Organization (NUMO) of Japan (e.g. NUMO, 2004). Those geological environments identified as having favourable characteristics for construction of the disposal system, and are interpreted as stable geologic setting(s), will dictate the requirements of the repository design. The major weighting of overall barrier performance of the disposal system is borne by the near-field (i.e. EBS). The multi-barrier system and its functions are depicted in Figure A3-38.

When a potential disposal site is selected in the future, an optimised design for the EBS will be determined based on both safety and economic considerations – including the geologic conditions specific to the site. The reference layout of the EBS in the H12 report assumes either axial, horizontal tunnel emplacement or vertical pit emplacement of vitrified waste as a generic concept (Figure A3-39). Any radioactivity (i.e. radionuclides) released from the EBS will decay, and concentrations will be reduced by dilution and retardation during the long migration period within the geosphere. The repository is designed to provide intrinsic, long-term passive safety.

Figure A3-38: **Basic concept for the geologic disposal system in Japan and expected barrier functions**

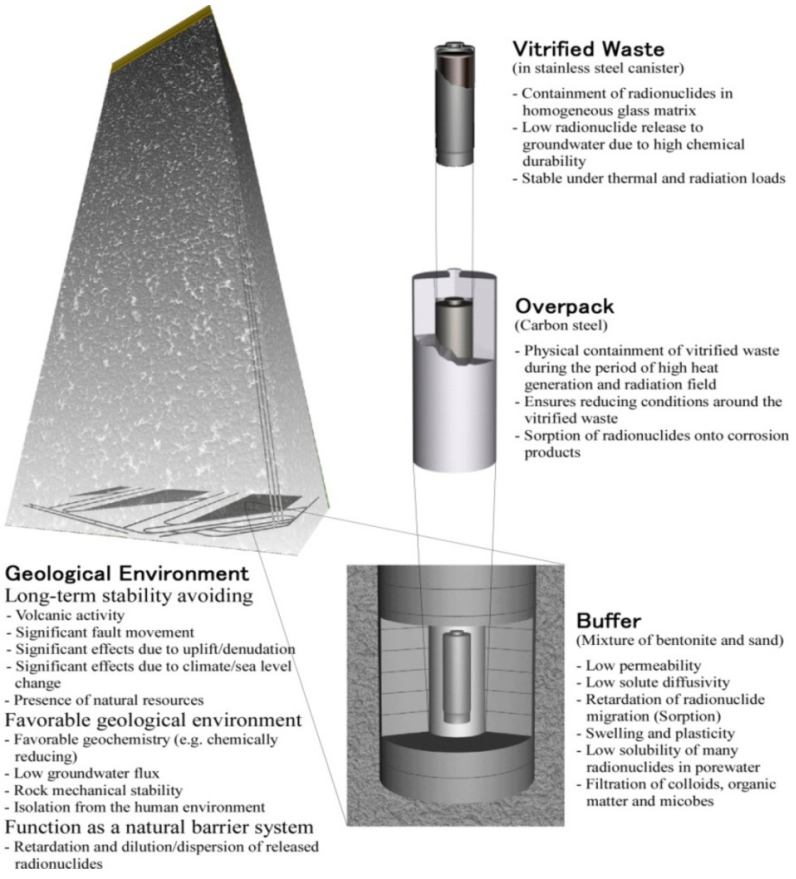

Source: JNC, 2000.

Figure A3-39: **Specifications of the disposal tunnels, disposal tunnel spacing and waste package pitch**

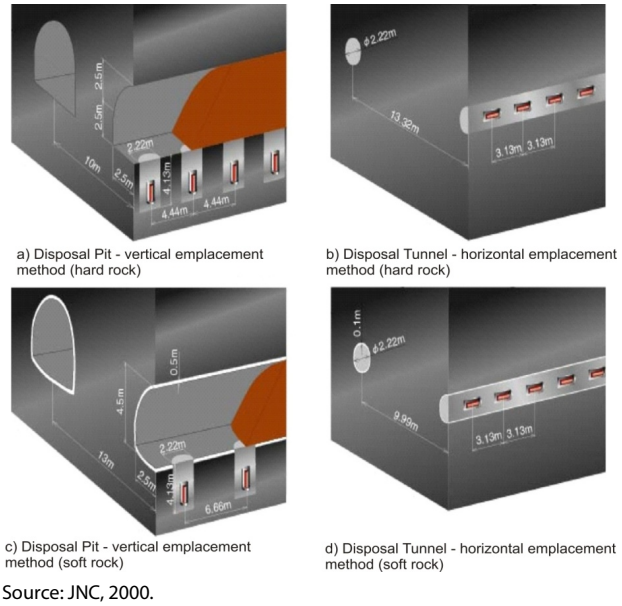

Source: JNC, 2000.

The H12 report demonstrated the basic technical feasibility of geological disposal in Japan without specifying any particular geological environment. The practicality and reliability of the technologies used in the H12 report should be confirmed by applying them to specific geological environments. Considering the range of characteristics and the distribution of the geology in Japan, two URL projects – the Horonobe URL for investigation of sedimentary rock with saline groundwater, and the Mizunami URL for investigation of crystalline rock with fresh groundwater – have been established (e.g. Ota et al., 2011). The experience and knowledge gained in the URL projects will support methodologies for investigations for NUMO's repository site selection and will be used to establish safety regulations; however, these URLs will never be transferred to the implementing entity.

Formation properties

An overview of the Horonobe URL is illustrated in Figure A3-40. In the Horonobe URL, the ventilation and two access shafts have been excavated through unconsolidated sediment (approximately 20 m thickness) into the sedimentary rocks (i.e. Koetoi and Wakkanai formations). As shown in Figure A3-40, horizontal galleries have been excavated at 140 m, 250 m and 350 m depth.

Figure A3-40: **Overview of the Horonobe URL**

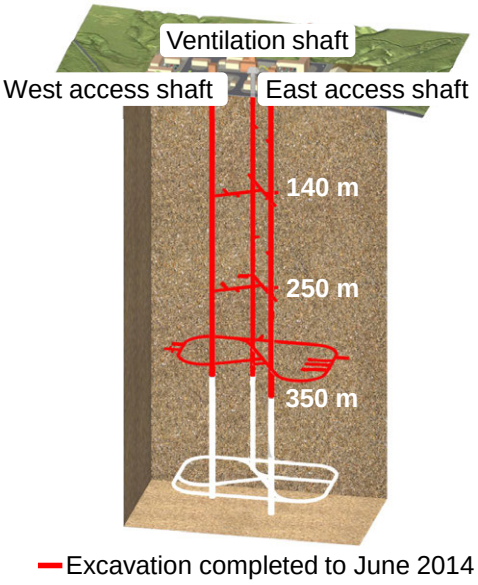

Note: Image of URL layout may change as investigation progress.

Source: Koide et al. 2015.

Geology/structure

The Horonobe URL site is located on the eastern margin of a Neogene- to Quaternary-aged sedimentary basin on the western side of northern Hokkaido. The site is located in an active Quaternary-aged foreland fold-and-thrust belt near the boundary between the Okhotsk and Amurian plates (e.g. Yamamoto, 1979; Wei and Seno, 1998; Ikeda, 2002) (Figure A3-41). The basin consists of the Wakkanai Formation (siliceous mudstones with opal-CT), the Koetoi Formation (diatomaceous mudstones with opal-A), the Yuchi Formation (fine to medium-grained sandstones) and the Sarabetsu Formation (alternating beds of conglomerate, sandstone and mudstone, intercalated with coal seams) (see Figure A3-42). The Koetoi and Wakkanai formations are the main target rocks for the Horonobe URL project.

With respect to distribution of the target rocks in the URL site, the Koetoi Formation is found at depth between 20 m and 250 m, and the Wakkanai Formation is observed at depths greater than approximately 250 m. Additionally, the boundary between the Koetoi and Wakkanai formations generally strikes northwest-southeast and dips moderately westward (Tokiwa et al., 2014).

Burial and subsidence of the Wakkanai, Koetoi and Yuchi formations occurred during the Neogene to Quaternary. The siliceous mudstone was buried to a depth of more than 1 km at the time of maximum burial (Ishii et al., 2008; Kai and Maekawa, 2009). Subsequently, uplift and denudation initiated approximately 1.0 Ma ago with the deposition of Sarabetsu Formation, which followed the flexural folding that began between 2.2 and 1.0 Ma in response to regional east-west compression (Ishii et al., 2008). Several anticline hinge lines, such as F1, F2 and F3 in Figure A3-41, developed with northwest-southeast to north-northwest-south-southeast trends, plunging gently to the northwest or southeast (Ishii, 2012).

With respect to mineralogy, X-ray diffraction analyses indicate that the Koetoi and Wakkanai formations consist mainly of amorphous materials (principally opal-A and/or opal-CT) in addition to trace amounts of quartz, K-feldspar, clay minerals (kaolinite, illite, smectite and chlorite), pyrite and carbonate (calcite, siderite) (Ota et al., 2011). The upper part of the Wakkanai Formation is thought to be a diagenetic transition zone, separating biogenic sediments consisting mainly of opal-A in the overlying Koetoi Formation from deeper zones in the Wakkanai Formation where opal-CT dominates.

Figure A3-41: **Geological map and geological cross-section of the Horonobe Area, showing locations of boreholes and the Horonobe URL**

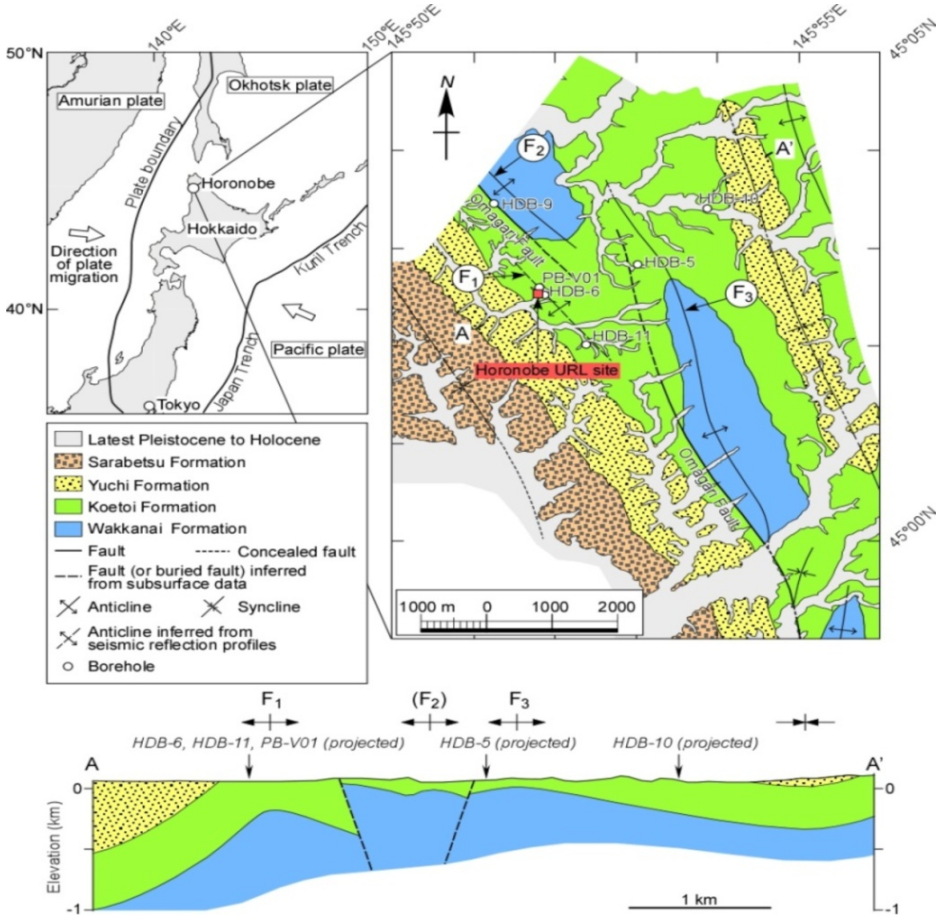

Note: Plate boundaries and directions of plate movement are defined based on information in Wei and Seno (1998). F1, F2 and F3 are specific fold hinges.

Source: Ishii et al., 2008.

Figure A3-42: **Schematic columnar section of the Horonobe area**

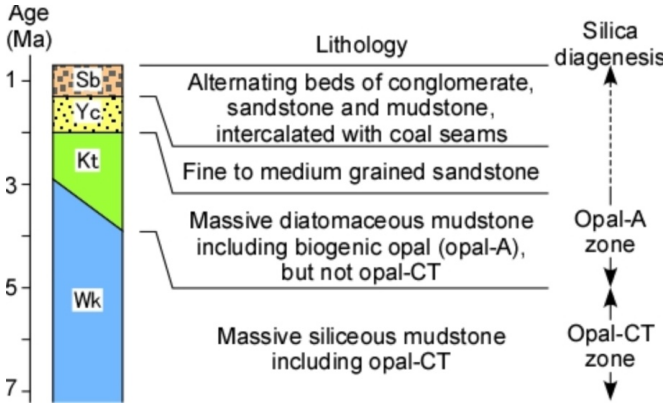

Note: Sb – Sarabetsu Formation, Yc – Yuchi Formation, Kt – Koetoi Formation and Wk – Wakkanai Formation.

Source: Modified from Ota et al., 2011.

Geochemistry, hydrogeology and transport properties

Geochemistry

Hydrochemical investigations demonstrate that at any given locality within the URL area, shallow, fresh, Na-HCO_3-dominated groundwater occurs above saline, Na-Cl-dominated groundwater (Hama et al., 2007; Ota et al., 2011). The most saline groundwater sampled in the vicinity of the URL has TDS of ~22 000 mg/L (Hama et al., 2007). With respect to the groundwater chemistry, both horizontal and vertical salinity gradients are recognised. The stable isotopes of oxygen and hydrogen, as well as salinity, increase with increasing depth (Hama et al., 2007; Sasamoto et al., 2011). The evolution of Na-Cl-dominated groundwater is provisionally interpreted to have involved the dilution of fossil seawater, accompanied by diagenetic mineral-water reactions, such as the alteration of opal-A to opal-CT (Hama et al., 2007). Furthermore, spatial variations in groundwater salinity are tentatively interpreted to be related to variations in the frequency and spatial distribution of fractures (Hama et al., 2007).

In situ measurement of pH and Eh has been conducted at about 600 mbgs in borehole HDB-11 for the groundwater in the Wakkanai Formation, and the resultant values are 6.2 and -166 mV, respectively (e.g. Ota et al., 2011). The groundwater contains high concentrations of dissolved gases, including $CH_4(g)$, $CO_2(g)$, $H_2S(g)$ and various hydrocarbons, which exsolve from the groundwaters as they are pumped. The effects of such degassing on the chemistry of groundwater was evaluated using a reaction-path model to simulate the titration of the gases exsolved (Sasamoto et al., 2011). Results suggest that undisturbed groundwaters have similar values for pH; however, the redox potentials calculated using the corrected groundwater compositions and assuming equilibrium for the $CH_4(aq)/CO_2(aq)$ redox couple are more negative than the in situ value (Sasamoto et al., 2011). Regarding a potential reaction governing redox potentials, the SO_4^{2-}/pyrite redox couple could be considered as a possible control on the Horonobe groundwaters (e.g. Amano et al., 2012).

Hydrogeology and transport properties

In the URL area, two major types of faults have been observed: faults cross-cutting bedding planes at a high angle (FCBs), and bedding faults parallel to bedding planes (Ishii and Fukushima, 2006). The former faults (i.e. FCBs) are generally strike-slip faults oblique to the fold axes, and the FCBs are believed to be the dominant flow paths based on the results of geological and hydrological investigations (Ishii and Fukushima, 2006; Kurikami et al., 2008).

Hydrological investigations (i.e. borehole televiewer and electromagnetic imaging logging, fluid logging, pressure build-up testing, hydraulic packer testing) in the deep boreholes, and supplemental permeability tests in the laboratory, were performed for the Horonobe URL area. Results indicate that permeability varies significantly when comparing measurements from both the field and laboratory; a close relationship between the fracture/fault distribution and heterogeneities in formation permeability is suggested (Kurikami et al., 2008). Additionally, the results of field measurement by hydraulic packer testing in the Wakkanai Formation suggest that the permeability generally seems to decrease with increasing depth, and the sections with the highest permeability (i.e. hydraulic conductivity higher than 10^{-5} m^2/s) are limited to depths of less than ~400 m b.g.s. (see Figure A3-43).

Figure A3-43: **Hydraulic conductivity derived from hydraulic packer tests**

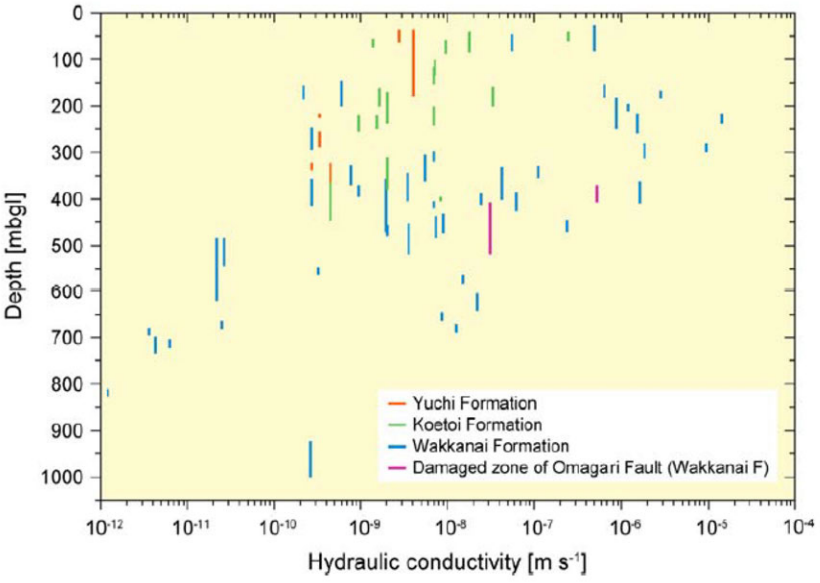

Source: Ota et al., 2011.

Considering the above hydrogeological features, the following hydrogeological conceptual model for both the Koetoi and Wakkanai formations (depending on the scale) has been proposed (Kurikami et al., 2008): a) the Koetoi Formation could be considered as homogeneous (porous) media under any scale; b) the Wakkanai Formation should be modelled as heterogeneous (fractured) media, considering the fracture distributions at the scales ranging from 10 to 200 m. At scales larger than 200 m, the Wakkanai could be considered homogeneous.

The nature and distribution of fractures is an important consideration for the evaluation of solute transport in the Wakkanai Formation, and non-sorbing tracer experiments using potassium iodide (KI) solution have been performed by using fractured cores (e.g. Hatanaka et al., 2004). The obtained breakthrough was evaluated by numerical calculations and the results indicate the importance of matrix diffusion for mass transport in fractured sedimentary rocks (Hatanaka et al., 2004).

Laboratory experiments focused on sorption and diffusion behaviours in samples from the Wakkanai Formation have been conducted using cationic Cs^+, anionic I^- and neutral HTO, in order to obtain relevant transport properties, such as K_d and D_e, for the development of the mechanistic sorption-diffusion model (Xia et al., 2006; Tachi et al., 2011). A clay-based modelling approach, assuming key contributions from the illite and smectite components, was proposed to interpret the observed diffusion and sorption behaviour (Tachi et al., 2011).

Diffusion and sorption behaviours in the Wakkanai Formation have been estimated by in situ dipole tracer experiments using both non-sorbing and sorbing tracers (Yokota and Tanaka, 2014). Preliminary interpretation of the experiments, based on a one-dimensional advection-dispersion equation, suggests the fracture surface of the Wakkanai Formation would have both reversible and irreversible sorption characteristics for Cs^{+} and Sr^{2+}, and irreversible sorption for Co^{2+} and Eu^{3+} (Yokota and Tanaka, 2014).

A brief summary of the key information presented in the included database is presented below.

- The age of the Koetoi and Wakkanai formations is 2 to 4 Ma and 3 to 7 Ma, respectively. The thickness for the combined formations in the URL is relatively thick (i.e. more than 400 m). The maximum burial depth for the formations is estimated at about 1 km.
- The dominant minerals (i.e. over 50 to 60 wt.%) in both the Koetoi and Wakkanai formations are amorphous silica minerals likely opal-A and opal-CT and the formations contain measurable quantities of clay minerals (e.g. illite, smectite). Trace amounts of sulfide and carbonate minerals are also present.
- With respect to rock chemistry, very limited information is available for the Wakkanai Formation, and the best estimated cation-exchange capacity value is relatively low in relation to the relatively low content of clay minerals.
- Porewater chemistry in both the Koetoi and Wakkanai formations are similar and indicate Na-Cl-type groundwaters.
- Water content and porosity of the Koetoi Formation is higher than that of the Wakkanai Formation.
- With regard to permeability, the measured values in laboratory for both the Koetoi and Wakkanai formations are generally low, though the measured porosities are higher. Regarding diffusion coefficients, the relevant data are limited to the Wakkanai Formation, and generally, there is no detailed description/explanation of the orientation of the samples with respect to bedding. The best-estimate values of D_e for HTO and I^{-} are average values reported in the database.
- Geomechanical parameters, such as uniaxial compressive strength and Young's moduli, are higher in the Koetoi Formation than in the Wakkanai Formation.

Favourable formation attributes

The areal extent and thickness of the lithological units allow for predictability at scales relevant to establishing safety

- Neogene sedimentary formations, which are widely distributed throughout Japan, were selected for investigation in the Horonobe URL project (Ota et al., 2011). Based on Japanese legislation, HLW should be disposed of in deep geological formations at depths greater than 300 m b.g.s. to isolate the waste from the human environment over the long-term. In addition, the required formation thickness in the Horonobe URL was defined assuming that the shaft would reach a maximum depth of ~500 m. Furthermore it was also required to select a site where the URL could be constructed and maintained safely.
  - Geophysical and borehole investigations around the URL site have confirmed that the target formations (Koetoi and Wakkanai) extend laterally over several kilometres and vertically, from near surface to at least 1 000 m, displaced/deformed by the Omagari Fault and related folds.
  - In the URL, the Koetoi and Wakkanai formations have been confirmed at depths of 20-250 m and 250-350 m (at present gallery level), respectively.

The presence of natural barriers (host and enclosing formations) acts to isolate the host rock and contain solutes for safety-relevant time frames

- Due to the nature of the generic URL project, performance evaluation of host rock for safety-relevant time frames has not been conducted.
  - The selected formations in the Horonobe URL project, however, could be considered as natural barriers due to their basic properties (e.g. low permeability, potential retardation capacity), which would be a factor in assessing the capacity of the formations to isolate radionuclides for the long-term.

Stability of the geosphere on safety-relevant time frames supported by multiple lines of geoscientific evidence/reasoning

- Natural events and processes which would occur over the next hundred thousand years and affect the stability of geosphere in Japan are: a) earthquakes and fault movement, b) volcanic and hydrothermal activity, c) uplift, subsidence, sedimentation and denudation, and d) climatic and sea level changes (JNC, 2000). Key natural phenomena which may have potential impacts on groundwater flow properties include past events (likely c and d above) (e.g. Niizato et al., 2008), and any more recent neo-tectonic activities around the URL area (Iwatsuki et al., 2009).
- A conceptual hydrogeological model considering the results of palaeo-hydrogeological study have been proposed, which defines three hydrogeological sub-systems as follows (see Figure A3-44 ; Iwatsuki et al., 2009): sub-system 1 is a porous-medium in the Koetoi Formation having low to moderate permeability (10^{-10} to 10^{-7} m/s); sub-system 2 is a fractured-medium in the upper Wakkanai Formation having low to high permeability (10^{-10} to 10^{-5} m/s); and, sub-system 3 represents a fracture-medium in the lower Wakkanai Formation (e.g. deeper than 400 m) having low to moderate permeability (10^{-10} to 10^{-7} m/s) (Iwatsuki et al., 2009). In both sub-system 1 and 2, mixing of groundwater between the recharged meteoric water and the connate seawater has been suggested due to uplift and denudation in the last 1 Ma (Iwatsuki et al., 2009). Connate seawater (resident in the formation in excess of 1.5 Ma – from Hama et al., 2007), having 1/3 to 1/2 of the salinity when compared with present-day seawater, has been preserved in sub-system 3 (Iwatsuki et al., 2009).
  - The relatively low-permeability sequence and deep section of the Horonobe URL area, represented by sub-system 3, suggest that natural events, such as climate change, uplift and denudation, may not affect the groundwater flow system at depth.
- In relation to the low-permeability conditions, geochemical stability of the groundwater over geologic time frames has also been investigated.
  - Horonobe groundwaters appear to be at equilibrium, or to closely approach equilibrium, with respect to carbonate and sulfide minerals (Hama et al., 2007; Iwatsuki et al., 2009; Sasamoto et al., 2011).
  - All of these minerals are observed as secondary minerals in the Wakkanai Formation.
  - It is, therefore, suggested that the geochemical conditions represented by pH (buffered by carbonate minerals) and redox condition (buffered by sulfide minerals) have been preserved for a long time since diagenesis, following formation deposition (Iwatsuki et al., 2009).

Figure A3-44: **Hydrogeological properties of sub-systems (above) and groundwater chemistry (below) around the Horonobe URL**

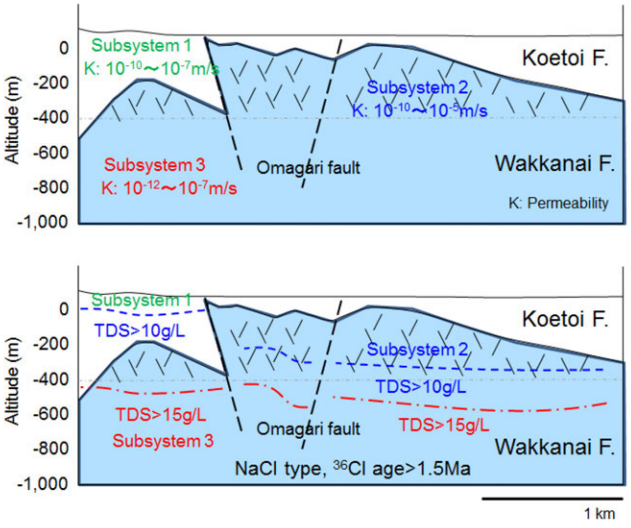

Source: Modified from Iwatsuki et al., 2009.

Summary and future work

The concept of geological disposal in Japan is based on a multi-barrier system approach that will combine the natural, isolating properties of the geosphere with the engineered barrier system (EBS). Evaluation of the long-term stability of the geological environment, particularly in Japan, is of key importance due its location within a tectonically active zone. EBS design must possess sufficient margins of safety to accommodate a wide range of geologic conditions. When a potential disposal site is selected in the future, an optimised EBS design will be determined based on both safety and economic considerations, with an aim to provide intrinsic, long-term passive safety.

Any investigations for repository site selection, which will be carried out by NUMO, established in 2000 as the implementation body for the geological disposal of high-level waste (HLW) in Japan, will be proceeded by a step-wise approach (i.e. literature surveys, and the subsequent investigation of preliminary surface-based and detailed sub-surface investigations).

Regarding the Horonobe URL project, future R&D projects have been proposed in response to the Japanese national programme requirements for research on HLW disposal. Ongoing (Phases II and III) investigations will continue and the tunnel excavation down to 500 m depth will be considered based on the plan for the "Deep Geological Research Laboratory (Tentative Name) Project", published in 1998 (JNC, 1998).

References

Amano, Y. et al. (2012), "Validation of surface-based hydrochemical investigation and the impact of underground facility construction at Horonobe URL", *Journal of Groundwater Hydrology*, No. 54(4), pp. 207-228 (in Japanese).

Hama, K. et al. (2007), "The hydrogeochemistry of argillaceous rock formation at the Horonobe URL site", *Physics and Chemistry of the Earth*, No. 32, pp. 170-180.

Hatanaka, K. et al. (2004), "Laboratory experiment on the hydraulic and transport properties of fractured soft sedimentary rock", Proceedings of the 33th international symposium of rock mechanics, pp. 313-318 (in Japanese).

Ikeda, Y. (2002), "The origin and mechanism of active folding in Japan", *Active Fault Research*, No. 22: pp. 67-70 (in Japanese).

Ishii, E. and T. Fukushima (2006), "A case study of analysis of faults in Neogene siliceous rocks", *Journal of the Japan Society of Engineering Geology*, No. 47, pp. 280-291 (in Japanese).

Ishii, E. et al. (2008), "Inception of anticline growth near the Omagari Fault, northern Hokkaido, Japan", *The Journal of the Geological Society of Japan*, No. 114, pp. 286-299 (in Japanese).

Ishii, E. (2012), "Microstructure and origin of faults in siliceous mudstone at the Horonobe Underground Research Laboratory site, Japan", *Journal of Structural Geology*, No. 34: pp. 20-29.

Iwatsuki, T., E. Ishii, and T. Niizato (2009), "Scenario development of long-term evolution for deep hydrochemical conditions in Horonobe area, Hokkaidok, Japan", *Journal of Geology*, 118(4): 700-716 (in Japanese).

JNC (1998), "Deep Geological Research Laboratory (Tentative Name) Project", JNC TN1410 98-002 (in Japanese).

JNC (2000), "Second Progress Report on Research and Development for the Geological Disposal of HLW in Japan, H12: Project to Establish the Scientific and Technical Basis for HLW Disposal in Japan Project Overview Report", JNC TN1410 2000-001.

Kai, K. and K. Maekawa (2009), "Oxygen and hydrogen isotopic ratios and Cl^- concentration of saline water in the Neogene siliceous sediments of Horonobe, Hokkaido, Japan", *Journal of the Japanese Association of Petroleum Technologists*, 74: pp. 96-106 (in Japanese).

Koide, K. et al. (2015), "Current status of R&D activities and future plan and role of JAEA's two generic URLs", WM2015 Conference, Phoenix, Arizona, United States, 15-19 March 2015.

Kurikami, H., R. Takeuchi and S. Yabuuchi (2008), "Scale effect and heterogeneity of hydraulic conductivity of sedimentary rocks at Horonobe URL site", *Physics and Chemistry of the Earth*, 33: S37-S44.

Niizato, T. et al. (2008), "Synthesising geoscientific data into a site model for performance assessment: A study on the long-term evolution of the geological environment in and around the Horonobe URL, Hokkaido, northern Japan", Proceedings of 3rd workshop on approaches and challenges for the use of geological information in the safety case, OECD/NEA, Nancy, France, 15-18 April 2008.

NUMO (2004), "Evaluating site suitability for a HLW repository – Scientific background and practical application of NUMO's siting factors", NUMO-TR-04-04.

Ota, K., H. Abe and T. Kunimaru (Eds.) (2011), "Horonobe Underground Research Laboratory Project Synthesis of Phase I Investigation 2001-2005 Volume Geoscienctific Research", JAEA-Research 2010-068.

Sasamoto, H., R.C. Arthur and K. Hama (2011), "Interpretation of undisturbed hydro-geochemical conditions in Neogene sediments of the Horonobe area, Hokkaido, Japan", *Applied Geochemistry*, 26: pp. 1467-1477.

Tachi, Y. et al. (2011), "Diffusion and sorption of Cs^+, I^- and HTO in samples of the argillaceous Wakkanai Formation from the Horonobe URL, Japan: Clay-based modeling approach", *Geochmica et Cosmochimica Acta*, 75: pp. 6742-6759.

Tokiwa, T. et al. (2014), "Fracture characterization around a gallery in soft sedimentary rock in Horonobe URL of Japan", *International Journal of Rock Mechanics & Mining Science*, 65: pp. 1-7.

Yamamoto, H. (1979), "The geologic structure and the sedimentary basin off northern part of the Hokkaido Island", *Journal of the Japanese Association of Petroleum Technologists*, 44: pp. 260-267 (in Japanese).

Yokota, H. and S. Tanaka. (2014), "Preliminary analysis of dipole tracer migration experiments in fractured sedimentary rock at Horonobe URL of Japan", Proceedings of the 19th Pacific Basin Nuclear Conference (PBNC 2014), Vancouver, British Columbia, Canada, 24-28 August 2014.

Wei, D. and T. Seno. (1998), "Determination of the Amurian plate motion", In: Flower, M., Chung, S.L., Lo, C.H., Lee, T.Y. (Eds.), *Mantle Dynamics and Plate Interactions in East Asia*. Geodynamics Series 27, American Geophysical Union, Washington, D.C., United States, pp. 337-346.

Xia., X. et al. (2006), "Comparative study of cesium sorption on crushed and intact sedimentary rock", *Radiochim. Acta*, 94: pp. 683-687.

Opalinus Clay – Switzerland

Introduction

In Switzerland, the Nuclear Energy Act (KEG, 2003) states that the waste producers are responsible for the safe management of their radioactive waste. In 1972, the operators of the nuclear power plants and the Swiss Confederation (responsible for radioactive waste from medicine, industry and research) set up Nagra to perform this task. Nagra stands for "National Cooperative for the Disposal of Radioactive Waste".

The "Sectoral Plan for Deep Geological Repositories" (SFOE, 2008) is the Swiss road map for the step-wise site selection process. Three major stages shall lead to the general licence application. At the present stage of planning, there exists the potential for one site to contain all waste forms or separate sites to accommodate low/intermediate and high-level wastes. In the synthesis report pertinent to Stage 2 (NAGRA, 2014a), a total of six Stage 1 candidate geological siting regions (five of them in northern Switzerland) were compared, and Nagra proposed to focus future siting activities on the regions of Zürich Nordost (formerly "Zürcher Weinland"; Nagra, 2002a, b) and Jura Ost, both located in northern Switzerland, with the Opalinus Clay as the preferred host rock (cf. Figure 3-3); the confining units contribute to the geological barrier properties of the rock mass. ENSI, the Swiss Federal Nuclear Safety Inspectorate, approved Nagra's proposals for the choice of Opalinus Clay as the host rock for both repository types and the two candidate regions for further investigation in Stage 3, and also recommended to include an addition region, Nördlich Lägern, in Stage 3 (ENSI, 2017).

The geoscientific description of the Opalinus Clay and its confining units, as well as the local geological situation in the areas of Zürich Nordost and Jura Ost, was recently synthesised (Nagra, 2014b). Investigations on drill cores were performed on samples from various boreholes in northern Switzerland, with particularly dense and large data sets from Benken and Schlattingen (e.g. Nagra, 2002a; Wersin et al., 2013).

The Opalinus Clay is also investigated in great detail at the Mont Terri Underground Rock Laboratory (URL) (www.mont-terri.ch). It is located in the Folded Jura of north-western Switzerland. This area is not suitable for a DGR, but the security gallery of the highway tunnel through the Mont Terri anticline provides easy access to the Opalinus Clay for in situ experiments. Due to differences in the geological evolution, in the tectonic setting and in the current burial depth, the properties of Opalinus Clay at Mont Terri differ slightly but systematically from those of the siting areas in northern Switzerland. Therefore, two separate datasets have been compiled for this report: i) one based on data from the Mont Terri URL, representative of shallow depth occurrence of the clay (250-300 m b.g.s., maximum burial 1 350 m) and with strong tectonic overprint; and ii) another representative of the candidate repository regions, based mainly on core data from the boreholes of Benken (approximately 600 m b.g.s.) and Schlattingen-1 (900 m b.g.s.), with a maximum burial of ~1 700 m.

Disposal concept

The Swiss Radioactive Waste Management Program (Nagra, 2008a) foresees two types of DGRs: a high-level waste repository[2] for spent fuel[3], vitrified high-level waste (HLW) and long-lived

2. In German: "HAA-Lager".
3. According to current legislation, spent fuel is classified as radioactive waste.

intermediate-level waste (ILW), and a repository for low- and intermediate-level waste (L/ILW repository[4]).

The post-closure safety of the repository systems relies upon a system of nested, passive engineered and geological barriers that complement one another. Figure A3-45 schematically illustrates the barrier systems for the different waste types. The barrier system includes the waste matrices, the disposal canisters/containers, the materials used for backfilling and sealing of the underground structures, and the host rock, along with other geological formations that may provide an additional geological barrier (confining units). Figures A3-46 and A3-47 show schematic layouts of the HLW repository and the L/ILW repository, respectively.

Figure A3-45: **Schematic illustration of the barrier systems for the different waste types**

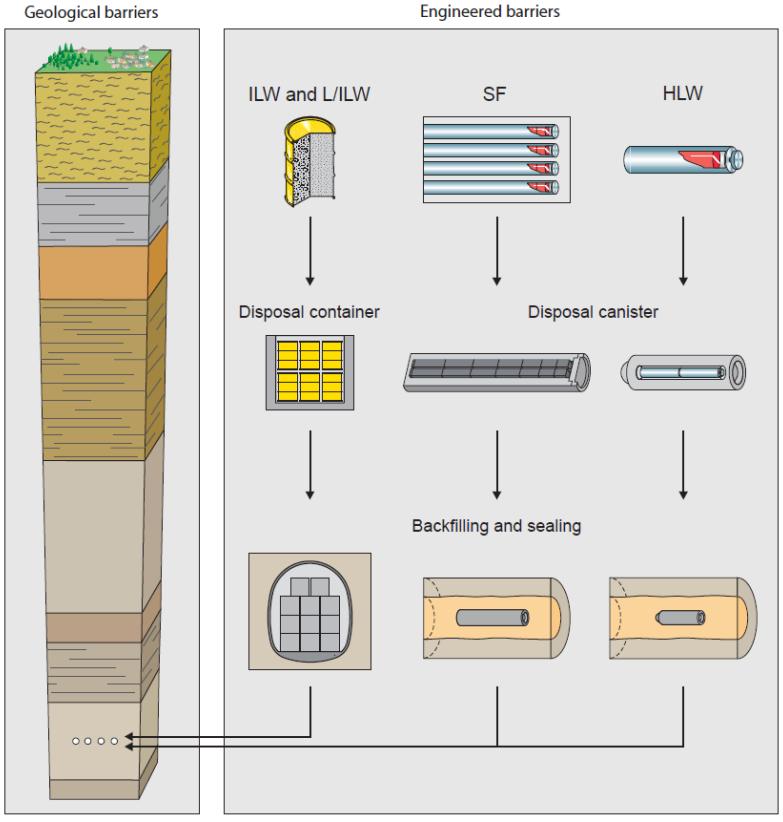

Source: Leupin et al., 2016.

Note: Not drawn to scale. Emplacement rooms in the left picture do not correspond to any specific repository type or layout.

In the case of the HLW repository, the underground facilities will be constructed in Opalinus Clay at a depth of 400-700 m b.g.s. The facilities would include a series of dead-end emplacement rooms for spent fuel and HLW, with initial diameters of about 2.5-3 m and lengths ranging from 300 m up to 1 000 m. According to the reference concept, the disposal canisters[5] will be emplaced co-axially with respect to the tunnel walls on pedestals of compacted bentonite blocks. Immediately after emplacement, the respective tunnel section will be backfilled with highly compacted granulated bentonite.

4 In German: "SMA-Lager".
5. The current reference concept foresees carbon steel canisters.

Figure A3-46: **Schematic layout of the HLW repository with its main features**

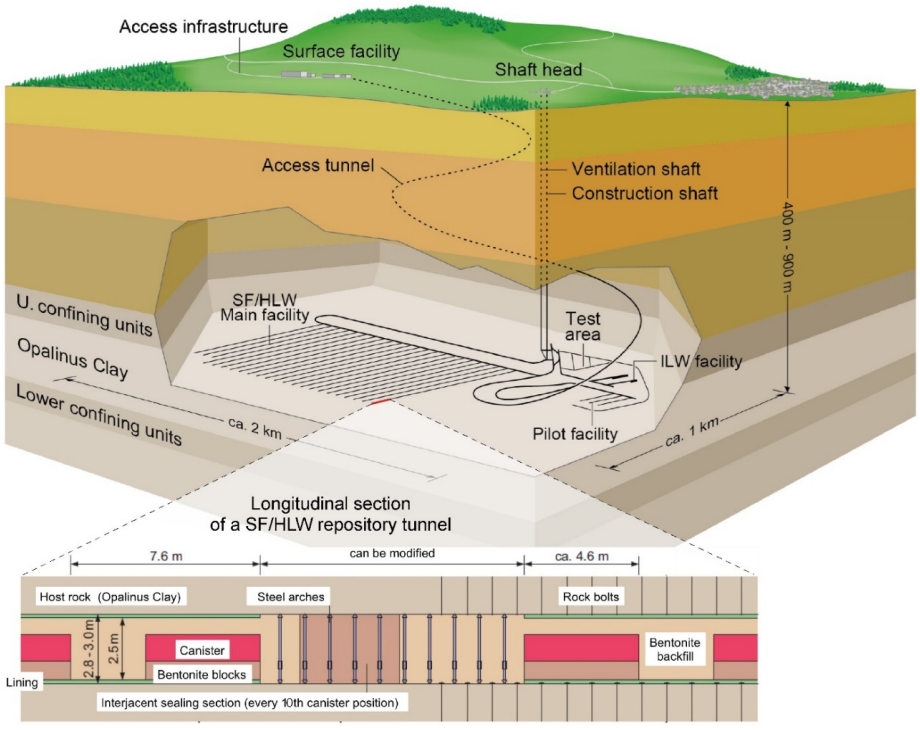

Note: Not to scale; combined figure from Nagra, 2016.

The current reference concept includes a liner along the spent fuel/HLW emplacement rooms. After every ~10th canister, the liner is interrupted by an intermediate seal, which ensures direct physical contact between the bentonite backfill and the Opalinus Clay host rock, thus interrupting potential preferential water flow and solute transport pathways along the liner (see Nagra, 2010).

Long-lived intermediate-level waste (ILW) will be packaged in concrete disposal containers. The containers will be stacked in dead-end emplacement caverns of about 7 m width and supported by concrete lining. The remaining void spaces will be backfilled with a specifically designed mortar. The current reference concept foresees a gas-permeable seal at the end of each ILW emplacement cavern.

The concept for waste emplacement in the L/ILW repository is more or less identical to that of the ILW portion of the HLW repository. The underground facilities of both the HLW repository and the L/ILW repository consist of:

- the main facility (i.e. the emplacement rooms in which the radioactive waste will be emplaced),
- the pilot facility with representative amounts of the radioactive waste,
- a test area, also called the Underground Research Laboratory (URL),
- a central area, and
- various types of seals at different locations within the underground structures.

The emplacement rooms will be arranged in disposal areas, the final size and shape of which will be determined based on in situ geological conditions. Access to both repositories will be provided, during construction and operation, by a ramp, by shafts or by any combination of these.

Figure A3-47: **Schematic layout of the L/ILW repository with its main features**

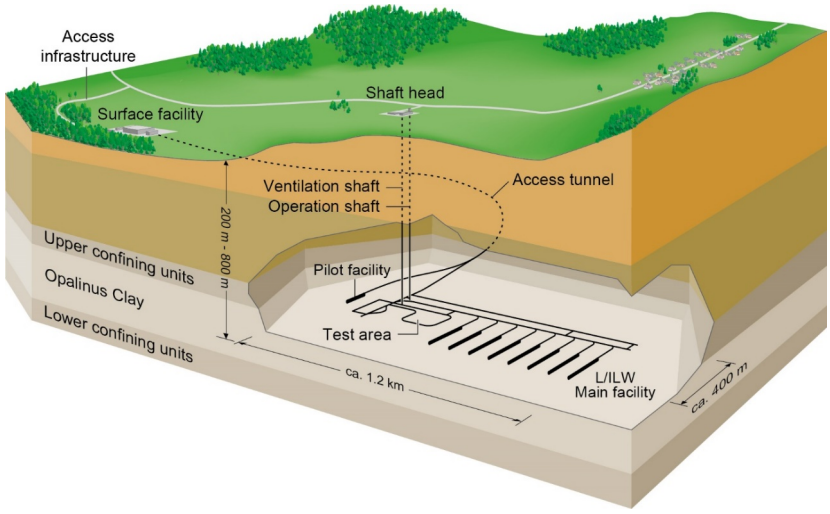

Source: Nagra, 2016.

Formation properties

Geology/structure

The Opalinus Clay is an over-consolidated Jurassic claystone with a typical thickness of approximately 100 m across northern Switzerland (112-120 m thickness in the potential siting regions). Compared to other Mesozoic sedimentary rocks in the area, the Opalinus Clay is a homogeneous formation with only minor vertical and lateral lithological variability (Figure A3-48). At the metre scale, some coarsening-upward cycles, with characteristic changes in grain size from clay to silt/sand particles, are observed. At the decimetre- to millimetre-scale, the preferred alignment of platy clay particles is responsible for a distinct fabric (bedding). The macro- to microscopic bedding is a very important characteristic of the Opalinus Clay texture and is responsible for the observed anisotropy in both mechanical and transport properties.

Figure A3-48: **Illustration of the lithological variability of the Opalinus Clay at different scales**

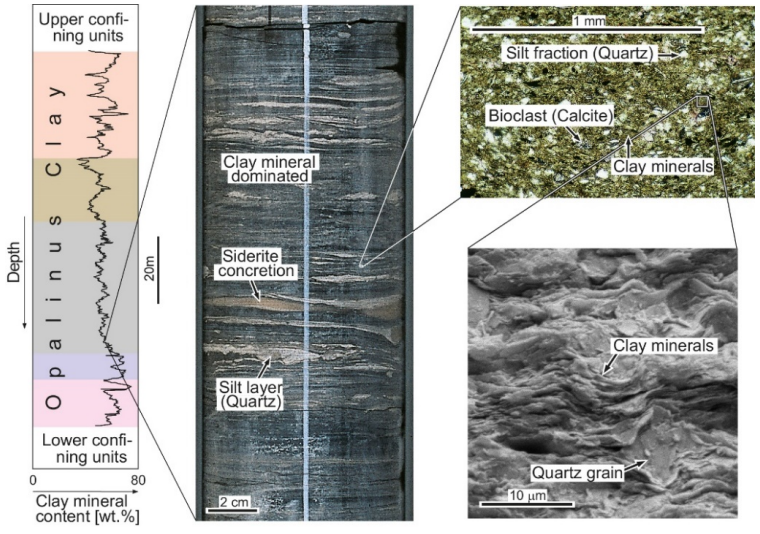

Source: Nagra 2014b.

Note: Coloured depth intervals on the left indicate sub-units (different lithological facies).

The Mesozoic sedimentary rocks in northern Switzerland experienced two major burial phases (Figure A3-49). A first, continent-scale, long-lasting phase occurred during the Cretaceous Period, when the Opalinus Clay was buried to a depth of about 1 100 m, after which about 600 m of Cretaceous and upper Malm were eroded during late Cretaceous and early Tertiary times. In the late Tertiary, the sedimentary pile was buried again below the Molasse (erosional debris of the rising Alpine mountain chain) and the Opalinus Clay at Benken reached a depth of about 1 650 m at 10 Ma before present. At the Mont Terri URL in north-western Switzerland, maximum burial is thought to have reached approximately 1 350 m (Mazurek et al., 2006).

Figure A3-49: **Reconstructed burial history for north-eastern Switzerland**

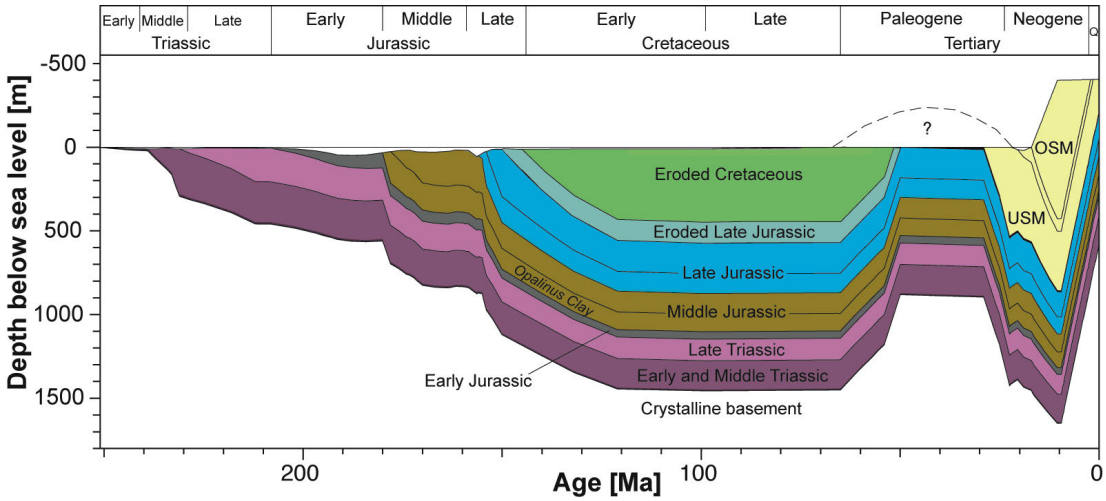

Source: Example for borehole Benken Mazurek et al., 2006; after Nagra, 2002a.

Considering the ratio of maximum burial and present burial depth, an over-consolidation ratio of approximately 2.5-5 at Mont Terri and 1.5-3 in the area of potential repositories in northern Switzerland is obtained. The maximum temperature reached at the level of the Opalinus Clay in the siting areas is estimated at approximately 85°C (Mazurek et al., 2006). Diagenetic cementation is generally weak and clearly detectable only in thin silty or sandy beds and lenses.

The Opalinus Clay outcrops in the vicinity of the German-Swiss border and gently dips to S-SE. With progressively deeper burial towards the Alps, the band in which it occurs at suitable depth is relatively narrow and is bounded by fault systems in the east (north of Zürich) and in the west (Rhenish system); see Figure A3-50.

The tectonic overprint of the Opalinus Clay is different at the Mont Terri URL when compared to the candidate regions in northern Switzerland (Figure A3-50). The URL is located on the south-eastern limb of the Mont Terri anticline and tectonically belongs to the Folded Jura of the detached Alpine foreland. The Folded Jura is the zone with the most intense deformation of the Jura fold-and-thrust belt, which developed during late Miocene north-south shortening. In contrast, the candidate regions are located within the (deformed) Tabular Jura and the Subjurassic Zone, which experienced much less internal deformation during Miocene shortening.

Figure A3-50: **Tectonic units at the level of the Opalinus Clay in northern Switzerland with locations of repository candidate regions (Stage 1), deep wells in Opalinus clay with core characterisation, and the Mont Terri URL**

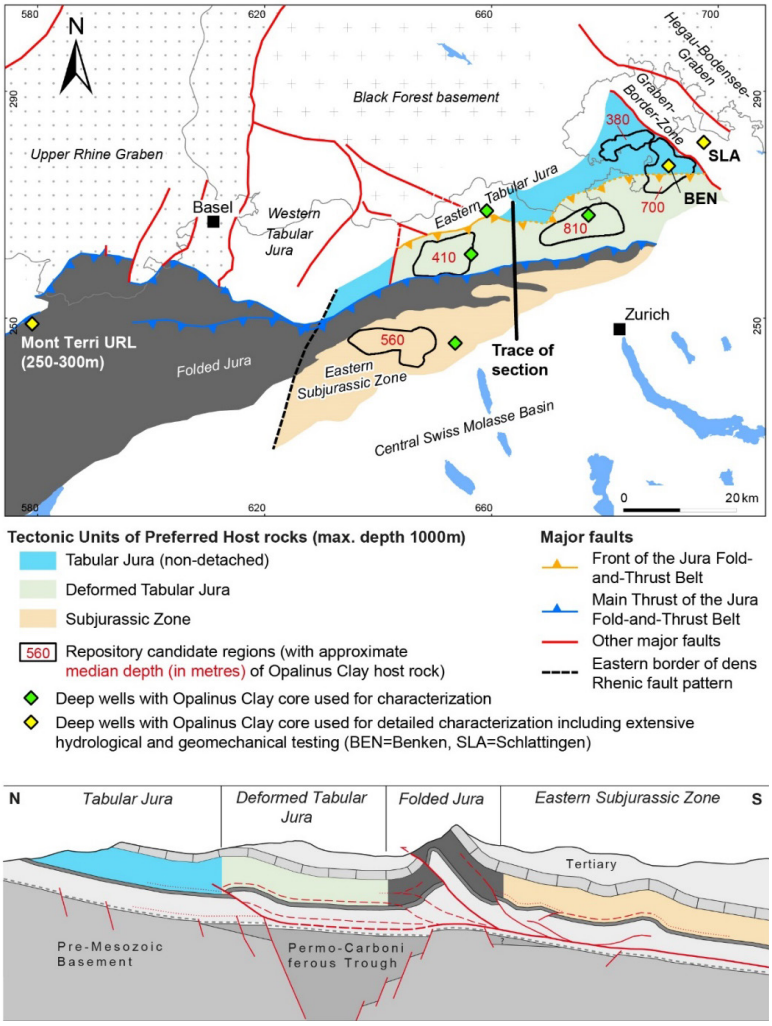

Source: Based on information from Nagra, 2014b.

Geotechnical classification and deformation behaviour

The Opalinus Clay is classified as a clayey (and sandy) siltstone, based on grain-size distribution, and as predominantly lean clay with low to medium plasticity (plasticity indices in the range of 10-25%).

The mechanical behaviour is characterised by features pertinent to both (stiff) soils and (weak) rocks. One-dimensional (oedometric) consolidation testing shows a significant volume reduction in the stress range above the apparent pre-consolidation stress (20 to 25 MPa for core samples in northern Switzerland). The very low hydraulic conductivity and a moderate swelling behaviour are additional clay-soil features of the Opalinus Clay.

On the other hand, results from Unconfined Compressive Strength tests suggest a weak to medium strong rock, according to international standards, and strain softening and development of discrete shear surfaces are typically observed in undrained triaxial testing. Observations at the Mont Terri URL also demonstrate that the excavation damage zone is of brittle nature.

A distinct anisotropy is observed in strength and stiffness, relating the micro- and macroscopic bedding structures to mechanical observations. Strength strongly depends on water content, and hence on burial depth and/or the over-consolidation ratio. Elastic properties (stiffness) are also stress-dependent.

Geochemistry, hydrogeology and transport properties

The mineralogical variability of the Opalinus Clay is minor (Figures A3-48 and A3-51). Clay mineral contents are typically 60±15 wt.%, with predominantly non-swelling clays (~50 wt.%) such as kaolinite, illite and chlorite, and approximately 10 wt.% of swelling illite-smectite mixed layers. Besides clay minerals, carbonates (20±15 wt.%) and quartz/feldspars (20±10 wt.%) are the other main constituents.

Figure A3-51: **Mineralogical composition of the Opalinus Clay**

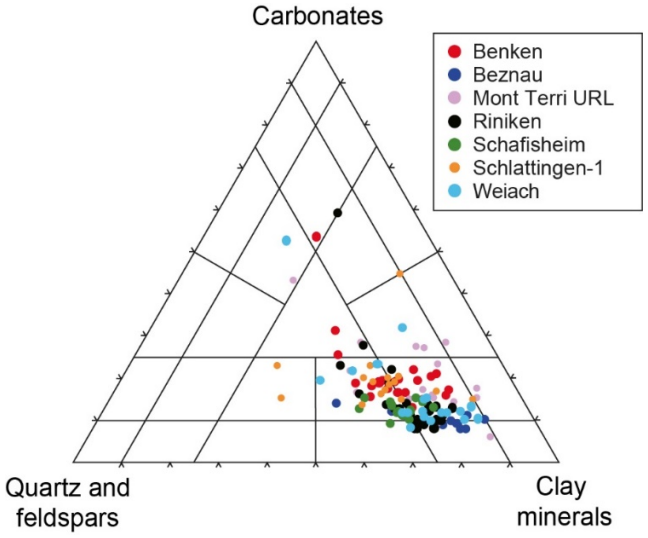

Source: Nagra, 2014b.

The porewater is of a general Na-Cl-type and can be explained by a marine component in addition to interaction(s) with the embedding aquifers. The redox conditions correspond to S^{VI}/S^{-II} equilibrium at saturation with pyrite and siderite. For the sites in northern Switzerland, the reference value of chloride is 5.7 g/l, and pCO_2 is $10^{-2.2}$ bar. To account for uncertainty and potential regional variations, variants of the reference porewater have been modelled (mainly pCO_2 and salinity).

In the two preferred siting areas (Zürich Nordost and Jura Ost), the Opalinus Clay is part of a succession of aquitards bounded by regional aquifers (Figure A3-52). Hydraulic tests in Opalinus Clay in boreholes of northern Switzerland indicate hydraulic conductivities $\leq 5 \times 10^{-13}$ m/s (Figure A3-53). In situ packer test data generally show good agreement with hydraulic testing of the rock matrix on drill cores, which supports the assumption of a homogeneous media. Various observations highlight the good self-sealing properties of Opalinus Clay, and dedicated experiments have been undertaken at the Mont Terri URL (e.g. Bock et al., 2010).

Typical physical porosities of the Opalinus Clay, calculated from density measurements, amount to about 11 vol.-% for northern Switzerland and about 16 vol.% for Mont Terri. The best estimate of the anion-accessible fraction is 0.5. The pore size spectra are dominated by mesopores (i.e. equivalent radii 1-25 nm). Modern methods of scanning electron microscopy allow visualisation of the pore types associated with different minerals (e.g. Figure A3-54).

Effective diffusion coefficients were obtained by laboratory and in situ experiments, and can also be estimated from porosity using the extended Archie's law (van Loon, 2014). Profiles of natural tracers (Mazurek et al., 2009, 2011) are compatible with diffusion coefficients measured on drill core samples and are in agreement with low Péclet numbers (Nagra, 2002a), which indicate diffusion-dominated transport.

Figure A3-52: **Geological profile of the Benken borehole and schematic geological isolation concept**

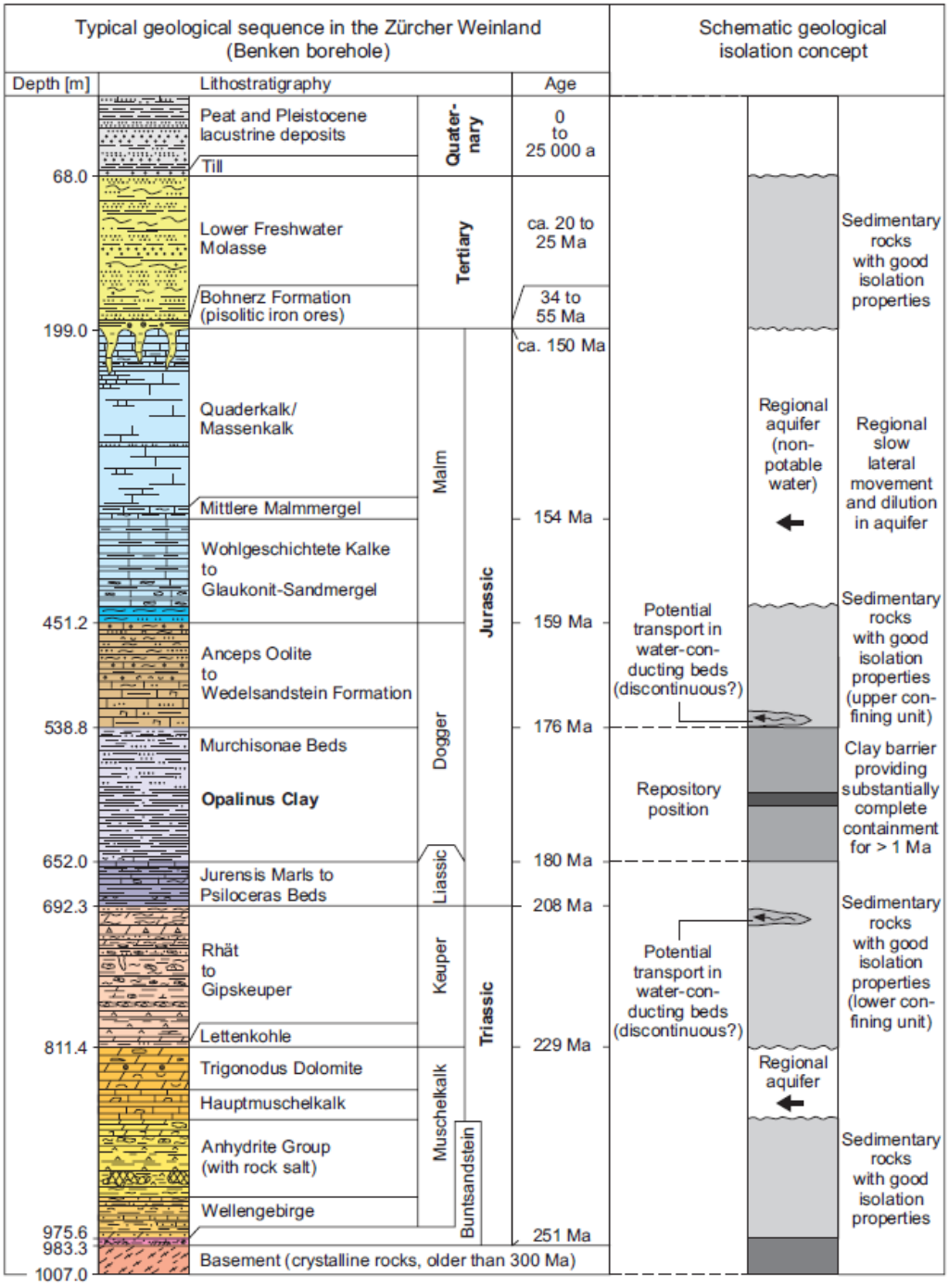

Source: Nagra, 2002b.

Figure A3-53: **Hydraulic conductivity of the Opalinus Clay as a function of depth**

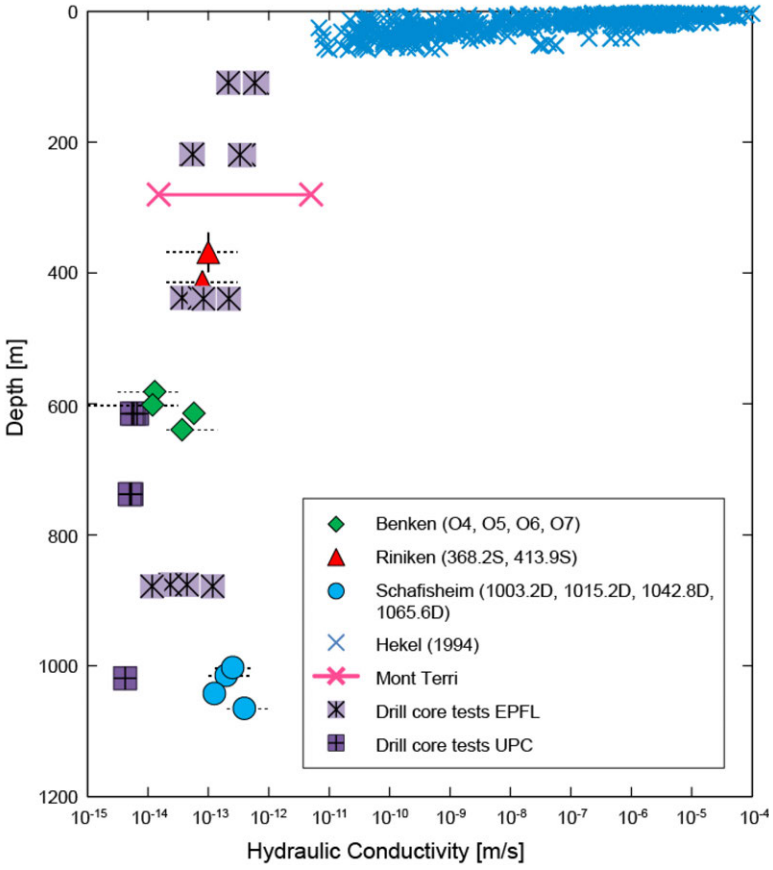

Source: Figure from Gautschi, 2017 (detailed references therein).

Note: Packer test data indicate best estimates and ranges. Data from drill cores re-calculated to depth based on average confining pressure.

Figure A3-54: **Pore geometries of Opalinus Clay visualised by BIB-SEM (a and b, Houben et al., 2013) and FIB nanotomography (FIB-nt) (c, Marschall et al., 2016)**

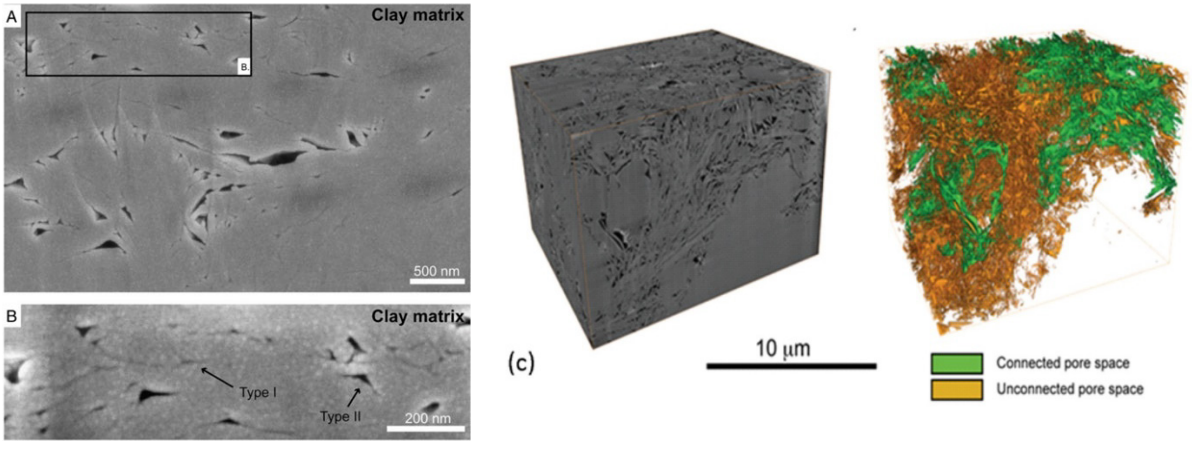

Note: Samples from the clay-rich facies at Mont Terri.

Favourable formation attributes

The areal extent and thickness of the lithological units allow for predictability at scales relevant to establishing safety

- The Opalinus Clay is an over-consolidated Jurassic claystone with average thickness of ~100 m across northern Switzerland, with favoured siting zones over an area of ~3 200 km^2 (~80 km x ~40 km).
- The Opalinus Clay is a homogeneous formation, with only minor vertical and lateral lithological variability.

The presence of natural barriers (host and enclosing formations) acts to isolate the host rock and contain solutes for safety-relevant time frames

- In the two preferred siting areas (Zürich Nordost and Jura Ost), the Opalinus Clay is part of a succession of aquitards bounded by regional aquifers.
- Various observations highlight the good self-sealing properties of Opalinus Clay.
- In the candidate repository regions, the formation is found at substantial depths (> 600 m b.g.s.).

Stability of the geosphere on safety-relevant time frames supported by multiple lines of geoscientific evidence/reasoning

Transport processes are anticipated to remain diffusion-dominated over geologic time frames (hundreds of thousands to millions of years)

- Very low hydraulic conductivities (10^{-12} to 10^{-14} m/s) are consistent with other parameters that suggest diffusion-dominated transport.

Geochemical stability of the groundwater-porewater system over geologic time frames

- Profiles of natural tracers are compatible with diffusion coefficients measured on drill core samples and are in agreement with low Péclet numbers – all suggesting diffusion-dominated transport.

Geomechanical stability of the formations to natural perturbations

- The candidate regions are located within the (deformed) Tabular Jura and the Subjurassic Zone, which experienced much less internal deformation than surrounding regions during Miocene tectonic events.
- Moderate swelling behaviour is another feature of the Opalinus Clay.

Summary and future work

The high clay mineral contents, the diffusion-dominated transport and the self-sealing properties are major arguments for Opalinus Clay as host rock for radioactive waste. The high clay mineral contents, the diffusion-dominated transport and the self-sealing properties are major arguments for Opalinus Clay as host rock for radioactive waste. Currently the siting activities for Sectoral Plan Stage 3 are ongoing.

References

Bock, H. et al. (2010), *Self-sealing of Fractures in Argillaceous Formations in the Context of Geological Disposal of Radioactive Waste – Review and Synthesis*, OECD Publishing, Paris, 310 p.

ENSI (2017), "Sicherheitstechnisches Gutachten zum Vorschlag der in Etappe 3 weiter zu untersuchenden geologischen Standortgebiete. Sachplan geologische Tiefenlager Etappe 2", Eidgenössisches Nuklearsicherheitsinspektorat ENSI, Brugg.

Gautschi, A. (2017), "Safety-relevant hydrogeological properties of the claystone barrier of a Swiss radioactive waste repository: An evaluation using multiple lines of evidence", *Grundwasser*, No. 22, pp. 221-233, DOI 10.1007/s00767-017-0364-1.

Houben, M.E., G. Desbois and J.L. Urai (2013), "Pore morphology and distribution in the shaly facies of Opalinus Clay (Mont Terri, Switzerland): insights from representative 2D BIB-SEM investigations on mm to nm scale", *Applied Clay Science*, No. 71, pp. 82-97.

KEG (2003), Kernenergiegesetz SR 732.1 (Nuclear Energy Act). Bern, Switzerland.

Leupin, O. et al. (2016), "High-level waste repository-induced effects", Nagra Tech. Rep. NTB 14-13, Nagra, Wettingen, Switzerland.

Marschall, P., et al. (2016), "Microstructural insights into the petrophysical characteristics of indurated clays", *The Clay Minerals Society Workshop Lectures Series*, Vol. 21, Ch. 14, 191-198.

Mazurek, M., A.J. Hurford and W. Leu (2006), "Unravelling the multi-stage burial history of the Swiss Molasse Basin: Integration of apatite fission track, vitrinite reflectance and biomarker isomerisation analysis", *Basin Research*, No. 18, pp. 27-50.

Mazurek, M. et al. (2009), *Natural Tracer Profiles Across Argillaceous Formations: The CLAYTRAC Project*, NEA No. 6253, OECD Publishing, Paris, 358 p.

Mazurek, M. et al. (2011), "Natural tracer profiles across argillaceous formations", *Applied Geochemistry*, No. 26, pp. 1035-1064.

Nagra (2002a), "Projekt Opalinuston: Synthese der geowissenschaftlichen Untersuchungsergebnisse: Entsorgungsnachweis für abgebrannte Brennelemente, verglaste hochaktive sowie langlebige mittelaktive Abfälle", Nagra Tech. Ber. NTB 02-03, Nagra, Wettingen, Switzerland.

Nagra (2002b), "Project Opalinus Clay, Safety Report. Demonstration of disposal feasibility for spent fuel, vitrified high-level waste and long-lived intermediate-level waste (Entsorgungsnachweis)", Nagra Tech. Rep. NTB 02-05, Nagra, Wettingen, Switzerland.

Nagra (2008), "Entsorgungsprogramm 2008 der Entsorgungspflichtigen", Nagra Tech. Ber. NTB 08-01, Nagra, Wettingen, Switzerland.

Nagra (2010), "Beurteilung der geologischen Unterlagen für die provisorischen Sicherheitsanalysen in SGT Etappe 2. Klärung der Notwendigkeit ergänzender geologischer Untersuchungen", Nagra Tech. Ber. NTB 10-01, Nagra, Wettingen, Switzerland.

Nagra (2014a), "SGT Etappe 2: Vorschlag weiter zu untersuchender geologischer Standortgebiete mit zugehörigen Standortarealen für die Oberflächenanlage. Sicherheitstechnischer Bericht zu SGT Etappe 2. Sicherheitstechnischer Vergleich und Vorschlag der in Etappe 3 weiter zu untersuchenden geologischen Standortgebiete", Nagra Tech. Ber. NTB 14-01, Nagra, Wettingen, Switzerland.

Nagra (2014b), "SGT Etappe 2: Vorschlag weiter zu untersuchender geologischer Standortgebiete mit zugehörigen Standortarealen für die Oberflächenanlage. Geologische Grundlagen", Nagra Tech. Ber. NTB 14-02, Nagra, Wettingen, Switzerland.

Nagra (2016), "The Nagra Research, Development and Demonstration (RD&D) Plan for the Disposal of Radioactive Waste in Switzerland", Nagra Tech. Rep. NTB 16-02, Nagra, Wettingen, Switzerland.

SFOE (2008), "Sectoral Plan for Deep Geological Repositories – Conceptual Part", Department of Environment, Transport, Energy and Communications (DETEC), Swiss Federal Office of Energy (SFOE) Bern, Switzerland.

Van Loon, L.R. (2014), "Effective Diffusion Coefficients and Porosity Values for Argillaceous Rocks and Bentonite: Measured and Estimated Values for the Provisional Safety Analyses for SGT-E2", Nagra Tech. Rep. NTB 12-03, Nagra, Wettingen, Switzerland.

Wersin, P. et al. (2013), "Rock and porewater characterization on drillcores from the Schlattingen borehole", Nagra Arbeitsbericht NAB 12-54, Nagra, Wettingen, Switzerland.

Citations list for Master Database

[1] Ishii, E., Sanada, H., Iwatsuki, T., Sugita, Y. and Kurikami, H. 2011. Mechanical strength of the transition zone at the boundary between opal-A and opal-CT zones in siliceous rocks. Engineering Geology, 122: 215-221.

[2] Ishii, E., Yasue, K., Ohira, H., Furusawa, A., Hasegawa, T. and Nakagawa, M. 2008. Inception of anticline growth near the Omagari Fault, northern Hokkaido, Japan. The Journal of the Geological Society of Japan, 114: 286-299.

[3] Ishii, E., Sanada, H., Funaki, H., Sugita, Y. and Kurikami, H. 2011. The relationships among brittleness, deformation behavior, and transport properties in mudstones: an example from the Horonobe Underground Research Laboratory, Japan. Journal of Geophysical Research, 116: B09206. doi:10.1029/2011JB008279.

[4] Ota, K., Abe, H. and Kunimaru, T. (Eds). 2010. Horonobe Underground Research Laboratory Project, synthesis of Phase I investigations 2001–2005. Volume Geoscientific Research, JAEA Technical Report, JAEA-Research 2010-068. Japan Atomic Energy Agency, Tokai-mura, Japan.

[5] Amo, M., Suzuki, N., Shinoda, T., Ratnayake, N.P. and Takahashi, K. 2007. Diagenesis and distribution of sterenes in Late Miocene to Pliocene marine siliceous rocks from Horonobe (Hokkaido, Japan). Organic Geochemistry, 38: 1132–1145.

[6] Ishii, E. 2012. Microstructure and origin of faults in siliceous mudstone at the Horonobe Underground Research Laboratory site, Japan. Journal of Structural Geology, 34: 20–29.

[7] Mazurek, M. and Eggenberger, U. 2005. Mineralogical Analysis of Core Samples from the Horonobe Area. Institute of Geological Sciences, University of Bern, Switzerland. RWI Technical Report 05–01.

[8] Amano, Y., Yamamoto, Y., Nanjyo, I., Murakami, H., Yokota, H., Yamazaki, M., Kunimaru, T., Oyama, T. and Iwatsuki, T. 2011. Data of Groundwater from Boreholes, River Water and Precipitation for the Horonobe Underground Research Laboratory Project (2001-2010). JAEA-data/code 2011-023 (Japanese).

[9] Kurikami, H., Takeuchi, R. and Yabuuchi, S. 2008. Scale effect and heterogeneity of hydraulic conductivity of sedimentary rocks at Horonobe URL site. Physics and Chemistry of the Earth, 33: S37–S44.

[10] Yamamot, T., Shimo, M., Fujiwara, Y., Hattori, H., Nago, M., Tadokoro, T. and Nakagaki, S. HDB-6 Borehole Investigations in the Horonobe Underground Research Program, JNC-TJ5400 2005-004.

[11] Ishii, E., Funaki, H., Tokiwa, T. and Ota, K. 2010. Relationship between fault growth mechanism and permeability variations with depth of siliceous mudstones in northern Hokkaido, Japan. Journal of Structural Geology, 32: 1792-1805.

[12] Tachi, Y., Yotsuji, K., Seida, Y. and Yui, M. 2011. Diffusion and sorption of Cs+, I- and HTO in samples of the argillaceous Wakkanai Formation form the Horonobe URL, Japan: Clay-based modeling approach. Geochemica et Cosmochimica Acta, 75: 6742-6759.

[13] Takahashi, H., Seida, Y. and Yui, M. 2009. 3D X-ray CT and diffusion measurements to assess tortuosity and constructivity in a sedimentary rock. Diffusion-fundamentals.org 11(86): 1-2. URN: http://nbn-resolving.de/urn:nbn:de:bsz:15-qucosa-191088.

[14] Steurbaut, E. 2006. Ypresian. In: L. Dejonghe (Ed.). Current status of chronostratigraphic units named from Belgium and adjacent areas, Geologica Belgica, Brussels. Geologica Belgica, 9(1-2): 73-93.

[15] Vandenberghe, N., Van Simaeys, S., Steurbaut, E., Jagt, J.W.M. and Fleder, P.J. 2004. Stratigraphic architecture of the Upper Cretaceous and Cenozoic along the southern border of the North Sea Basin in Belgium. Netherlands Journal of Geosciences/Geologie en Mijnbouw, 83(3): 155-171.

[16] Mertens, J. 2005. Burial history of two potential host formations (Boom Clay, Ypresian Clays). ONDRAF/NIRAS Note, 2005-0062, 10p.

[17] Cammaer, C., Cockaerts, G. and Schiltz, M. 2009. Drilling and Geological Report: ON-Kallo-1; ON-Kallo-2; ON-Kallo-3. Report of Samsuffit bvba (Samsuffit R2009-01), commissioned by ONDRAF/NIRAS, 93.

[18] Mohammad, W., Vandenberghe, N. and Zeelmaekers, E. 2009. The NIRAS-ONDRAF Kallo 1&2 boreholes. The Ypresian cored section: 254-410m depth. Report by the Laboratory for Applied Geology & Mineralogy (K.U.Leuven) – December 2009, 142p.

[19] Van Marcke, P. and Laenen, B. 2005. The Ypresian Clays as Possible Host Rock for Radioactive Waste Disposal: An Evaluation. NIROND TR-2005-01, 150p.

[20] Lima, A. 2011. Thermo-Hydro-Mechanical Behaviour of two deep Belgian clay formations: Boom and Ypresian clays. PhD-thesis, Universitat politècnica de Catalunya, 221p.

[21] Nguyen, X.P. 2013. Etude du comportement chimico-hydro-mécanique des argiles raides dans le contexte du stockage de déchets radioactifs. PhD-thesis, Université Paris-Est, 396p.

[22] ONDRAF/NIRAS. 2001. Safety Assessment and Feasibility Interim Report 2 (SAFIR 2), NIROND 2001-06E.

[23] Walraevens, K. and Mahauden, M. 1998. Mineralogische, geochemische en chemische analysen van de Ieperiaan-kleien uit boring DOEL1. Project nummer TGO 97/05, Universiteit Gent, Rapporten oktober 1998, december 1998, februari 1999.

[24] Aertsens, M., Dierckx, A., Put, M., Moors, H., Janssen, K., Van Ravestyn, V., Van Gompel, M., Van Gompel, M. and De Cannière, P. 2005. Determination of the Hydraulic conductivity, ηR and the apparent diffusion coefficient on Ieper Clay and Boom Clay cores from the Doel-1 and Doel-2b drillings. Report N° SCK·CEN-R-3589, commissioned by NIRAS/ONDRAF (contract N° CCHO-98/332), reported by SCK·CEN (contract N° KNT 90 98 1042), 18p.

[25] Fernández, A.M, Sánchez, M., Sánchez, M., Galán, P., Melón, A. and González, A.E. (in prep). Pore water extraction and geomechanical analysis of the Ypresian clays. First preliminary results, Report by Ciemat CIEMAT/DMA/2G209/1/13, 58p.

[26] I.N.I.S.Ma. 1998. Report on physical and thermal properties (bulk and grain density, water content, porosity, specific surface, thermal conductivity and heat capacity) of core samples of the Doel 1 borehole. Technical Report N°74.252 by the Institut National Interuniversitaire des Silicates Sols et Matériaux a.s.b.l., Mons, commissioned by ONDRAF/NIRAS, 12p.

[27] LGC (Henriet, G. & Sine, B.). 1998. Report of physical and mechanical properties (Young's & Poisson's ratios, cohesion and angle of internal friction, swelling pressure, Atterberg limits and grain-size distribution) of core samples of the Doel 1 borehole. Rapport d'essais N°254/78-98 by the Laboratoire du Génie Civil, Université Catholique de Louvain, commissioned by NIRAS/ONDRAF, Order N° BESTEL Bon 9702856, 171p.

[28] Wouters, L., Mertens, J. and Moermans, G. 2014. Seismic reconnaissance campaigns in the vicinity of the Mol-Dessel nuclear zone. NIROND-TR 2014-01 (ONDRAF/NIRAS)

[29] Horseman S.T., Winter M.G. and Entwistle, D.C. 1993. Triaxial experiments on Boom Clay. In The Engineering Geology of Weak Rock, Balkema, Rotterdam.

[30] Cui Y.J., Sultan N. and Delage P. 2000. A thermomechanical model for saturated clays. Canadian Geotechnical Journal, 37(3): 607-620.

[31] Zeelmaekers, E. 2011. Computerized qualitative and quantitative clay mineralogy. Introduction and application to known geological cases. Doctoral Thesis KU Leuven, Belgium, 397 p.

[32] Zeelmaekers, E., Honty, M., Derkowski, A., Środoń, J., De Craen, M., Vandenberghe, N., Adriaens, R., Ufer, K. and Wouters, L. 2015. Qualitative and quantitative mineralogy of the Rupelian Boom Clay in Belgium. Clays and Clay Minerals, 50(2): 249-272.

[33] De Craen, M., Wang, L., Van Geet, M. and Moors, H. 2004. Geochemistry of Boom Clay pore water at the Mol Site. SCK•CEN-BLG-990.

[34] De Cannière, P., Fonteyne, A., Moors, H., Put, M. and Van Gomplel, M. 1994. Continuation of the migration experiments in the Boom Clay (laboratory and in situ). Report NIROND 94-06.

[35] Honty, M. 2010. CEC of the Boom Clay – a review. SCK-CEN ER-134.

[36] FUNMIG (Fundamental Processes of Radionuclide Migration). FP6-5165514.

[37] Aertsens, M., Wemaere, I. and Wouters, L. 2004. Spatial variability of transport parameters in the Boom Clay. Applied Clay Science, 26: 37-45.

[38] Digital data of wireline loggings in borehole Mol-1: Schlumberger.

[39] Digital data of wireline loggings in borehole Dessel-1: Schlumberger.

[40] Verbeeck, K., Vanneste, K., and Camelbeeck, T. 2013. Velocity profiles extrapolation in the Campine Basin, Belgium: Technical report, Royal Observatory of Belgium, Brussels, 38p.

[41] Ter Burg, T.K. 1993. Borehole Seismic Survey Summary (Dessel-1 well). Schlumberger, 156p.

[42] Weist, W.-R. 1997. Well Mol-1: Check shot survey, sonic calibration, synthetic seismograms – Processing report: Schlumberger, 259p.

[43] François B., Labiouse V., Dizier A., Marinelli F. and Charlier, R. 2014. Hollow Cylinder Tests on Boom Clay: Modelling of Strain Localization in the Anisotropic Excavation Damaged Zone. Rock Mechanics and Rock Engineering, 47(1): 71–86.

[44] TIMODAZ. 2010a. Deliverable D5 – THM characterisation and input for simulation (WP 3.1, D5). European commission.

[45] TIMODAZ. 2010b. Deliverable D13 – Simulation of lab and in situ tests. European commission.

[46] TIMODAZ. 2010c. Deliverable D07 – Laboratory simulation tests. European commission.

[47] Bernier F., Li X.L. and Bastiaens W. 2007. Twenty-five years' geotechnical observation and testing in the Tertiary Boom clay formation. Géotechnique 57(2): 229-237.

[48] Chen G.J., Sillen X., Verstricht J. and Li X.L. 2011. ATLAS III in situ heating test in Boom Clay: Field data, observation and interpretation. Computers and geotechnics 38(5): 683-696.

[49] Mertens J., Bastiaens W. and Dehandschutter B. 2004. Characterisation of induced discontinuities in the Boom Clay around the underground excavations (URF, Mol, Belgium). Applied Clay Science, 26: 413-428.

[50] Yu, L., Gedeon, M., Wemaere, I., Marivoet, J. and De Craen, M. 2011. Boom Clay Hydraulic Conductivity. SCK•CEN-ER-122.

[51] Bruggeman, C., Maes, N., Aertsens, M. and De Cannière, P. 2009. Tritiated water retention and migration behaviour in Boom Clay. NIROND-TR 2009-16.

[52] Bruggeman, C., Aertsens, M., Maes, N. and Salah, S. 2010. Iodine retention and migration behaviour in Boom Clay. SCK•CEN-ER-119.

[53] Decleer, J., Viaene, W. and Vandenberghe, N. 1983. Relationships between chemical, physical and mineralogical characteristics of the Rupelian Boom Clay, Belgium. Clay Minerals, 18: 1-10.

[54] Thury, M. and Bossart P. 1999. Mont Terri Rock laboratory: Results of the hydrogeological, geochemical and geotechnical experiments performed in 1996-1997. Geologische Berichte Nr. 23, Landeshydrologie und –geologie, Bern, Schweiz.

[55] Mazurek, M., Hurford, A. J. and Leu, W. 2006. Unravelling the multi-stage burial history of the Swiss Molasse Basin: Integration of apatite fission track, vitrinite reflectance and biomarker isomerisation analysis. Basin Research, 18: 27-50.

[56] Giger, S. & Marschall, P. 2014. Geomechanical properties, rock models and in-situ stress conditions for Opalinus Clay in Northern Switzerland. Nagra Arb. Ber. NAB 14-01, Nagra, Wettingen, Switzerland.

[57] Freivogel, M. and Huggenberger, P. 2003. Modellierung bilanzierter Profile im Gebiet Mont Terri – La Croix (Kanton Jura). In: Heitzmann, P., Tripet, J.P. (Eds.), Geology, Paleohydrology and Stress Field of the Mont Terri Region. Reports of the Federal Office for Water and Geology (FOWG), Geology Series, No 4, Bern, Switzerland.

[58] NAGRA. 2002. Projekt Opalinuston. Synthese der geowissenschaftlichen Untersuchungsergebnisse. Entsorgungsnachweis für abgebrannte Brennelemente, hochaktive sowie langlebig-mittelaktive Abfälle. Nagra Technischer Bericht NTB 02-03. (Nagra Techn. Report), NAGRA, Wettingen, Switzerland.

[59] Calculated based on data in Mazurek. 2011. Aufbau und Auswertung der Gesteinsparameter-Datenbank fu¨r Opalinuston, den ´Braunen Dogger´, Effinger Schichten und Mergel-Formationen des Helvetikums, Nagra Arbeitsbericht NAB 11-20, Nagra, Wettingen, Switzerland.

[60] Pearson, F.J., Arcos, D., Bath, A., Boisson, J.Y., Fernandez, A.M., Gäbler, H.E., Gaucher, E., Gautschi, A., Griffault, L., Hernan, P. and Waber, H.N. 2003. Mont Terri project – Geochemistry of water in the Opalinus Clay formation at the Mont Terri Rock Laboratory. Reports of the Federal Office for Water and Geology (FOWG), Geology Series, No 5, Bern, Switzerland.

[61] Fernández, A.M., et al. 2014. Applying the squeezing technique to highly consolidated clayrocks for pore water characterisation: Lessons learned from experiments at the Mont Terri Rock Laboratory. Appl. Geochem. http://dx.doi.org/10.1016/j.apgeochem.2014.07.003

[62] Bock, H. 2009. RA Experiment – Updated review of the rock mechanics properties of the Opalinus Clay of the Mont Terri URL based on laboratory and field testing. Mont Terri Project Technical Report TR 2008-04, swisstopo, Wabern/CH.

[63] Rübel, A.P., Sonntag, C., Lippmann, J., Pearson, F.J. and Gautschi, A. 2002. Solute transport in formations of very low permeability: profiles of stable isotope and dissolved noble gas contents of pore water in the Opalinus Clay, Mont Terri, Switzerland. Geochimica et Cosmochimica Acta, 66: 1311 – 1321.

[64] Mazurek, M., Alt-Epping, P., Bath, A., Gimmi, T., Waber, H. N., Buschaert, S., De Canniére, P., De Craen, M., Gautschi, A., Savoye, S., Vinsot, A., Wemaere, I. and Wouters, L. 2011. Natural tracer profiles across argillaceous formations. Applied Geochemistry, 26: 1035-1064

[65] Schuster, K. 2007. Ventilation Test (VE) Experiment: final activity report on high resolution seismic investigations within the VE-Experiment. Mont Terri Technical Report TR 2007-06.

[66] AF Consult. 2012. Mont Terri TN 2010-74.

[67] Nagra. 2014. Based on Marschall et al. 2003 (Mont Terri TR 2001-02).

[68] Nagra. 2014. SGT Etappe 2: Vorschlag weiter zu untersuchender geologischer Standortgebiete mit zugehörigen Standortarealen für die Oberflächenanlage: Geologische Grundlagen. Nagra Tech. Ber. NTB 14-02 (Dossier VI).

[69] Wersin, P., Mazurek, M., Waber, H.N., Mäder, U.K., Gimmi, T., Rufer, D. and De Haller, A. 2013. Rock and porewater characterisation on drillcores from the Schlattingen borehole. Nagra Arbeitsbericht NAB 12-54, Nagra, Wettingen, Switzerland.

[70] Calculated based on data in Wersin, P., Mazurek, M., Waber, H.N., Mäder, U.K., Gimmi, T., Rufer, D. and De Haller, A. 2013. Rock and porewater characterisation on drillcores from the Schlattingen borehole. Nagra Arbeitsbericht NAB 12-54, Nagra, Wettingen, Switzerland.

[71] Gimmi, T. and Waber, H.N. 2004. Modelling of tracer profiles in pore waters of argillaceous rocks in the Benken borehole: stable water isotopes, chloride, and chlorine isotopes. Nagra Technical Report NTB 04-05, Nagra, Wettingen, Switzerland.

[72] Gimmi, T., Waber, H.N., Gautschi, A. and Rübel, A. 2007. Stable water isotopes in pore water of Jurassic argillaceous rocks as tracers for solute transport over large spatial and temporal scales. Water Resources Research, 43: W04410, doi:10.1029/2005WR004774.

[73] Gesteinslabor, J. 2013. Geomechanical laboratory tests on Opalinus Clay cores from the borehole Schlattingen SLA-1. Nagra Arbeitsbericht NAB 13-18. Nagra, Wettingen, Switzerland.

[74] Debelmas, J. 1974. Géologie de la France, Vol 1 et 2. Doin Editeur, Paris, France.

[75] Rouire J. and Rousset C. 1980. Causses, Cévennes, Aubrac. Guide Géologiques Régionaux, Masson (Ed.), Paris 190 p.

[76] Barbarand J., Lucazeau, F., Pagel, M. and Séranne, M. 2001. Burial and exhumation history of the south-eastern Massif Central (France) constrained by apatite fission-track thermochronology. Tectonophysics, 335: 275-290.

[77] Peyaud, J.-B. 2002. Diagenèse et transferts en milieu argileux fracturé : l'argilite de Tournemire (Aveyron, France). Thèse Docteur en Sciences Université Paris XI Paris Sud-Orsay (France).

[78] Barbreau, A. and Boisson, J.-Y. 1994. Caractérisation d'une formation argileuse. Synthèse des principaux résultats obtenus à partir du tunnel de Tournemire de janvier 1992 à juin 1993 Rapport d'activité 1991-1993. EC Rapport d'avancement n° 1 (contrat CCE-CEA n° FI 2W CT91-0115) EUR 15756 fr CEC Nuclear Science & Technology Series, Euroffice. Luxembourg.

[79] Boisson J.-Y., Bertrand L., Heitz, J.-F. and Moreau-le Golvan, Y. 2001. In situ and laboratory investigations of fluid flow through an argillaceous formation at different scales of space and time, Tournemire tunnel, southern France. Special issue on "Confining units". Hydrogeology Journal, 9(1): 108-123.

[80] Beaucaire, C., Pearson, F.J. and Gautschi, A. 2005. Chemical buffering capacity of clay rock. OECD/NEA/RWMC/IGSC Workshop on Stability and buffering capacity of the geosphere for long term isolation of radioactive waste: application to argillaceous media. AEN/NEA 66 2005 05 1 P/ Braunschweig (Germany) 9-11 dec 2003 ISBN 92-64-00908-6 OECD/NEA Paris (France) pp. 147-154.

[81] De Windt, L., Cabrera, J. & Boisson, J.-Y. 1998. Hydrochemistry of an indurated argillaceous formation (Tournemire site, France). 9th WRI '09 International Symp. on Water-Rock Interaction (Int. Assoc. of Geochemistry) Taupo (New Zeland) 30 march-3 april 1998. Greg B. Arehart & John R. Hulston (Eds.) A.A. Balkema, Rotterdam, Holland pp. 145-148.

[82] De Windt, L., Cabrera, J. & Boisson, J.-Y. 1999. Radioactive waste containment in indurated claystones : comparison between the chemical containment properties of matrix and fractures. Chemical Containment of Wastes in the Geosphere Geological Society of London, Special Publications, n° SP 157, Metcalfe R. & Rochelle C.A. (eds.) Blackwell Scientific Publications Oxford (UK) pp. 169-181.

[83] Altinier, M.-V., Savoye, S., Michelot, J.-L., Beaucaire, C., Massault, M., Tessier, D. and Waber, H.N. 2007. The isotopic composition of pore-water from Tournemire argillite (France): an inter-comparaison study. Physics and Chemistry of the Earth, Parts A/B/C, 32 (1-7): 209-218. In Natural and engineered Barriers For Radioactive Waste Confinement Int. Meet., Andra, Tours 2005, part 1. Aranyossy J.-F. (Ed.), Elsevier Amsterdam (Holland), pp. 209-218.

[84] Bensenouci, F., Michelot, J.-L., Matray, J.-M., Savoye, S., Lavielle, B., Thomas, B. and Dick, P. 2011. A profile of Helium-4 concentration in pore-water for assessing the transport phenomena through an argillaceous formation (Tournemire, France). Physics and

Chemistry of the Earth, Parts A/B/C, 36 (17-18). In Natural & engineered Barriers for Radioactive Waste Confinement Int. Meet., Andra, Nantes 2010. [Geological and hydrological properties] Guest Editor: J.-F. Aranyossy (& associated editors), Elsevier Amsterdam (Holland) pp. 1521-1530.

[85] Moreau-le Golvan, Y., Michelot, J.-L. and Boisson J.-Y. 1997. Stable isotope contents of porewater in a claystone formation (Tournemire, France): assessment of the extraction technique and preliminary results. Applied Geochemistry, 12: 739-745.

[86] Patriarche, D., Ledoux, E., Michelot, J.-L., Simon-Coinçon, R. and Savoye, S. 2004a. Diffusion as the main process for mass transport in very low water content argillites: 2. Fluid flow and mass transport modelling. A.G.U. Water Resources Research, 40: 20-39.

[87] Patriarche, D., Ledoux, E., Simon-Coinçon, R., Michelot, J.-L. and Cabrera, J. 2004b. Characterization and modelling of diffusion process for mass transport through the Tournemire argillites (Aveyron, France). Applied Clay Science, 26(1-4): 109-122. In "Clays in Natural and engineered Barriers for Radioactive Waste Confinement" Elsevier Amsterdam (Holland).

[88] Patriarche, D., Michelot, J.-L., Ledoux, E. and Savoye, S. 2004c. Diffusion as the main process for mass transport in very low water content argillites: 1. Chloride as a natural tracer for mass transport-Diffusion coefficient and concentration measurements in interstitial water. A.G.U. Water Resources Research, 40: 1-19 (W01516).

[89] Savoye, S., Michelot, J.-L., Wittebroodt, C. and Altinier, M.-V. 2006a Contribution of the diffusive exchange method to the characterization of pore-water in consolidated argillaceous rocks. Journal of Contaminant Hydrology, 86(1-2): 87-104.

[90] Trémosa, J., Gonçalvès, J., Matray, J.-M. and Violette, S. 2010. Estimating thermo-osmotic coefficients in clay-rocks: II – In situ experimental approach. Journal of Colloid and Interface Science, 342(1): 175-184.

[91] Maßmann, J., Uehara, S., Rejeb, A. and Millard, A. 2009. Investigation of desaturation in an old tunnel and new galleries at an argillaceous site. Special Issue of Environmental Geology, 57(6): 1437-1445.

[92] Daupley, X. 1997. Etude du potentiel de l'eau interstitielle d'une roche argileuse et de relations entre ses propriétés hydriques et mécaniques – Application aux argilites du Toarcien de la région de Tournemire (Aveyron). Thèse Docteur en Sciences (Géologie de l'Ingénieur) Ecole Nationale Supérieure des Mines de Paris (France).

[93] IPSN internal reports.

[94] Alheid, H.-J., Knecht, M., Boisson, J.-Y., Hommand-Etienne, F. and Pepa, S. 1999. Comparison of in situ hydraulic and seismic measurements in the excavation damaged zone of underground drifts. 9th ISRM 1999 International Congress on Rock Mechanics (International Soc. for Rock. Mech.), Paris (France) 1999, Aug 25-28 [Poster]. Vouille and Berest (Eds.) A.A. Balkema, Rotterdam, Holland pp. 1263-1266.

[95] Bertrand, L., Laviguerie, R., Cabrera, J., Matray, J.-M. and Savoye, S. 2002. Instrument for measuring pore pressure and permeability in low-permeability clay/rock. 1st Clays In Natural And Engineered Barriers For Radioactive Waste Confinement International Meet, Reims (France) Dec 9-12 [Poster]. Proc.: Book of abstracts Poster session on Mass transfer n° P-MT-16 Andra Science and Technology Series pp. 321.

[96] Boisson, J.-Y., Cabrera, J. and De Windt, L. 1998). Etude des écoulements dans un massif argileux : laboratoire souterrain de Tournemire. EC Rapport final (contrat CCE-CEA n° FI 2W CT9-0115 et Avenants 1 et 2) EUR 18338 fr CEC Nuclear Science & Technology Series, Euroffice. Luxembourg 300 p.

[97] Matray, J.-M., Savoye, S. and Cabrera, J. 2007. Desaturation and structure relationships around drifts excavated in the well-compacted Tournemire's argillite (Aveyron, France). Engineering Geology, 90(1-2): 1-16.

[98] Rouire, J. and Rousset, C. 1980. Causses, Cévennes, Aubrac. Guide Géologiques Régionaux, Masson (Eds.), Paris 190 p.

[99] Savoye, S., Michelot, J.-L. and Wittebroodt, C. 2006b. Evaluation of the reversibility of iodide uptake by argillaceous rocks by the radial diffusion method. Radiochimica Acta, 94 (9-11): 699-704.

[100] Motellier, S., Devol-Brown, I., Savoye, S., Thoby, D. and Alberto J.-C. 2007. Evaluation of tritiated water diffusion through the Toarcian clayey formation of the Tournemire experimental site (France). Journal of Contaminant Hydrology, 94(1-2): 99-108.

[101] NWMO. 2011. Geosynthesis. NWMO DGR-TR-2011-11 R000. Toronto, Canada.

[102] Intera. 2011. Descriptive Geosphere Site Model. Intera Engineering Ltd. report for the Nuclear Waste Management Organization NWMO DGR-TR-2011-24 R000. Toronto, Canada.

[103] Jackson, R. 2010. Organic Geochemistry and Clay Mineralogy for DGR-3 and DGR-4 Core. Intera Engineering DGR Site Characterization report TR-08-29.

[104] Wigston, A. and Jackson, R. 2010. Mineralogy and Geochemistry of DGR-3 Core. Intera Engineering DGR Site Characterization report TR-08-22.

[105] Wigston, A. and Jackson, R. 2010. Mineralogy and Geochemistry of DGR-4 Core. Intera Engineering DGR Site Characterization report TR-08-23.

[106] Clark, I., Mohapatra, R., Mohammadzadeh, H. and Kotzer, T. 2010a. Porewater and Gas Analyses in DGR-1 and DGR-2 Core. Intera Engineering DGR Site Characterization report TR-07-21.

[107] Clark, I., Liu, I., Mohammadzadeh, M., Mohapatra, R., Zhang, P. and Wilk, M. 2010b. Porewater and Gas Analyses in DGR-3 and DGR-4 Core. Intera Engineering DGR Site Characterization report TR-08-19.

[108] Kovács, L. (Ed). 1998. Digest on the Results of Short-Term Characterisation Programme of Boda Claystone Formation. Special edition of PURAM.

[109] Kovács, L., Hámos, G. and Csicsák, J. 2000. Actual State of the Site Characterisation Programme of the Boda Siltstone Formation. Bulletin of the Hungarian Geological Society, 130(2): 197-206.

[110] Konrád, G., Sebe, K., Halász, A. and Babinszki, E. 2010. Sedimentology of a Permian playa lake: the Boda Claystone Formation, Hungary. Geologos, 16(1): 27-41.

[111] Máthé, Z and Varga, A. 2015. Late Permian in the Mecsek Unit ont he basis of the mineralogical, petrological and textural features of the Boda Claystone Formation (BCF). In Dályay V. and Sámson M. (Eds.): Issue of Tisia Conference, pp. 58-62 (in Hungarian with English abstract).

[112] Konrád, G. 1999. The Boda Claystone Formation: "The Geology of Today for Tomorrow (A Satellite Conference of the World Conference on Science)." Excursion Guide Book (23-24 June, 1999, Hungary), pp 65-74.

[113] Hámos, G., Máthé, Z. and Majoros, G. 1996. The Geology of Boda Site (Hungary); Surface and URL-based Investigations. TOPSEAL '96 Stockholm, Sweden, 1996. Transactions, Vol. II., pp. 196-199.

[114] Császár, G. (Ed.). 1997. Lithostratigraphic chart of the Hungarian Stratigraphic Commission. Hungarian Geological Institute, Budapest, p. 114 (in Hungarian with English text).

[115] Kovács, L. 1999. Short-term programme of characterisation of Boda Claystone Formation. Final report – Volume 6: Rock mechanical, geotechnical investigations (in Hungarian). Internal report (March). Manuscript – MECSEKÉRC Inc.

[116] Kovács, L. 2004. Report on the primary stress field (overcoring) measurements performed in Bak-5, Eg-2 and Het-6 boreholes (in Hungarian). Internal report (December). Manuscript – Bomix Ltd.

[117] Sipos, P., Németh, T. and Máthé, Z. 2010. Preliminary results on the Co, Sr and Cs sorption properties of the analcime-containing rock type of the Boda Siltstone Formation. Central European Geology, 53(1): 67-78.

[118] Lázár, K. and Máthé, Z. 2012. Claystone as a potential host rock for nuclear waste storage. Clay minerals in Nature – Their Characterization, Modification and Application. M. Valaškova and G.S. Martynkova (Eds.), ISBN 978-953-51-0738; DOI: 10.5772/48123.

[119] Kovács, L. (Ed.). 2010. Contract finalizing summarizing report on the research of BCF performed between 2004 and 2010 (in Hungarian). Internal report (March). Manuscript – MECSEKÉRC Inc.

[120] Parneix, J.-C., Bouchet, A., Mazurier, A., Bétin, N., Ramirez, S. and Robinet, J.C. (Eds.). 2008. Synthesis of the characterization of Callovo-Oxfordian, Opalinus, Boom and Boda clays. FUNDAMENTAL PROCESSES OF RADIONUCLIDE MIGRATION (FUNMIG) project PID 3.2.18.

[121] Fernandes, M.M., Vér, N. and Baeyens, B. 2015. Predicting the uptake of Cs, Ni, Co, Eu, Th and U on argillaceous rocks using sorption models for illite. Submitted to Applied Geochemistry

[122] Nagykanizsa. 1990. Determination of the permeability of Lower Permian BCF samples by constant reservoir pressure at changing pore pressure and temperature. Hungarian Hydrocarbon Institute report (in Hungarian).

[123] Fedor, F. (Ed). 2013. The complex investigation series on samples from the Ib-4 borehole. Research report (in Hungarian).

[124] Van Loon, L.R. and Mibus, J. 2015. A modified version of Archie's law to estimate effective diffusion coefficients of radionuclides in argillaceous rocks and its application in safety analysis studies. Submitted to Applied Geochemistry.

[125] Lázár, K., Megyeri, J., Szarvas, T., Parneix, J.-C. and Máthé, Z. 2008. Diffusion of anionic species (99TcO4- and H14CO3-) and HTO in Boda Claystone borecore samples. 4th Annual Wokshop Proceedings 6th EC FP – FUNMIG IP (Karlruhe, Germany, Nov 24.-27), pp. 199-204.

[126] Máthé, Z. and Varga, A. 2015. Late Permian in the Mecsek Unit on the basis of the mineralogical, petrological and textural features of the Boda Claystone Formation (BCF). In Dályay, V. and Sámson, M. (Eds.), Issue of Tisia Conference, pp. 58-62 (in Hungarian with English abstract).

[127] Árkai, P., Balogh, K., Demény, A., Fórizs, I., Máthé, Z., Nagy, Z. 2000. Composition, Diagenetic and Post-diagenetic Alterations of a Possible Radioactive Waste Repository Site: the Boda Albitic Claystone Formation, Southern Hungary. Acta Geologica Hungarica, 43(4): 351-378.

[128] Ormai, P., Frigyesi, F., Benkovics, I., Kovács, L., Csicsák, J., Majoros, G., Érdi-Krausz, G. and Bárdossy, G. 1996. Hungarian Approach For Final Disposal of High Level Radioactive Waste. Geological Problems in Radioactive Waste Isolation (Second Worldwide Review), P.A. Witherspoon (Ed.), LBNL – University of California.

[129] Ormai, P., Frigyesi, F., Balla, Z., Kovács, L. and Hámos, G. 2001. Geological Disposal as the Preferred Option in the Hungarian Radioactive Waste Management Program. Geological Challenges in Radioactive Waste Isolation (Third Worldwide Review). P.A. Witherspoon and G. S. Bodvarsson (Eds.), LBNL – University of California.

[130] Hámos, G. and Kovács, L. 1999. Potential site for high level radioactive waste: "The Geology of Today for Tomorrow (A Satellite Conference of the World Conference on Science.)" Excursion Guide Book (23-24 June, 1999, Hungary), pp 53-64.

[131] Csicsák, J. 1996. Hydrogeological Investigations on a Claystone Formation in the URL of Hungary. TOPSEAL '96 Stockholm, Sweden. Transactions, Vol. II., pp. 201-204.

[132] Kovács, L. 1996. Engineering Investigations Inside a Claystone URL in Hungary. TOPSEAL'96 Stockholm, Sweden. Transactions, Vol. II., pp. 205-208.

[133] Sámson, M. (Ed.). 2015. BAF-2 drilling documentation and assessment report (in Hungarian).

[134] Ács, P. and Fedor, F. 2015. Pore structure of Boda Claystone Formation, W-Mecsek, Hungary. 6th International Meeting on Clays in Natural and Engineered Barriers for Radioactive Waste Confinement, Brussels, March 23-26.

[135] Lakatos, I., Fedor, F. and Tóth, J. 2002. Hydrodynamic investigations on samples from the Boda Claystone Formation. Internal report, Mecsekérc Plc. (in Hungarian).

[136] Demény, I., Fórizs, I. and Máthé, Z. 1996. A Preliminary Stable Isotope Study on a Potential Radioactive Waste Repository Site in the Mecsek Mountains, Southern Hungary. Rapid Communications in Mass Spectrometry, 10: 1415-1417.

[137] Berta, Z. 1999. Short-term programme of characterisation of Boda Claystone Formation. Final report – Volume 7: Geophysical investigations (in Hungarian). Internal report (March). Manuscript – MECSEKÉRC Inc.

[138] Kovács, L. 2001. Partial Self-Healing Effects of a Highly Indurated Claystone Formation (BCF) Discovered by In Situ Measurements. Proceedings of Topical Session "Evidences of, and Approaches to, Self Healing in Argillaceous Media". Clay Club Meeting (Nance, France, 16 May 2001). NEA/RWM/CLAYCLUB (2001)5.

[139] Mell P., Megyeri, J., Riess, L., Máthé, Z., Hámos, G. and Lázár, K. 2006. Diffusion of Sr, Cs, Co and I in argillaceous rock as studied by radiotracers. Journal of Radioanalytical and Nuclear Chemistry, 268(2): 411-417.

[140] Vandenberghe, N., De Craen, M. and Wouters, L. 2014. The Boom Clay Geology from Sedimentation to Present-day Occurrence: A Review. Memoirs of the Geol. Survey of Belgium, N° 60.

[141] Blaise, T., Barbarand, J., Kars, M., Ploquin, F., Aubourg, C., Brigaud, B., Cathelineau, M., El Albani, A., Gautheron, C., Izart, A., Janots, D., Michels, R., Pagel, M., Pozzi, J-P., Boiron, M-C., and Landrein, P. 2013. Reconstruction of low temperature (<100°C) burial in sedimentary Basins: A comparison of geothermometer in the intracontinental Paris Basin. Marine and Petroleum Geology (1-17 in press).

[142] Garcia, M.H., Rabaute, A., Yven, B. and Guillemot, D. 2011. Multivariate and spatial statistical analysis of Callovo-Oxfordian physical properties from lab and borehole logs data: Towards a characterization of lateral and vertical spatial trends in the Meuse/Haute-Marne Transposition Zone. Physics and Chemistry of the Earth, 36(17–18): 1469–1485.

[143] Gaucher, E., Robelin, C., Matray, J. M., Négrel, G., Gros, Y., Heitz, J. and Bouchet, A. 2004. Andra Underground Research Laboratory: interpretation of the mineralogical and geochemical data acquired in the Callovian–Oxfordian formation by investigative drilling. Physics and Chemistry of the Earth, Parts A/B/C, 29(1): 55-77.

[144] Cosenza, P., Robinet, J.C., Prêt, D., Huret, E., Fleury, M., Géraud, Y. and Zamora, M. 2013. Indirect estimation of the clay content of clay-rocks using acoustic measurements: New insights from the Montiers-sur-Saulx deep borehole (Meuse, France). Marine and Petroleum Geology.

[145] Lerouge, C., Grangeon, S., Gaucher, E.C., Tournassat, C., Agrinier, P., Guerrot, C. and Buschaert, S. 2011. Mineralogical and isotopic record of biotic and abiotic diagenesis of the Callovian–Oxfordian clayey formation of Bure (France). Geochimica et Cosmochimica Acta, 75(10): 2633-2663.

[146] Sammartino, S., Bouchet, A., Prêt, D., Parneix, J.C. and Tevissen, E. 2003. Spatial distribution of porosity and minerals in clay rocks from the Callovo-Oxfordian formation (Meuse/Haute-Marne, Eastern France) — implications on ionic species diffusion and rock sorption capability. Applied Clay Science, 23(1): 157-166.

[147] Grasset, L., Brevet, J., Schäfer, T., Claret, F., Gaucher, E.C., Albrecht, A., and Amblès, A. 2010. Sequential extraction and spectroscopic characterisation of organic matter from the Callovo-Oxfordian formation. Organic Geochemistry, 41(3): 221-233.

[148] Elie, M., Faure, P., Michels, R., Landais, P., and Griffault, L. 2000. Natural and laboratory oxidation of low-organic-carbon-content sediments: comparison of chemical changes in hydrocarbons. Energy & fuels, 14(4): 854-861.

[149] Pellenard, P. and Deconinck, J. F. 2006. Mineralogical variability of Callovo-Oxfordian clays from the Paris Basin and the Subalpine Basin. Comptes Rendus Geoscience, 338(12): 854-866.

[150] Vinsot, A., Mettler, S., and Wechner, S. 2008. In situ characterization of the Callovo-Oxfordian pore water composition. Physics and Chemistry of the Earth, Parts A/B/C, 33: S75-S86.

[151] Tournassat C., Vinsot A., Gaucher E.C., Altmann S. 2015. Chapter 3, Chemical conditions in clay-rocks. In: C. Tournassat, C.I. Steefel, I.C. Bourg, F. Bergaya (Eds.). Natural and Engineered Clay Barriers, Developments in Clay Science, 6. Elsevier, ISBN 9780081000274.

[152] Battani, A., Smith, T., Robinet, J.C., Brulhet, J., Lavielle, B., and Coelho, D. 2011. Contribution of logging tools to understanding helium porewater data across the Mesozoic sequence of the East of the Paris Basin. Geochimica et Cosmochimica Acta, 75(23): 7566-7584.

[153] Yven, B., Sammartino, S., Geraud, Y., Homand, F. and Villieras, F. 2007. Mineralogy, texture and porosity of Callovo-Oxfordian argillites of the Meuse/Haute-Marne region (eastern Paris basin). Mémoires de la Société géologique de France, 178: 73-90.

[154] Gaucher, É.C., Blanc, P., Bardot, F., Braibant, G., Buschaert, S., Crouzet, C. and Altmann, S. 2006. Modelling the porewater chemistry of the Callovian–Oxfordian formation at a regional scale. Comptes Rendus Geoscience, 338(12): 917-930.

[155] Robinet, J.C., Sardini, P., Siitari-Kauppi, M., Prêt, D. and Yven, B. 2015. Upscaling the porosity of the Callovo-Oxfordian mudstone from the pore scale to the formation scale; insights from the 3H-PMMA autoradiography technique and SEM BSE imaging. Sedimentary Geology, 321: 1-10.

[156] Savoye, S., Page, J., Puente, C., Imbert, C. and Coelho, D. 2010. New experimental approach for studying diffusion through an intact and unsaturated medium: a case study with Callovo-Oxfordian argillite. Environmental science & technology, 44(10): 3698-3704.

[157] Savoye, S., Goutelard, F., Beaucaire, C., Charles, Y., Fayette, A., Herbette, M. and Coelho, D. 2011. Effect of temperature on the containment properties of argillaceous rocks: The case study of Callovo-Oxfordian claystones. Journal of contaminant hydrology, 125(1): 102-112.

[158] Savoye, S., Frasca, B., Grenut, B. and Fayette, A. 2012. How mobile is iodide in the Callovo-Oxfordian claystones under experimental conditions close to the in situ ones? Journal of contaminant hydrology, 142: 82-92.

[159] Descostes, M., Blin, V., Bazer-Bachi, F., Meier, P., Grenut, B., Radwan, J. and Tevissen, E. 2008. Diffusion of anionic species in Callovo-Oxfordian argillites and Oxfordian limestones (Meuse/Haute-Marne, France). Applied Geochemistry, 23(4): 655-677.

[160] Melkior, T., Yahiaoui, S., Thoby, D., Motellier, S. and Barthes, V. 2007. Diffusion coefficients of alkaline cations in Bure mudrock. Physics and Chemistry of the Earth, Parts A/B/C, 32(1): 453-462.

[161] Jacquier, P., Hainos, D., Robinet, J.C., Herbette, M., Grenut, B., Bouchet, A. and Ferry, C. 2013. The influence of mineral variability of Callovo-Oxfordian clay rocks on radionuclide transfer properties. Applied Clay Science, 83: 129-136.

[162] Altmann, S., Tournassat, C., Goutelard, F., Parneix, J.C., Gimmi, T. and Maes, N. 2012. Diffusion-driven transport in clayrock formations. Applied Geochemistry, 27(2): 463-478.

[163] Andra report: D.RP.AMFS.12.0024.

[164] Granbow, B. 2016. Geological Disposal of Radioactive Waste in Clay. *In*: Elements, Deep-Mined Geological Disposal of Radioactive Waste, 12(4): 239-245.

[165] Hobbs, M., de Haller, A., Koroleva, M., Mazurek, M., Spangenberg, J., Mäder, U. and Meier, D. 2011. Borehole DGR-3 and DGR-4 Porewater Investigations. DGR Site Characterization Document, Geofirma Engineering Project 08-200, TR-08-40.

[166] Schuster, K. Internal BGR Compilation.

[167] Amann, F., Button, E., Evans, K., Gischig, V. and Blümel, M. 2011a. Experimental Study of the Brittle Behavior of Clay shale in Rapid Unconfined Compression. Rock Mech. Rock Eng.

[168] Amann, F., Kaiser, P. and Button, E. 2011b. Experimental Study of Brittle Behavior of Clay Shale.

[169] Favero, V. 2017. Multiphysical behaviour of shales from Northern Switzerland. Thèse École polytechnique fédérale de Lausanne EPFL, n° 7539.

[170] Marschall, P. and Giger, S. 2016. ENSI-Nachforderung zum Indikator "Tiefenlage im Hinblick auf bautechnische Machbarkeit" in Etappe 2 SGT. Geomechanische Unterlagen. Nagra Arb. Ber. NAB 16-43, Nagra, Wettingen, Schweiz.

[171] Al, T., Xiang, Y., Loomer, D. and Cavé, L. 2010. Measurement of diffusion properties by X-ray radiography and by through-diffusion techniques using iodide and tritium tracers: core samples from DGR-3 and DGR-4. DGR Site Characterization Document, Intera Engineering Project 08-200, TR-08-27.

[172] Sterling, S., Jackson, R., Walsh, R., Heagle, D. and Clark, I. 2011. Assessment of Porosity Data and Gas Phase Presence in DGR Cores. DGR Site Characterization Document, Intera Engineering Project 08-200, TR-08-34.

[173] Clark, I., Scharf, V., Zuliani, J. and Herod, M. 2011. Porewater Analyses in DGR-5 and DGR-6 Core. DGR Site Characterization Document, Intera Engineering Project 08-200, TR-09-04.

Table 1 – Master Database

GEOLOGICAL PARAMETERS

Formation	Depositional Environment			
	Depositional environment		Confidence	Reference
JPN_Koetoi	Marine		High	[1]
JPN_Wakkanai	Marine		High	[2]
BEL_Ypresian	Littoral to bathyal oxic to anoxic environment		Moderate	[14]
BEL_Boom	Open marine (50 to 150 m deep sea)		High	[140]
FRA_Callovo-Oxfordian	Marine, External platform		High	[ ]
FRA_Toarcian-Domerian	Marine		[ ]	[74]
CH_Opalinus_MTerri	Shallow marine		High	[54]
CH_Opalinus_NE	Shallow marine		High	[58]
CAN_Georgian Bay	Marine, Shelf (storm-dominated)		High	[101]
CAN_Queenston	Marine, Platform, Delta (sub-aerial exposure)		High	[101]
HUN_Boda-Gorica Block	Intermittent lacustrine (saline playa mudflat, playa lake)		[ ]	[108-111]
HUN_Boda-Boda Block	Intermittent lacustrine (saline playa mudflat, playa lake)		[ ]	[108-111, 126]
	Age [Ma]			
	Minimum	Maximum	Best Estimate	Confidence	Reference
JPN_Koetoi	2	4	[ ]	Moderate	[2]
JPN_Wakkanai	3	7	[ ]	Moderate	[11]
BEL_Ypresian	51	55	[ ]	Moderate	[15]
BEL_Boom	28	32	[ ]	High	[140]
FRA_Callovo-Oxfordian	158	163	[ ]	[ ]	[164]
FRA_Toarcian-Domerian	175	185	180	High	[74, 75]
CH_Opalinus_MTerri	[ ]	[ ]	172	High	[54]
CH_Opalinus_NE	[ ]	[ ]	172	High	[58]
CAN_Georgian Bay	440	460	450	High	[101]
CAN_Queenston	440	460	450	High	[101]
HUN_Boda-Gorica Block	255	270	260-265	High	[108, 109, 112, 113]
HUN_Boda-Boda Block	255	270	260-265	High	[108, 109, 112, 113]
	Maximum Burial Depth [m]			
	Minimum	Maximum	Best Estimate	Confidence	Reference
JPN_Koetoi	800	1100	1000	Moderate	[2, 3]
JPN_Wakkanai	1000	1300	1200	Moderate	[2, 3]
BEL_Ypresian	[ ]	[ ]	450	Moderate	[16]
BEL_Boom	205	225	215	Moderate	[140]
FRA_Callovo-Oxfordian	645	1045	[ ]	[ ]	[141]
FRA_Toarcian-Domerian	900	1700	1300	Low	[74, 76, 77]
CH_Opalinus_MTerri	[ ]	[ ]	1350	Moderate	[55, 56]
CH_Opalinus_NE	[ ]	[ ]	1650	Moderate	[55, 56]
CAN_Georgian Bay	[ ]	[ ]	1520	High	[101]
CAN_Queenston	[ ]	[ ]	1450	High	[101]
HUN_Boda-Gorica Block	3500	4500	[ ]	Moderate	[108, 109, 112, 113]
HUN_Boda-Boda Block	3500	4500	[ ]	Moderate	[108, 109, 112, 113]

Table 1 – Master Database (continued)

	Present Burial Depth - top of formation [m]				
	Minimum	Maximum	Best Estimate	Confidence	Reference
JPN_Koetoi	0	20	[ ]	High	[4]
JPN_Wakkanai	230	350	[ ]	High	[4]
BEL_Ypresian	289	329	[ ]	Moderate	[17, 18]
BEL_Boom	145	205	190	High	[22, 28]
FRA_Callovo-Oxfordian	[ ]	[ ]	490	[ ]	[164]
FRA_Toarcian-Domerian	200	300	250	High	[78, 79]
CH_Opalinus_MTerri	[ ]	[ ]	220	High	[57]
CH_Opalinus_NE	540	830	[ ]	High	[58, 69]
CAN_Georgian Bay	510	530	520	High	[102]
CAN_Queenston	440	460	450	High	[102]
HUN_Boda-Gorica Block	350	600	[ ]	Moderate	[108, 109, 112, 113]
HUN_Boda-Boda Block	0	600	[ ]	Moderate	[108, 109, 112, 113]
	Present Burial Depth - bottom of formation [m]				
	Minimum	Maximum	Best Estimate	Confidence	Reference
JPN_Koetoi	230	350	[ ]	High	[4]
JPN_Wakkanai	1000	1200	[ ]	Low	[4]
BEL_Ypresian	401	441	[ ]	Moderate	[19]
BEL_Boom	247	307	292	High	[22, 28]
FRA_Callovo-Oxfordian	[ ]	[ ]	643	[ ]	[164]
FRA_Toarcian-Domerian	400	560	500	High	[78, 79]
CH_Opalinus_MTerri	[ ]	[ ]	300	High	[57]
CH_Opalinus_NE	652	950	[ ]	High	[58, 69]
CAN_Georgian Bay	610	620	610	High	[102]
CAN_Queenston	510	530	520	High	[102]
HUN_Boda-Gorica Block	600	850	[ ]	Low	[108, 109, 112, 113]
HUN_Boda-Boda Block	700	1600	[ ]	Moderate	[108, 109, 112, 113]
	Maximum Temperature During Diagenesis (°C)				
	Minimum	Maximum	Best Estimate	Confidence	Reference
JPN_Koetoi	30	45	[ ]	Low	[5]
JPN_Wakkanai	45	60	[ ]	Low	[5]
BEL_Ypresian	[ ]	[ ]	[ ]	[ ]	[ ]
BEL_Boom	[]	[ ]	20	Moderate	[ ]
FRA_Callovo-Oxfordian	47	52	[ ]	[ ]	[141]
FRA_Toarcian-Domerian	[ ]	[ ]	[ ]	[ ]	[ ]
CH_Opalinus_MTerri	[ ]	[ ]	85	High	[55]
CH_Opalinus_NE	[ ]	[ ]	85	High	[55]
CAN_Georgian Bay	60	90	70	High	[101]
CAN_Queenston	60	90	70	High	[101]
HUN_Boda-Gorica Block	140	180	[ ]	Low	[114]
HUN_Boda-Boda Block	150	200	160	High	[108, 127]

Table 1 – Master Database (continued)

Formation	Over-consolidation Ratio				
	Minimum	Maximum	Best Estimate	Confidence	Reference
JPN_Koetoi	3.2	4.4	4.0	Moderate	[3]
JPN_Wakkanai	2.0	2.6	2.4	Moderate	[3]
BEL_Ypresian	[ ]	[ ]	1.4	Moderate	[20, 21]
BEL_Boom	2.0	2.4	2.4	High	[29, 30]
FRA_Callovo-Oxfordian	[ ]	[ ]	[ ]	[ ]	[ ]
FRA_Toarcian-Domerian	[ ]	[ ]	[ ]	[ ]	[ ]
CH_Opalinus_MTerri	2.5	5.0	4.0	Low	[58, 56]
CH_Opalinus_NE	1.5	3.0	2.0 (Schlattingen); 2.5 (Benken)	Moderate	[58, 56]
CAN_Georgian Bay	[ ]	[ ]	[ ]	[ ]	[ ]
CAN_Queenston	[ ]	[ ]	[ ]	[ ]	[ ]
HUN_Boda-Gorica Block	4.1	4.6	4.2	Moderate	[115, 116]
HUN_Boda-Boda Block	4.1	4.6	4.2	Moderate	[115, 116]
	Thickness (m)				
	Minimum	Maximum	Best Estimate	Confidence	Reference
JPN_Koetoi	[ ]	[ ]	350	Moderate	[4]
JPN_Wakkanai	600	1000	[ ]	Moderate	[4]
BEL_Ypresian	[ ]	[ ]	110	Moderate	[1, 18, 19]
BEL_Boom	[ ]	[ ]	102	High	[22]
FRA_Callovo-Oxfordian	130	160	153	[ ]	[142, 164]
FRA_Toarcian-Domerian	200	260	250	High	[74, 75, 78, 79]
CH_Opalinus_MTerri	90	160	[ ]	High	[57]
CH_Opalinus_NE	[ ]	[ ]	110	High	[58, 69]
CAN_Georgian Bay	88	90	90	High	[102]
CAN_Queenston	70	74	70	High	[102]
HUN_Boda-Gorica Block	210	[ ]	350	Low	[108, 109, 112, 113]
HUN_Boda-Boda Block	700	1000	800	High	[108, 109, 112, 113]

MINERALOGICAL PARAMETERS

	Total Clay Minerals (weight %)				
	Minimum	Maximum	Best Estimate	Confidence	Reference
JPN_Koetoi	17.0	25.0	21.0	Moderate	[6]
JPN_Wakkanai	19.0	33.0	26.0	Moderate	[6]
BEL_Ypresian	25.0	65.0	50.0	Moderate	[18]
BEL_Boom	25.0	71.0	51.5	High	[31, 32]
FRA_Callovo-Oxfordian (USC)	3.0	51.0	29.0	High	[143-146, 149]
FRA_Callovo-Oxfordian (UA)	29.0	59.0	49.0	High	[143-146, 149]
FRA_Toarcian-Domerian	25.0	50.0	29.5	Moderate	[79]
CH_Opalinus_MTerri	45.0	72.0	59.0	High	[59]
CH_Opalinus_NE	43.0	63.0	54.0	High	[59, 70]
CAN_Georgian Bay	8.0	71.0	48.5	High	[102]
CAN_Queenston	5.5	55.0	41.5	High	[102]
HUN_Boda-Gorica Block	15.0	45.0	40.0	Moderate	[117, 118]
HUN_Boda-Boda Block	11.0	56.0	41.5	High	[112, 113, 127-131]

Table 1 – Master Database (continued)

	Clay Minerals - Illite [% total dry weight]				
	Minimum	Maximum	Best Estimate	Confidence	Reference
JPN_Koetoi	7.0	12.0	7.0	Moderate	[7]
JPN_Wakkanai	7.0	11.0	7.0	Moderate	[7]
BEL_Ypresian	2.0	16.0	6.0	Moderate	[]
BEL_Boom	4.0	18.0	11.4	High	[31, 32]
FRA_Callovo-Oxfordian (USC)	1.0	30.0	9.0	High	[143-146, 149]
FRA_Callovo-Oxfordian (UA)	9.0	23.0	15.0	High	[143-146, 149]
FRA_Toarcian-Domerian	[ ]	[ ]	[ ]	[ ]	[ ]
CH_Opalinus_MTerri	15.0	27.0	21.3	High	[59]
CH_Opalinus_NE	8.0	18.0	14.0	High	[59, 70]
CAN_Georgian Bay	0.0	51.0	28.0	High	[102]
CAN_Queenston	3.5	39.0	25.0	High	[102]
HUN_Boda-Gorica Block	10.0	40.0	33.0	Moderate	[117, 118]
HUN_Boda-Boda Block	5.0	45.0	31.0	High	[112, 113, 127-132]
	Clay Minerals - Smectite [% total dry weight]				
	Minimum	Maximum	Best Estimate	Confidence	Reference
JPN_Koetoi	8.0	11.0	8.0	Moderate	[7]
JPN_Wakkanai	10.0	16.0	10.0	Moderate	[7]
BEL_Ypresian	10.0	36.0	26.0	Moderate	[18]
BEL_Boom	7.0	24.0	14.2	High	[31, 32]
FRA_Callovo-Oxfordian	[ ]	[ ]	[ ]	[ ]	[]
FRA_Toarcian-Domerian	[ ]	[ ]	[ ]	[ ]	[]
CH_Opalinus_MTerri	[ ]	[ ]	0.0	High	[59]
CH_Opalinus_NE	[ ]	[ ]	0.0	High	[59, 70]
CAN_Georgian Bay	[ ]	[ ]	0.5	High	[103]
CAN_Queenston	[ ]	[ ]	0.5	High	[103]
HUN_Boda-Gorica Block	2.0	5.0	2.0	Moderate	[117, 118]
HUN_Boda-Boda Block	0.5	5.0	1.0	High	[112, 113, 127-131]
Formation	**Clay Minerals - Chlorite [% total dry weight]**				
	Minimum	Maximum	Best Estimate	Confidence	Reference
JPN_Koetoi	0.0	4.0	1.0	Moderate	[7]
JPN_Wakkanai	0.0	5.0	3.0	Moderate	[7]
BEL_Ypresian	0.0	6.0	3.0	Moderate	[18]
BEL_Boom	1.0	4.0	2.8	High	[31, 32]
FRA_Callovo-Oxfordian (USC)	0.0	3.0	2.0	High	[143-146, 149]
FRA_Callovo-Oxfordian (UA)	1.0	8.0	3.0	High	[143-146, 149]
FRA_Toarcian-Domerian	1.0	5.0	2.5	Moderate	[79]
CH_Opalinus_MTerri	5.0	11.0	8.0	High	[59]
CH_Opalinus_NE	3.0	5.0	4.0	High	[59, 70]
CAN_Georgian Bay	8.0	25.5	13.0	High	[102]
CAN_Queenston	2.0	15.5	10.0	High	[102]
HUN_Boda-Gorica Block	2.0	8.0	2.0	Moderate	[117, 118]
HUN_Boda-Boda Block	1.0	31.0	8.0	High	[112, 113, 127-132]

Table 1 – Master Database (continued)

	Clay Minerals - Kaolinite [% total dry weight]				
	Minimum	Maximum	Best Estimate	Confidence	Reference
JPN_Koetoi	1.0	7.0	2.0	Moderate	[7]
JPN_Wakkanai	0.0	4.0	2.0	Moderate	[7]
BEL_Ypresian	1.0	9.0	4.0	Moderate	[18]
BEL_Boom	2.0	16.0	8.0	High	[31, 32]
FRA_Callovo-Oxfordian (USC)	0.0	2.0	0.0	High	[143-146, 149]
FRA_Callovo-Oxfordian (UA)	0.0	9.0	3.0	High	[143-146, 149]
FRA_Toarcian-Domerian	5.0	25.0	15.0	Moderate	[79]
CH_Opalinus_MTerri	14.0	27.0	21.0	High	[59]
CH_Opalinus_NE	10.0	20.0	15.0	High	[59, 70]
CAN_Georgian Bay	1.0	2.0	2.0	High	[102]
CAN_Queenston	[ ]	[ ]	2.0	High	[102]
HUN_Boda-Gorica Block	0.0	0.0	0.0	Moderate	[117, 118]
HUN_Boda-Boda Block	0.0	10.0	0.0	High	[112, 113, 127-131]
	Clay Minerals - Illite/Smectite [% total dry weight]				
	Minimum	Maximum	Best Estimate	Confidence	Reference
JPN_Koetoi	3.0	6.0	3.0	Moderate	[7]
JPN_Wakkanai	3.0	7.0	4.0	Moderate	[7]
BEL_Ypresian	6.0	14.0	11.0	Moderate	[18]
BEL_Boom	7.0	23.0	15.3	High	[31, 32]
FRA_Callovo-Oxfordian (USC)	1.0	30.0	18.0	High	[143-146, 149]
FRA_Callovo-Oxfordian (UA)	12.0	33.0	28.0	High	[143-146, 149]
FRA_Toarcian-Domerian	9.0	15.0	12.0	Moderate	[79]
CH_Opalinus_MTerri	6.0	13.0	10.0	High	[59]
CH_Opalinus_NE	14.0	26.0	21.0	High	[59, 70]
CAN_Georgian Bay	1.5	8.0	5.0	High	[102]
CAN_Queenston	[ ]	[ ]	4.0	High	[102]
HUN_Boda-Gorica Block	4.0	6.0	3.0	Moderate	[117, 118]
HUN_Boda-Boda Block	0.0	1.0	0.5	High	[112, 113, 127-131]
	Quartz [% total dry weight %]				
	Minimum	Maximum	Best Estimate	Confidence	Reference
JPN_Koetoi	7.0	10.0	8.5	Moderate	[6]
JPN_Wakkanai	9.0	13.0	11.0	Moderate	[6]
BEL_Ypresian	24.0	72.0	37.0	Moderate	[18]
BEL_Boom	21.0	61.0	34.3	High	[31, 32]
FRA_Callovo-Oxfordian (USC)	12.0	52.0	25.0	High	[143-146, 149]
FRA_Callovo-Oxfordian (UA)	10.0	36.0	18.0	High	[143-146, 149]
FRA_Toarcian-Domerian	10.0	30.0	17.5	Moderate	[79]
CH_Opalinus_MTerri	9.0	22.0	15.0	High	[59]
CH_Opalinus_NE	14.0	28.0	21.0	High	[59, 70]
CAN_Georgian Bay	0.0	53.5	29.0	High	[102]
CAN_Queenston	4.0	34.0	17.5	High	[102]
HUN_Boda-Gorica Block	3.0	30.0	11.0	Moderate	[117, 118]
HUN_Boda-Boda Block	1.0	28.0	8.5	High	[112, 113, 127-131]

Table 1 – Master Database (continued)

Formation	Feldspars [% total dry weight %]				
	Minimum	Maximum	Best Estimate	Confidence	Reference
JPN_Koetoi	5.0	10.0	7.5	Moderate	[6]
JPN_Wakkanai	7.0	13.0	10.0	Moderate	[6]
BEL_Ypresian	3.0	15.0	10.0	Moderate	[18]
BEL_Boom	4.7	14.0	9.3	High	[31, 32]
FRA_Callovo-Oxfordian (USC)	[ ]	[ ]	1.0	High	[143-146, 149]
FRA_Callovo-Oxfordian (UA)	[ ]	[ ]	1.0	High	[143-146, 149]
FRA_Toarcian-Domerian	[ ]	[ ]	[ ]	[ ]	[ ]
CH_Opalinus_MTerri	0.0	5.0	3.0	High	[59]
CH_Opalinus_NE	1.0	5.0	3.0	High	[59, 70]
CAN_Georgian Bay	[ ]	[ ]	2.0	High	[102]
CAN_Queenston	[ ]	[ ]	0.0	High	[102]
HUN_Boda-Gorica Block	7.0	30.0	19.5	Moderate	[117, 118]
HUN_Boda-Boda Block	5.0	59.0	32.5	High	[112, 113, 127-131]
Formation	**Total Carbonates [% total dry weight %]**				
	Minimum	Maximum	Best Estimate	Confidence	Reference
JPN_Koetoi	0.0	2.0	1.0	Moderate	[6]
JPN_Wakkanai	0.0	1.0	0.5	Moderate	[6]
BEL_Ypresian	0.0	9.0	2.0	Moderate	[18, 23]
BEL_Boom	0.0	5.5	1.2	Moderate	[31, 32]
FRA_Callovo-Oxfordian (USC)	11.0	76.0	42.0	High	[143-146, 149]
FRA_Callovo-Oxfordian (UA)	15.0	53.0	28.0	High	[143-146, 149]
FRA_Toarcian-Domerian	18.0	54.0	46.0	Moderate	[79]
CH_Opalinus_MTerri	9.0	34.0	21.3	High	[59]
CH_Opalinus_NE	12.0	28.0	20.0	High	[59, 70]
CAN_Georgian Bay	[ ]	[ ]	20.0	High	[102]
CAN_Queenston	[ ]	[ ]	39.5	High	[102]
HUN_Boda-Gorica Block	9.0	16.0	10.0	Moderate	[117, 118]
HUN_Boda-Boda Block	4.0	50.0	10.0	High	[112, 113, 127-132]
	Calcite [% total dry weight]				
	Minimum	Maximum	Best Estimate	Confidence	Reference
JPN_Koetoi	[ ]	[ ]	[ ]	[ ]	[ ]
JPN_Wakkanai	[ ]	[ ]	[ ]	[ ]	[ ]
BEL_Ypresian	0.0	3.0	1.0	Moderate	[18]
BEL_Boom	0.0	4.0	1.0	Moderate	[31, 32]
FRA_Callovo-Oxfordian (USC)	9.0	71.0	36.0	High	[143-146, 149]
FRA_Callovo-Oxfordian (UA)	13.0	51.0	24.0	High	[143-146, 149]
FRA_Toarcian-Domerian	10.0	45.0	33.0	Moderate	[79]
CH_Opalinus_MTerri	6.0	31.0	19.0	High	[59]
CH_Opalinus_NE	7.0	23.0	15.0	High	[59, 70]
CAN_Georgian Bay	0.0	71.0	10.0	High	[102]
CAN_Queenston	8.0	81.0	25.5	High	[102]
HUN_Boda-Gorica Block	8.0	15.0	9.0	Moderate	[117, 118]
HUN_Boda-Boda Block	1.0	15.0	6.0	High	[112, 113, 127-132]

Table 1 – Master Database (continued)

	Dolomite/ankerite [% total dry weight]				
	Minimum	Maximum	Best Estimate	Confidence	Reference
JPN_Koetoi	[ ]	[ ]	[ ]	[ ]	[ ]
JPN_Wakkanai	[ ]	[ ]	[ ]	[ ]	[ ]
BEL_Ypresian	0.0	1.0	1.0	Moderate	[18]
BEL_Boom	0.0	1.0	0.1	Moderate	[31, 32]
FRA_Callovo-Oxfordian (USC)	0.0	17.0	6.0	High	[143-146, 149]
FRA_Callovo-Oxfordian (UA)	1.0	8.0	4.0	High	[143-146, 149]
FRA_Toarcian-Domerian	3.0	25.0	10.0	Moderate	[79]
CH_Opalinus_MTerri	0.0	1.0	0.3	High	[59]
CH_Opalinus_NE	0.0	2.0	1.0	High	[59, 70]
CAN_Georgian Bay	0.0	55.0	10.0	High	[102, 104, 105]
CAN_Queenston	0.0	31.5	14.0	High	[102, 104, 105]
HUN_Boda-Gorica Block	0.5	4.0	1.0	Moderate	[117, 118]
HUN_Boda-Boda Block	0.5	45.0	4.0	High	[112, 113, 127-131]
	Pyrite [% total dry weight %]				
	Minimum	Maximum	Best Estimate	Confidence	Reference
JPN_Koetoi	0.0	2.0	1.0	Moderate	[7]
JPN_Wakkanai	0.0	4.0	2.0	Moderate	[6]
BEL_Ypresian	0.3	1.0	1.0	Moderate	[18]
BEL_Boom	0.5	3.0	1.7	Moderate	[31, 32]
FRA_Callovo-Oxfordian (USC)	0.0	2.0	1.0	High	[143-146, 149]
FRA_Callovo-Oxfordian (UA)	0.0	4.0	1.0	High	[143-146, 149]
FRA_Toarcian-Domerian	2.0	9.0	7.0	Moderate	[79]
CH_Opalinus_MTerri	0.4	2.2	1.3	High	[59]
CH_Opalinus_NE	0.2	2.2	1.2	High	[59, 70]
CAN_Georgian Bay	0.0	4.7	0.5	High	[104]
CAN_Queenston	0.0	2.5	1.0	High	[104]
HUN_Boda-Gorica Block	0.0	1.0	0.0	Moderate	[117, 118]
HUN_Boda-Boda Block	0.0	1.0	0.0	High	[112, 113, 127-131]
	Organic Carbon [%]				
	Minimum	Maximum	Best Estimate	Confidence	Reference
JPN_Koetoi	0.8	1.4	1.1	Moderate	[5]
JPN_Wakkanai	0.8	1.2	1.0	Moderate	[5]
BEL_Ypresian	0.4	1.1	1.0	Moderate	[23]
BEL_Boom	0.3	2.4	1.0	Moderate	[31, 32]
FRA_Callovo-Oxfordian	0.0	2.0	1.0	High	[143, 147, 148]
FRA_Toarcian-Domerian	0.7	1.6	[ ]	Moderate	[79]
CH_Opalinus_MTerri	0.2	1.2	0.7	High	[59]
CH_Opalinus_NE	0.3	0.7	0.5	High	[59, 70]
CAN_Georgian Bay	0.0	0.7	0.2	High	[102]
CAN_Queenston	0.0	0.3	0.1	High	[102]
HUN_Boda-Gorica Block	0.0	0.3	0.1	Moderate	[117, 118]
HUN_Boda-Boda Block	0.0	0.3	0.1	High	[112, 113, 127-131]

Table 1 – Master Database (continued)

Formation	Other Minerals (% total dry weight)			
	Mineral Identification and Fraction	Best Estimate	Confidence	Reference
JPN_Koetoi	Opal-A ($SiO_2 nH_2O$), Calcite/Dolomite/Siderite/ Magnetite (1.0)	59.5	[ ]	[ ]
JPN_Wakkanai	Opal-CT ($SiO_2 nH_2O$), Calcite/Dolomite/Siderite/ Magnetite (0.5)	49.5	[ ]	[ ]
BEL_Ypresian	Opal-CT ($SiO_2 nH_2O$)	[ ]	Moderate	[18]
BEL_Boom	Anatase (.7), Apatite (.2), Gypsum (.1), Siderite (.1) for 'Total Carbonates'	1.0	Moderate	[31, 32]
FRA_Callovo-Oxfordian (USC)	Apatite, Siderite, Fe minerals	1.0	High	[143-146, 149]
FRA_Callovo-Oxfordian (UA)	Apatite, Siderite, Fe minerals	2.0	High	[143-146, 149]
FRA_Toarcian-Domerian	[ ]	[ ]	[ ]	[ ]
CH_Opalinus_MTerri	Siderite (1.7) for 'Total Carbonates'	[ ]	[ ]	[59]
CH_Opalinus_NE	Siderite (4.0) for 'Total Carbonates'	[ ]	[ ]	[59, 70]
CAN_Georgian Bay	Brookite, Rutile, Anatase, Halite, Covellite	[ ]	Moderate	[104]
CAN_Queenston	Hematite, Rutile, Anatase, Halite	0.5	Moderate	[104]
HUN_Boda-Gorica Block	Analcime (13.0), Hematite (6.0), Muscovite + Biotite + Apatite (.4)	19.4	Moderate	[117, 118]
HUN_Boda-Boda Block	Hematite (7.0), Muscovite + Biotite + Apatite (0.4), Vermiculite + Chlorite/Smectite (1.0) for 'Total Clays'	7.4	Moderate	[112, 113, 127-131]

PORE WATER CHEMISTRY PARAMETERS

	Porewater Type		
	Porewater type	Confidence	Reference
JPN_Koetoi	Na-Cl	High	[8]
JPN_Wakkanai	Na-Cl	High	[8]
BEL_Ypresian	Na-Cl	Moderate	[23]
BEL_Boom	Na-HCO_3	High	[33]
FRA_Callovo-Oxfordian	[ ]	[ ]	[ ]
FRA_Toarcian-Domerian	Na-HCO3--Cl- type (interstitial fluid)	Low	[79, 80, 81, 82]
CH_Opalinus_MTerri	Na-Cl-(SO4)	High	[61]
CH_Opalinus_NE	Na-Cl-(SO4)	High	[68]
CAN_Georgian Bay	Na-Cl	High	[101, 102]
CAN_Queenston	Na-Cl	High	[101, 102]
HUN_Boda-Gorica Block	Na-HCO3-SO4	Moderate	[119]
HUN_Boda-Boda Block	Na-SO4-HCO3 & Na-HCO3-SO4	Moderate	[108, 109, 131]

	Salinity (TDS) [mg/L]				
	Minimum	Maximum	Best Estimate	Confidence	Reference
JPN_Koetoi	1500	22000	9600	Moderate	[8]
JPN_Wakkanai	130	20000	10000	Moderate	[8]
BEL_Ypresian	11153	16796	13810	Moderate	[23, 24]
BEL_Boom	1230	2076	1360	High	[34]
FRA_Callovo-Oxfordian	[ ]	[ ]	4100	[ ]	[ ]
FRA_Toarcian-Domerian	1350	5560	1980	Low	[79, 80, 81, 82]
CH_Opalinus_MTerri	7701	21929	15350	High	[61]
CH_Opalinus_NE	[ ]	[ ]	12810	High	[68]
CAN_Georgian Bay	268000	360000	295020	High	[102]
CAN_Queenston	260000	320000	285420	High	[102]
HUN_Boda-Gorica Block	650	1445	1350	Moderate	[119]
HUN_Boda-Boda Block	420	7300	3500	Moderate	[108, 109, 119, 131, 132]

Table 1 – Master Database (continued)

	pH				
	Minimum	Maximum	Best Estimate	Confidence	Reference
JPN_Koetoi	7.6	7.7	7.7	Moderate	[8]
JPN_Wakkanai	6.8	6.9	6.9	Moderate	[8]
BEL_Ypresian	[ ]	[ ]	[ ]	[ ]	[ ]
BEL_Boom	8.2	9.7	8.2	Moderate	[33]
FRA_Callovo-Oxfordian	7.0	7.2	7.2	Moderate	[150, 151]
FRA_Toarcian-Domerian	[ ]	[ ]	[ ]	[ ]	[ ]
CH_Opalinus_MTerri	6.9	8.1	[ ]	High	[61]
CH_Opalinus_NE	[ ]	[ ]	7.2	High	[68]
CAN_Georgian Bay	[ ]	[ ]	5.5	Low	[102]
CAN_Queenston	[ ]	[ ]	5.7	Low	[102]
HUN_Boda-Gorica Block	[ ]	[ ]	[ ]	[ ]	[ ]
HUN_Boda-Boda Block	7.4	10.0	8.0	High	[108, 109, 110, 131, 133]
	Eh (mV)				
	Minimum	Maximum	Best Estimate	Confidence	Reference
JPN_Koetoi	[ ]	[ ]	[ ]	[ ]	[ ]
JPN_Wakkanai	[ ]	[ ]	[ ]	[ ]	[ ]
BEL_Ypresian	[ ]	[ ]	[ ]	[ ]	[ ]
BEL_Boom	-368	-250	-274	Moderate	[33]
FRA_Callovo-Oxfordian	[ ]	[ ]	-200	[ ]	[150, 151]
FRA_Toarcian-Domerian	[ ]	[ ]	[ ]	[ ]	[ ]
CH_Opalinus_MTerri	[ ]	[ ]	-175	Moderate	[60]
CH_Opalinus_NE	[ ]	[ ]	-170	Moderate	[58]
CAN_Georgian Bay	[ ]	[ ]	-150	Moderate	[102]
CAN_Queenston	[ ]	[ ]	-150	Moderate	[102]
HUN_Boda-Gorica Block	-219	-47	-100	High	[119]
HUN_Boda-Boda Block	-342	233	-50	High	[108, 109, 119, 131, 132]
Formation	**Ca Concentration [mg/L]**				
	Minimum	Maximum	Best Estimate	Confidence	Reference
JPN_Koetoi	3.8	220.0	60.0	Moderate	[8]
JPN_Wakkanai	0.4	250.0	69.0	Moderate	[8]
BEL_Ypresian	132.0	360.9	270.0	Moderate	[23, 24]
BEL_Boom	1.5	2.9	2.0	Moderate	[33]
FRA_Callovo-Oxfordian	200.0	320.0	200.0	[ ]	[150, 151]
FRA_Toarcian-Domerian	27.2	295.2	60.0	Low	[79, 80, 81]
CH_Opalinus_MTerri	235.0	925.0	[ ]	High	[61]
CH_Opalinus_NE	[ ]	[ ]	501.0	High	[68]
CAN_Georgian Bay	33000.0	50700.0	42200.0	Moderate	[102]
CAN_Queenston	26800.0	53000.0	42000.0	Moderate	[102]
HUN_Boda-Gorica Block	3.2	4.4	3.9	High	[119]
HUN_Boda-Boda Block	4.0	280.0	72.0	High	[119, 131, 133]

Table 1 – Master Database (continued)

	Mg Concentration [mg/L]				
	Minimum	Maximum	Best Estimate	Confidence	Reference
JPN_Koetoi	5.7	210.0	46.0	Moderate	[8]
JPN_Wakkanai	ND	170.0	49.0	Moderate	[8]
BEL_Ypresian	83.0	204.5	120.0	Moderate	[23, 24]
BEL_Boom	1.3	2.6	1.6	Moderate	[33]
FRA_Callovo-Oxfordian	102.0	170.0	102.0	[ ]	[150, 151]
FRA_Toarcian-Domerian	8.0	92.3	18.2	Low	[79, 80, 81]
CH_Opalinus_MTerri	255.0	950.0	[ ]	High	[61]
CH_Opalinus_NE	[ ]	[ ]	234.0	High	[68]
CAN_Georgian Bay	4010.0	12500.0	6900.0	Moderate	[102]
CAN_Queenston	4900.0	12500.0	9000.0	Moderate	[102]
HUN_Boda-Gorica Block	0.7	2.0	1.3	High	[119]
HUN_Boda-Boda Block	4.0	69.0	22.0	High	[119, 131, 133]
	Na Concentration [mg/L]				
	Minimum	Maximum	Best Estimate	Confidence	Reference
JPN_Koetoi	370.0	6900.0	2900.0	Moderate	[8]
JPN_Wakkanai	22.0	6600.0	3100.0	Moderate	[8]
BEL_Ypresian	4060.0	5654.0	4900.0	Moderate	[23, 24]
BEL_Boom	348.0	431.0	359.0	Moderate	[33]
FRA_Callovo-Oxfordian	1010.0	1270.0	1035.0	[ ]	[150, 151]
FRA_Toarcian-Domerian	324.0	1326.0	520.0	Low	[79, 80, 81]
CH_Opalinus_MTerri	2100.0	6200.0	[ ]	High	[61]
CH_Opalinus_NE	[ ]	[ ]	3780.0	High	[68]
CAN_Georgian Bay	37000.0	91000.0	48000.0	High	[102]
CAN_Queenston	21900.0	98000.0	41500.0	High	[102]
HUN_Boda-Gorica Block	350.0	380.0	367.5	High	[119]
HUN_Boda-Boda Block	160.0	2300.0	940.0	High	[119, 131, 133]
	K Concentration [mg/L]				
	Minimum	Maximum	Best Estimate	Confidence	Reference
JPN_Koetoi	18.0	320.0	91.0	Moderate	[8]
JPN_Wakkanai	1.8	180.0	69.0	Moderate	[8]
BEL_Ypresian	67.5	210.1	110.0	Moderate	[23, 24]
BEL_Boom	6.7	8.3	7.2	Moderate	[33]
FRA_Callovo-Oxfordian	19.0	39.0	19.0	[ ]	[150, 151]
FRA_Toarcian-Domerian	16.4	77.8	30.1	Low	[79, 80, 81]
CH_Opalinus_MTerri	48.0	69.0	[ ]	High	[61]
CH_Opalinus_NE	[ ]	[ ]	102.0	High	[68]
CAN_Georgian Bay	7300.0	20900.0	11700.0	Moderate	[102]
CAN_Queenston	6950.0	19200.0	12500.0	Moderate	[102]
HUN_Boda-Gorica Block	2.0	7.0	4.1	High	[119]
HUN_Boda-Boda Block	1.7	70.0	22.0	High	[119, 131, 133]

Table 1 – Master Database (continued)

	Sr Concentration [mg/L]				
	Minimum	Maximum	Best Estimate	Confidence	Reference
JPN_Koetoi	0.1	5.7	1.1	Moderate	[8]
JPN_Wakkanai	ND	20.0	1.0	Moderate	[8]
BEL_Ypresian	[ ]	[ ]	[ ]	[ ]	[ ]
BEL_Boom	46.0	90.0	69.0	Moderate	[33]
FRA_Callovo-Oxfordian	15.0	23.0	17.0	[ ]	[150, 151]
FRA_Toarcian-Domerian	0.9	19.3	2.6	Low	[79, 80, 81]
CH_Opalinus_MTerri	45.0	46.0	[ ]	High	[61]
CH_Opalinus_NE	[ ]	[ ]	18.5	High	[68]
CAN_Georgian Bay	590.0	1500.0	1300.0	Moderate	[102]
CAN_Queenston	610.0	1200.0	960.0	Moderate	[102]
HUN_Boda-Gorica Block	[ ]	[ ]	[ ]	[ ]	[ ]
HUN_Boda-Boda Block	0.0	14.5	2.8	High	[119, 131, 133]
	Cl Concentration [mg/L]				
	Minimum	Maximum	Best Estimate	Confidence	Reference
JPN_Koetoi	200.0	12000.0	3400.0	Moderate	[8]
JPN_Wakkanai	14.0	10000.0	3610.0	Moderate	[8]
BEL_Ypresian	6320.0	9563.0	7900.0	Moderate	[23, 24]
BEL_Boom	24.0	30.0	26.0	Moderate	[33]
FRA_Callovo-Oxfordian	990.0	1780.0	1240.0	[ ]	[150, 151]
FRA_Toarcian-Domerian	71.0	533.0	160.0	Low	[79, 80, 81]
CH_Opalinus_MTerri	2500.0	12000.0	[ ]	High	[61]
CH_Opalinus_NE	3455.0	8905.0	5686.0	High	[58, 69, 71]
CAN_Georgian Bay	160000.0	210000.0	184000.0	High	[102]
CAN_Queenston	86000.0	251000.0	178000.0	High	[102]
HUN_Boda-Gorica Block	15.0	25.0	19.3	High	[119]
HUN_Boda-Boda Block	4.0	760.0	170.0	High	[119, 131, 133]
Formation	**Br Concentration [mg/L]**				
	Minimum	Maximum	Best Estimate	Confidence	Reference
JPN_Koetoi	ND	99.0	23.0	Moderate	[8]
JPN_Wakkanai	ND	83.0	24.0	Moderate	[8]
BEL_Ypresian	23.7	30.0	25.0	Moderate	[23, 24]
BEL_Boom	[ ]	[ ]	0.6	Moderate	[33]
FRA_Callovo-Oxfordian	4.8	6.2	5.0	[ ]	[151]
FRA_Toarcian-Domerian	< d. l.	< d. l.	< d. l.	Low	[79, 80, 81]
CH_Opalinus_MTerri	7.0	35.0	[ ]	High	[61]
CH_Opalinus_NE	5.9	7.1	[ ]	High	[69]
CAN_Georgian Bay	880.0	2850.0	1920.0	High	[102]
CAN_Queenston	1100.0	2700.0	2100.0	High	[102]
HUN_Boda-Gorica Block	[ ]	[ ]	[ ]	[ ]	[ ]
HUN_Boda-Boda Block	[ ]	[ ]	[ ]	[ ]	[ ]

Table 1 – Master Database (continued)

	SO_4 Concentration [mg/L]				
	Minimum	Maximum	Best Estimate	Confidence	Reference
JPN_Koetoi	ND	38.0	<0.1	Moderate	[8]
JPN_Wakkanai	ND	140.0	0.2	Moderate	[8]
BEL_Ypresian	306.0	821.0	480.0	Moderate	[23, 24]
BEL_Boom	0.6	2.3	2.2	Moderate	[33]
FRA_Callovo-Oxfordian	1060.0	1540.0	1250.0	[ ]	[150, 151]
FRA_Toarcian-Domerian	480.0	3168.0	912.0	Low	[79, 80, 81]
CH_Opalinus_MTerri	1700.0	2500.0	[ ]	High	[61]
CH_Opalinus_NE	[ ]	[ ]	2375.0	Moderate	[68]
CAN_Georgian Bay	110.0	310.0	210.0	Moderate	[102]
CAN_Queenston	140.0	310.0	220.0	Moderate	[102]
HUN_Boda-Gorica Block	110.0	210.0	160.0	High	[119]
HUN_Boda-Boda Block	28.0	5650.0	2040.0	High	[119, 131, 133]
	HCO_3 Concentration [mg/L]				
	Minimum	Maximum	Best Estimate	Confidence	Reference
JPN_Koetoi	840.0	3700.0	2900.0	Moderate	[8]
JPN_Wakkanai	47.0	3200.0	2800.0	Moderate	[8]
BEL_Ypresian	[ ]	[ ]	[ ]	[ ]	[ ]
BEL_Boom	[ ]	[ ]	878.9	Moderate	[33]
FRA_Callovo-Oxfordian	85.0	220.0	220.0	[ ]	[150, 151]
FRA_Toarcian-Domerian	118.0	375.0	270.0	Low	[79, 80, 81]
CH_Opalinus_MTerri	52.0	1098.0	[ ]	High	[60]
CH_Opalinus_NE	[ ]	[ ]	125.0	Moderate	[68]
CAN_Georgian Bay	[ ]	[ ]	[ ]	[ ]	[ ]
CAN_Queenston	[ ]	[ ]	[ ]	[ ]	[ ]
HUN_Boda-Gorica Block	769.0	799.0	785.3	High	[119]
HUN_Boda-Boda Block	10.0	512.0	220.0	High	[119, 131, 133]
	Other Chemical Species Concentrations [mg/L]				
	Species & (Best Estimate Concentrations >0.1 mg/L)			Confidence	Reference
JPN_Koetoi	Fe (0.6), Si (29.0), NH_4 (140.0), I (8.0)			Moderate	[8]
JPN_Wakkanai	Fe (0.5), NH_4 (120.0), B (120.0), I (12.0)			Moderate	[8]
BEL_Ypresian	[ ]			[ ]	[ ]
BEL_Boom	Fe (0.2), U (0.7), Si (3.4), NO_3 (0.4), F (2.9), B (0.7)			Moderate	[33]
FRA_Callovo-Oxfordian	Fe (0.2), Si (0.2), NH_4 (2.0), I (3.5), NO_3 (<5.0), F (0.7)			[ ]	[150, 151]
FRA_Toarcian-Domerian	Si (0.2)			Low	[79, 80, 81]
CH_Opalinus_MTerri	[ ]			[ ]	[ ]
CH_Opalinus_NE	Fe (2.9)			Moderate	[68]
CAN_Georgian Bay	B (80.0)			Moderate	[102]
CAN_Queenston	B (90.0)			Moderate	[102]
HUN_Boda-Gorica Block	NH_4 (0.2)			High	[119]
HUN_Boda-Boda Block	Fe (1.0), NH_4 (0.9), B (1.7), Mn (0.3), NO_3 (0.8), F (1.6)			High	[119, 131, 133]

Table 1 – Master Database (continued)

	$\delta^{18}O$ [‰ vs SMOW]				
	Minimum	Maximum	Best Estimate	Confidence	Reference
JPN_Koetoi	-10.4	1.5	-4.1	Moderate	[8]
JPN_Wakkanai	-11.0	3.5	-3.1	Moderate	[8]
BEL_Ypresian	[ ]	[ ]	[ ]	[ ]	[ ]
BEL_Boom	[ ]	[ ]	[ ]	[ ]	[ ]
FRA_Callovo-Oxfordian	-8.2	-5.0	[ ]	[ ]	[64]
FRA_Toarcian-Domerian	-7.0	-5.0	-6.0	Moderate	[83-90]
CH_Opalinus_MTerri	-9.3	-6.6	[ ]	High	[60, 63, 64]
CH_Opalinus_NE	-8.1	-4.6	[ ]	High	[58, 69, 72]
CAN_Georgian Bay	-4.8	-2.5	-3.8	High	[102]
CAN_Queenston	-4.7	-2.4	-3.5	High	[102]
HUN_Boda-Gorica Block	-12.2	-11.6	-11.7	High	[119]
HUN_Boda-Boda Block	-11.0	-6.7	-10.5	High	[108, 119, 131, 133, 136]
	$\delta^{2}H$ [‰ vs SMOW]				
	Minimum	Maximum	Best Estimate	Confidence	Reference
JPN_Koetoi	-72.0	-27.0	-52.6	Moderate	[8]
JPN_Wakkanai	-71.2	-21.0	-46.0	Moderate	[8]
BEL_Ypresian	[ ]	[ ]	[ ]	[ ]	[ ]
BEL_Boom	[ ]	[ ]	[ ]	[ ]	[ ]
FRA_Callovo-Oxfordian	-54.0	-25.0	[ ]	[ ]	[64]
FRA_Toarcian-Domerian	-50.0	-35.0	-20.0	Moderate	[83-90]
CH_Opalinus_MTerri	-64.7	-47.1	[ ]	High	[60, 63, 64]
CH_Opalinus_NE	-52.8	-39.3	[ ]	High	[58, 69, 72]
CAN_Georgian Bay	-55.9	-41.9	-47.9	High	[102]
CAN_Queenston	-50.7	-42.7	-47.3	High	[102]
HUN_Boda-Gorica Block	-85.5	-82.6	-83.7	High	[119]
HUN_Boda-Boda Block	-86.0	-54.0	-74.0	High	[108, 119, 131, 133, 136]

PETROPHYSICAL PARAMETERS

Formation	CEC [meq/kg rock]				
	Minimum	Maximum	Best Estimate	Confidence	Reference
JPN_Koetoi	[ ]	[ ]	[ ]	[ ]	[ ]
JPN_Wakkanai	[ ]	[ ]	200.0	High	[12]
BEL_Ypresian	131.0	420.0	300.0	Moderate	[18, 23, 25, 26]
BEL_Boom	130.0	270.0	182.0 (Boeretang Mbr); 227.0 (Putte Mbr); 210.0 (Terhagen Mbr); 177.0 (Belsele-Waas Mbr.)	High	[35]
FRA_Callovo-Oxfordian (USC)	10.0	250.0	130.0	High	[143, 154]
FRA_Callovo-Oxfordian (UA)	60.0	250.0	160.0	High	[143, 154]
FRA_Toarcian-Domerian	[ ]	[ ]	100-200	Moderate	[79, 81]
CH_Opalinus_MTerri	92.0	195.0	128.0	High	[60]
CH_Opalinus_NE	101.0	120.0	111.0	High	[59, 70]
CAN_Georgian Bay	[ ]	[ ]	[ ]	[ ]	[ ]
CAN_Queenston	[ ]	[ ]	[ ]	[ ]	[ ]
HUN_Boda-Gorica Block	112.0	162.0	120.0	High	[120, 121]
HUN_Boda-Boda Block	40.0	42.0	41.0	High	[121]

Table 1 – Master Database (continued)

	Total Specific Surface [m²/g]				
	Minimum	Maximum	Best Estimate	Confidence	Reference
JPN_Koetoi	[ ]	[ ]	[ ]	[ ]	[ ]
JPN_Wakkanai	[ ]	[ ]	191.5	High	[4]
BEL_Ypresian	23.0	85.0	50.0	Moderate	[26]
BEL_Boom	130.0 (76.0)	148.0 (184.0)	139.0 (140.0)	Moderate	[36] ([53])
FRA_Callovo-Oxfordian	40.0	80.0	70.0	Low	[154]
FRA_Toarcian-Domerian	[ ]	[ ]	[ ]	[ ]	[ ]
CH_Opalinus_MTerri	112.0	195.0	155.0	High	[60]
CH_Opalinus_NE	29.0	104.0	84.0	High	[59, 70]
CAN_Georgian Bay	[ ]	[ ]	[ ]	[ ]	[ ]
CAN_Queenston	[ ]	[ ]	[ ]	[ ]	[ ]
HUN_Boda-Gorica Block	9.8	20.8	15.4	Moderate/High	[122]
HUN_Boda-Boda Block	2.5	12.0	8.0	Low/High	[133, 134]
	External Specific Surface [m²/g]				
	Minimum	Maximum	Best Estimate	Confidence	Reference
JPN_Koetoi	[ ]	[ ]	[ ]	[ ]	[ ]
JPN_Wakkanai	[ ]	[ ]	70.5	High	[4]
BEL_Ypresian	[ ]	[ ]	[ ]	[ ]	[ ]
BEL_Boom	36.6	43.5	41.7	Moderate	[30]
FRA_Callovo-Oxfordian (USC)	4.0	40.0	20.0	High	[144, 146, 153]
FRA_Callovo-Oxfordian (UA)	12.0	45.0	31.0	High	[144, 146, 153]
FRA_Toarcian-Domerian	26.0	37.0	29.0	Moderate	[79]
CH_Opalinus_MTerri	24.0	37.0	31.0	High	[60]
CH_Opalinus_NE	9.8	33.6	23.0	High	[59, 70]
CAN_Georgian Bay	0.8	17.0	6.0	Moderate	[102]
CAN_Queenston	2.1	13.3	9.3	Moderate	[102]
HUN_Boda-Gorica Block	7.6	24.5	15.3	Moderate/High	[122]
HUN_Boda-Boda Block	4.5	15.9	9.4	Low/High	[133, 134]
	Density Bulk Saturated [kg/m³]				
	Minimum	Maximum	Best Estimate	Confidence	Reference
JPN_Koetoi	1465	1635	1545	High	[4]
JPN_Wakkanai	1919	1974	1950	High	[4]
BEL_Ypresian	1790	2090	1980	Moderate	[20, 21, 25-27]
BEL_Boom	[ ]	[ ]	[ ]	[ ]	[ ]
FRA_Callovo-Oxfordian (USC)	2380	2650	2470	High	[143]
FRA_Callovo-Oxfordian (UA)	2380	2520	2450	High	[143]
FRA_Toarcian-Domerian	2300	2600	2600	Moderate	[78, 79]
CH_Opalinus_MTerri	2410	2450	2430	High	[62]
CH_Opalinus_NE	2509	2565	2535	High	[69]
CAN_Georgian Bay	2540	2750	2640	High	[102]
CAN_Queenston	2560	2690	2660	High	[102]
HUN_Boda-Gorica Block	[ ]	[ ]	[ ]	[ ]	[ ]
HUN_Boda-Boda Block	[ ]	[ ]	[ ]	[ ]	[ ]

Table 1 – Master Database (continued)

Formation	Bulk Dry Density [kg/m³]				
	Minimum	Maximum	Best Estimate	Confidence	Reference
JPN_Koetoi	814	1054	929	High	[4]
JPN_Wakkanai	1577	1618	1595	High	[4]
BEL_Ypresian	1330	1800	1570	Moderate	[20, 21, 25-27]
BEL_Boom	1630	1760	1700	Moderate	[36]
FRA_Callovo-Oxfordian (USC)	2230	2450	2340	High	[143]
FRA_Callovo-Oxfordian (UA)	2250	2330	2290	High	[143]
FRA_Toarcian-Domerian	2400	3060	2460	Moderate	[78, 79]
CH_Opalinus_MTerri	2280	2380	2330	Moderate	[62]
CH_Opalinus_NE	2367	2528	2449	Moderate	[59, 70]
CAN_Georgian Bay	2470	2740	2610	High	[102]
CAN_Queenston	2530	2650	2580	High	[102]
HUN_Boda-Gorica Block	2430 / 1709	2682 / 2740	2620 / 2557	Moderate (volume and weight measurement) / Moderate/High (He-pycnometry)	[119, 122]
HUN_Boda-Boda Block	2600 / 2668	2820 / 2711	2730 / 2695	Low (MSZ 18284/2 norm) / Low/Moderate (He-pycnometry)	[108, 133, 134]
	Grain Density (kg/m³)				
	Minimum	Maximum	Best Estimate	Confidence	Reference
JPN_Koetoi	1906	3029	2419	High	[4]
JPN_Wakkanai	2408	2564	2477	High	[4]
BEL_Ypresian	2633	2800	2700	Moderate	[20, 21, 25-27]
BEL_Boom	2661	2711	2695	Moderate	[36]
FRA_Callovo-Oxfordian (USC)	2660	2710	2690	High	[143]
FRA_Callovo-Oxfordian (UA)	2670	2740	2700	High	[143]
FRA_Toarcian-Domerian	2600	2700	2650	Moderate	[78, 79]
CH_Opalinus_MTerri	2680	2760	2700	High	[62]
CH_Opalinus_NE	2658	2800	2732	High	[59, 70]
CAN_Georgian Bay	2690	2860	2760	High	[102]
CAN_Queenston	2660	2830	2770	High	[102]
HUN_Boda-Gorica Block	1745	2911	2683	Moderate	[119]
HUN_Boda-Boda Block	2710	2782	2734	Low/High	[133-135]
	Water Content (water weight /dry weight) [%]				
	Minimum	Maximum	Best Estimate	Confidence	Reference
JPN_Koetoi	54.2	78.1	66.4	High	[4]
JPN_Wakkanai	21.2	23.1	22.0	High	[4]
BEL_Ypresian	19.1	35.0	26.0	Moderate	[20, 21, 25-27]
BEL_Boom	13.7	29.9	19.2	Moderate	[ ]
FRA_Callovo-Oxfordian (USC)	1.0	9.5	6.2	Moderate	[143, 154]
FRA_Callovo-Oxfordian (UA)	3.7	9.0	7.0	Moderate	[143, 154]
FRA_Toarcian-Domerian	1.0	6.0	4.0	Moderate	[78, 79]
CH_Opalinus_MTerri	3.5	8.0	6.4	High	[62]
CH_Opalinus_NE	3.6	5.1	4.4	High	[70]
CAN_Georgian Bay	1.6	3.4	2.5	High	[106, 107, 165]
CAN_Queenston	2.1	3.2	2.7	High	[106, 107, 165]
HUN_Boda-Gorica Block	0.6	36.4	2.3	Moderate	[123]
HUN_Boda-Boda Block	0.0	3.1	<1	Low/High	[133, 135]

Table 1 – Master Database (continued)

	Porosity Calculated from Water Content at 105-110C° or Water Loss [%vol]				
	Minimum	Maximum	Best Estimate	Confidence	Reference
JPN_Koetoi	57.3	65.2	61.6	High	[4]
JPN_Wakkanai	34.5	36.9	35.6	High	[4]
BEL_Ypresian	32.5	50.8	43.0	Moderate	[20, 21, 25-27]
BEL_Boom	27.0	44.7	34.3	[ ]	[ ]
FRA_Callovo-Oxfordian (USC)	2.6	19.5	14.9	Moderate	[143]
FRA_Callovo-Oxfordian (UA)	9.1	19.5	15.9	Moderate	[143]
FRA_Toarcian-Domerian	7.0	14.0	10.5	Moderate	[78, 79]
CH_Opalinus_MTerri	11.2	16.2	13.7	High	[62]
CH_Opalinus_NE	5.5	12.6	10.9	High	[70]
CAN_Georgian Bay	8.3	12.1	9.4	Moderate	[102, 165, 172, 173]
CAN_Queenston	5.8	10.9	8.4	Moderate	[102, 165, 172, 173]
HUN_Boda-Gorica Block	0.5	6.0	2.0	Moderate	[122]
HUN_Boda-Boda Block	1.1	2.2	1.4	Low/High	[108, 109, 119, 122, 131, 133]
Formation	**Porosity - other methods (%)**				
	Minimum	Maximum	Best Estimate	Confidence	Reference
JPN_Koetoi	50.6	58.6	53.7	High	[10]
JPN_Wakkanai	30.7	34.5	33.6	High	[10]
BEL_Ypresian	30.0	47.0	40.0	[ ]	[24]
BEL_Boom	31.0	45.0	[ ]	Moderate	[37]
FRA_Callovo-Oxfordian (USC)	3.0/5.0 (Water content 150°C/NMR)	23.0 (Water content 150°C & NMR)	15.3/14.1 (Water content 150°C/NMR)	High	[144, 152, 153, 155]
FRA_Callovo-Oxfordian (UA)	8.0/13.0 (Water content 150°C/NMR)	22.0/23.0 (Water content 150°C/NMR)	16.2/18.3 (Water content 150°C/NMR)	High	[144, 152, 153, 155]
FRA_Toarcian-Domerian	8.0	11.0	10.5	Moderate	[78, 96]
CH_Opalinus_MTerri	14.0	17.0	15.9	High	[60]
CH_Opalinus_NE	8.8	13.8	11.4	High	[69]
CAN_Georgian Bay	5.5	11.0	7.2	High	[102]
CAN_Queenston	5.5	9.7	6.2	High	[102]
HUN_Boda-Gorica Block	[ ]	[ ]	[ ]	[ ]	[ ]
HUN_Boda-Boda Block	0.4	1.5	0.8	Moderate	[133]

Table 1 – Master Database (continued)

	Effective Porosity [% vol]				
	Minimum	Maximum	Best Estimate	Confidence	Reference
JPN_Koetoi	50.6	58.6	53.7	High (Hg intrusion technique)	[10]
JPN_Wakkanai	30.7	34.5	33.6	High (Hg intrusion technique)	[10]
BEL_Ypresian	30.0	47.0	40.0	[] (HTO pressure-pulse test)	[24]
BEL_Boom	31.0	45.0	[ ]	Moderate	[37]
FRA_Callovo-Oxfordian	[ ]	[ ]	[ ]	[ ]	[ ]
FRA_Toarcian-Domerian	8.0	11.0	10.5	Moderate (Hg intrusion & BET isotherms)	[78, 79]
CH_Opalinus_MTerri	14.0	17.0	15.9	High (Pycnometer porosity)	[60]
CH_Opalinus_NE	8.8	13.8	11.4	High (Pycnometer porosity)	[69]
CAN_Georgian Bay	5.5	11.0	7.2	High (gravimetric; Dean Stark fluid saturation method; boyle's law gas (He) expansion method; nuclear magnetic resonance)	[102]
CAN_Queenston	5.5	9.7	6.2	High (gravimetric; Dean Stark fluid saturation method; boyle's law gas (He) expansion method; nuclear magnetic resonance)	[102]
HUN_Boda-Gorica Block	[ ]	[ ]	[ ]	[ ]	[ ]
HUN_Boda-Boda Block	1.2	2.4	[ ]	Moderate (Pycnometer porosity)	[135]
	Anion-accessible Porosity [% vol]				
	Minimum	Maximum	Best Estimate	Confidence	Reference
JPN_Koetoi	[ ]	[ ]	[ ]	[ ]	[ ]
JPN_Wakkanai	[ ]	[ ]	[ ]	[ ]	[ ]
BEL_Ypresian	17.0	32.0	23.0	Moderate	[24]
BEL_Boom	5.0	20.0	16.0	Moderate	[52]
FRA_Callovo-Oxfordian (USC)	0.1	24.0	6.8	Moderate	[156-162]
FRA_Callovo-Oxfordian (UA)	1.1	27.0	8.0	Moderate	[156-162]
FRA_Toarcian-Domerian	2.0	4.0	3.0	Moderate (Cl-)	[86, 87, 88, 99]
CH_Opalinus_MTerri	5.8	7.7	7.1	High	[68]
CH_Opalinus_NE	3.9	5.1	4.4	Low	[68]
CAN_Georgian Bay	3.9	6.7	4.8	High	[102, 171]
CAN_Queenston	2.9	5.2	3.9	High	[102, 171]
HUN_Boda-Gorica Block	1.8	2.7	2.4	High (Cl-)	[124]
HUN_Boda-Boda Block	[ ]	[ ]	[ ]	[ ]	[ ]

Table 1 – Master Database (continued)

Formation	Seismic Velocity Vp Laboratory Tests (km/s)								
	Minimum (⊥)	Minimum (//)	Maximum (⊥)	Maximum (//)	Best Estimate (⊥)	Best Estimate (//)	Confidence (⊥)	Confidence (//)	Reference
JPN_Koetoi	1.7	1.6	1.8	1.8	1.8	1.7	High	High	[4]
JPN_Wakkanai	1.2	2.2	2.4	2.3	2.2	2.2	High	High	[4]
BEL_Ypresian	[ ]	[ ]	[ ]	[ ]	[ ]	[ ]	[ ]	[ ]	[ ]
BEL_Boom	[ ]	[ ]	[ ]	[ ]	[ ]	[ ]	[ ]	[ ]	[ ]
FRA_Callovo-Oxfordian	[ ]	[ ]	[ ]	[ ]	[ ]	[ ]	[ ]	[ ]	[ ]
FRA_Toarcian-Domerian	4.4	3.2	4.4	3.3	4.4	3.3	Moderate	Moderate	[94]
CH_Opalinus_MTerri	2.2	3.1	3.0	3.6	2.6	3.4	Low	Low	[62]
CH_Opalinus_NE	2.8	4.0	3.3	4.1	3.0	4.0	Low	Low	[58]
CAN_Georgian Bay	3.2	[ ]	5.7	[ ]	4.1	[ ]	High	[ ]	[101]
CAN_Queenston	1.9	[ ]	5.3	[ ]	4.2	[ ]	High	[ ]	[101]
HUN_Boda-Gorica Block	2.6	2.6	3.5	3.4	3.0	3.0	Low/Moderate	Low/Moderate	[123]
HUN_Boda-Boda Block	4.4	4.9	5.1	5.4	4.8	5.1	Moderate	Moderate	[133]
	Seismic Velocity Vs Laboratory Tests (km/s)								
	Minimum (⊥)	Minimum (//)	Maximum (⊥)	Maximum (//)	Best Estimate (⊥)	Best Estimate (//)	Confidence (⊥)	Confidence (//)	Reference
JPN_Koetoi	0.6	0.4	0.7	0.5	0.6	0.5	High	High	[4]
JPN_Wakkanai	0.7	0.9	1.0	0.9	0.9	0.9	High	High	[4]
BEL_Ypresian	[ ]	[ ]	[ ]	[ ]	[ ]	[ ]	[ ]	[ ]	[ ]
BEL_Boom	[ ]	[ ]	[ ]	[ ]	[ ]	[ ]	[ ]	[ ]	[ ]
FRA_Callovo-Oxfordian	[ ]	[ ]	[ ]	[ ]	[ ]	[ ]	[ ]	[ ]	[ ]
FRA_Toarcian-Domerian	[ ]	[ ]	[ ]	[ ]	[ ]	[ ]	[ ]	[ ]	[ ]
CH_Opalinus_MTerri	1.3	1.8	1.8	2.1	1.5	1.9	Low	Low	[62]
CH_Opalinus_NE	1.6	2.2	1.9	2.4	1.7	2.3	Low	Low	[58]
CAN_Georgian Bay	1.7	[ ]	3.3	[ ]	2.2	[ ]	High	[ ]	[101]
CAN_Queenston	0.9	[ ]	3.2	[ ]	2.2	[ ]	High	[ ]	[101]
HUN_Boda-Gorica Block	1.6	1.8	2.1	1.9	1.8	1.8	Low/Moderate	Low/Moderate	[123]
HUN_Boda-Boda Block	2.1	2.5	2.8	2.9	2.6	2.8	Moderate	Moderate	[133]

Table 1 – Master Database (continued)

	Seismic Velocity Vp In Situ Tests [km/s]				
	Minimum	Maximum	Best Estimate	Confidence	Reference
JPN_Koetoi	1.6	1.7	1.7	High	[4]
JPN_Wakkanai	2.3	2.4	2.3	High	[4]
BEL_Ypresian	[ ]	[ ]	[ ]	[ ]	[ ]
BEL_Boom	1.7	2.1	1.9±0.1 (Boeretang Mbr); 1.9±.8 (Putte Mbr); 1.9±.6 (Terhagen Mbr); 1.9±1.4 (Belsele-Waas Mbr.)	High	[38-40]
FRA_Callovo-Oxfordian	[ ]	[ ]	[ ]	[ ]	[ ]
FRA_Toarcian-Domerian	3.4	4.2	4.0	Moderate	[94]
CH_Opalinus_MTerri	2.4-2.8 / 2.8-3.4	2.5-3.4 / 3.2-4.6	2.5-3.2 / 3.0-4.0 (⊥/ // to fabric)	High	[65, 166]
CH_Opalinus_NE	2.8	3.6	3.2	Low	[58]
CAN_Georgian Bay	3.8	4.2	4.0	Moderate/High	[107]
CAN_Queenston	3.9	4.3	4.2	Moderate/High	[107]
HUN_Boda-Gorica Block	[ ]	[ ]	[ ]	[ ]	[ ]
HUN_Boda-Boda Block	4.4	6.5	5.3	High	[137]
	Seismic Velocity Vs In Situ Tests [km/s]				
	Minimum	Maximum	Best Estimate	Confidence	Reference
JPN_Koetoi	0.8	0.8	0.8	High	[4]
JPN_Wakkanai	1.1	1.2	1.2	High	[4]
BEL_Ypresian	[ ]	[ ]	[ ]	[ ]	[ ]
BEL_Boom	0.5	0.7	0.5±0.1 (Boeretang Mbr); 0.5±0.1 (Putte Mbr); 0.6±0.1 (Terhagen Mbr); 0.6±0.1 (Belsele-Waas Mbr.)	Moderate	[40-42]
FRA_Callovo-Oxfordian	[ ]	[ ]	[ ]	[ ]	[ ]
FRA_Toarcian-Domerian	1.6	1.8	1.7	Moderate	[94]
CH_Opalinus_MTerri	0.9-1.5 / 1.0-1.9	1.1-1.7 / 1.0-2.2	1.0-1.6 / 1.0-2.1 (⊥/ // to fabric)	High	[166]
CH_Opalinus_NE	1.4	1.9	1.7	Low	[58]
CAN_Georgian Bay	1.5	2.3	2.0	Moderate/High	[102]
CAN_Queenston	2.1	2.3	2.2	Moderate/High	[102]
HUN_Boda-Gorica Block	[ ]	[ ]	[ ]	[ ]	[ ]
HUN_Boda-Boda Block	2.5	4.2	2.9	High	[137]

FLOW AND SOLUTE TRANSPORT PARAMETERS

	Hydraulic Conductivity In Situ [m/s]				
	Minimum	Maximum	Best Estimate	Confidence	Reference
JPN_Koetoi	9.0E-10	3.0E-08	5.2E-09	Moderate (combined ∥ and ⊥ data)	[9]
JPN_Wakkanai	1.0E-12	1.0E-05	1.0E-09	Moderate (combined ∥ and ⊥ data)	[9]
BEL_Ypresian	[ ]	[ ]	[ ]	[ ]	[ ]
BEL_Boom	1.6E-12	8.6E-12	4.7E-12	High	[50]
FRA_Callovo-Oxfordian	1.2E-14	3.1E-12	1.9E-13	Moderate	[ ]
FRA_Toarcian-Domerian	1.0E-15	1.0E-13	1.0E-14	Moderate (// to bedding)	[79, 95-98]
CH_Opalinus_MTerri	2.0E-14	2.3E-10	3.1E-13	High (// to bedding)	[66]
CH_Opalinus_NE	1.2E-14	4.0E-13	8.0E-14	Moderate (// to bedding)	[68]
CAN_Georgian Bay	2.9E-15	3.3E-13	3.0E-14	High	[102]
CAN_Queenston	1.6E-14	1.5E-13	3.0E-14	High	[102]
HUN_Boda-Gorica Block	2.0E-13	8.0E-08	1.0E-12	High	[119]
HUN_Boda-Boda Block	1.0E-13	5.0E-09	1.0E-12	High	[108, 109, 131, 133, 138]

Table 1 – Master Database (continued)

Formation	Hydraulic Conductivity Laboratory Tests (m/s)									
	Minimum (⊥)	Minimum (//)	Maximum (⊥)	Maximum (//)	Best Estimate (⊥)	Best Estimate (//)	Anisotropy* (‖/⊥)	Confidence (⊥)	Confidence (//)	Reference
JPN_Koetoi	[ ]	[ ]	[ ]	[ ]	[ ]	[ ]	[ ]	[ ]	[ ]	[ ]
JPN_Wakkanai	7.0E-13	[ ]	5.0E-12	[ ]	1.9E-12	[ ]	[ ]	[ ]	Moderate	[9]
BEL_Ypresian	8.2E-13	[ ]	5.7E-11	[ ]	5.0E-12	[ ]	[ ]	[ ]	Moderate	[13]
BEL_Boom	[ ]	[ ]	[ ]	[ ]	4.6E-12 (1.7E-12*)	9.2E-12 (4.4E-12*)	2.0 (2.6)	High	High	[50]
FRA_Callovo-Oxfordian	2.1E-15	9.1E-15	2.1E-12	5.5E-12	2.3E-13	6.2E-13	2.7 (calculated from best estimates)	Moderate	Moderate	[]
FRA_Toarcian-Domerian	[ ]	[ ]	[ ]	[ ]	1.0E-14	[ ]	[ ]	[ ]	Moderate	[79, 95-98]
CH_Opalinus_MTerri	6.0E-14	1.0E-13	2.0E-13	2.0E-13	[ ]	[ ]	[ ]	Moderate	Moderate	[67]
CH_Opalinus_NE	6.0E-15	3.0E-14	1.2E-13	6.0E-14	2.5E-14	[ ]	[ ]	Low	High	[68]
CAN_Georgian Bay	2.8E-14/2.8E-14	6.4E-12/[ ]	1.3E-11/6.8E-11	1.1E-11/[ ]	5.1E-13/1.3E-11	8.8E-12/2.8E-13	17.3/.02 (calculated from best estimates)	High (Brine pulse/gas pulse)	High (Brine pulse/gas pulse)	[102]
CAN_Queenston	2.8E-14/2.8E-14	2.8E-14/[ ]	2.6E-12/6.8E-10	3.5E-12/[ ]	9.2E-13/1.2E-10	1.3E-12/2.7E-11	1.4/.2 (calculated from best estimates)	High (Brine pulse/gas pulse)	High (Brine pulse/gas pulse)	[102]
HUN_Boda-Gorica Block	[ ]	[ ]	[ ]	[ ]	[ ]	[ ]	[ ]	[ ]	[ ]	[ ]
HUN_Boda-Boda Block	[ ]	[ ]	[ ]	[ ]	[ ]	[ ]	[ ]	[ ]	[ ]	[ ]
	Diffusion Coefficient De (^{3}H) Laboratory Tests (m^2/s)									
	Minimum (⊥)	Minimum (//)	Maximum (⊥)	Maximum (//)	Best Estimate (⊥)	Best Estimate (//)	Anisotropy* (‖/⊥)	Confidence (⊥)	Confidence (//)	Reference
JPN_Koetoi	[ ]	[ ]	[ ]	[ ]	[ ]	[ ]	[ ]	[ ]	[ ]	[ ]
JPN_Wakkanai	[ ]	1.1E-10	[ ]	1.8E-10	8.8E-11	1.0E-10	1.2	High	High	[13]
BEL_Ypresian	2.0E-10	[ ]	5.8E-10	[ ]	3.0E-10	[ ]	[ ]	Moderate	[ ]	[24]
BEL_Boom	7.5E-11	9.0E-11	1.1E-10	2.2E-10	9.4E-11	1.5E-10	1.6	Moderate	Moderate	[51]
FRA_Callovo-Oxfordian (USC)	4.0E-14	[ ]	8.0E-11	[ ]	2.5E-11	[ ]	[ ]	High	[ ]	[156-162]
FRA_Callovo-Oxfordian (UA)	9.9E-12	[ ]	3.1E-11	[ ]	2.2E-11	[ ]	[ ]	High	[ ]	[156-162]
FRA_Toarcian-Domerian	7.0E-12	2.0E-11	8.0E-12	3.0E-11	7.5E-12	2.5E-11	3.3	Moderate	Moderate	[86, 87, 88, 96, 100]
CH_Opalinus_MTerri	1.2E-11	[ ]	1.5E-11	[ ]	1.4E-11	5.4E-11	3.9	High	High	[68]
CH_Opalinus_NE	5.4E-12	3.1E-11	8.8E-12	3.3E-11	6.4E-12	3.2E-11	5.0	High	High	[68]
CAN_Georgian Bay	1.5E-13	[ ]	3.3E-12	[ ]	1.0E-12	[ ]	[ ]	High	[ ]	[102]
CAN_Queenston	9.3E-14	[ ]	4.8E-12	[ ]	1.8E-12	[ ]	[ ]	High	[ ]	[102]
HUN_Boda-Gorica Block	[ ]	1.1E-11	[ ]	1.4E-11	[ ]	1.2E-11	[ ]	[ ]	High	[118, 124, 125]
HUN_Boda-Boda Block	[ ]	[ ]	[ ]	[ ]	[ ]	[ ]	[ ]	[ ]	[ ]	[ ]

Table 1 – Master Database (continued)

	Diffusion Coefficient De (I) [m²/s]									
	Minimum (⊥)	Minimum (//)	Maximum (⊥)	Maximum (//)	Best Estimate (⊥)	Best Estimate (//)	Anisotropy* (‖/⊥)	Confidence (⊥)	Confidence (//)	Reference
JPN_Koetoi	[ ]	[ ]	[ ]	[ ]	[ ]	[ ]	[ ]	[ ]	[ ]	[ ]
JPN_Wakkanai	[ ]	2.7E-11	[ ]	9.7E-11	[ ]	5.7E-11	[ ]	[ ]	High	[12]
BEL_Ypresian	1.3E-10	[ ]	4.5E-10	[ ]	2.0E-10	[ ]	[ ]	Moderate	[ ]	[24]
BEL_Boom	2.5E-11	[ ]	2.0E-10	[ ]	1.4E-10	3.4E-10	2.4	Moderate	Moderate	[52]
FRA_Callovo-Oxfordian (USC)	2.8E-13	[ ]	4.7E-12	[ ]	2.6E-12	[ ]	[ ]	Moderate	[ ]	[156, 158, 159]
FRA_Callovo-Oxfordian (UA)	5.0E-13	[ ]	7.7E-12	[ ]	4.5E-12	[ ]	[ ]	Moderate	[ ]	[156, 158, 159]
FRA_Toarcian-Domerian	1.4E-13	[ ]	2.4E-13	[ ]	2.0E-13	[ ]	[ ]	Moderate	[ ]	[86, 87, 88, 99]
CH_Opalinus_MTerri	3.4E-12	[ ]	4.8E-12	[ ]	4.1E-12	[ ]	[ ]	High	[ ]	[68]
CH_Opalinus_NE	4.5E-13	[ ]	6.6E-13	[ ]	5.4E-13	[ ]	[ ]	High	[ ]	[68]
CAN_Georgian Bay	5.3E-14	2.3E-12	5.3E-12	5.3E-12	1.3E-12	4.2E-12	3.1	High	High	[102]
CAN_Queenston	3.2E-14	2.5E-12	2.8E-12	4.0E-12	1.6E-12	3.0E-12	1.9	High	High	[102]
HUN_Boda-Gorica Block	[ ]	[ ]	[ ]	[ ]	[ ]	[ ]	[ ]	[ ]	[ ]	[ ]
HUN_Boda-Boda Block	[ ]	1.5E-12	[ ]	1.0E-11	[ ]	2.0E-12	[ ]	[ ]	High	[139]
	Diffusion Coefficient De (Cl) (m²/s)									
	Minimum (⊥)	Minimum (//)	Maximum (⊥)	Maximum (//)	Best Estimate (⊥)	Best Estimate (//)	Anisotropy* (‖/⊥)	Confidence (⊥)	Confidence (//)	Reference
JPN_Koetoi	[ ]	[ ]	[ ]	[ ]	[ ]	[ ]	[ ]	[ ]	[ ]	[ ]
JPN_Wakkanai	[ ]	[ ]	[ ]	[ ]	[ ]	[ ]	[ ]	[ ]	[ ]	[ ]
BEL_Ypresian	[ ]	[ ]	[ ]	[ ]	[ ]	[ ]	[ ]	[ ]	[ ]	[ ]
BEL_Boom	[ ]	[ ]	[ ]	[ ]	[ ]	[ ]	[ ]	[ ]	[ ]	[ ]
FRA_Callovo-Oxfordian (USC)	6.0E-14	[ ]	6.0E-11	[ ]	8.3E-11	[ ]	[ ]	High	[]	[156-162]
FRA_Callovo-Oxfordian (UA)	7.0E-13	[ ]	9.1E-12	[ ]	4.7E-12	[ ]	[ ]	High	[]	[156-162]
FRA_Toarcian-Domerian	3.8E-12	[ ]	4.4E-12	[ ]	4.0E-12	[ ]	[ ]	Moderate	[ ]	[86, 87, 88, 99]
CH_Opalinus_MTerri	4.1E-12	[ ]	5.7E-12	[ ]	4.9E-12	1.6E-11	3.3	High	High	[68]
CH_Opalinus_NE	6.7E-13	[ ]	1.0E-12	[ ]	8.1E-13	3.4E-12	4.2	High	High	[68]
CAN_Georgian Bay	[ ]	[ ]	[ ]	[ ]	[ ]	[ ]	[ ]	[ ]	[ ]	[ ]
CAN_Queenston	[ ]	[ ]	[ ]	[ ]	[ ]	[ ]	[ ]	[ ]	[ ]	[ ]
HUN_Boda-Gorica Block	[ ]	3.3E-13	[ ]	4.0E-13	[ ]	3.7E-13	[ ]	[ ]	High	[124]
HUN_Boda-Boda Block	[ ]	[ ]	[ ]	[ ]	[ ]	[ ]	[ ]	[ ]	[ ]	[ ]

Table 1 – Master Database (continued)

GEOMECHANICAL PARAMETERS

	Uniaxial Compressive Strength Laboratory Tests (MPa)									
	Minimum (⊥)	Minimum (//)	Maximum (⊥)	Maximum (//)	Best Estimate (⊥)	Best Estimate (//)	Anisotropy* (⊥/‖)	Confidence (⊥)	Confidence (//)	Reference
JPN_Koetoi	5.1	1.4	9.8	7.4	7.6	4.0	1.9	High	High	[4]
JPN_Wakkanai	11.3	11.1	22.6	21.8	16.9	14.6	1.2	High	High	[4]
BEL_Ypresian	0.2	[ ]	2.0	[ ]	1.3	[ ]	[ ]	Moderate	[ ]	[27]
BEL_Boom	2.0	[ ]	3.0	[ ]	2.0	[ ]	[ ]	Moderate	[ ]	[47, 48, 49]
FRA_Callovo-Oxfordian (UA)	10.0	12.3	43.8	34.6	26.3 ± 6.4	20 ± 6.6	1.3	High	High	[163]
FRA_Toarcian-Domerian	12.0	33.0	18.0	38.0	13.0	37.0	0.4	Moderate	Moderate	[78, 79, 91]
CH_Opalinus_MTerri	5.0	4.0	24.4	19.5	7.0-16.0	10.0-18.0	[]	Moderate	Moderate	[56, 167, 168]
CH_Opalinus_NE	17.0	21.8	38.3	41.7	31.0	36.0	0.9	Low	Low	[56]
CAN_Georgian Bay	15.0	[ ]	63.0	[ ]	32.0	[ ]	[ ]	High	[ ]	[101, 102]
CAN_Queenston	19.0	[ ]	70.0	[ ]	48.0	[ ]	[ ]	High	[ ]	[101, 102]
HUN_Boda-Gorica Block	7.6	[ ]	160.0	[ ]	70.0	[ ]	[ ]	Moderate	[ ]	[119]
HUN_Boda-Boda Block	16.0	11.0	250.0	210.0	110.0	90.0	1.2	Moderate	Moderate	[108, 109, 115, 132, 133]
Formation	**Young's Modulus Static Laboratory Tests (MPa)**									
	Minimum (⊥)	Minimum (//)	Maximum (⊥)	Maximum (//)	Best Estimate (⊥)	Best Estimate (//)	Anisotropy* (⊥/‖)	Confidence (⊥)	Confidence (//)	Reference
JPN_Koetoi	556	376	1398	935	1030	686	1.5	High	High	[4]
JPN_Wakkanai	1710	2410	5220	3500	3614	2872	1.3	High	High	[4]
BEL_Ypresian	[ ]	[ ]	[ ]	[ ]	[ ]	[ ]	[ ]	[ ]	[ ]	[ ]
BEL_Boom	[ ]	[ ]	[ ]	[ ]	200	400	[ ]	Moderate	Moderate	[43-46]
FRA_Callovo-Oxfordian	3252	7118	8638	15738	5945	11428	0.5	High	High	[163]
FRA_Toarcian-Domerian	14757	8000	32309	14336	27680	9270	3.0	Moderate	Moderate	[78, 79, 91]
CH_Opalinus_MTerri	2200	4300	8500	17000	3300	6600	0.5	Low	Low	[62]
CH_Opalinus_NE	2900	5800	9300	18500	4400	8800	0.5	Low	Low	[73]
CAN_Georgian Bay	3000	[ ]	18000	[ ]	12000	[ ]	[ ]	High	[ ]	[101, 102]
CAN_Queenston	5000	[ ]	25000	[ ]	15000	[ ]	[ ]	High	[ ]	[101, 102]
HUN_Boda-Gorica Block	1700	[ ]	52000	[ ]	22500 (20000-25000)	[ ]	[ ]	Moderate	[ ]	[119]
HUN_Boda-Boda Block	79000	52000	110000	69000	83000	57000	1.5	Moderate	Moderate	[115]
	Young's Modulus Dynamic Laboratory Tests (MPa)									
	Minimum (⊥)	Minimum (//)	Maximum (⊥)	Maximum (//)	Best Estimate (⊥)	Best Estimate (//)	Anisotropy* (⊥/‖)	Confidence (⊥)	Confidence (//)	Reference
JPN_Koetoi	1550	558	1840	1380	1816	999	1.8	High	High	[4]
JPN_Wakkanai	2390	4270	5640	4750	4432	4503	1.0	High	High	[4]
BEL_Ypresian	[ ]	[ ]	[ ]	[ ]	[ ]	[ ]	[ ]	[ ]	[ ]	[ ]
BEL_Boom	[ ]	[ ]	[ ]	[ ]	[ ]	[ ]	[ ]	[ ]	[ ]	[ ]
FRA_Callovo-Oxfordian	10822	19565	16222	25165	13522	22365	0.6	High	High	[163]
FRA_Toarcian-Domerian	[ ]	[ ]	[ ]	[ ]	[ ]	[ ]	[ ]	[ ]	[ ]	[ ]
CH_Opalinus_MTerri	[ ]	[ ]	[ ]	[ ]	14000	22000	[ ]	High	High	[62]
CH_Opalinus_NE	16000	30000	22000	36000	19000	33000	0.6	Low	Low	[58]
CAN_Georgian Bay	20170	[ ]	73300	[ ]	34400	[ ]	[ ]	Moderate/High	[ ]	[101, 102]
CAN_Queenston	6000	[ ]	61700	[ ]	36200	[ ]	[ ]	Moderate/High	[ ]	[101, 102]
HUN_Boda-Gorica Block	[ ]	[ ]	[ ]	[ ]	[ ]	[ ]	[ ]	[ ]	[ ]	[ ]
HUN_Boda-Boda Block	18000	18000	79000	79000	45000 - 50000	45000 - 50000	[ ]	High (mixed orientation)	High (mixed orientation)	[115, 133, 137]

Table 1 – Master Database (continued)

	Young's Modulus Static In Situ Tests (MPa)													
	Minimum (⊥)	Minimum (//)	Minimum (-)	Maximum (⊥)	Maximum (//)	Maximum (-)	Best Estimate (⊥)	Best Estimate (//)	Best Estimate (-)	Anisotropy* (⊥/‖)	Confidence (⊥)	Confidence (//)	Confidence (-)	Reference
JPN_Koetoi	[ ]	[ ]	[ ]	[ ]	[ ]	[ ]	[ ]	[ ]	1250 - 1750	[ ]	[ ]	[ ]	Moderate (Orientation of bedding towards borehole axis:55°)	[4]
JPN_Wakkanai	[ ]	[ ]	4350	[ ]	[ ]	7070	[ ]	[ ]	5710	[ ]	[ ]	[ ]	Moderate (Oblique to bedding (30 to 60°)	[4]
BEL_Ypresian	[ ]	[ ]	[ ]	[ ]	[ ]	[ ]	[ ]	[ ]	[ ]	[ ]	[ ]	[ ]	[ ]	[ ]
BEL_Boom	[ ]	[ ]	[ ]	[ ]	[ ]	[ ]	700	1400	[ ]	0.5	Moderate	Moderate	[ ]	[48]
FRA_Callovo-Oxfordian	[ ]	[ ]	[ ]	[ ]	[ ]	[ ]	[ ]	[ ]	[ ]	[ ]	[ ]	[ ]	[ ]	[ ]
FRA_Toarcian-Domerian	[ ]	[ ]	[ ]	[ ]	[ ]	[ ]	[ ]	[ ]	[ ]	[ ]	[ ]	[ ]	[ ]	[ ]
CH_Opalinus_MTerri	1900	5900	[ ]	3100	7700	[ ]	2500	6800	[ ]	0.4	Low	Low	[ ]	[62]
CH_Opalinus_NE	[ ]	10500	[ ]	[ ]	13500	[ ]	[ ]	12000	[ ]	[ ]	[ ]	Low	[ ]	[58]
CAN_Georgian Bay	[ ]	[ ]	[ ]	[ ]	[ ]	[ ]	[ ]	[ ]	[ ]	[ ]	[ ]	[ ]	[ ]	[ ]
CAN_Queenston	[ ]	[ ]	[ ]	[ ]	[ ]	[ ]	[ ]	[ ]	[ ]	[ ]	[ ]	[ ]	[ ]	[ ]
HUN_Boda-Gorica Block	[ ]	[ ]	[ ]	[ ]	[ ]	[ ]	[ ]	[ ]	[ ]	[ ]	[ ]	[ ]	[ ]	[ ]
HUN_Boda-Boda Block	[ ]	[ ]	14000	[ ]	[ ]	98000	[ ]	[ ]	52000	[ ]	[ ]	[ ]	Moderate (mixed orientation)	[115]

Table 1 – Master Database (continued)

	Poisson's Ratio Static Laboratory Tests									
	Minimum (⊥)	Minimum (//)	Maximum (⊥)	Maximum (//)	Best Estimate (⊥)	Best Estimate (//)	Anisotropy* (⊥/‖)	Confidence (⊥)	Confidence (//)	Reference
JPN_Koetoi	0.21	0.22	0.33	0.47	0.25	0.33	0.76	High	High	[4]
JPN_Wakkanai	0.20	0.21	0.29	0.27	0.23	0.24	0.96	High	High	[4]
BEL_Ypresian	[ ]	[ ]	[ ]	[ ]	[ ]	[ ]	[ ]	[ ]	[ ]	[ ]
BEL_Boom	[ ]	[ ]	[ ]	[ ]	0.13	0.25	0.50	Moderate	Moderate	[43-46]
FRA_Callovo-Oxfordian	[ ]	[ ]	[ ]	[ ]	[ ]	[ ]	[ ]	[ ]	[ ]	[ ]
FRA_Toarcian-Domerian	[ ]	[ ]	[ ]	[ ]	0.17	0.14	1.21	Moderate	Moderate	[78, 79, 91]
CH_Opalinus_MTerri	0.31	0.16	0.39	0.34	0.35	0.25	1.40	Low	Low	[62]
CH_Opalinus_NE	0.17	0.17	0.37	0.37	0.27	0.27	1.00	Moderate	Moderate	[58]
CAN_Georgian Bay	0.02	[ ]	0.50	[ ]	0.23	[ ]	[ ]	High	[ ]	[101, 102]
CAN_Queenston	0.10	[ ]	0.40	[ ]	0.30	[ ]	[ ]	High	[ ]	[101, 102]
HUN_Boda-Gorica Block	0.12	[ ]	0.42	[ ]	0.22 - 0.24	[ ]	[ ]	Moderate	[ ]	[119]
HUN_Boda-Boda Block	0.13	[ ]	0.43	[ ]	0.29	[ ]	[ ]	Moderate	[ ]	[133]
	Poisson's Ratio Dynamic Laboratory Tests									
	Minimum (⊥)	Minimum (//)	Maximum (⊥)	Maximum (//)	Best Estimate (⊥)	Best Estimate (//)	Anisotropy* (⊥/‖)	Confidence (⊥)	Confidence (//)	Reference
JPN_Koetoi	0.42	0.44	0.44	0.48	0.43	0.46	0.94	High	High	[4]
JPN_Wakkanai	0.25	0.40	0.41	0.41	0.37	0.40	0.92	High	High	[4]
BEL_Ypresian	[ ]	[ ]	[ ]	[ ]	[ ]	[ ]	[ ]	[ ]	[ ]	[ ]
BEL_Boom	[ ]	[ ]	[ ]	[ ]	[ ]	[ ]	[ ]	[ ]	[ ]	[ ]
FRA_Callovo-Oxfordian	0.23	0.13	0.37	0.21	0.30	0.17	1.76	High	High	[163]
FRA_Toarcian-Domerian	[ ]	[ ]	[ ]	[ ]	[ ]	[ ]	[ ]	[ ]	[ ]	[ ]
CH_Opalinus_MTerri	[ ]	[ ]	[ ]	[ ]	0.25	0.26	0.96	High	High	[62]
CH_Opalinus_NE	0.26	0.26	0.28	0.28	0.27	0.27	1.00	Low	Low	[58]
CAN_Georgian Bay	0.27	[ ]	0.37	[ ]	0.30	[ ]	[ ]	Moderate/High	[ ]	[101, 102]
CAN_Queenston	0.11	[ ]	0.38	[ ]	0.30	[ ]	[ ]	Moderate/High	[ ]	[101, 102]
HUN_Boda-Gorica Block	[ ]	[ ]	[ ]	[ ]	[ ]	[ ]	[ ]	[ ]	[ ]	[ ]
HUN_Boda-Boda Block	0.10	0.10	0.42	0.42	0.29 - 0.31	0.29 - 0.31	1.00	Moderate (mixed orientation)	Moderate (mixed orientation)	[115, 137]
Formation	**Swelling Pressure Laboratory Tests [MPa]**									
	Minimum (⊥)	Minimum (//)	Maximum (⊥)	Maximum (//)	Best Estimate (⊥)	Best Estimate (//)	Anisotropy* (⊥/‖)	Confidence (⊥)	Confidence (//)	Reference
JPN_Koetoi	[ ]	0.00	[ ]	0.03	[ ]	0.01	[ ]	[ ]	High	[4]
JPN_Wakkanai	0.00	0.00	0.06	0.02	0.02	0.01	3.43	High	High	[4]
BEL_Ypresian	[ ]	[ ]	[ ]	[ ]	[ ]	[ ]	[ ]	[ ]	[ ]	[ ]
BEL_Boom	[ ]	[ ]	[ ]	[ ]	[ ]	[ ]	[ ]	[ ]	[ ]	[ ]
FRA_Callovo-Oxfordian	[ ]	[ ]	[ ]	[ ]	[ ]	[ ]	[ ]	[ ]	[ ]	[ ]
FRA_Toarcian-Domerian	0.14	0.33	0.61	0.46	0.50	0.40	1.25	Low	Low	[79, 92]
CH_Opalinus_MTerri	0.44	0.08	0.61	0.16	0.50	0.20	2.50	Moderate	Low	[56]
CH_Opalinus_NE	0.80	0.10	1.40	0.20	1.10	0.20	5.50	Moderate	Low	[56]
CAN_Georgian Bay	[ ]	[ ]	[ ]	[ ]	[ ]	[ ]	[ ]	[ ]	[ ]	[ ]
CAN_Queenston	[ ]	[ ]	[ ]	[ ]	[ ]	[ ]	[ ]	[ ]	[ ]	[ ]
HUN_Boda-Gorica Block	[ ]	[ ]	[ ]	[ ]	[ ]	[ ]	[ ]	[ ]	[ ]	[ ]
HUN_Boda-Boda Block	[ ]	[ ]	[ ]	[ ]	[ ]	[ ]	[ ]	[ ]	[ ]	[ ]

Table 1 – Master Database (continued)

	Cohesion Laboratory Tests									
	Minimum (⊥)	Minimum (//)	Maximum (⊥)	Maximum (//)	Best Estimate (⊥)	Best Estimate (//)	Anisotropy* (⊥/‖)	Confidence (⊥)	Confidence (//)	Reference
JPN_Koetoi	[ ]	1.6	[ ]	1.7	[ ]	1.7	[ ]	[]	Moderate	[4]
JPN_Wakkanai	3.1	4.1	6.8	4.6	4.4	4.4	1.0	Moderate	Moderate	[4]
BEL_Ypresian	0.2	[ ]	0.8	[ ]	0.5	[]	[ ]	Moderate	[]	[21, 27]
BEL_Boom	[ ]	[ ]	[ ]	[ ]	0.3	0.3	[ ]	Low	Low	[43-46]
FRA_Callovo-Oxfordian	[ ]	[ ]	[ ]	[ ]	[ ]	[ ]	[ ]	[ ]	[ ]	[ ]
FRA_Toarcian-Domerian	1.0	[ ]	1.8	[ ]	1.5	[ ]	[ ]	Moderate	[ ]	[93]
CH_Opalinus_MTerri	[ ]	[ ]	[ ]	[ ]	2.0-10.0	2.0-10.0	[ ]	Low	Low	[56, 170]
CH_Opalinus_NE	[ ]	[ ]	[ ]	[ ]	3.0-10.0	3.0-10.0	[ ]	Low	Low	[56, 170]
CAN_Georgian Bay	[ ]	[ ]	[ ]	[ ]	[ ]	[ ]	[ ]	[ ]	[ ]	[ ]
CAN_Queenston	[ ]	[ ]	[ ]	[ ]	[ ]	[ ]	[ ]	[ ]	[ ]	[ ]
HUN_Boda-Gorica Block	[ ]	[ ]	[ ]	[ ]	[ ]	[ ]	[ ]	[ ]	[ ]	[ ]
HUN_Boda-Boda Block	[ ]	[ ]	[ ]	[ ]	[ ]	[ ]	[ ]	[ ]	[ ]	[ ]
	Internal Friction Angle Laboratory Tests [°]									
	Minimum (⊥)	Minimum (//)	Maximum (⊥)	Maximum (//)	Best Estimate (⊥)	Best Estimate (//)	Anisotropy* (⊥/‖)	Confidence (⊥)	Confidence (//)	Reference
JPN_Koetoi	[ ]	14.2	[ ]	18.5	[ ]	16.4	[ ]	[ ]	Moderate	[4]
JPN_Wakkanai	24.1	28.5	30.3	30.6	26.1	29.6	0.9	Moderate	Moderate	[4]
BEL_Ypresian	7.8	[ ]	38.0	[ ]	16.0	[ ]	[ ]	Moderate	[ ]	[21, 27]
BEL_Boom	[ ]	[ ]	[ ]	[ ]	[ ]	[ ]	[ ]	[ ]	[ ]	[ ]
FRA_Callovo-Oxfordian	[ ]	[ ]	[ ]	[ ]	[ ]	[ ]	[ ]	[ ]	[ ]	[ ]
FRA_Toarcian-Domerian	19.0	[ ]	35.0	[ ]	25.0	[ ]	[ ]	Moderate	[ ]	[93]
CH_Opalinus_MTerri	[ ]	[ ]	[ ]	[ ]	20.0	29.0	0.7	Low	Low	[56, 170]
CH_Opalinus_NE	[ ]	[ ]	[ ]	[ ]	20.0	33.0	0.6	Moderate	Low	[56, 170]
CAN_Georgian Bay	[ ]	[ ]	[ ]	[ ]	[ ]	[ ]	[ ]	[ ]	[ ]	[ ]
CAN_Queenston	[ ]	[ ]	[ ]	[ ]	[ ]	[ ]	[ ]	[ ]	[ ]	[ ]
HUN_Boda-Gorica Block	[ ]	[ ]	[ ]	[ ]	[ ]	[ ]	[ ]	[ ]	[ ]	[ ]
HUN_Boda-Boda Block	[ ]	[ ]	[ ]	[ ]	[ ]	[ ]	[ ]	[ ]	[ ]	[ ]

Table 2 – Methods and scales of measurement

GEOLOGICAL PARAMETERS - METHODS	JPN - Koetoi	JPN - Wakkanai	BEL - Ypresian	BEL - Boom	FRA - Callovo-Oxfordian	FRA - Domerian-Toarcian	CH - Opalinus_ MTerri	CH - Opalinus_NE	CAN - Georgian Bay	CAN - Queenston	HUN - Boda-Gorica Block	HUN - Boda-Boda Block
Depositional Environment	[ ]	[ ]	[ ]	[ ]	[ ]	[ ]	[ ]	[ ]	[ ]	[ ]	[ ]	[ ]
Age [Ma]	[ ]	[ ]	[ ]	[ ]	Ammonite determination cyclostrati-graphy	Regional study; km scale	Biostratigraphy; borehole scale	Biostratigraphy; borehole scale	Geologic time scale	Geologic time scale	Stratigraphical analyses; formation scale	stratigraphical analyses; formation scale
Burial Depth Present-day [m, top formation]	[ ]	[ ]	Geophysical logs; Doel and Kallo locations	[ ]; Nuclear zone of Mol-Dessel (reference research site); Best estimate corresponds to borehole ON-Mol-1	[ ]	Regional study; km scale	Borehole & surface data, balanced cross-sections; km scale	Borehole data; borehole scale	Drill core logging - true vertical depth; km scale	Drill core logging - true vertical depth; km scale	Surface boreholes, geological mapping; 15-20 km^2 scale	Surface boreholes, geological mapping; 20-25 km^2 scale
Burial Depth Present-day [m, bottom formation]	[ ]	[ ]	Geophysical logs; Doel and Kallo locations	[ ]; Nuclear zone of Mol-Dessel (reference research site); Best estimate corresponds to borehole ON-Mol-2	[ ]	Regional study; km scale	Borehole & surface data, balanced cross-sections; km scale	Borehole data; borehole scale	Drill core logging - true vertical depth; km scale	Drill core logging - true vertical depth; km scale	Surface boreholes; 15-20 km^2 scale	Surface boreholes; 20-25 km^2 scale
Thickness [m]	[ ]	[ ]	Geophysical logs; Doel and Kallo locations	[ ]	modelling from boreholes; Thickness range defined on the basis of the Callovo-Oxfordian 3D modelling Cox at the scale of the Transposition Zone; Thickness uncertainty: ± 10 m (maximum)	Regional study; km scale	Borehole & surface data; balanced cross-sections; borehole km scale; Max. number is due to tectonic thickening, the primary thickness is 90 m	Borehole data & 3D seismics; borehole scale	meters - drill core logging	meters - drill core logging	surface boreholes; 15-20 km2 scale	surface boreholes, geological mapping; 20-25 km2 scale

Table 2 – Methods and scales of measurement (continued)

GEOLOGICAL PARAMETERS - METHODS	JPN - Koetoi	JPN - Wakkanai	BEL - Ypresian	BEL - Boom	FRA - Callovo-Oxfordian	FRA - Domerian-Toarcian	CH - Opalinus_ MTerri	CH - Opalinus_NE	CAN - Georgian Bay	CAN - Queenston	HUN - Boda-Gorica Block	HUN - Boda-Boda Block
Burial Depth Maximum [m]	[ ]	[ ]	Thickness data - sedimentary cover; Doel location	[ ]; Nuclear zone of Mol-Dessel (reference research site)	Inferred from thermal modelling (organic matter maturity, apatite fission track) and thermal indicators (fluid inclusions, clay mineralogy); 545 m (depth of top of COX in EST433) + 300 m ± 200 m of overburden	Regional study; km scale	Stratigraphy, vitrinite reflectance & basin modelling, one-dimensional consolidation; cm to basin scale	Stratigraphy, vitrinite reflectance, organic geochemistry, apatite fission track analyses, fluid inclusions & basin modelling, one-dimensional consolidation; cm to basin scale	Estimated from regional studies and burial history curve for S. Ontario; meters to tens of meters scale	Estimated from regional studies and burial history curve for S. Ontario; meters to tens of meters scale	Stratigraphical analyses, mineralogy-lithology; formation scale	Stratigraphical analyses, mineralogy-lithology; formation scale
Over-consolidation ratio	[ ]	[ ]	Oedometer test, n≤5; Kallo location, observed range	[ ]	[ ]	[ ]	Basin modelling & one-dimensional consolidation; dm to m scale	Basin modelling & one-dimensional consolidation; dm scale	[ ]	[ ]	[ ]	Recent primary stress state: overcoring; formation scale
Maximum temperature reached during diagenesis [°C]	[ ]	[ ]	[ ]	[ ]	Thermal modelling (organic matter maturity, apatite fission track) and thermal indicators (fluid inclusions, clay mineralogy)	[ ]	Stratigraphy, vitrinite reflectance & basin modelling; cm to basin scale	Stratigraphy, vitrinite reflectance, organic geochemistry, apatite fission track analyses, fluid inclusions & basin modelling; cm to basin scale	Based on regional observations (CAI, peak burial depth, hydrocarbon characterization - maturity)	Based on regional observations (CAI, peak burial depth, hydrocarbon characterization - maturity)	Stratigraphical analyses; formation scale	Vitrinite-reflection, illite crystallinity index; formation scale

Table 2 – Methods and scales of measurement (continued)

MINERALOGICAL PARAMETERS - METHODS	JPN - Koetoi	JPN - Wakkanai	BEL - Ypresian	BEL - Boom	FRA - Callovo-Oxfordian	FRA - Domerian-Toarcian	CH - Opalinus_ MTerri	CH - Opalinus_NE	CAN - Georgian Bay	CAN - Queenston	HUN - Boda-Gorica Block	HUN - Boda-Boda Block
Clay minerals - sum of all [% total dry weight]	Normative calculation; best estimate = median value; cm scale	Normative calculation; best estimate = median value; cm scale	XRD bulk; Kallo location; observed range; n≤15; cm^3 scale	XRD	XRD and bulk chemical analysis; Measurement and analytical uncertainties (semi-quantitative estimate)= ± 5 %; Best estimate = mean; cm scale	XRD; rock samples from borehole	XRD + IR spectroscopy; Min/Max values represent values of mean ± 1 sigma standard deviation; cm to dm scale	XRD + IR spectroscopy; Min/Max values represent values of mean ± 1 sigma standard deviation; cm to dm scale	XRD; core samples from DGR boreholes; cm to tens of cm scale	XRD; core samples from DGR boreholes; cm to tens of cm scale	XRD, thermal analysis; n=50; formation scale	XRD, thermal analysis; n=200; Best estimate = median; formation scale
Clay Minerals-Illite [% total dry weight]	Normative calculation; best estimate = median value; cm scale	Normative calculation; best estimate = median value; cm scale	XRD bulk & CEC +XRD <2µm; Kallo location; observed range; n≤15; cm^3 scale	XRD	XRD and bulk chemical analysis; Measurement and analytical uncertainties (semi-quantitative estimate)= ± 5 %; Best estimate = mean; cm scale	[ ]	XRD + IR spectroscopy; Min/Max values represent values of mean ± 1 sigma standard deviation; cm to dm scale	XRD + IR spectroscopy; Min/Max values represent values of mean ± 1 sigma standard deviation; cm to dm scale	XRD; core samples from DGR boreholes; cm to tens of cm scale	XRD; core samples from DGR boreholes; cm to tens of cm scale	XRD, thermal analysis, TEM; n=50; formation scale	XRD, thermal analysis, TEM; n=200; Best estimate = median; formation scale
Clay Minerals-Smectite [% total dry weight]	Normative calculation; best estimate = median value; cm scale	Normative calculation; best estimate = median value; cm scale	XRD bulk & CEC +XRD <2µm; Kallo location; observed range; n≤16; cm^3 scale	XRD	[ ]	[ ]	XRD + IR spectroscopy; Min/Max values represent values of mean ± 1 sigma standard deviation; cm to dm scale	XRD + IR spectroscopy; Min/Max values represent values of mean ± 1 sigma standard deviation; cm to dm scale	XRD; core samples from DGR boreholes; calculated from % clay fraction in the rock; cm to tens of cm scale	XRD; core samples from DGR boreholes; calculated from % clay fraction in the rock; cm to tens of cm scale	XRD, thermal analysis; n=50; formation scale	XRD, thermal analysis; n=200; Best estimate = median; formation scale
Clay Minerals-Chlorite [% total dry weight]	Normative calculation; best estimate = median value; cm scale	Normative calculation; best estimate = median value; cm scale	XRD bulk & CEC; Kallo location; observed range; n≤15	XRD	XRD and bulk chemical analysis; Measurement and analytical uncertainties (semi-quantitative estimate)= ± 5 %; Best estimate = mean; cm scale	XRD; rock samples from borehole	XRD + IR spectroscopy; Min/Max values represent values of mean ± 1 sigma standard deviation; cm to dm scale	XRD + IR spectroscopy; Min/Max values represent values of mean ± 1 sigma standard deviation; cm to dm scale	XRD; core samples from DGR boreholes; cm to tens of cm scale	XRD; core samples from DGR boreholes; cm to tens of cm scale	XRD, thermal analysis, TEM; n=50; formation scale	XRD, thermal analysis, TEM; n=200; Best estimate = median; formation scale

Table 2 – Methods and scales of measurement (continued)

MINERALOGICAL PARAMETERS - METHODS	JPN - Koetoi	JPN - Wakkanai	BEL - Ypresian	BEL - Boom	FRA - Callovo-Oxfordian	FRA - Domerian-Toarcian	CH - Opalinus_ MTerri	CH - Opalinus_NE	CAN - Georgian Bay	CAN - Queenston	HUN - Boda-Gorica Block	HUN - Boda-Boda Block
Clay Minerals-Kaolinite [% total dry weight]	Normative calculation; best estimate = median value; cm scale	Normative calculation; best estimate = median value; cm scale	XRD bulk & CEC; Kallo location; observed range; n≤15	XRD	XRD and bulk chemical analysis; cm scale	XRD; rock samples from borehole	XRD + IR spectroscopy; Min/Max values represent values of mean ± 1 sigma standard deviation; cm to dm scale	XRD + IR spectroscopy; Min/Max values represent values of mean ± 1 sigma standard deviation; cm to dm scale	XRD; core samples from DGR boreholes; cm to tens of cm scale	XRD; core samples from DGR boreholes; cm to tens of cm scale	XRD, thermal analysis; n=50; formation scale	XRD, thermal analysis; n=200; Best estimate = median; formation scale
Clay Minerals-Illite/Smectite [% total dry weight]	Normative calculation; best estimate = median value; cm scale	Normative calculation; best estimate = median value; cm scale	XRD bulk & CEC +XRD <2µm; Kallo location; observed range; n≤15	XRD	XRD and bulk chemical analysis; cm scale	XRD; rock samples from borehole	XRD + IR spectroscopy; Min/Max values represent values of mean ± 1 sigma standard deviation; cm to dm scale	XRD + IR spectroscopy; Min/Max values represent values of mean ± 1 sigma standard deviation; cm to dm scale	XRD; core samples from DGR boreholes; cm to tens of cm scale	XRD; core samples from DGR boreholes; cm to tens of cm scale	thermal analysis; n=50; formation scale	XRD, thermal analysis; n=200; Best estimate = median; formation scale
Quartz [% total dry weight]	Normative calculation; best estimate = median value; cm scale	Normative calculation; best estimate = median value; cm scale	XRD bulk; Kallo location; observed range; n≤15; cm^3 scale	XRD	XRD and bulk chemical analysis; Measurement and analytical uncertainties (semi-quantitative estimate)= ± 5 %; Best estimate = mean; cm scale	XRD; rock samples from borehole	XRD + IR spectroscopy; Min/Max values represent values of mean ± 1 sigma standard deviation; cm to dm scale	XRD + IR spectroscopy; Min/Max values represent values of mean ± 1 sigma standard deviation; cm to dm scale	XRD; core samples from DGR boreholes; cm to tens of cm scale	XRD; core samples from DGR boreholes; cm to tens of cm scale	XRD; n=50; formation scale	XRD; n=200; Best estimate = median; formation scale
Feldspars [% total dry weight]	Normative calculation; best estimate = median value; cm scale	Normative calculation; best estimate = median value; cm scale	XRD bulk; Kallo location; observed range; n≤15; cm^3 scale	XRD	XRD and bulk chemical analysis; cm scale	[ ]	XRD + IR spectroscopy; Min/Max values represent values of mean ± 1 sigma standard deviation; cm to dm scale	XRD + IR spectroscopy; Min/Max values represent values of mean ± 1 sigma standard deviation; cm to dm scale	XRD - semi-quantitative analysis; core samples from DGR boreholes; cm to tens of cm scale	XRD - semi-quantitative analysis; core samples from DGR boreholes; cm to tens of cm scale	XRD; n=50; formation scale	XRD; n=200; Best estimate = median; formation scale
Carbonates [% total dry weight]	Normative calculation; best estimate = median value; cm scale	Normative calculation; best estimate = median value; cm scale	XRD bulk, calcimetry; Kallo & Doel locations; observed range; n≤65	XRD	XRD and bulk chemical analysis; Measurement and analytical uncertainties (semi-quantitative estimate)= ± 5 %; Best estimate = mean; cm scale	XRD; rock samples from borehole	XRD + IR spectroscopy; Min/Max values represent values of mean ± 1 sigma standard deviation; cm to dm scale	XRD + IR spectroscopy; Min/Max values represent values of mean ± 1 sigma standard deviation; cm to dm scale	XRD; core samples from DGR boreholes; cm to tens of cm scale	XRD; core samples from DGR boreholes; cm to tens of cm scale	XRD, thermal analysis; n=50; formation scale	XRD, thermal analysis; n=200; Best estimate = median; formation scale

Table 2 – Methods and scales of measurement (continued)

MINERALOGICAL PARAMETERS - METHODS	JPN - Koetoi	JPN - Wakkanai	BEL - Ypresian	BEL - Boom	FRA - Callovo-Oxfordian	FRA - Domerian-Toarcian	CH - Opalinus_ MTerri	CH - Opalinus_NE	CAN - Georgian Bay	CAN - Queenston	HUN - Boda-Gorica Block	HUN - Boda-Boda Block
Calcite [% total dry weight]	[ ]	[ ]	XRD bulk; Kallo location; observed range; n≤15; cm^3 scale	XRD	XRD and bulk chemical analysis; cm scale	XRD; rock samples from borehole	XRD + IR spectroscopy; Min/Max values represent values of mean ± 1 sigma standard deviation; cm to dm scale	XRD + IR spectroscopy; Min/Max values represent values of mean ± 1 sigma standard deviation; cm to dm scale	XRD; core samples from DGR boreholes; cm to tens of cm scale	XRD; core samples from DGR boreholes; cm to tens of cm scale	XRD, thermal analysis; n=50; formation scale	XRD, thermal analysis; n=200; Best estimate = median; formation scale
Dolomite/ ankerite [% total dry weight]	[ ]	[ ]	XRD bulk; Kallo location; observed range; n≤15; cm^3 scale	XRD	XRD and bulk chemical analysis; cm scale	XRD; rock samples from borehole	XRD + IR spectroscopy; Min/Max values represent values of mean ± 1 sigma standard deviation; cm to dm scale	XRD + IR spectroscopy; Min/Max values represent values of mean ± 1 sigma standard deviation; cm to dm scale	XRD - semi-quantitative analysis; core samples from DGR boreholes; cm to tens of cm scale	XRD - semi-quantitative analysis; core samples from DGR boreholes; cm to tens of cm scale	XRD, thermal analysis; n=50; formation scale	XRD, thermal analysis; n=200; Best estimate = median; formation scale
Pyrite [% total dry weight]	Normative calculation; best estimate = median value; cm scale	Normative calculation; best estimate = median value; cm scale	XRD bulk; Kallo location; observed range; n≤15; cm^3 scale	XRD	XRD and bulk chemical analysis; cm scale	XRD; rock samples from borehole	XRD + IR spectroscopy; Min/Max values represent values of mean ± 1 sigma standard deviation; cm to dm scale	XRD + IR spectroscopy; Min/Max values represent values of mean ± 1 sigma standard deviation; cm to dm scale	XRD - semi-quantitative analysis; core samples from DGR boreholes; cm to tens of cm scale	XRD - semi-quantitative analysis; core samples from DGR boreholes; cm to tens of cm scale	XRD, thermal analysis; n=50; formation scale	XRD, thermal analysis; n=200; Best estimate = median; formation scale
Carbon Organic [%]	CHNS, cm scale, best estimate: median value	CHNS, cm scale, best estimate: median value	Walkley-Black Method; Doel location; observed range; n≤50	IR	TOC; best estimate = mean	Rock-Eval Pyrolysis; rock samples from borehole	XRD + IR spectroscopy; Min/Max values represent values of mean ± 1 sigma standard deviation; cm to dm scale	XRD + IR spectroscopy; Min/Max values represent values of mean ± 1 sigma standard deviation; cm to dm scale	[ ]	[ ]	TOC; n=50; formation scale	TOC; n=200; best estimate = median; formation scale

Table 2 – Methods and scales of measurement (continued)

PORE WATER CHEMISTRY PARAMETERS - METHODS	JPN - Koetoi	JPN - Wakkanai	BEL - Ypresian	BEL - Boom	FRA - Callovo-Oxfordian	FRA - Domerian-Toarcian	CH – Opalinus MTerri	CH - Opalinus_NE	CAN - Georgian Bay	CAN - Queenston	HUN - Boda-Gorica Block	HUN - Boda-Boda Block
Pore Water Type	[ ]	[ ]	Squeezing (<10 MPa); n≤15; Doel location; cm^3 samples	Piezometer samples; cm^3 scale	[ ]	Leaching - cationic exchange, leaching-squeezing and modelling; rock samples from boreholes and fractures (meter scale)	[ ]	Squeezing; cm-dm scale	[ ]	[ ]	[ ]	[ ]
TDS - salinity [mg/L]	[ ]	[ ]	Squeezing (<10 MPa); n≤15	cm^3 scale	[ ]	Leaching - cationic exchange, leaching-squeezing and modelling; rock samples (cm scale)	Core squeezing; Samples BWS-E4 4.28–4.65 (min) and BWS-A6 4.1–4.3 (max); dm scale	Aqueous extraction, squeezing, modelling; reference water; cm-dm scale	[ ]	[ ]	Gravimetric; rock samples from URL & surface outcrops	Gravimetric; rock samples from URL & surface outcrops, surface boreholes
Eh [mV]	[ ]	[ ]	[ ]	Pt electrode and Ag/AgCl electrode; cm^3 samples	[ ]	[ ]	Geochemical modelling of reference waters (A1 and A3); assuming equilibrium between pyrite and SO4(2-); meter scale	Calculated on the assumption of equilibrium between pyrite and SO4(2-)	Estimate only; calculated using PHREEQC	Estimate only; calculated using PHREEQC	In-situ; water samples	In-situ; water samples; URL & surface borehole water sample
pH	pH electrode; meters to tens of meters	pH electrode; meters to tens of meters	[ ]	[ ]	Online; PAC1002 experiment for best estimate; min/max from Analytical results on samples EST02361,02363,02364,02382,02618; URL scale	[ ]	Core squeezing; Samples BWS-E4 4.28–4.65 (min) and BWS-A6 4.1–4.3 (max); dm scale	Aqueous extraction, squeezing, modelling; reference water; cm-dm scale	Calculated in PHREEQC from CO_2 and major ion concentrations in DGR2 only; not measured	Calculated in PHREEQC from CO_2 and major ion concentrations in DGR2 only; not measured	[ ]	In-situ; water samples

Table 2 – Methods and scales of measurement (continued)

PORE WATER CHEMISTRY PARAMETERS - METHODS	JPN - Koetoi	JPN - Wakkanai	BEL - Ypresian	BEL - Boom	FRA - Callovo-Oxfordian	FRA - Domerian-Toarcian	CH – Opalinus MTerri	CH - Opalinus_NE	CAN - Georgian Bay	CAN - Queenston	HUN - Boda-Gorica Block	HUN - Boda-Boda Block
$\delta^{18}O$ [‰ vs SMOW]	Mass spectrometry; meters to tens of meters	Mass spectrometry; meters to tens of meters	[ ]	[ ]	Rock core samples	Vapour exchange, radial diffusion, distillations under vacuum; rock samples (cm scale)	Vacuum distillation, squeezing, diffusive exchange, in-situ borehole sampling; cm-dm scale	Benken: vacuum distillation and diffusive exchange; Schlattingen: squeezing and diffusive exchange; cm-dm scale	Vacuum distillation at 150°C for 6 hours; high-temperature vacuum distillation: ICP-MS; VSMOW; core samples from DGR boreholes; min/max represent lowest/highest values measured; best estimate = central tendency; cm to tens of cm scale	Vacuum distillation at 150°C for 6 hours; high-temperature vacuum distillation: ICP-MS; VSMOW; core samples from DGR boreholes; min/max represent lowest/highest values measured; best estimate = central tendency; cm to tens of cm scale	Water sample	Mass spectrometry; groundwater sample
$\delta^{2}H$ [‰ vs SMOW]	Mass spectrometry; meters to tens of meters	Mass spectrometry; meters to tens of meters	[ ]	[ ]	Rock core samples	Vapour exchange, radial diffusion, distillations under vacuum; rock samples (cm scale)	Vacuum distillation, squeezing, diffusive exchange, in-situ borehole sampling; cm-dm scale	Benken: vacuum distillation and diffusive exchange; Schlattingen: squeezing and diffusive exchange; cm-dm scale	Vacuum distillation at 150°C for 6 hours; high-temperature vacuum distillation: ICP-MS; VSMOW; core samples from DGR boreholes; min/max represent lowest/highest values measured; best estimate = central tendency; cm to tens of cm scale	Vacuum distillation at 150°C for 6 hours; high-temperature vacuum distillation: ICP-MS; VSMOW; core samples from DGR boreholes; min/max represent lowest/highest values measured; best estimate = central tendency; cm to tens of cm scale	Water sample	Mass spectrometry; water sample
Cations: Ca, Mg, K, Na [mg/L]	IC; meters to tens of meters	IC; meters to tens of meters	Squeezing (<10 MPa), AAS; n≤15; Doel location; non-oxidised samples; observed range	[ ]	Seepage waters from boreholes; Best estimate value is the minimum because disturbing effects, like evaporation, while drilling induced less representative larger values; PAC1002 experiment, URL scale	Leaching - cationic exchange, leaching-squeezing and modelling; rock samples (cm scale)	Core squeezing; Samples BWS-E4 4.28–4.65 (min) and BWS-A6 4.1–4.3 (max); dm scale	Aqueous extraction, squeezing, modelling; reference water; cm-dm scale	Crush and leach; porewater concentrations normalized to extracted porewater volume, and corrected, assuming $CaCO_3$ and gypsum equilibration, using PHREEQC; units mg/L_{H2O}; min/max represent lowest/highest values measured; best estimate = central tendency; cm to tens of cm scale	Crush and leach; porewater concentrations normalized to extracted porewater volume, and corrected, assuming $CaCO_3$ and gypsum equilibration, using PHREEQC; units mg/L_{H2O}; min/max represent lowest/highest values measured; best estimate = central tendency; cm to tens of cm scale	Ca, Mg: complexometry ; SO4, HCO3: flame photometry ICP-OES; water samples	Ca, Mg: complexometry ; SO4, HCO3: flame photometry ICP-OES; water samples

Table 2 – Methods and scales of measurement (continued)

PORE WATER CHEMISTRY PARAMETERS - METHODS	JPN - Koetoi	JPN - Wakkanai	BEL - Ypresian	BEL - Boom	FRA - Callovo-Oxfordian	FRA - Domerian-Toarcian	CH – Opalinus MTerri	CH - Opalinus_NE	CAN - Georgian Bay	CAN - Queenston	HUN - Boda-Gorica Block	HUN - Boda-Boda Block
Cations: Ca, Mg, K, Na [mg/L]	IC; meters to tens of meters	IC; meters to tens of meters	Squeezing (<10 MPa), AAS; n≤15; Doel location; non-oxidised samples; observed range	[ ]	Seepage waters from boreholes; Best estimate value is the minimum because disturbing effects, like evaporation, while drilling induced less representative larger values; PAC1002 experiment, URL scale	Leaching - cationic exchange, leaching-squeezing and modelling; rock samples (cm scale)	Core squeezing; Samples BWS-E4 4.28–4.65 (min) and BWS-A6 4.1–4.3 (max); dm scale	Aqueous extraction, squeezing, modelling; reference water; cm-dm scale	Crush and leach; porewater concentrations normalized to extracted porewater volume, and corrected, assuming $CaCO_3$ and gypsum equilibration, using PHREEQC; units mg/L_{H2O}; min/max represent lowest/highest values measured; best estimate = central tendency; cm to tens of cm scale	Crush and leach; porewater concentrations normalized to extracted porewater volume, and corrected, assuming $CaCO_3$ and gypsum equilibration, using PHREEQC; units mg/L_{H2O}; min/max represent lowest/highest values measured; best estimate = central tendency; cm to tens of cm scale	Ca, Mg: complexometry; SO4, HCO3: flame photometry ICP-OES; water samples	Ca, Mg: complexometry; SO4, HCO3: flame photometry ICP-OES; water samples
Anions: Cl, SO4, HCO3, Br [mg/L]	Cl and Br - IC; SO4 - absorption spectrophotometry; HCO3 - calculated from alkalinity; all data shown in this table is obtained from groundwater taken by pumping or batch sampler, NOT squeezing of pore water; meters to tens of meters scale	Cl and Br - IC; SO4 - absorption spectrophotometry; HCO3 - calculated from alkalinity; all data shown in this table is obtained from groundwater taken by pumping or batch sampler, NOT squeezing of pore water. "Best estimate" data is obtained using surface based borehole (SAB-1 borehole) at GL -350m depth in research drift of Horonobe URL; meters to tens of meters scale	Squeezing (<10MPa) Cl: chloridometer, n≤15; Br: selective electrode n≤2; SO4: turbidimetry, n≤15	[ ]	Seepage waters from boreholes; Best estimate value is the minimum because disturbing effects, like evaporation, while drilling induced less representative larger values (except for HCO3, where BE = maximum); PAC1002 experiment; URL scale	Cl, SO4: leaching - cationic exchange, leaching-squeezing and modelling; rock samples (cm scale); Br: no data; HCO3: cm scale	Cl, Br, SO4: core squeezing, dm scale, Samples BWS-E4 4.28–4.65 (min) and BWS-A6 4.1–4.3 (max); HCO3: in-situ sampling, meter scale	Cl, SO4, HCO3: aqueous extraction, squeezing, modelling; Br: squeezing; Cl: Best estimate = reference water; min/max: based on aqueous extraction of Benken & Schlattingen cores and an assumed anion-accessible porosity fraction of 0.5; SO4 and HCO3 - reference water; cm-dm scale	Crush and leach; porewater concentrations normalized to extracted porewater volume, and corrected, assuming $CaCO_3$ and gypsum equilibration, using PHREEQC; units mg/L_{H2O}; Cl and Br - IC; min/max represent lowest/highest values measured; best estimate = central tendency; cm to tens of cm scale	Crush and leach; porewater concentrations normalized to extracted porewater volume, and corrected, assuming $CaCO_3$ and gypsum equilibration, using PHREEQC; units mg/L_{H2O}; Cl and Br - IC; min/max represent lowest/highest values measured; best estimate = central tendency; cm to tens of cm scale	Cl, HCO3: titrimetry; SO4: gravimetric; Br: NA; water samples	Cl, HCO3: titrimetry; SO4: gravimetric; Br: NA; water samples

Table 2 – Methods and scales of measurement (continued)

PETROPHYSICAL PARAMETERS - METHODS	JPN - Koetoi	JPN - Wakkanai	BEL - Ypresian	BEL - Boom	FRA - Callovo-Oxfordian	FRA - Domerian-Toarcian	CH - Opalinus_ MTerri	CH - Opalinus_NE	CAN - Georgian Bay	CAN - Queenston	HUN - Boda-Gorica Block	HUN - Boda-Boda Block
CEC [meq/100g of rock]	[ ]	[ ]	NH4OAc/Co-hexamine/CsNO4/Cu-Trien/Cu-Trien; Doel and Kallo locations; observed range; n≤50; cm^3 samples	Ag-thiourea, Sr-85 & Ca-45 labelled, Co-hexamine, Cu-trien; Best estimate = average	Cobalt hexamine - total fraction; Best estimate = mean; cm scale	[ ]	Ni-en, Co-hex, Acetate; CEC approximated by consumption of index cation (and not by the sum of desorbed cations); cm scale	Ni-en method, CEC approximated by Ni consumption; cm scale	[ ]	[ ]	Ammonium acetate; Cs isotope dilution	Cs isotope dilution; crushed rock samples
Specific Surface External [m^2/g]	[ ]	[ ]	[ ]	4 samples around HADES	Measured by N2-adsorbsion (BET method); Best estimate = mean; mm scale	N2-adsorbsion (BET method); rock samples from boreholes - cm scale	[ ]	Measured by N2-adsorbsion (BET method); cm scale	BET; core samples from DGR boreholes; cm to tens of cm scale	BET; core samples from DGR boreholes; cm to tens of cm scale	Physisorption; measured systematically on 46 samples of Ib-4 borehole (598.12-608.58 m)	Physisorption; rock fragments - small plugs; measured systematically on 13 samples of BAF-2 borehole
Specific Surface Total [m^2/g]	[ ]	[ ]	BET-Method, 1g samples; Doel location; observed range; n≤25	Water absorption; EGME - 4 samples around HADES	Using H2O isotherms; n=4	[ ]	[ ]	Benken: EGME and H2O adsorption; cm scale. Schlattingen: Keeling's hygroscopic method; cm scale	[ ]	[ ]	Physisorption; measured by CO_2 on 33 samples systematically on 71 samples of Ib-4 borehole (598.12-608.58 m) and interpreted on the basis of Dubinin-Radushkevich theory	Physisorption; rock fragments - small plugs; measured by CO_2 on 14 samples of BAF-2 borehole (and interpreted on the basis of Dubinin-Radushkevich theory
Density Bulk Saturated [kg/m3]	Size of specimen: f50 x H100 [mm]	Size of specimen: f35 x H70 [mm]	Volume and weight at saturated conditions; Doel and Kallo locations; observed range; n≤50; cm^3 samples	[ ]	Water content 150°C + Grain density; Best estimate = mean; mm-cm scale	Weight loss at 105°C / conventional method; rock samples from boreholes (cm scale / tenth of sample)	Min/Max values represent values of mean ± 1 sigma standard deviation; cm scale	Paraffin displacement; cm scale	Paraffin displacement; 75 mm diameter core samples from DGR boreholes; Best estimate = mean; cm to tens of cm scale	Paraffin displacement; 75 mm diameter core samples from DGR boreholes; best estimate = mean; cm to tens of cm scale	[ ]	[ ]

Table 2 – Methods and scales of measurement (continued)

PETROPHYSICAL PARAMETERS - METHODS	JPN - Koetoi	JPN - Wakkanai	BEL - Ypresian	BEL - Boom	FRA - Callovo-Oxfordian	FRA - Domerian-Toarcian	CH - Opalinus_ MTerri	CH - Opalinus_NE	CAN - Georgian Bay	CAN - Queenston	HUN - Boda-Gorica Block	HUN - Boda-Boda Block
Density Bulk Dry [kg/m3]	Size of specimen: f50 x H100 [mm]	Size of specimen: f35 x H70 [mm]	Based on density bulk saturated and water content; Doel and Kallo locations; observed range; n≤50; cm^3 samples	Directly measured UNE Standard 7045	Water content 150°C + Grain density; Best estimate = mean; mm-cm scale	Weight loss at 105°C / conventional method; rock samples from boreholes (cm scale / tenth of sample)	Min/Max values represent values of mean ± 1 sigma standard deviation; cm scale	Paraffin displacement; refers to directly measured densities. Values calculated from measured bulk wet density and water content are lower; cm scale	Paraffin displacement; 75 mm diameter core samples from DGR boreholes; paraffin displacement method - "dry or wet"; best estimate = mean; cm to tens of cm scale	Paraffin displacement; 75 mm diameter core samples from DGR boreholes; based on borehole data from Bruce site; best estimate = mean. Paraffin displacement method - samples analysed "dry or wet"; cm to tens of cm scale	Volume and weight measurements - rock samples; He pycnometry - measured systematically on 48 plug with 1" and 1.5" diameter samples of Ib-4 borehole (598.12-608.58 m), rock samples (plugs)	He-pycnometry; 21 samples; rock fragments/plugs
Density Grain Average [kg/m3]	Size of specimen: f50 x H100 [mm]	Size of specimen: f35 x H70 [mm]	Pyncnometry (different fluids); Doel and Kallo locations; observed range; n≤50; cm^3 samples	[ ]	Helium pycnometry; Best estimate = mean; mm-cm scale	Estimated from literature	Min/Max values represent values of mean ± 1 sigma standard deviation; cm scale	He pycnometry (Benken), kerosene pycnometry (Schlattingen); cm scale	Kerosene-pycnometry; 75 mm diameter core samples from DGR boreholes; cm to tens of cm scale	Kerosene-pycnometry; cm to tens of cm scale	He-pycnometry; measured systematically on 126 samples of Ib-4 borehole (598,12-608,58 m); rock samples (plugs and fragments)	He-pycnometry; 3 samples from URL and 21 samples from borehole; rock fragments/plugs
Water Content (water weight / dry weight) [%]	Size of specimen: f50 x H100 [mm]	Size of specimen: f35 x H70 [mm]	Wet, dry weighting; Doel and Kallo locations; observed range; n≤50; cm^3 samples	[ ]	Water Content as water weight loss (150°C/24h) / dry solid weight; Best estimate = mean; cm scale	Weight loss at 105°C / conventional method; rock samples from boreholes (cm scale / tenth of sample)	Water Content as water weight loss (105°C/24h) / dry solid weight; Drying at 105–110 °C; cm-dm samples	Water Content as water weight loss (105°C/24h) / dry solid weight; drying at 105 °C; cm-dm scale	Water Content as water weight loss (150°C) / dry solid weight; cm-dm scale	Water Content as water weight loss (150°C) / dry solid weight; cm-dm scale	Saturation under a given pressure; measured on plugs saturated under pressure; rock samples (plugs)	Calculated from weight loss; 10-30 days required to reach dry state; rock fragments/plugs
Porosity calculated from Water content at 105-110 C° [%vol]	Size of specimen: f50 x H100 [mm]	[ ]	[ ]	[ ]	Water content 105°C + Grain density; Best estimate = mean; cm scale	Weight loss at 105°C / conventional method; rock samples from boreholes (cm scale / tenth of sample)	Drying at 105–110 °C	Drying at 105 °C; cm-dm scale	Water-loss porosity by drying at 105°C; sub-samples of 76 mm diameter cores from boreholes; cm scale	Water-loss porosity by drying at 105°C; sub-samples of 76 mm diameter cores from boreholes; cm scale	He-pycnometry; rock samples (plugs); measured systematically on 48 plug with 1" and 1.5" diameter samples of Ib-4 borehole (598.12-608.58m)	He-pycnometry; 3 samples from URL and 21 samples from borehole; rock fragments/plugs

Table 2 – Methods and scales of measurement (continued)

PETROPHYSICAL PARAMETERS - METHODS	JPN - Koetoi	JPN - Wakkanai	BEL - Ypresian	BEL - Boom	FRA - Callovo-Oxfordian	FRA - Domerian-Toarcian	CH - Opalinus_ MTerri	CH - Opalinus_NE	CAN - Georgian Bay	CAN - Queenston	HUN - Boda-Gorica Block	HUN - Boda-Boda Block
Porosity - other methods [%vol]	Hg intrusion technique	Hg intrusion technique; Size of specimen: f35 x H70 [mm]	Wet volume and weight, dry weight; Doel and Kallo locations; observed range; n≤50; cm^3 samples	[ ]	NMR; borehole logging; the total porosity is based on log measurements acquired at high-resolution (every 10 cm) to achieve fine-scale variability on the complete geological formation; Uncertainties on diagraphic measurement NMR (TCMR tool): 1 %; Best estimate = mean	Hg injection porosimetry & BET isotherms; rock samples from boreholes (cm scale / tenth of sample)	Pycnometer porosity (sometimes called physical porosity); calculated from bulk wet and grain densities; cm scale	Pycnometer porosity (sometimes called physical porosity); calculated from bulk wet and grain densities; cm scale	Dean Stark fluid saturation method; DGR-5/6 data: boyle's law gas (He) expansion method; nuclear magnetic resonance; 75 mm diameter core samples from DGR boreholes; based on borehole data from Bruce site; water loss porosity values; cm to tens of cm scale	Dean Stark fluid saturation method; DGR-5/6 data: boyle's law gas (He) expansion method; nuclear magnetic resonance; based on borehole data from Bruce site; water-loss porosity values, Best estimate = mean; cm to tens of cm scale	[ ]	Calculated on the basis weight loss, during drying, geometry and estimated free pore water density and modified by He-pycnometry - measured on wet samples; rock plugs
Effective Porosity [% vol]	Hg intrusion technique	Hg intrusion technique; Size of specimen: f35 x H70 [mm]	[ ]	[ ]	NMR; borehole logging; the total porosity is based on log measurements acquired at high-resolution (every 10 cm) to achieve fine-scale variability on the complete geological formation; Uncertainties on diagraphic measurement NMR (TCMR tool): 1 %; Best estimate = mean	Hg injection porosimetry & BET isotherms; rock samples from boreholes (cm scale / tenth of sample)	Pycnometer porosity (sometimes called physical porosity); calculated from bulk wet and grain densities; cm scale	Pycnometer porosity (sometimes called physical porosity); calculated from bulk wet and grain densities; cm scale	Gravimetric; Dean Stark fluid saturation method; DGR-5/6 data: boyle's law gas (He) expansion method; nuclear magnetic resonance; 75 mm dia. core samples from DGR boreholes; based on borehole data from Bruce site; water loss porosity values; cm to tens of cm scale	Gravimetric; Dean Stark fluid saturation method; DGR-5/6 data: boyle's law gas (He) expansion method; nuclear magnetic resonance; based on borehole data from Bruce site; water loss porosity values, Best estimate value = mean value; cm to tens of cm scale	[ ]	[ ]
Porosity Other Methods [%vol]	[ ]	[ ]	HTO pressure-pulse test; Doel location; observed range; n≤50; cm^3 samples	[ ]	[ ]	[ ]	[ ]	[ ]	[ ]	[ ]	[ ]	Mercury injection; rock samples
Anion-accessible porosity	[ ]	[ ]	Pressure-pulse test, iodide; Doel location; observed range; n≤25; cm^3 scale	[ ]	Through-diffusion for Cl; Best estimate = mean; mm-cm samples	Through-diffusion cell, axial confining pressure: 1.9 Mpa; rock samples from boreholes (D:35 mm / e:10 mm)	Through-diffusion (lab); n=5; cm scale	Through-diffusion, cm scale; 6 measurements. Data are biased because they all refer to a small, very clay-rich core section in Benken -> not representative	Through-diffusion and x-ray radiography; cm to tens of cm scale	Through-diffusion and x-ray radiography; cm to tens of cm scale	Through-diffusion test; rock samples	[ ]

Table 2 – Methods and scales of measurement (continued)

PETROPHYSICAL PARAMETERS - METHODS	JPN - Koetoi	JPN - Wakkanai	BEL - Ypresian	BEL - Boom	FRA - Callovo-Oxfordian	FRA - Domerian-Toarcian	CH - Opalinus_ MTerri	CH - Opalinus_NE	CAN - Georgian Bay	CAN - Queenston	HUN - Boda-Gorica Block	HUN - Boda-Boda Block
Seismic Velocity Vp (⊥) lab. tests [m/s]	Size of specimen: f50 x H100 [mm]	Size of specimen: f35 x H70 [mm]	[ ]	[ ]	[ ]	Ultrasonic velocity laboratory tests; rock samples from boreholes (cm scale / tenth of sample)	Benchtop measurement of P-wave velocity ⊥ to fabric, at an excitation frequency of typically 1MHz and unconstrained (no external stress applied); cm-dm scale	Benchtop measurement of P-wave velocity ⊥ to fabric, at an excitation frequency of 1MHz and unconstrained (no external stress applied); Best estimate is average of 68 test results, Min/Max values are average ±1 Standard deviation. All results are from Benken; cm-dm scale	UT; 75 mm diameter core samples from DGR boreholes; cm to tens of cm scale	UT; 75 mm diameter core samples from DGR boreholes; cm to tens of cm scale	AVS; measured on 6 saturated samples in lab, perpendicular to bedding; rock plugs	Acoustic velocity measurement in reservoir conditions (confining and pore pressure) at room temperature; acoustic waves; measured on 4 saturated samples; rock plugs
Seismic Velocity Vp (∕) lab. tests [m/s]	Size of specimen: f50 x H100 [mm]	Size of specimen: f35 x H70 [mm]	[ ]	[ ]	[ ]	Ultrasonic velocity laboratory tests; rock samples from boreholes (cm scale / tenth of sample)	Benchtop measurement of P-wave velocity ‖ to fabric, at an excitation frequency of typically 1MHz and unconstrained (no external stress applied); cm-dm scale	Benchtop measurement of P-wave velocity ‖ to fabric, at an excitation frequency of typically 1MHz and unconstrained (no external stress applied); Best estimate is average of 71 test results, Min/Max values are average ±1 Standard deviation; cm-dm scale	[ ]	[ ]	AVS; measured on 3 saturated samples in lab, parallel to bedding; rock plugs	Acoustic velocity measurement in reservoir conditions (confining and pore pressure) at room temperature; acoustic waves; 8 saturated samples; rock plugs
Seismic Velocity Vs (⊥) lab. tests [m/s]	Size of specimen: f50 x H100 [mm]	Size of specimen: f35 x H70 [mm]	[ ]	[ ]	[ ]	Ultrasonic velocity laboratory tests; rock samples from boreholes (cm scale / tenth of sample)	Benchtop measurement of S-wave velocity ⊥ to fabric, at an excitation frequency of typically 1MHz and unconstrained (no external stress applied); cm-dm scale	Benchtop measurement of S-wave velocity ⊥ to fabric, at an excitation frequency of 1MHz and unconstrained (no external stress applied); Best estimate is average of 68 test results, Min/Max values are average ±1 Standard deviation. All results are from Benken.	UT; 75 mm diameter core samples from DGR boreholes; cm to tens of cm scale	UT; 75 mm diameter core samples from DGR boreholes; cm to tens of cm scale	AVS; measured on 6 saturated samples in lab, perpendicular to bedding; rock plugs	Acoustic velocity measurement in reservoir conditions (confining and pore pressure) at room temperature; 4 saturated samples; rock plugs

Table 2 – Methods and scales of measurement (continued)

PETROPHYSICAL PARAMETERS - METHODS	JPN - Koetoi	JPN - Wakkanai	BEL - Ypresian	BEL - Boom	FRA - Callovo-Oxfordian	FRA - Domerian-Toarcian	CH - Opalinus_ MTerri	CH - Opalinus_NE	CAN - Georgian Bay	CAN - Queenston	HUN - Boda-Gorica Block	HUN - Boda-Boda Block
Seismic Velocity Vs (⁄) lab. tests [m/s]	Size of specimen: f50 x H100 [mm]	Size of specimen: f35 x H70 [mm]	[ ]	[ ]	[ ]	Ultrasonic velocity laboratory tests; rock samples from boreholes (cm scale / tenth of sample)	Benchtop measurement of S-wave velocity ∥ to fabric, at an excitation frequency of typically 1MHz and unconstrained (no external stress applied); cm-dm scale	Benchtop measurement of S-wave velocity ∥ to fabric, at an excitation frequency of 1MHz and unconstrained (no external stress applied); Best estimate is average of 71 test results, Min/Max values are average ±1 Standard deviation. All results are from Benken; cm-dm scale	[ ]	[ ]	AVS; measured on 3 saturated samples in lab, parallel to bedding; rock plugs	Acoustic velocity measurement in reservoir conditions (confining and pore pressure) at room temperature; 8 saturated samples; rock plugs
Seismic Velocity Vp in situ tests [m/s]	Data measured in a 158.7 mm dia. borehole	Data measured in a 158.7 mm dia. borehole	[ ]	Wireline logging of (DTCO) compressive slowness in 2 boreholes ON-Mol-1 and ON-Dessel-1; 0.5m intervals; In situ vertical logging; averages and 2σ ranges from the two boreholes and for the layer thickness	[ ]	Interval sonic velocity; horizontal boreholes (tenth of meters scale)	In Situ measurement of P-wave velocity ∥ to fabric, at an excitation frequency of 3-15 kHz; In Situ measurement of P-wave velocity ⊥ to fabric, at an excitation frequency of 3-15 kHz	In Situ measurement of P-wave velocity ⊥ to fabric, at an excitation frequency of 5-15 kHz	Sonic velocity measurement; geophysical logging in a 6" diameter borehole; meter scale	Sonic velocity measurement; geophysical logging in a 6" diameter borehole; meter scale	[ ]	Seismic tomography; in-situ (borehole tunnel)
Seismic Velocity Vs in situ tests [m/s]	Data measured in a 158.7 mm dia. borehole	Data measured in a 158.7 mm dia. borehole	[ ]	Vertical seismic profiles in 2 boreholes ON-Dessel-1 and some additional data from ON-Mol-1; 5m intervals; In situ vertical logging between surface source and borehole receiver; averages and 2σ ranges from the two boreholes (and from VS-horizontal and VS-vertical at ON-Dessel-1) and for the layer thickness	[ ]	Interval sonic velocity; horizontal boreholes (tenth of meters scale)	[ ]	In Situ measurement of S-wave velocity ⊥ to fabric, at an excitation frequency of 5-15 kHz	Sonic velocity measurement; geophysical logging in a 6" diameter borehole; meter scale	Sonic velocity measurement; geophysical logging in a 6" diameter borehole; meter scale	[ ]	Seismic tomography; in-situ (borehole tunnel)

Table 2 – Methods and scales of measurement (continued)

SOLUTE TRANSPORT PARAMETERS - METHODS	JPN - Koetoi	JPN - Wakkanai	BEL - Ypresian	BEL - Boom	FRA - Callovo-Oxfordian	FRA - Domerian-Toarcian	CH - Opalinus_ MTerri	CH - Opalinus_NE	CAN - Georgian Bay	CAN - Queenston	HUN - Boda-Gorica Block	HUN - Boda-Boda Block
Hydraulic Conductivity (⊥) lab. tests [m/s]	Transient pulse test on core; Transient pulse tests were performed in the laboratory tests. The length of the test specimens was less than 10 cm. The confining pressure and the pore water pressure were controlled to simulate overburden and hydrostatic pressures, respectively, according to the depth at which the specimen was sampled. oblique to bedding only 30-60 degrees; cm scale	Transient pulse test on core; Transient pulse tests were performed in the laboratory tests. The length of the test specimens was less than 10 cm. The confining pressure and the pore water pressure were controlled to simulate overburden and hydrostatic pressures, respectively, according to the depth at which the specimen was sampled. oblique to bedding only 30-60 degrees; cm scale	Pressure-pulse test; Doel location; observed range; n≤25; cm^3 samples	permeameter; ON-Mol-1; n=23; cm^3 samples	Pulse test; best estimate = mean; dm-cm scale	pulses tests with fresh water, axial confining pressure: 4 to 8 Mpa; rock samples from boreholes (D:35 mm / e:10 mm)	Permeameter; drill core samples	Permeameter; tests in the range 10 - 12.5 MPa for 5 Schlattingen samples & 12-16 MPa for 2 Benken samples; cm scale	Gas and brine pulse on as received and dried samples; tens of cm scale	Gas and brine pulse on as received and dried samples; derived from permeability results; tens of cm scale	[ ]	[ ]
Hydraulic Conductivity (/) lab. tests [m/s]	[ ]	[ ]	[ ]	permeameter; ON-Mol-1; n=20; cm^3 samples	Pulse test; best estimate = mean; dm-cm scale	[ ]	Permeameter; data from suspected disturbed sample SED-B3 06 excluded; drill core samples	Permeameter; n=2; cm scale	Gas and brine pulse on as received and dried samples; derived from permeability results; tens of cm scale	Gas and brine pulse on as received and dried samples; derived from permeability results; tens of cm scale	[ ]	[ ]
Hydraulic Conductivity in situ tests [m/s]	Packer test; In-situ packer test. A single hydraulic packer test includes a pulse test, a slug test and a pumping test in sequence, followed by a recovery test. The length of test intervals vary from 10 m to 150 m in the investigations; 10-150 m scale	Packer test; In-situ packer test. A single hydraulic packer test includes a pulse test, a slug test and a pumping test in sequence, followed by a recovery test. The length of test intervals vary from 10 m to 150 m in the investigations; 10-150 m scale	[ ]	Piezometer tests - n=72; large-scale hydraulic testing m3 - n=1; dm^3	Pulse test; in boreholes and URL; best estimate = mean	long term pulses tests (1 m packer interval / ~ 24 h)	Packer tests, boreholes drilled from URL; overburden around 280 m; hydrotests outside EDZ; Best estimate = geometric mean; It cannot be excluded that the highest values in the data set are affected by tunnel excavation effects; meters (packer test interval length)	Packer testing in borehole (parallel only), depth >330 m; 10 reliable packer tests in boreholes Benken, Schafisheim, Riniken. Depth-range 330 - 1080 m. Statistics based on best estimates; interval lengths 3-60 m	Borehole straddle packer, 12-30 m intervals; tens of meters scale	Borehole straddle packer, 12-30 m intervals; tens of meters scale	Pumping slug test (Pulse Withdrawal, Constant Rate Withdrawal, Slug Withdrawal); 25 meter intervals	Pumping slug test (Pulse Withdrawal, Constant Rate Withdrawal); borehole test intervals of 25 m and 100 m

Table 2 – Methods and scales of measurement (continued)

SOLUTE TRANSPORT PARAMETERS - METHODS	JPN - Koetoi	JPN - Wakkanai	BEL - Ypresian	BEL - Boom	FRA - Callovo-Oxfordian	FRA - Domerian-Toarcian	CH - Opalinus_ MTerri	CH - Opalinus_NE	CAN - Georgian Bay	CAN - Queenston	HUN - Boda-Gorica Block	HUN - Boda-Boda Block
Diffusion Effective Coeff. De (3H) (⊥) lab. tests [m²/s] :	[ ]	Through-diffusion; test conditions: argon atmospheric condition, no filter was used, synthetic groundwater was used; 20 cm diameter and thickness samples	Pressure-pulse test; Doel location; observed range; n≤25; cm^3 samples	pulse injection & through-diffusion experiment; cm^3	through-diffusion method on samples; best estimate = mean; mm-cm scale	Through-diffusion cell, axial confining pressure: 1.9 Mpa; rock samples from boreholes (D:35 mm / e:10 mm)	Through-diffusion; n=6; cm scale	Through-diffusion; n=10; cm scale	Through-diffusion; no confining pressure; ambient temperature and pressure; values were also determined via through-diffusion under confining pressure of 15 MPa (2.8E-12); cm to tens of cm scale	Through-diffusion; no confining pressure; ambient temperature and pressure; values were also determined under confining pressure of 12.0 Mpa (4.2E-12); cm to tens of cm scale	[ ]	[ ]
Diffusion Effective Coeff. De (3H) (∕) lab. tests [m²/s]	[ ]	Through-diffusion; Test conditions: room temperature (20-25°C), aerobic conditions, filters were not used since low swelling deformation of rock sample due to low smectite contents and high porosity, 45° to the bedding plane data included in the data of [14], synthetic groundwater was used; Lab test, tracer as HTO = 270 Bq/cm^3, pH 8.5; HDB-6 GL-450 to 600 m, best estimate: average value; 5 and 10 mm diameter samples	[ ]	pulse injection & through-diffusion experiment; cm^3	[ ]	Through diffusion cell, axial confining pressure: 1.9 Mpa; rock samples from boreholes (D:35 mm / e:10 mm)	Through-diffusion; n=2; cm scale	Through-diffusion; n=4; cm scale	[ ]	[ ]	Through-diffusion test; HTO, lab, no clear bedding orientation; rock core samples	[ ]
Diffusion Effective Coeff. De (I-) (⊥) lab. tests [m²/s]	[ ]	[ ]	Pressure-pulse test; Doel location; observed range; n≤25; cm^3 samples	pulse injection & through-diffusion experiment; cm^3	through-diffusion method on samples; best estimate = mean; mm-cm scale	Through-diffusion cell, axial confining pressure: 1.9 Mpa; rock samples from boreholes (D:35 mm / e:10 mm)	Through-diffusion; n=2; cm scale	Through-diffusion; n=3; cm scale	Through-diffusion; no confining pressure; ambient temperature and pressure; values were also determined via through-diffusion under confining pressure of 15 MPa (1.4E-12); cm to tens of cm scale	Through-diffusion; no confining pressure; ambient temperature and pressure; values were also determined under confining pressure of 12.0 Mpa (2.4E-12); cm to tens of cm scale	[ ]	[ ]

Table 2 – Methods and scales of measurement (continued)

SOLUTE TRANSPORT PARAMETERS - METHODS	JPN - Koetoi	JPN - Wakkanai	BEL - Ypresian	BEL - Boom	FRA - Callovo-Oxfordian	FRA - Domerian-Toarcian	CH - Opalinus_ MTerri	CH - Opalinus_NE	CAN - Georgian Bay	CAN - Queenston	HUN - Boda-Gorica Block	HUN - Boda-Boda Block
Diffusion Effective Coeff. De (I-) (//) lab. tests [m²/s]	[ ]	Through-diffusion; lab test, tracer as I- = 320 Bq/cm³, pH 8.5; HDB-6 GL-450 to 600 m, best estimate = average value; 5 and 10 mm thickness samples	[ ]	pulse injection & through-diffusion experiment; cm³	[ ]	[ ]	[ ]		Through-diffusion; no confining pressure; ambient temperature and pressure	Through-diffusion; no confining pressure; ambient temperature and pressure	[ ]	Through-diffusion test; high-pressure diffusion test; rock samples
Diffusion Effective Coeff. De (Cl-) (⊥) lab. tests [m²/s]	[ ]	[ ]	[ ]	[ ]	through-diffusion method on samples; best estimate = mean; mm-cm scale	Through-diffusion cell, axial confining pressure: 1.9 Mpa; rock samples from boreholes (D:35 mm / e:10 mm)	Through-diffusion; n=5; cm scale	Through-diffusion; n=6; cm scale	[]	[]	[]	[ ]
Diffusion Effective Coeff. De (Cl-) (//) lab. tests [m²/s]	[ ]	[ ]	[ ]	[ ]	[ ]		Through-diffusion; n=1; cm scale	Through-diffusion; n=1; cm scale	[]	[]	Through diffusion test; HTO, lab, no clear bedding orientation; rock core samples	[ ]

Table 2 – Methods and scales of measurement (continued)

GEOMECHANICAL PARAMETERS - METHODS	JPN - Koetoi	JPN - Wakkanai	BEL - Ypresian	BEL - Boom	FRA - Callovo-Oxfordian	FRA - Domerian-Toarcian	CH - Opalinus_MTerri	CH - Opalinus_NE	CAN - Georgian Bay	CAN - Queenston	HUN - Boda-Gorica Block	HUN - Boda-Boda Block
Uniaxial Compressive Strength (⊥) lab. tests [MPa]	Size of specimen: f50 x H100 [mm]; strain rate ca 0.5%/min	Size of specimen: f35 x H70 [mm]; strain rate: ca.0.5%/min	Uniaxial compression test; strain rate 0.3mm/min; Doel location; observed range; n≤10; cm^3 samples	Back-analysis of uniaxial compression tests; rock sample	UCS tests; tangent modulus at 50% uniaxial strength; sample not resaturated before the test; loading rate: 10E-5 s-1; Best estimate = mean +/- standard deviation; cm scale	Uniaxial compression; rock samples from boreholes (room temperature, saturated, cm scale)	Min and max values from 6 test results; best estimate = median; cm-dm scale	Unconfined compressive tests in the laboratory, loading direction ⊥ to dominant fabric; min/max values from 11 test results; Best estimate = median; test results between Benken and Schlattingen nearly identical; dm scale	Uniaxial Compression Test; 76 mm diameter rock core from boreholes; natural or close to natural water content; tested @ room temperature; based on 11 samples from DGR 1 to 6 boreholes; outliers representing hard layers have been excluded when calculating the mean value; best estimate = mean; tens of cm scale	Uniaxial Compression Test; 75 mm diameter core sample; natural or close to natural water content; tested @ room temperature; based on 14 samples from DGR 1 to 6 boreholes; best estimate = mean; tens of cm scale	Rock samples (46mm<D<64 mm; L/D=2)	Short-term laboratory tests on samples of orientation near perpendicular to beddings (±20°); n>500; rock samples (46mm<D<64 mm; L/D=2)
Uniaxial Compressive Strength (/) lab. tests [MPa]	Size of specimen: f50 x H100 [mm]; strain rate ca 0.5%/min	Size of specimen: f35 x H70 [mm]; strain rate: ca.0.5%/min	[ ]	[ ]	UCS tests; tangent modulus at 50% uniaxial strength; sample not resaturated before the test; loading rate: 10E-5 s-1; Best estimate = mean +/- standard deviation; cm scale	Uniaxial compression; rock samples from boreholes (room temperature, saturated, cm scale)	Min and max values from 8 test results; best estimate = median; cm-dm scale	Unconfined compressive tests in the laboratory, loading direction ∥ to dominant fabric; min/max values from 9 test results; Best estimate = median; average value of test results from Benken are only 70% of the average value from Schlattingen; dm scale	[ ]	[ ]	[ ]	Short-term laboratory tests on samples of orientation near perpendicular to beddings (±20°); n>500; rock samples (46mm<D<64 mm; L/D=2)

Table 2 – Methods and scales of measurement (continued)

GEOMECHANICAL PARAMETERS - METHODS	JPN - Koetoi	JPN - Wakkanai	BEL - Ypresian	BEL - Boom	FRA - Callovo-Oxfordian	FRA - Domerian-Toarcian	CH - Opalinus_MTerri	CH - Opalinus_NE	CAN - Georgian Bay	CAN - Queenston	HUN - Boda-Gorica Block	HUN - Boda-Boda Block
Young's Modulus Static (⊥) lab. tests [MPa]	Size of specimen: f50 x H100 [mm]; Secant Young's modulus at 50 % of the ultimate uniaxial compressive strength	Size of specimen: f35 x H70 [mm]; Secant Young's modulus at 50 % of the ultimate uniaxial compressive strength	Triaxial tests; confining pressure equal to in situ stress, secant modulus; strain rate 1µm/min; Kallo location; observed range; n≤5; cm^3 scale	Back-analysis of hollow cylinder tests; rock samples	UCS tests; tangent modulus at 50% uniaxial strength; sample not resaturated before the test; loading rate: 10E-5 s-3; the min/max Young Modulus are calculated with the standard deviation (best estimate = mean +/- standard deviation); cm scale	triaxial test; rock samples from boreholes (room temperature, saturated, cm scale)	Best estimate = average of 5 test results; min/max values are average ±1 Standard deviation. Experiments conducted at a confining stress between 2 and 4 Mpa; cm-dm scale	Undrained triaxial testing with loading ⊥ to dominant fabric, secant modulus of unload-reload-cycle at 30-70% of peak strength; Best estimate = median of 5 test results; min/max values refer to lowest and highest observed values; experiments conducted at a confining pressure of 22MPa and a pore fluid pressure of 9MPa; all results from samples of the borehole Schlattingen; cm-dm scale	Uniaxial Compression Test; 76 mm diameter rock core from boreholes; natural or close to natural water content; tested @ room temperature; based on 11 samples from DGR 1 to 6 boreholes; outliers representing hard layers have been excluded when calculating the mean value; Best estimate = mean; tens of cm scale	Uniaxial Compression Test; 75 mm diameter core sample; natural or close to natural water content; tested @ room temperature; based on 14 samples from DGR 1 to 6 boreholes; Best estimate = mean; tens of cm scale	Rock samples (46mm<D<64 mm; L/D=2)	Short-term laboratory tests on samples of orientation near perpendicular to beddings (±20°); short-term biaxial test with 10-15 MPa cylindrical load (Hooke's biaxial load device with Doorstopper-cells); rock samples (overcored - D=55mm, 100mm<L< 150mm)

Table 2 – Methods and scales of measurement (continued)

GEOMECHANICAL PARAMETERS - METHODS	JPN - Koetoi	JPN - Wakkanai	BEL - Ypresian	BEL - Boom	FRA - Callovo-Oxfordian	FRA - Domerian-Toarcian	CH - Opalinus_MTerri	CH - Opalinus_NE	CAN - Georgian Bay	CAN - Queenston	HUN - Boda-Gorica Block	HUN - Boda-Boda Block
Young's Modulus Static (//) lab. tests [MPa]	Size of specimen: f50 x H100 [mm]; secant Young's modulus at 50 % of the ultimate uniaxial compressive strength	Size of specimen: f35 x H70 [mm]; secant Young's modulus at 50 % of the ultimate uniaxial compressive strength	[ ]	Back-analysis of hollow cylinder tests; rock samples	UCS tests; tangent modulus at 50% uniaxial strength; sample not resaturated before the test; loading rate: 10E-5 s-3; the min/max Young Modulus are calculated with the standard deviation (best estimate = mean +/- standard deviation); cm scale	Triaxial test; rock samples from boreholes (room temperature, saturated, cm scale)	Best estimate = average of 8 test results; min/max values are average ±1 Standard deviation. Experiments conducted at a confining stress between 2 and 4 Mpa; cm-dm scale	Undrained triaxial testing with loading ⊥ to dominant fabric, secant modulus of unload-reload-cycle at 30-70% of peak strength; Best estimate = median of 2 test results; min/max values refer to lowest and highest observed values; experiments conducted at a confining pressure of 22MPa and a pore fluid pressure of 9MPa; all results from samples of the borehole Schlattingen; cm-dm scale	[ ]	[ ]	[ ]	Short-term laboratory tests on samples of orientation near perpendicular to beddings (±20°); short-term biaxial test with 10-15 MPa cylindrical load (Hooke's biaxial load device with Doorstopper-cells); rock samples (overcored - D=55mm, 100mm<L< 150mm)
Young's Modulus Dynamic (⊥) lab. tests [MPa]	Size of specimen: f50 x H100 [mm]; values calculated by sonic wave velocity of cores	Size of specimen: f35 x H70 [mm]; values calculated by sonic wave velocity of cores	[ ]	[ ]	Lab test on cubic sample with P and S wave measurement (NF P 94-411); sample not resaturated before the test; the min/max Young Modulus are calculated with the standard deviation (best estimate = mean +/- standard deviation); cm scale	[ ]	Calculated from P-wave and S-wave velocities ⊥ fabric and using a bulk density of 2430 kg/m3 (cf. Petrophysical parameters); cm-dm scale	cm-dm; Calculated from P-wave and S-wave velocities ⊥ fabric and using a bulk density of 2430 kg/m3 (cf. Petrophysical parameters); Best estimate is average of 68 test results, Min and Max values are average ±1 Standard deviation; all results from samples of the borehole Benken; cm-dm scale	Uniaxial Compression Test; natural or close to natural water content; tested @ room temperature; 76 mm dia. core samples from DGR boreholes; tens of cm scale	Uniaxial Compression Test; 75 mm diameter cores; based on 14 samples from DGR 1 to 6 boreholes; Best estimate = mean; tens of cm scale	[ ]	[ ]

Table 2 – Methods and scales of measurement (continued)

GEOMECHANICAL PARAMETERS - METHODS	JPN - Koetoi	JPN - Wakkanai	BEL - Ypresian	BEL - Boom	FRA - Callovo-Oxfordian	FRA - Domerian-Toarcian	CH - Opalinus_MTerri	CH - Opalinus_NE	CAN - Georgian Bay	CAN - Queenston	HUN - Boda-Gorica Block	HUN - Boda-Boda Block
Young's Modulus Dynamic (∥) lab. tests [MPa]	Size of specimen: f50 x H100 [mm]; values calculated by sonic wave velocity of cores	Size of specimen: f35 x H70 [mm]; values calculated by sonic wave velocity of cores	[ ]	[ ]	Lab test on cubic sample with P and S wave measurement (NF P 94-411); sample not saturated before the test; the min/max Young Modulus are calculated with the standard deviation (best estimate = mean +/- standard deviation); cm scale	[ ]	Calculated from P-wave and S-wave velocities ∥ fabric and using a bulk density of 2430 kg/m3 (cf. Petrophysical parameters); cm-dm scale	Calculated from P-wave and S-wave velocities ∥ fabric and using a bulk density of 2430 kg/m3 (cf. Petrophysical parameters); Best estimate = average of 71 test results; min/max values are average ±1 Standard deviation; all results from samples of the borehole Benken; cm-dm scale	[ ]		[ ]	[ ]
Young's Modulus Static (⊥) in situ tests [MPa]	[ ]	[ ]	[ ]	Back-analysis of ATLAS experiment (small strain); undisturbed Boom Clay - small strain	[ ]	[ ]	Derived from dilatometer tests; calculated from 30 test results assuming a Poisson ratio of n=0.35; cm-dm scale	[ ]	[ ]		[ ]	[ ]
Young's Modulus Static (∥) in situ tests [MPa]	Dilatometer test in a 158.7 mm diameter borehole; loading span: 1 m depth of test: from 200 m to 550 m depth range of pressure: 0 - 6.8 MPa	Dilatometer test in a 158.7 mm diameter borehole; loading span: 1 m depth of test: from 400 m to 550 m depth range of pressure: 0 - 7.6 MPa	[ ]	Back-analysis of ATLAS experiment (small strain); undisturbed Boom Clay - small strain	[ ]	[ ]	Derived from dilatometer tests; calculated from 9 test results assuming a Poisson ratio of n=0.27; cm-dm scale	Derived from dilatometer tests at a depth range of 598-628m b.g.; meter scale	[ ]		[ ]	[ ]

Table 2 – Methods and scales of measurement (continued)

GEOMECHANICAL PARAMETERS - METHODS	JPN - Koetoi	JPN - Wakkanai	BEL - Ypresian	BEL - Boom	FRA - Callovo-Oxfordian	FRA - Domerian-Toarcian	CH - Opalinus_MTerri	CH - Opalinus_NE	CAN - Georgian Bay	CAN - Queenston	HUN - Boda-Gorica Block	HUN - Boda-Boda Block
Poisson's Ratio Static lab. tests (⊥) [-]	Size of specimen: f50 x H100 [mm]; value at 50 % of the ultimate uniaxial compressive strength	Size of specimen: f35 x H70 [mm]; A value at 50 % of the ultimate uniaxial compressive strength	[ ]	Back-analysis of hollow cylinder tests; rock samples	[ ]	Triaxial test; rock samples from boreholes (room temperature, saturated, cm scale)	Best estimate = average of 7 test results; min and max values are average ±1 standard deviation; cm-dm scale	Constrained from undrained triaxial testing with loading ⊥ to dominant fabric; Best estimate = average of 22 test results; min/max values are average ±1 standard deviation; all results from samples of the borehole Benken; cm-dm scale	Uniaxial Compression Test; natural or close to natural water content; tested @ room temperature; based on 11 samples from DGR 1 to 6 boreholes; outliers representing hard layers have been excluded when calculating the mean value; best estimate = mean; tens of cm scale	Uniaxial Compression Test; 75 mm diameter cores; natural or close to natural water content; tested @ room temperature; based on 14 samples from DGR 1 to 6 boreholes; best estimate = mean; tens of cm scale	Rock samples (46mm<D <64mm; L/D=2)	Short-term laboratory tests on samples of orientation near perpendicular to beddings (±20°); n>500; rock samples (46mm<D<64mm; L/D=2)
Poisson's Ratio Static lab. tests (//) [-]	Size of specimen: f50 x H100 [mm]; value at 50 % of the ultimate uniaxial compressive strength	Size of specimen: f35 x H70 [mm]; value at 50 % of the ultimate uniaxial compressive strength	[ ]	Back-analysis of drained triaxial tests; rock samples	[ ]	Triaxial test; rock samples from boreholes (room temperature, saturated, cm scale)	Best estimate = average of 8 test results' min/max values are average ±1 standard deviation; cm-dm scale	Constrained from undrained triaxial testing with loading direction ∥ to dominant fabric; Best estimate = average of 21 test results; min/max values are average ±1 standard deviation; all results from samples of the borehole Benken; cm-dm scale	[ ]	[ ]	[ ]	[ ]
Poisson's Ratio Dynamic (⊥) lab. tests [-]	Size of specimen: f50 x H100 [mm]; values calculated by sonic wave velocity of cores	Size of specimen: f35 x H70 [mm]; values calculated by sonic wave velocity of cores	[ ]	[ ]	Lab test on cubic sample with P and S wave measurement (NF P 94-411); sample not resaturated before the test; the min/max Young Modulus are calculated with the standard deviation (best estimate = mean +/- standard deviation); cm scale	[ ]	Calculated from P-wave and S-wave velocities ⊥ fabric (cf. Petrophysical parameters); cm-dm scale	Calculated from P-wave and S-wave velocities ⊥ fabric (cf. Petrophysical parameters); Best estimate = average of 68 test results; min/max values are average ±1 standard deviation; all results from samples of the borehole Benken; cm-dm scale	Uniaxial Compression Test; natural or close to natural water content; tested @ room temperature; 76 mm dia. core samples from DGR boreholes; tens of cm scale	Uniaxial Compression Test; 75 mm diameter cores; based on 14 samples from DGR 1 to 6 boreholes; Best estimate = mean; tens of cm scale	[ ]	[ ]

Table 2 – Methods and scales of measurement (continued)

GEOMECHANICAL PARAMETERS - METHODS	JPN - Koetoi	JPN - Wakkanai	BEL - Ypresian	BEL - Boom	FRA - Callovo-Oxfordian	FRA - Domerian-Toarcian	CH - Opalinus_MTerri	CH - Opalinus_NE	CAN - Georgian Bay	CAN - Queenston	HUN - Boda-Gorica Block	HUN - Boda-Boda Block
Poisson's Ratio Dynamic (⁄) lab. tests [-]	Size of specimen: f50 x H100 [mm]; values calculated by sonic wave velocity of cores	Size of specimen: f35 x H70 [mm]; values calculated by sonic wave velocity of cores	[ ]	[ ]	Lab test on cubic sample with P and S wave measurement (NF P 94-411); sample not resaturated before the test; the min/max Young Modulus are calculated with the standard deviation (best estimate = mean +/- standard deviation); cm scale	[ ]	Calculated from P-wave and S-wave velocities ∥ fabric (cf. Petrophysical parameters); cm-dm scale	Calculated from P-wave and S-wave velocities ∥ fabric (cf. Petrophysical parameters); Best estimate = average of 71 test results; min/max values are average ±1 standard deviation; all results from samples of the borehole Benken; cm-dm scale	[ ]	[ ]	[ ]	[ ]
Cohesion (⊥) lab. tests [MPa]	[ ]	Size of specimen: f35 x H70 [mm]; drain condition, confining pressure: 1.35 - 14.3 MPa, strain rate: 0.02%/min, parallel to almost perpendicular to bedding	Triaxial tests; strain rate: 0.001mm/min [9]; 1mm/min [14]; Doel & Kallo locations; observed range; n≤15; cm^3 samples	Back-analysis of hollow cylinder test; rock samples	[ ]	Triaxial test; rock samples from boreholes (room temperature, saturated, cm scale)	Test results with loading direction ⊥ and ∥ to the dominant fabric were analysed in combination as 'matrix' values; cm-dm scale	Test results with loading direction ⊥ and ∥ to the dominant fabric were analysed in combination as 'matrix' values; cm-dm scale	[ ]	[ ]	[ ]	[ ]
Cohesion (⁄) lab. tests [MPa]	Size of specimen: f50 x H100 [mm]; drain condition, confining pressure: 0.86 - 6.51 MPa, strain rate: 0.02%/min, orientation towards bedding: 50 degrees	Size of specimen: f35 x H70 [mm]; drain condition, confining pressure: 2 - 14.3 MPa, strain rate: 0.02%/min, oblique to bedding (30 to 60 degrees)	[ ]	Back-analysis of hollow cylinder test; rock samples	[ ]	[ ]	Test results with loading direction ⊥ and ∥ to the dominant fabric were analysed in combination as 'matrix' values; cm-dm scale	Test results with loading direction ⊥ and ∥ to the dominant fabric were analysed in combination as 'matrix' values; cm-dm scale	[ ]	[ ]	[ ]	[ ]

Table 2 – Methods and scales of measurement (continued)

GEOMECHANICAL PARAMETERS - METHODS	JPN - Koetoi	JPN - Wakkanai	BEL - Ypresian	BEL - Boom	FRA - Callovo-Oxfordian	FRA - Domerian-Toarcian	CH - Opalinus_MTerri	CH - Opalinus_NE	CAN - Georgian Bay	CAN - Queenston	HUN - Boda-Gorica Block	HUN - Boda-Boda Block
Internal Friction Angle (⊥) lab. tests [°]	[ ]	Size of specimen: f35 x H70 [mm]; drain condition, confining pressure: 1.35 - 14.3 MPa, strain rate: 0.02%/min, parallel to almost perpendicular to bedding	Triaxial tests; strain rate: 0.001mm/min [9]; 1mm/min [14]; Doel & Kallo locations; observed range; n≤15; cm^3 samples	[ ]	[ ]	Triaxial test; rock samples from boreholes (room temperature, saturated, cm scale)	Test results with loading direction ⊥ and ∥ to the dominant fabric were analysed in combination as 'matrix' values; cm-dm scale	Test results with loading direction ⊥ and ∥ to the dominant fabric were analysed in combination as 'matrix' values; cm-dm scale	[ ]	[ ]	[ ]	[ ]
Internal Friction Angle (∕) lab. tests [°]	Size of specimen: f50 x H100 [mm]; drain condition, confining pressure: 0.86 - 6.51 MPa, strain rate: 0.02%/min, orientation towards bedding: 50 degrees	Size of specimen: f35 x H70 [mm]; drain condition, confining pressure: 2 - 14.3 MPa, strain rate: 0.02%/min, oblique to bedding (30 to 60 degrees)	[ ]	[ ]	[ ]	[ ]	Test results with loading direction ⊥ and ∥ to the dominant fabric were analysed in combination as 'matrix' values; cm-dm scale	Test results with loading direction ⊥ and ∥ to the dominant fabric were analysed in combination as 'matrix' values; cm-dm scale	[ ]	[ ]	[ ]	[ ]
Swelling Pressure (⊥) lab. tests [MPa]	[ ]	Size of specimen: f60 x H20 [mm]; parallel to almost perpendicular to bedding	[ ]	[ ]	[ ]	Equiv. oedo cell with "natural water"; rock samples from boreholes (room temperature, saturated, cm scale)	Constrained swelling test using a chemically balanced, synthetic pore fluid (Pearson 1998); Best estimate = average of 5 test results; min/max values refer to lowest and highest recorded values; cm-dm scale	Constrained swelling test using a chemically balanced, synthetic pore fluid (Pearson 1998); Best estimate = average of 2 test results; min/max values refer to lowest and highest recorded values; cm-dm scale	[ ]	[ ]	[ ]	[ ]

Table 2 – Methods and scales of measurement (continued)

GEOMECHANICAL PARAMETERS - METHODS	JPN - Koetoi	JPN - Wakkanai	BEL - Ypresian	BEL - Boom	FRA - Callovo-Oxfordian	FRA - Domerian-Toarcian	CH - Opalinus_MTerri	CH - Opalinus_NE	CAN - Georgian Bay	CAN - Queenston	HUN - Boda-Gorica Block	HUN - Boda-Boda Block
Swelling Pressure (/) lab. tests [MPa]	Size of specimen: f60 x H20 [mm]; drain condition, orientation towards bedding: 50 degrees; for testing at natural initial water content, preparation performed such as to retain water content to within 1% of its in situ value. At least three specimens per sample were prepared.	Size of specimen: f60 x H20 [mm]; oblique to bedding (30 to 60 degrees); for testing at natural initial water content, preparation performed such as to retain water content to within 1% of its in situ value. At least three specimens per sample were prepared.	[ ]	[ ]	[ ]	Equiv. oedo cell with "natural water"; rock samples from boreholes (room temperature, saturated, cm scale)	Constrained swelling test using a chemically balanced, synthetic pore fluid (Pearson 1998); Best estimate = average of 2 test results; min/max values refer to lowest and highest recorded values; cm-dm scale	Constrained swelling test using a chemically balanced, synthetic pore fluid (Pearson 1998); Best estimate = average of 5 test results; min/max values refer to lowest and highest recorded values; cm-dm scale	[ ]	[ ]	[ ]	[ ]

NEA PUBLICATIONS AND INFORMATION

The **full catalogue of publications** is available online at www.oecd-nea.org/pub.

In addition to basic information on the Agency and its work programme, the NEA website offers free downloads of hundreds of technical and policy-oriented reports. The professional journal of the Agency, **NEA News** – featuring articles on the latest nuclear energy issues – is available online at www.oecd-nea.org/nea-news.

An **NEA monthly electronic bulletin** is also distributed free of charge to subscribers, providing updates of new results, events and publications. Sign up at www.oecd-nea.org/bulletin.

Visit us on **Facebook** at www.facebook.com/OECDNuclearEnergyAgency or follow us on **Twitter** @OECD_NEA.

OECD/NEA PUBLISHING, 2 rue André-Pascal, 75775 PARIS CEDEX 16

Clay Club Catalogue of Characteristics of Argillaceous Rocks: 2022 Update

The NEA Clay Club has been gathering the key geoscientific characteristics of the various argillaceous formations that are – or have been – studied in NEA member countries in the context of radioactive waste disposal, resulting in the publication of the Clay Club Catalogue of Characteristics of Argillaceous Rocks in 2005.

This publication builds upon the 2005 NEA report by providing updated datasets for a select number of argillaceous formations presented in the previous report, as well as an expanded discussion of: the formations and their properties; the nuclear waste management organisations responsible for the implementation of the deep geological repository concept; the design concept proposed for a deep geological repository in the respective countries and rock formations; and some of the favourable properties of said argillaceous formations.

A key goal of this report is to present the data in a manner that allows reasonable comparability (in both scale and methods) of the included parameters, in order to support the formal assessment and demonstration of the capacity of clay-rich formations to securely contain and isolate nuclear waste from the natural environment.

Nuclear Energy Agency (NEA)
46, quai Alphonse Le Gallo
92100 Boulogne-Billancourt, France
Tel.: +33 (0)1 73 21 28 19
nea@oecd-nea.org www.oecd-nea.org

NEA No. 7249